THE UNIVERSITY OF ADELAIDE

DEPARTMENT OF MECHANICAL ENGINEERING

A Study of Pressure Fluctuations in Turbulent Shear Flows Under the Effects of Mean Pressure Gradients

By

Kim Boon Lim, B.E.

Thesis for the Degree of Doctor of Philosophy

December, 1971

TABLE OF CONTENTS

SUMMARY.

The work described in this thesis represents part of a programme undertaken with the aim of obtaining a better insight into the mechanism associated with the generation of wall pressure fluctuations in turbulent shear flows with and without mean streamwise pressure gradients.

Reliable routine procedures were developed for the calculation of the wall pressure fluctuations and results are presented for the boundary layer with zero mean pressure gradient. These were based on the assumptions that:-

(1) turbulence/mean-shear interaction contributes mainly to the pressure fluctuations.

(2) the boundary layer exhibits statistical stationarity in time and homogeneity in planes parallel to the boundary.

(3) the boundary layer grows sufficiently slowly so that the mean velocity parallel to the boundary, and the root mean square velocity fluctuation normal to the boundary are functions only of the co-ordinate normal to the boundary.

The boundary layer models which have been employed allow an examination of the effects of the changes of the specification of the mean shear, the eddy scales and the correlation coefficient on the overall values of the mean square pressure fluctuations. The variation of these pressures with Reynolds number was also examined.

It is shown that the correct interpretation of contributions of

various regions of a turbulent boundary layer to the space-time covariance of the pressure fluctuations at the wall requires consideration of the "joint contribution density function". This function represents the joint contribution of a pair of infinitesimally thin strata of the boundary layer, parallel to the wall, per unit thickness of each to the space-time covariance. It is essentially a second spatial derivative, and its use leads to the conclusion that earlier interpretations based on functions which are only first derivatives are liable to error. Contributions of finite regions can be obtained in terms of this function, but must be carefully defined. Representative calculated values of the function are given for the case of the mean square wall pressure fluctuation, and it is shown that the inner region of the boundary layer accounts for the major contribution to the pressures.

The results also indicate that

(1) A single representative value of p'/τ_w obtained in previous calculations is typical of only a limited range of Reynolds number, and that over the Reynolds number range for which $10^3 \leq Re_\delta^* \leq 10^7$ the variation in contribution of the turbulence/mean-shear interaction to p'/τ_w is from 1.10 to 6.51. Over the limited Reynolds number range for which experimental results are available, the variation of the calculated values of p'/τ_w is in accord with that of experimental results.

(2) At low Reynolds numbers, the small eddies make a dominant contribution to $\langle p^2 \rangle$ (over 90% at $Re_\delta^* = 10^3$). The proportion of the contribution falls off with increase in Reynolds number to a value of about 20% at $Re_\delta^* = 10^7$.

(3) The variation of the total value of $\langle p^2 \rangle$ with Reynolds number is predominantly a reflection of the variation of the value of the large eddy contribution with Reynolds number and is a function also of the correlation scales assigned to the eddy structure in the turbulence.

(4) The value of the mean square pressure is sensitive to the choice of the eddy scales and the correlation function. Slight variation in the specification of the mean shear in the transition region has an insignificant effect on the overall value.

(5) For a two-dimensional incompressible turbulent boundary layer, turbulence/mean-shear interaction is the dominant process in the generation of the wall pressure fluctuations, and accounts for about 80% of the overall mean square value.

(6) Comparison of the calculated auto-covariance and the frequency power spectral density distribution with experimental results from various sources show that the calculated values fall within the range covered by the experimental curves. This lends further weight to the credibility of the assumption that the turbulence/mean-shear interaction plays a dominant role in the generation of the wall pressure fluctuations.

(7) The experimental results for which good transducer resolution at the higher frequencies is claimed indicate that the high frequency characteristics of the theoretical model may not be representative of that in the actual boundary layer. This could be due to a deficiency of the model and/or the neglect of the other pressure source terms which provide relatively small but not negligible contributions to the pressures.

Measurements were made of the mean flow properties and of the spectral

density distributions of the wall pressure fluctuations in a constant pressure turbulent boundary layer. The good agreement between the present results and those of previous investigators confirms the validity of the present results and proves the proper functioning of the experimental equipment.

The root mean square values of the wall pressure fluctuations obtained from the integration of the spectral density distributions indicate that p'/τ_w varies from 2.3 to 2.5 over the Reynolds number range of $7.0 \times 10^3 \leq Re_{\delta^*} \leq 1.5 \times 10^4$. It is found that the effect of the transducer size on its resolution at the high frequencies is not negligible for the present measurements for which $0.14 \leq d/\delta^* \leq 0.30$.

It is believed that the pressure gradient results presented in this thesis represent the first measurements of the wall pressure fluctuations in an equilibrium turbulent boundary layer under the effects of a mean streamwise pressure gradient. The measurements were made in an adverse pressure gradient layer for which the pressure gradient parameter $\beta = 1.37$ and were limited to the spectral density distributions at two locations in the working section of the wind tunnel. The relatively small size of the transducers used resulted in a value of d/δ^* of approximately 0.06, a value which is believed the smallest to date. The results indicate that

(1) The spectral density distribution for the pressure gradient layer is similar to that of the constant pressure layer in the frequency range for which $1 < \omega\delta^*/U_\infty < 3$. For frequencies where $\omega\delta^*/U_\infty > 3$ or $\omega\delta^*/U_\infty < 1$, the spectra from the adverse pressure gradient layer are higher than those of the constant pressure layer.

(2) The root mean square value of the wall pressure fluctuations expressed as p'/τ_w is greater in the adverse pressure gradient layer than that in the constant pressure layer.

(3) For Reynolds numbers, Re_δ^*, in the region of 3×10^4, p'/τ_w has the value of 4.2 although the corresponding value of p'/q_∞, namely 7.0×10^{-3}, is not much greater than the value of 6.3×10^{-3} for the constant pressure layer at $Re_\delta^* = 1.5\times10^4$.

STATEMENT OF ORIGINALITY.

This thesis contains no material which has been accepted for the award of any other degree or diploma in any University. To the best of the author's knowledge and belief, this thesis contains no material previously published or written by another person, except where due reference is made in the text.

K.B. Lim

December, 1971.

ACKNOWLEDGEMENTS.

The work described in this thesis has been carried out in the Department of Mechanical Engineering of the University of Adelaide under the aegis of Professor H.H. Davis. The author is indebted to Professor Davis for the opportunity to carry out this research.

To Dr. M.K. Bull, who supervised the work, the author is deeply indebted, both for his help, constant interest and encouragement throughout the course of the research and for his assistance during the preparation of this thesis.

Greatful acknowledgements are made to Dr. G.L. Brown for fruitful discussions of the work.

The author is indebted to his family for their encouragement and support without which the completion of the thesis would certainly have been in doubt.

To the workshop staff, thanks are due for their assistance in the manufacture and assembly of the test equipment, and in particular to Mr. G. Osborne for his invaluable help during the experimental work.

Acknowledgements are also made to the Australian Research Grants Committee and to the Australian Institute of Nuclear Science and Engineering for providing financial grants, without which this work would not have been possible.

PRINCIPAL NOTATIONS.

a, b, c	constants
C_f	skin friction coefficient
C(a,b)	contribution to the pressure covariance from sources within the region $a \leq y_2 \leq b$
d	diameter of transducer sensing element
f	frequency
f(r)	longitudinal velocity correlation coefficient in isotropic turbulence
G	Clauser boundary layer family parameter
H	boundary layer shape parameter = δ^*/θ
i, j, k, l, m, n	tensor notation suffices
$M(y_2)$	mean shear = $\partial U_1(y_2)/\partial x_2$
M_s	shock Mach number
p	pressure (generally denotes fluctuating value)
p'	root mean square pressure
$Q_{pp}(\tau)$	auto-covariance of the fluctuating pressure
q	pressure source
Re_{δ^*}	Reynolds number based on boundary layer displacement thickness = $\delta^* U_\infty/\nu$
$R_{ij}(\vec{r})$	velocity correlation coefficient
$R_{pp}(\vec{r},\tau)$	space-time pressure correlation coefficient
$\vec{r}$	separation vector = $\vec{z} - \vec{y}$
s	eddy scale
T	temperature
t, t'	time and retarded time

u_i	velocity component in the x_i-direction (generally denotes fluctuating value)
u_i'	root mean square velocity fluctuations
U_1	mean velocity in direction of free stream
U_c	convection velocity
U_τ	friction velocity
U_∞	free stream velocity
$\vec{x}$, $\vec{x}'$	usually denotes field point co-ordinates
x_2^*	$= x_2 U_\tau/\nu$
$\vec{y}$, $\vec{z}$	usually denotes source point co-ordinates
y^*	$= yU_\tau/\nu$
α_i	anisotropy factor
β	pressure gradient parameter
γ	ratio of specific heat of a gas at constant pressure to the specific heat at constant temperature
Δ	Clauser thickness
δ	boundary layer thickness
δ_c	boundary layer thickness at which $\partial U_1/\partial \ln y = 1/\kappa$
δ^*	boundary layer displacement thickness
δ_ℓ^*	thickness of viscous sublayer
δ_0	boundary layer thickness at which $U_\infty - U_1 = U_\tau$
ζ	$= x_2/\delta$
θ	boundary layer momentum thickness
κ	von Karman constant
$(\Lambda_1)_{pp}$	longitudinal integral scale
ν	fluid kinematic viscosity
$\vec{\xi}$	field point separation vector $= \vec{x}' - \vec{x}$

Π	Coles's profile parameter
ρ	fluid density
τ	time delay = t' - t
τ_Λ	integral time scale
τ_w	wall shear stress
$\phi_p(\omega)$	frequency power spectral density
$\phi_{pp}(\vec{r})$	covariance of the fluctuating pressure
ω	circular frequency
$w(\zeta)$	Coles's wake function
$<...>$	denotes statistical mean value

1. REVIEW OF PREVIOUS WORK AND OBJECTIVES OF THE PRESENT RESEARCH.

1.1 Introduction.

The initial concept of turbulence in fluid flow can be attributed to Reynolds (1883) in his study of pipe flow. Since then, and particularly in recent years, much effort has been spent in the study of the structure and characteristics of turbulent fluid motion. Turbulent motion, whether it be the idealised homogeneous isotropic type considered by, for example, Batchelor (1953) or the homogeneous anisotropic category of which the turbulent shear flow treated by, for example, Townsend (1956) is a particular example, is a complex phenomenon and the progress in the development of the theory was restricted until Taylor ((1921) and (1935)) showed that statistical theory could be used to a great advantage in this field. However, due to the complexity of the mathematical equations involved, the development has been limited to the formation of general principles and hypotheses concerning the nature of the turbulent motion through the accumulation of experimental data.

Further, the experimental data are predominantly those relating to velocity fluctuations, mainly as a result of the fact that the hot-wire anemometer has been the only instrument capable of measuring fluctuating quantities in the flow without creating significant additional disturbance of its own.

While velocity fluctuations are obviously quantities of primary

interest, experimental results for other quantities could be just as significant if they could be obtained. Pressure fluctuations could well be included in this category.

There are, in fact, two very good reasons for investigating the properties of the fluctuating pressure field in a turbulent flow:

(a) to improve understanding of the mechanisms operating in turbulent flows, and

(b) to provide data for the solution of practical engineering problems to which pressure fluctuations may give rise.

The experimental investigation of pressure fluctuations is difficult because virtually the only reliable means of measuring the fluctuating pressure is in the use of small microphones or transducers mounted flush with a solid surface as it has been claimed (see Hodgson (1962)) that the use of such devices in the midst of the flow region invariably creates a major flow disturbance whose frequencies are about the same as those to be measured with a relative amplitude of at least an order of magnitude higher. Hence, the available results have been limited to surface or wall pressure fluctuations obtained from boundary layer as well as wall jet (see Lilley and Hodgson (1960)) measurements. It should be noted, however, that the argument referred to above is not universally accepted - the author has been informed that recent work at the University of Toronto indicates that useful pressure fluctuation measurements within a turbulent flow may well be possible.* However, even though most existing pressure fluctuation measurements are limited to those made at the solid surface

* Siddon, T.E. 1969 On the Response of Pressure Measuring Instrumentation in Unsteady Flow. University of Toronto, U.T.I.A.S., Report No. 136

under a boundary layer or a wall jet, they are applicable to several areas of considerable engineering importance, including , for example, boundary layer noise generation at both rigid and flexible surfaces, fatigue of aircraft structures, and underwater detection.

1.2 Survey of Previous Work on Turbulent Pressure Fluctuations.

1.2.1 Isotropic Turbulence.

The early investigations into pressure fluctuations in turbulent flows were reported by Heisenberg (1948), Obukhoff (1949), and Batchelor (1951) and were limited to the case of isotropic turbulence. It was assumed that the joint probability function for the velocity fluctuations at any two points was Gaussian thus simplifying the relationship between the fourth order and the second order correlations and at the same time making equivalent to zero all odd order correlations. The resultant expression for the pressure covariance was given by Batchelor (1951) as

$$\phi_{pp}(\vec{r}) = \langle p(\vec{x})p(\vec{x}+\vec{r})\rangle = 2u'^4 \int_r^\infty (y - \frac{r^2}{y}) \{f'(y)\}^2 \, dy \quad , \qquad \ldots(1.2.1)$$

where $f'(y) = \frac{\partial f(y)}{\partial y}$, u' is the root mean square velocity fluctuations, $\langle \ldots \rangle$ represents the statistical mean value and $f(r)$ is the correlation scalar of the homogeneous isotropic turbulence. When $f(r)$ obtained by Proudman (1951) from measurements behind a grid in a uniform flow was used, the root mean square pressure was obtained by Batchelor as

$$p' = 0.58 \, \rho u'^2 \quad , \qquad \ldots(1.2.2)$$

where ρ is the fluid density.

Uberoi (1953) argued that simple relationships for the correlation functions could be assumed without invoking the Gaussian condition for the joint probability function for the fluctuating velocity components and obtained

$$p' = \begin{cases} 1.0\ \rho u'^2 & - \text{ for low Reynolds number} \\ 0.55\ \rho u'^2 & - \text{ for high Reynolds number} \end{cases} \qquad \ldots(1.2.3)$$

1.2.2 Turbulent Shear Flow with Zero Mean Pressure Gradient.

The late 1950's and early 1960's were a period of fairly intense activity in both theoretical and experimental investigations of pressure fluctuations in turbulent shear flow with zero mean pressure gradient.

The experimental work established fairly well the general characteristics (mean square pressure, spectra, space-time correlations and convection properties) of the wall pressure field in subsonic turbulent boundary layers. However, there were, and remain, experimental problems such as that of adequate spatial resolution of the pressure transducers, a problem first treated by Corcos (1963) and later by Willmarth and Roos (1965). The results obtained were very valuable as engineering data, but were also important in relation to the identification of the flow processes contributing to the generation of pressure fluctuations.

The first attempt to calculate the statistical properties of the pressure fluctuations in turbulent shear flow was made by Kraichnan ((1956a) and (1956b)). The mathematical models which were used represented homogeneous isotropic and homogeneous anisotropic turbulence with a superimposed mean shear structure. Kraichnan's work was aimed at estimating the order of magnitude of the mean square wall pressure fluctuation in a two-dimensional incompressible turbulent boundary layer and determining which velocity interactions are mainly responsible for it. To this end, the approximation to the turbulent boundary layer flow was taken as an homogeneous anisotropic turbulence with a "mirror flow" characteristic. Laufer's (1954) experimental data were used in his analysis and he concluded that the interactions between the turbulence and the mean shear, through the gradient normal to the boundary of the mean velocity component parallel to the boundary and the gradient in the streamwise direction of the fluctuating velocity component normal to the boundary, was the dominant effect in producing wall pressure fluctuations. This "dominance of turbulence/mean-shear interaction" has been used extensively by later workers as the basis for further calculations of the statistical properties of the wall pressure fluctuations. Kraichnan himself estimated the turbulence/mean-shear contribution to the pressure fluctuations as

$$\frac{p'}{\tau_w} \simeq 6 \quad , \qquad \ldots(1.2.4)$$

where τ_w is the wall shear stress.

Kraichnan's calculations were refined and extended by Lilley and Hodgson (1960) and Hodgson (1962) on the basis of the assumption of the dominance of the turbulence/mean-shear interaction. They gave estimates

of the ratio of the root mean square wall pressure fluctuation to the mean wall shear stress which were in considerably better agreement with experimental values than those obtained by Kraichnan, and also an indication of which region of the boundary layer is the most important in generating wall pressure fluctuations. The value obtained by Lilley and Hodgson was

$$\frac{p'}{\tau_w} = 3 \quad , \qquad \ldots(1.2.5)$$

and Lilley (1960) in an extension of the analysis derived

$$\frac{p'}{\tau_w} = 3.1 \quad . \qquad \ldots(1.2.6)$$

Hodgson, on the assumption that the correlation coefficient for the fluctuating component of the velocity normal to the boundary can be taken as

$$R_{22}(y_2;\vec{r}) = \frac{\langle u_2(y_2)u_2(y_2;\vec{r})\rangle}{\left[u_2^2(y_2)\right]^{\frac{1}{2}}\left[u_2^2(y_2;\vec{r})\right]^{\frac{1}{2}}} = e^{-r^2/y_2^2} \quad , \qquad \ldots(1.2.7)$$

where $u_2(y_2)$ is the normal velocity component at a distance y_2 from the boundary and $\vec{r}$ is the separation vector between the points, obtained the value

$$\frac{p'}{\tau_w} = 2.56 \quad . \qquad \ldots(1.2.8)$$

As the result of a re-calculation, Hodgson, in a private communication, revised this value to

$$\frac{p'}{\tau_w} > 4 \quad . \qquad \ldots(1.2.9)$$

These values are of about the same magnitude as those measured experimentally.

Hodgson also concluded that the major contribution to the calculated wall pressure came from the region $0.02 < y_2/\delta < 0.4$, where δ is the boundary layer thickness. From an idealised model of the boundary layer velocity field, Hodgson calculated the one-dimensional wave-number spectra and space-correlations of the wall pressure field resulting solely from turbulence/mean-shear interaction, and found that the longitudinal integral scale and the integral time scale represented by

$$(\Lambda_1)_{pp} = \int_{-\infty}^{\infty} R_{pp}(\xi_1,0,0)\, d\xi_1 \qquad \ldots(1.2.10)$$

and

$$\tau_\Lambda = \int_{-\infty}^{\infty} R_{pp}(0,0,\tau)\, d\tau \qquad \ldots(1.2.11)$$

respectively, gave zero values, and the lateral correlation $R_{pp}(0,\xi_3,0)$ was positive for all ξ_3. (Here $R_{pp}(\xi_1,\xi_3,\tau)$ has been written for the correlation coefficient $\langle p(\vec{x},t)p(\vec{x}+\vec{\xi},t+\tau)\rangle/\langle p^2\rangle$ in a homogeneous field). Hence, the longitudinal space-correlation, which is positive at all small ξ_1, should be negative at large ξ_1, and the positive and negative areas under the curve should be equal. Hodgson's own measurements of the longitudinal space-correlation and to a lesser extent those of Bull (1967) and Blake (1970) show these characteristics, and in each case the lateral space-correlation is positive for all ξ_3, indicating that a significant part of the mean square pressure does result from turbulence/mean-shear interaction.

Willmarth and Wooldridge (1963) report measurements of correlations between the wall pressure fluctuations and the turbulence velocity components. They found that these correlations also take the forms which would be expected if the wall pressure fluctuations were mainly due to turbulence/mean-shear interaction.

However, Corcos (1964) using Willmarth's and Wooldridge's data has produced evidence to the contrary. His calculations which include the turbulence/mean-shear source terms as well as some of the other terms neglected previously gave results of the mean square wall pressure fluctuations which were about 32% only of the observed values with the contributions confined to the high frequency region of the pressure power spectrum and with the most significant contribution coming from the region of the boundary layer between the boundary surface and $y_2/\delta^* = 1.0$ (y_2/δ of about 0.12), that is, from a much narrower region of the boundary layer than indicated by Hodgson's calculations, with a peak contribution in the vicinity of $y_2/\delta^* = 0.2$ (y_2/δ of about 0.025), where δ^* is the displacement thickness of the boundary layer given by

$$\delta^* = \int_0^\infty (1 - \frac{U_1}{U_\infty})\, dy_2 \quad , \qquad \ldots(1.2.12)$$

U_1 is the mean velocity in the boundary layer and U_∞ is the free stream velocity. He therefore concluded that the turbulence/mean-shear interaction makes a significant contribution to the wall pressure fluctuations, but that it is not the dominant effect. The results of Bull (1967) appear to be consistent with Corcos's conclusion on the location of the turbulence/

mean-shear interaction sources as they indicate that the motion in the constant stress layer (where y_2/δ is less than about 0.2) is responsible for the high frequency portion ($\omega\delta/U_\infty > 2$, where ω is the frequency in rad/sec) of the pressure power spectrum which amounts to about 75% of the mean square pressure, and that significant contributions come from the innermost part of the fully turbulent region of the constant stress layer and probably also from sources located in the transition region ($5 < y_2 U_\tau/\nu < 30$, where $U_\tau = (\tau_w/\rho)^{\frac{1}{2}}$ is the friction velocity and ν is the kinematic viscosity). However, the general character of the results tends to be that of a pressure field with a dominant contribution (certainly greater than 32% of the mean square pressure) from the turbulence/mean-shear interaction.

So the work referred to does not clearly resolve the question of the dominance of turbulence/mean-shear interaction.

In none of the theoretical work was any attempt made to calculate the effects of Reynolds number on the wall pressure fluctuations. A Reynolds number effect on the wall pressure fluctuations in turbulent boundary layers was observed by Bull (1967) whose experimental results showed p'/τ_w increasing at the rate of about the 0.17 power of the Reynolds number, from 2.1 to 2.8 over the Reynolds number range $6\times10^3 < Re_\delta^* < 4\times10^5$, where Re_δ^* is the Reynolds number based on the displacement thickness. This was given a measure of support by the results of Harrison (1958), Willmarth (1959), Skudrzyk and Haddle (1960), Bull and Willis (1961), Willmarth and Wooldridge (1962) and Serafini (1963)

although these data were very scattered as a result of variations in the resolution of the pressure transducers used in the various experiments. This is in direct contrast to the results obtained by Corcos (1964) and Bakewell et. al. (1962) which indicate a monotonic decrease in p'/τ_w with increasing Reynolds number from their fully developed pipe flow data. However, in the case of the pipe flow experiments, it has been assumed that variations in pipe Reynolds number, obtained by varying the velocity in a given pipe, should have no effect on the resolving power of the same transducer, but, if one considers that the increase in Reynolds number causes the thickness of the viscous region to decrease, with presumably an increase in the frequency of the pressure fluctuations generated by this portion of the flow, the assumption may not be correct, and the observed decrease of p'/τ_w with increasing Reynolds number may possibly be a transducer resolution effect.

The results of a series of experiments in low speed wind tunnels and on a glider wing led Hodgson (1962) to conclude that

$$\frac{p'}{\tau_w} = 2.2 \quad . \qquad \ldots(1.2.13)$$

The recent work of Blake (1970) gave

$$\frac{p'}{\tau_w} = 3.6 \quad , \qquad \ldots(1.2.14)$$

where the experimental measurements were made with the use of a pinhole microphone to give a better high frequency resolution. Richards, Bull and Willis (1960), in their summary of earlier works on subsonic turbulent boundary layers, showed that there were wide differences in the experiment-

ally derived values for the mean square wall pressure fluctuations. It can be seen that this situation has not improved to any great extent and the question of the dominance or otherwise of the turbulence/mean-shear interaction in the contribution to the wall pressures and of Reynolds number effects are still open to conjecture. However, out of the scatter of the results, it has been possible to establish the order of magnitude of the fluctuating pressure and the form of its frequency power spectral density. It has also been deduced from correlation measurements that the convection velocity of the pressure field varies from about $0.5U_\infty$ to $0.8U_\infty$, the lower velocities being attributed to eddies in the inner part of the layer where the mean velocity is correspondingly lower.

1.2.3 Turbulent Shear Flow with Finite Mean Pressure Gradient.

For reasons of computational as well as experimental expediency, practically all previous effort in the study of wall pressure fluctuations have been concentrated on that resulting from the constant pressure or zero mean pressure gradient layers. One of the first theoretical treatment of boundary layers under the effects of mean pressure gradients was reported by White (1964). His results included calculated and experimental values of the longitudinal and lateral cross-spectral density of the wall pressure fluctuations, and the effect of spacing on the convection velocities. The latest report of work on pressure fluctuations due to boundary layers generated under the effects of mean pressure gradients was by Schloemer (1967). His effort covered the conditions of both mild adverse and mild favourable pressure gradients in the mean flow

in a low turbulence wind tunnel ($u_2'/U_\infty \leq 0.2\%$). The results for the adverse pressure gradient case indicate an increase in the spectral density, the effect being more marked at the low frequency end, that is, for $f\delta^*/U_\infty < 0.25$, where f is the frequency in Hz. The effect of the mild favourable pressure gradient was found to be a marked reduction of the high frequency portion of the spectral density and the increase of the convection velocity.

1.3 Objectives of the Present Work.

The work reported in this thesis represents part of a programme undertaken with the aim of obtaining a better insight into the mechanism associated with the generation of wall pressure fluctuations in turbulent shear flows with and without mean streamwise pressure gradients.

The specific objectives, all related to turbulent boundary layer flow, were as follows.

(1) The first objective was to develop reliable routine procedures for the calculation of wall pressure fluctuations in flows with zero and non-zero pressure gradients with the aid of the more powerful digital computers which have become available since previous calculations were made. The calculation programme was to be based on the assumption of the dominance of turbulence/mean-shear interaction, but otherwise kept as general as possible to allow the inclusion of the most representative turbulent velocity field data available and to allow investigation of the effects of the various flow parameters such as Reynolds number.

(2) The second objective was to find, from the calculated results, which regions of the boundary layer make the most significant contributions to the wall pressure fluctuations.

In the course of the work, this soon led to the realisation that in the past expressions such as "the contribution made by a region of the boundary layer to the wall pressure fluctuations" have tended to be used in rather a loose way, and that it is necessary to define quite carefully exactly what is meant by such expressions.

(3) The third objective was the measurement of the properties of the fluctuating wall pressure field in equilibrium turbulent boundary layers developed under the effects of various mean streamwise pressure gradients. To this end, a subsonic boundary layer tunnel was to be built and equipped with the necessary instrumentation and their associated calibration rigs. It was decided to use piezo-electric pressure transducers and to aim at achieving as small a value of the ratio of d/δ^* as possible (where d is the diameter of the sensing element of the transducer) to prevent excessive attenuation of the pressure signal at the higher frequencies (see Corcos (1963)).

(4) The fourth objective was to establish theoretically and experimentally, the variation of various wall pressure fluctuation parameters, in particular p'/τ_w, with Reynolds number.

(5) The fifth objective was to obtain a firm indication of whether or not turbulence/mean-shear interaction is the dominant process in the production of the wall pressure fluctuations, by comparing calculated mean square

pressure, spectra, and correlations with measured values, for a variety of pressure gradient conditions.

The objectives stated above imply a very extensive theoretical investigation and an equally extensive experimental one. It was appreciated at the onset that if both of these investigations were to be carried out carefully and thoroughly, it was unlikely that both, or perhaps either, could be completed in the time available. However, since the two aspects of the problem are complementary and are very much interdependent, it was considered that work on the two should proceed in parallel, even if this meant that one or both investigations would not be as complete as the achievement of all the set objectives would require.

As will be seen later, both investigations were limited. The complexity of the required numerical calculation procedures dictated that the theoretical work be confined to boundary layers with zero mean pressure gradient in the stream direction, although some indication of the applicability of these procedures to layers developing in non-zero pressure gradients is given. The experimental work was restricted to measurements of the root mean square value and frequency spectrum of the wall pressure fluctuations for two self-preserving boundary layers, one with zero mean pressure gradient and one with an adverse pressure gradient.

2. THE EQUATIONS FOR THE FLUCTUATING COMPONENT OF THE PRESSURE AND THE CONTRIBUTIONS MADE BY VARIOUS REGIONS OF THE BOUNDARY LAYER TO THE WALL PRESSURE FLUCTUATIONS.

2.1 The Equations for the Fluctuating Pressure.

The Navier-Stokes equations of motion which express the conservation of momentum, and the continuity equation which describes the conservation of mass form the basis of the theoretical study. For a turbulent fluid moving under the influence of some external force F and wherein the compressive effects are sufficiently small as to have negligible effect on the density ρ, these equations take the form

$$\frac{\partial (U_i+u_i)}{\partial t} + (U_j+u_j)\frac{\partial (U_i+u_i)}{\partial x_j} = -\frac{1}{\rho}\frac{\partial (P+p)}{\partial x_i} + \nu\nabla^2(U_i+u_i) + F_i \qquad \ldots(2.1.1)$$

and

$$\frac{\partial (U_i+u_i)}{\partial x_i} = 0 \ , \qquad \ldots(2.1.2)$$

where P and U_i represent respectively the mean pressure and the mean velocity in the x_i-direction at the point whose position vector is $\vec{x}$, p and u_i represent the corresponding time dependent quantities, and i and j taking the values of 1, 2 and 3 so that x_1, x_2 and x_3 form an orthogonal set of axes. The kinematic viscosity of the fluid is represented by ν.

In most situations of interest, the extraneous force F denoting the

gravitational influence throughout the mass of the fluid may be neglected. The relation between the pressure and the velocity fields obtained by taking the divergence of Equation (2.1.1) and then using the condition set by Equation (2.1.2) can be written as

$$\frac{\partial^2 (P+p)}{\partial x_k^2} = -\rho \frac{\partial^2 (U_i+u_i)(U_j+u_j)}{\partial x_i \partial x_j} \quad . \qquad \ldots(2.1.3)$$

Since

$$\frac{\partial^2 p}{\partial x_k^2} = \frac{\partial^2 (P+p)}{\partial x_k^2} - \frac{\partial^2 \langle P+p \rangle}{\partial x_k^2} \quad , \qquad \ldots(2.1.4)$$

where <.....> denotes the statistical mean value, the fluctuating component of the pressure can be obtained from Equation (2.1.3) to give

$$\frac{\partial^2 p}{\partial x_k^2} = -\rho q(\vec{x},t) \quad , \qquad \ldots(2.1.5)$$

where

$$q(\vec{x},t) = 2 \frac{\partial U_i}{\partial x_j} \frac{\partial u_j}{\partial x_i} + \frac{\partial u_i}{\partial x_j} \frac{\partial u_j}{\partial x_i} - \overleftarrow{\frac{\partial u_i}{\partial x_j}} \overrightarrow{\frac{\partial u_j}{\partial x_i}} \quad . \qquad \ldots(2.1.6)$$

Consider now the flow over a boundary surface formed by an infinite plane with a co-ordinate system set up such that x_1 denotes the distance in the direction of the free stream, x_2 denotes the distance perpendicular to the boundary surface and x_3 representing the distance in the direction orthogonal to both x_1 and x_2. It has been justified by Kraichnan (1956b) and by Lilley and Hodgson (1960) that the gradient of the fluctuating

pressure (generated by the turbulent boundary layer formed on the plane) in the direction normal to the boundary can be taken to be zero at the boundary, that is,

$$\left(\frac{\partial p}{\partial x_2}\right)_{x_2=0} = 0 \quad . \qquad \ldots(2.1.7)$$

The solution of the wall pressure fluctuations given by Equation (2.1.5) can then be obtained with the aid of the appropriate Green's function to give

$$p(\vec{x},t) = \frac{\rho}{2\pi} \int_{y_2>0} q(\vec{y},t) \frac{dV(\vec{y})}{|\vec{x}-\vec{y}|} \quad , \qquad \ldots(2.1.8)$$

where dV represents a volume element.

The space-time covariance of the pressure fluctuations at two points $\vec{x}$ and $\vec{x}'$ on the boundary surface is then given by

$$\langle p(\vec{x},t)p(\vec{x}',t')\rangle = \frac{\rho^2}{4\pi^2} \int_{y_2>0} \int_{z_2>0} \langle q(\vec{y},t)q(\vec{z},t')\rangle \frac{dV(\vec{y})}{|\vec{x}-\vec{y}|} \frac{dV(\vec{z})}{|\vec{x}'-\vec{z}|} \quad , \qquad \ldots(2.1.9)$$

where,

$$\langle q(\vec{y},t)q(\vec{z},t')\rangle = 4\frac{\partial U_i}{\partial y_j}\frac{\partial U_k}{\partial z_m}\left\langle \frac{\partial u_j}{\partial y_i}\frac{\partial u_m}{\partial z_k}\right\rangle + 2\frac{\partial U_i}{\partial y_j}\left\langle \frac{\partial u_j}{\partial y_i}\frac{\partial u_k}{\partial z_m}\frac{\partial u_m}{\partial z_k}\right\rangle +$$

$$+ 2\frac{\partial U_k}{\partial z_m}\left\langle \frac{\partial u_i}{\partial y_j}\frac{\partial u_j}{\partial y_i}\frac{\partial u_m}{\partial z_k}\right\rangle + \left\langle \frac{\partial u_i}{\partial y_j}\frac{\partial u_j}{\partial y_i}\frac{\partial u_k}{\partial z_m}\frac{\partial u_m}{\partial z_k}\right\rangle =$$

$$- \left\langle \frac{\partial u_i}{\partial y_j} \frac{\partial u_j}{\partial y_i} \right\rangle \left\langle \frac{\partial u_k}{\partial z_m} \frac{\partial u_m}{\partial z_k} \right\rangle , \qquad \ldots(2.1.10)$$

and all derivatives at $\vec{y}$ are for time t and all at $\vec{z}$ are for time t'.

2.2 Contribution to the Wall Pressure Fluctuation made by Turbulence in a Stratum Parallel to the Boundary.

As we are mainly concerned with either the overall value of the space-time covariance or the variation with distance from the boundary of the contribution to it, it will be an advantage to formulate the mathematical expressions which will facilitate the physical interpretation of the mechanisms giving rise to the fluctuating pressures. The covariance given by Equation (2.1.9) is a double volume integral and as such the overall value obtained cannot give any detail of the parts played by the various sources throughout the boundary layer. Previous attempts to provide an insight into the contributions to the space-time covariance of the wall pressure fluctuations have been through the formation of a first spatial derivative of the expression for the pressure in the direction normal to the boundary. It is realised that although the intended meaning of the derivative has been sufficiently well defined, the expression itself cannot be interpreted in a way that will give a physical insight into the contributions. Since meaningful expressions for the contributions have yet to be formulated and precisely defined, in what follows, an attempt will be made to define contributions from regions of the boundary layer and to keep attention focussed on the physical interpretation of the various mathematical expressions.

An examination of Equation (2.1.5) which is analogous to the equation relating electrostatic potential and electrostatic charge (p being analogous to the potential and ρq to the electrostatic charge density per unit volume), allows us to write the contribution to the instantaneous wall pressure fluctuations $p(\vec{x},t)$ made by the turbulence within a volume element $(dy_1 dy_2 dy_3)$ at $\vec{y}$ as

$$\frac{\rho}{2\pi} \frac{q(\vec{y},t)}{|\vec{x}-\vec{y}|} dy_1 dy_2 dy_3 \quad . \qquad \ldots(2.2.1)$$

This expression for the contribution can also be obtained by the direct consideration of Equation (2.1.8).

Consider now a stratum of the boundary layer and let it be infinitesimally thin and parallel to the boundary. The term "stratum" has been chosen to designate such a slice of the boundary layer in preference to "layer", which might lead to confusion with the boundary layer itself, or "lamina", which has strong associations with non-turbulent flow. The contribution to $p(\vec{x},t)$ made by a stratum within a boundary layer at a distance y_2 from the boundary and of thickness dy_2 is therefore

$$dp(\vec{x},t) = dy_2 \frac{\rho}{2\pi} \int_{-\infty}^{\infty} dy_1 \int_{-\infty}^{\infty} dy_3 \frac{q(\vec{y},t)}{|\vec{x}-\vec{y}|}$$

$$= \rho f_{13}(y_2,\vec{x},t)\, dy_2 \quad , \qquad \ldots(2.2.2)$$

where

$$f_{13}(y_2,\vec{x},t) = \frac{1}{2\pi}\int_{-\infty}^{\infty} dy_1 \int_{-\infty}^{\infty} dy_3 \frac{q(\vec{y},t)}{|\vec{x}-\vec{y}|} \quad . \qquad \ldots(2.2.3)$$

Note that, although the contribution to p has been designated dp, it is not permissible to form from Equation (2.2.2) a derivative $\partial p(\vec{x},t)/\partial y_2$; this is in fact a meaningless expression since the fluctuating component of the wall pressure is the value of the definite integral in Equation (2.1.8) at a particular value of x_2 (=0), and is not itself a function of x_2 or y_2.

2.3 Joint Contribution of Two Strata to the Space-Time Covariance of the Wall Pressure Fluctuations.

Because, in the expression for the space-time covariance of the wall pressure fluctuations, Equation (2.1.9), each spatial co-ordinate direction enters twice, in considering the contribution of various strata of the boundary layer, it becomes necessary to consider the joint contribution made by pairs of strata each of which may be at a different distance from the boundary.

The stratum or layer of pressure sources of thickness dy_2 at a distance y_2 from the boundary, by Equation (2.2.2), contributes $\rho f_{13}(y_2,\vec{x},t)dy_2$ to the wall pressure fluctuations at $\vec{x}$ at time t, and $\rho f_{13}(y_2,\vec{x}',t')dy_2$ to the pressure at $\vec{x}'$ at time t'. There will be two similar expressions with z_2 replacing y_2 for the corresponding contributions from the stratum of thickness dz_2 at a distance z_2 from the boundary.

The joint contribution of the two strata to the product $p(\vec{x},t)p(\vec{x}',t')$ is therefore

$$\rho^2 \{f_{13}(y_2,\vec{x},t)f_{13}(z_2,\vec{x}',t') + f_{13}(z_2,\vec{x},t)f_{13}(y_2,\vec{x}',t')\}\, dy_2\, dz_2 \quad , \qquad \ldots(2.3.1)$$

and the joint contribution to the space-time covariance (resulting from statistical space-time correlation between the turbulent velocity fluctuations in the two strata) is

$$\rho^2\, G_{13}(y_2,z_2,\vec{x},\vec{x}',t,t')\, dy_2\, dz_2 \quad , \qquad \ldots(2.3.2)$$

where

$$G_{13}(y_2,z_2,\vec{x},\vec{x}',t,t') = F_{13}(y_2,z_2,\vec{x},\vec{x}',t,t') + F_{13}(z_2,y_2,\vec{x},\vec{x}',t,t') \quad , \qquad \ldots(2.3.3)$$

and

$$F_{13}(y_2,z_2,\vec{x},\vec{x}',t,t') = \langle f_{13}(y_2,\vec{x},t)f_{13}(z_2,\vec{x}',t')\rangle \quad . \qquad \ldots(2.3.4)$$

As we are most concerned with variations normal to the boundary, we shall abbreviate F_{13} and G_{13} to $F_{13}(y_2,z_2)$ and $G_{13}(y_2,z_2)$ respectively and take as understood that they are also functions of $\vec{x}$, $\vec{x}'$, t, and t'.

It can be seen that G_{13} is a symmetric function of y_2 and z_2. Since it represents the joint contribution to the space-time covariance of the wall pressure fluctuations of a pair of strata, at distances from the boundary of y_2 and z_2 respectively, per unit thickness of each of these strata, it can therefore be referred to as the "joint contribution density

function".

The important point is that in considering contributions to the space-time covariance of the wall pressure fluctuations it is necessary, in general, to consider the joint contributions of pairs of strata of the boundary layer rather than the contribution of a particular stratum, and these contributions are correctly represented by G_{13}. The total space-time covariance will be obtained by taking account of all possible pairs of strata.

Only if it so happens that the values of G_{13} are very large for $y_2 = z_2$ and fall rapidly as y_2 and z_2 become increasingly different might it become justifiable to speak of the contribution of one stratum (or a set of strata which have a total thickness small compared with the total thickness of the boundary layer), in which case $G_{13}(y_2,y_2)$ would be the value of the joint contribution density function characterising the contribution of the stratum at $x_2 = y_2$ (as a result of correlation of this stratum with itself).

2.4 Contribution of a Finite Region of the Boundary Layer to the Space-Time Correlation of the Wall Pressure Fluctuations.

We shall now attempt to look into the possibility of representing, in a meaningful way, the contribution of a finite set of strata to the space-time covariance. It should be noted that in considering the contribution of a region of finite thickness to the space-time covariance of the wall pressure fluctuations it is necessary to define carefully what

is meant. We shall, therefore, define the contribution of the region $a \leq x_2 \leq b$ as that resulting from correlation of every elementary pressure source within this region with every other elementary pressure source within the region. It should be particularly emphasised that this does not include any contribution to the space-time covariance resulting from correlation between sources within the finite region considered and sources within some other finite region of the boundary layer.

The correlation between sources in the stratum at $x_2 = y_2$ and all other strata (at $x_2 = z_2$) located between this particular stratum and one at a distance $x_2 = a$ from the boundary (where $a < y_2$) gives rise to the contribution to $\langle p(\vec{x},t)p(\vec{x}',t')\rangle$ which can be obtained from the expression (2.3.2) as

$$\rho^2 \, dy_2 \int_a^{y_2} dz_2 \, G_{13}(y_2,z_2) \quad , \qquad \ldots(2.4.1)$$

and the contribution of all pairs of strata at distances from the boundary between $x_2 = a$ and $x_2 = b$ $(a < b)$ as a result of correlation of sources within the region $a \leq x_2 \leq b$ with all other sources within this region is

$$C(a,b) = \rho^2 \int_a^b dy_2 \int_a^{y_2} dz_2 \, G_{13}(y_2,z_2) \quad . \qquad \ldots(2.4.2)$$

Like G_{13} and F_{13}, C is also a function of $\vec{x}$, $\vec{x}'$, t, and t'. Equation (2.4.2) may also be written, by reversing the order of integration, as

$$C(a,b) = \rho^2 \int_a^b dz_2 \int_{z_2}^b dy_2 \, G_{13}(y_2,z_2) \quad . \qquad \ldots(2.4.3)$$

Similarly, the contribution to $\langle p(\vec{x},t)p(\vec{x}',t')\rangle$ can also be considered as that resulting from correlation between sources in the stratum at $x_2 = y_2$ and all other strata between y_2 and $x_2 = b$ and is

$$\rho^2 \, dy_2 \int_{y_2}^{b} dz_2 \; G_{13}(y_2,z_2) \quad , \qquad \ldots(2.4.4)$$

and the contribution resulting from correlations among all strata within the region $a \leq x_2 \leq b$ is

$$C(a,b) = \rho^2 \int_{a}^{b} dy_2 \int_{y_2}^{b} dz_2 \; G_{13}(y_2,z_2) \quad . \qquad \ldots(2.4.5)$$

This may also be written as

$$C(a,b) = \rho^2 \int_{y_2}^{b} dz_2 \int_{a}^{z_2} dy_2 \; G_{13}(y_2,z_2) \quad . \qquad \ldots(2.4.6)$$

The Equations (2.4.5) and (2.4.6) could have been obtained formally from Equations (2.4.3) and (2.4.2) respectively simply by interchanging the (dummy) variables y_2 and z_2 and making use of the fact that $G_{13}(y_2,z_2)$ is symmetrical with respect to y_2 and z_2. However, the longer procedure has been given in the endeavour to preserve the physical picture.

In the same way, the overall space-time covariance of the wall pressure can be obtained by first considering the correlation among sources in the stratum at $x_2 = y_2$ and all other strata either between the boundary and y_2 or more remote from the boundary than y_2, and then integrating over all y_2. This results in the expressions for the overall

space-time covariance of the wall pressure fluctuations, similar to the expressions (2.4.2) and (2.4.5), as

$$\langle p(\vec{x},t)p(\vec{x}',t')\rangle = C(0,\infty) = \rho^2 \int_0^{\infty} dy_2 \int_0^{y_2} dz_2 \; G_{13}(y_2,z_2) \qquad \ldots(2.4.7)$$

$$= \rho^2 \int_0^{\infty} dy_2 \int_{y_2}^{\infty} dz_2 \; G_{13}(y_2,z_2) \; . \qquad \ldots(2.4.8)$$

These equations also follow directly from Equations (2.4.2) and (2.4.5) by putting $a = 0$ and $b = \infty$. There will also be two similar relations to Equations (2.4.7) and (2.4.8), analogous to Equations (2.4.3) and (2.4.6), with the order of the y_2 and z_2 integrations reversed.

It is important to note here that the overall space-time covariance, as given by Equation (2.4.7) cannot be obtained simply by summing the $C(a,b)$ terms over a series of regions of finite thickness whose total thickness encompasses the boundary layer. This restriction exists due to the fact that as soon as two regions are combined, there enters, as well as the direct contribution represented by the C terms resulting from correlation within each of the regions, an additional contribution resulting from correlation of sources in one region with those in the other. As an illustration, consider the combination of two regions, one $a \leq x_2 \leq b$ and the other $b \leq x_2 \leq c$, to form the larger region $a \leq x_2 \leq c$. From Equation (2.4.2) we have

$$C(a,c) = \rho^2 \int_a^{c} dy_2 \int_a^{y_2} dz_2 \; G_{13}(y_2,z_2)$$

$$= \rho^2 \int_a^b dy_2 \int_a^{y_2} dz_2 \; G_{13}(y_2,z_2) + \rho^2 \int_b^c dy_2 \int_b^{y_2} dz_2 \; G_{13}(y_2,z_2) +$$

$$+ \rho^2 \int_b^c dy_2 \int_a^b dz_2 \; G_{13}(y_2,z_2)$$

$$= C(a,b) + C(b,c) + \rho^2 \int_b^c dy_2 \int_a^b dz_2 \; G_{13}(y_2,z_2) \qquad \ldots(2.4.9)$$

Here $C(a,b)$ represents the contribution of the finite region $a \leq x_2 \leq b$ and $C(b,c)$ the contribution of the finite region $b \leq x_2 \leq c$ as a result of correlation within each of the respective regions, while the third term represents the effect of correlation of sources in the former region with those of the latter. The example could clearly be extended to any number of finite regions.

This emphasises, in the general case, the difficulty, or, to be more precise, the impossibility of defining satisfactorily the contribution of a finite region of the boundary layer to the space-time covariance of the wall pressure fluctuations, even though the procedure given above leads to the correct overall value for this covariance. In general, therefore, it really only makes sense, in talking of contributions of various regions of the boundary layer to the space-time covariance of the wall pressure fluctuations, to consider not the contributions of finite regions but the joint contributions made by pairs of infinitesimally thin strata. These are correctly represented by the funtion G_{13}. The point may be made here, however, that it may be convenient in certain cases to use the expressions given above for the contribution of a finite region of the boundary layer.

In such cases, it is permissible only so long as care has been taken to define clearly what is meant.

But, even so, some qualifications need to be made. As in the case of the joint contribution to the space-time covariance of the wall pressure fluctuations resulting from a pair of strata, it is possible to envisage a situation where the contribution to the space-time covariance made by a finite region $a \leqslant x_2 \leqslant b$ of the boundary layer, as defined above, becomes essentially the total contribution of this region, even when correlation between sources within it and outside it is taken into account. In this case, the total contribution comes almost entirely from the correlation within the region itself, and again this implies that the function G_{13} must be large for $y_2 = z_2$ and fall rapidly to insignificant values as z_2 differs from y_2. (Quantitatively, this implies that

$$\{\rho^2 \int_0^a dy_2 \int_a^b dz_2\, G_{13}(y_2,z_2) + \rho^2 \int_b^\infty dy_2 \int_a^b dz_2\, G_{13}(y_2,z_2)\} << C(a,b) \ , \qquad \ldots(2.4.10)$$

where the first and second term on the left hand side result from correlation of sources in the region $a \leqslant x_2 \leqslant b$ with those in the regions $0 \leqslant x_2 \leqslant a$ and $b \leqslant x_2 \leqslant \infty$ respectively.)

Equations (2.4.2), (2.4.3), (2.4.5) and (2.4.6) could have been obtained more directly although more formally and without considering in detail the contributions of various strata, in the following way. For source terms confined to the region $a \leqslant x_2 \leqslant b$, Equation (2.1.9) written in full, gives for the contribution of this region (defined in the same way

as above) to the space-time covariance of the wall pressure fluctuations

$$C(a,b) = \frac{\rho^2}{4\pi^2} \int_{-\infty}^{\infty} dy_1 \int_{a}^{b} dy_2 \int_{-\infty}^{\infty} dy_3 \int_{-\infty}^{\infty} dz_1 \int_{a}^{b} dz_2 \int_{-\infty}^{\infty} dz_3 \frac{\langle q(\vec{y},t) q(\vec{z},t') \rangle}{|\vec{x}-\vec{y}| \quad |\vec{x}'-\vec{z}|}$$

$$= \rho^2 \int_{a}^{b} dy_2 \int_{a}^{b} dz_2 \, F_{13}(y_2,z_2) \qquad \ldots(2.4.11)$$

$$= \rho^2 \int_{a}^{b} dy_2 \int_{a}^{b} dz_2 \, F_{13}(z_2,y_2) \qquad \ldots(2.4.12)$$

with the use of Equations (2.2.3) and (2.3.4). To show that Equations (2.4.5) and (2.4.11) are equivalent, we have from Equation (2.4.11)

$$C(a,b) = \rho^2 \int_{a}^{b} dy_2 \int_{a}^{y_2} dz_2 \, F_{13}(y_2,z_2) + \rho^2 \int_{a}^{b} dy_2 \int_{y_2}^{b} dz_2 \, F_{13}(y_2,z_2)$$

$$= \rho^2 \int_{a}^{b} dz_2 \int_{a}^{z_2} dy_2 \, F_{13}(z_2,y_2) + \rho^2 \int_{a}^{b} dy_2 \int_{y_2}^{b} dz_2 \, F_{13}(y_2,z_2)$$

$$= \rho^2 \int_{a}^{b} dy_2 \int_{y_2}^{b} dz_2 \, F_{13}(z_2,y_2) + \rho^2 \int_{a}^{b} dy_2 \int_{y_2}^{b} dz_2 \, F_{13}(y_2,z_2)$$

$$= \rho^2 \int_{a}^{b} dy_2 \int_{y_2}^{b} dz_2 \, G_{13}(y_2,z_2) \quad ,$$

which is Equation (2.4.5). In a similar way, Equations (2.4.2), (2.4.3) and (2.4.6) could be obtained.

2.5 Representation of the Joint Contribution of Two Strata to the Space-Time Covariance of the Wall Pressure Fluctuations as a Derivative.

It was pointed out earlier that any attempt to formulate a derivative from Equation (2.2.2) would not result in a meaningful expression. This applies equally well to the expression (2.3.2) which represents an elementary contribution to $\langle p(\vec{x},t)p(\vec{x}',t')\rangle$. However, the function G_{13} itself may be represented as a derivative of a function which is closely related to the space-time covariance of the wall pressure fluctuations.

Let $P(y_2,z_2)/\rho^2$ be any indefinite integral of $G_{13}(y_2,z_2)$ over y_2 and z_2 so that

$$\frac{\partial^2 P(y_2,z_2)}{\partial y_2\, \partial z_2} = \rho^2 G_{13}(y_2,z_2) \quad . \qquad \ldots(2.5.1)$$

Like G_{13}, P will be a symmetric function of y_2 and z_2 and is written in the abbreviated form. It then follows from Equations (2.4.7) and (2.4.8) that

$$\langle p(\vec{x},t)p(\vec{x}',t')\rangle = \tfrac{1}{2}P(\infty,\infty) + \tfrac{1}{2}P(0,0) - P(0,\infty) \quad . \qquad \ldots(2.5.2)$$

Consider now the more specific definition of P given by

$$P(y_2,z_2) = \rho^2 \int_0^{y_2} dy \int_0^{z_2} dz \; G_{13}(y,z) \quad . \qquad \ldots(2.5.3)$$

Also, let

$$P^*(y_2,z_2) = \rho^2 \int_0^{y_2} dy \int_0^{z_2} dz \; F_{13}(y,z) \quad , \qquad \ldots(2.5.4)$$

so that by Equation (2.3.3)

$$P(y_2,z_2) = P^*(y_2,z_2) + P^*(z_2,y_2) \quad . \qquad \ldots(2.5.5)$$

With the preceeding definitions, we have, instead of Equation (2.5.2),

$$\langle p(\vec{x},t)p(\vec{x}',t')\rangle = \tfrac{1}{2}P(\infty,\infty) = P^{*}(\infty,\infty) = C(0,\infty). \quad \ldots(2.5.6)$$

From Equation (2.5.3) we have (taking $z_2 > y_2$ for convenience)

$$P(y_2,z_2) = \rho^2 \int_0^{y_2} dy \int_0^{y} dz\, G_{13}(y,z) + \rho^2 \int_0^{z_2} dy \int_y^{z_2} dz\, G_{13}(y,z) - \rho^2 \int_{y_2}^{z_2} dy \int_y^{z_2} dz\, G_{13}(y,z)$$

$$= C(0,y_2) + C(0,z_2) - C(y_2,z_2) \quad ,$$

$$= \left[\begin{array}{c}\text{contribution of} \\ \text{region } 0 \leq x_2 \leq y_2\end{array}\right] + \left[\begin{array}{c}\text{contribution of} \\ \text{region } 0 \leq x_2 \leq z_2\end{array}\right] - \left[\begin{array}{c}\text{contribution of} \\ \text{region } y_2 \leq x_2 \leq z_2\end{array}\right]. \quad \ldots(2.5.7)$$

Thus P represents a combination of the contributions of three finite regions of the boundary layer (as defined in Section 2.4) to the space-time covariance of the wall pressure fluctuations. The function P^{*} represents the contribution to the space-time covariance of the wall pressure fluctuations resulting from correlation of sources in the region $0 \leq x_2 \leq y_2$ with sources in the region $0 \leq x_2 \leq z_2$.

In considering the mean square wall pressure fluctuation $\langle p^2\rangle = \langle p(\vec{x},t)p(\vec{x},t)\rangle$ and the root mean square fluctuation $p' = \langle p^2\rangle^{\frac{1}{2}}$, Corcos (1964) and Bull and Lim (1968) have used the nomenclature (in the notation presented here) "$\partial\langle p^2\rangle/\partial y_2$" and "$\partial p'/\partial y_2$", and shown distributions of these

quantities across the boundary layer; the values at a particular y_2 have then been broadly interpreted as giving the contributions of a stratum at that y_2 to the mean square wall pressure fluctuation and the root mean square wall pressure fluctuation respectively. Although in both cases the meaning intended by the authors is probably fairly clear, it is also clear, following what has already been said in Section 2.2, that, strictly, the "derivatives" referred to have no meaning. This can perhaps be clarified by expressing these functions in terms of functions which have been clearly defined above.

It will be implied in the following that various functions, such as F_{13} and P^*, which have been written in the abbreviated form as functions of y_2 and z_2 only, are in this case evaluated for $\vec{x} = \vec{x}'$ and $t = t'$. Hence,

$$\frac{\text{"}\partial\langle p^2\rangle\text{"}}{\partial y_2} = \rho^2 \int_0^\infty dz_2 \, F_{13}(y_2, z_2) \qquad \ldots(2.5.8)$$

$$= \frac{\partial P^*(y_2, \infty)}{\partial y_2} \qquad \ldots(2.5.9)$$

and

$$\int_0^{y_2} \frac{\text{"}\partial\langle p^2\rangle\text{"}}{\partial y} \, dy = P^*(y_2, \infty) \; . \qquad \ldots(2.5.10)$$

The second quantity can be written

$$\frac{\text{"}\partial p'\text{"}}{\partial y_2} = \frac{\partial}{\partial y_2} \{P^*(y_2, \infty)\}^{\frac{1}{2}} \qquad \ldots(2.5.11)$$

$$= \frac{1}{2\{P^*(y_2,\infty)\}^{\frac{1}{2}}} \frac{\partial P^*(y_2,\infty)}{\partial y_2} \qquad \ldots(2.5.12)$$

and

$$\int_0^{y_2} \left| \frac{\partial p'}{\partial y} \right| dy = \{P^*(y_2,\infty)\}^{\frac{1}{2}} . \qquad \ldots(2.5.13)$$

Thus it will be seen from Equation (2.5.8) that, in fact, $\left| \partial\langle p^2\rangle/\partial y_2 \right| . dy_2$ represents the contribution to the mean square wall pressure fluctuation resulting from the correlation of sources in a stratum at y_2 with the sources in all other strata in the boundary layer. From Equations (2.5.11), (2.5.12) and (2.5.13) it is clear that the interpretation of $\left| \partial p'/\partial y_2 \right|$ has to be made in a very specialised way indeed, but it also contains contributions from all strata in the boundary layer. This raises a second objection to the use of these "derivatives", which is that, quite apart from the question of nomenclature, they are first derivatives rather than second derivatives, and as such already contain contributions from all strata in the boundary layer; in consequence their use to characterise contributions to $\langle p^2\rangle$ or p' from particular regions of the boundary layer could be very misleading. This brings us back to our earlier conclusion that, in general, the most satisfactory way of considering contributions from various regions of the boundary layer is by considering the joint contribution of pairs of strata as represented by the function G_{13}.

The variation of G_{13} over the boundary layer will be shown later for

a particular case as an illustration of the correct representation of the contributions of various strata of the boundary layer to the mean square wall pressure fluctuations. The G_{13} values presented will be those calculated on the basis of the assumptions that the boundary layer grows slowly in the streamwise direction, that the turbulence is statistically stationary in time and homogeneous in planes parallel to the boundary, and that the turbulence/mean-shear interaction gives rise to the dominant term of the source function, q (Equation (2.1.6)).

2.6 G_{13} for a Slowly Growing Boundary Layer with Statistically Homogeneous Strata and Dominance of Turbulence/Mean-Shear Interaction.

The source function q giving rise to the fluctuating component of the wall pressure is given by Equation (2.1.6) as

$$q(\vec{x},t) = 2\frac{\partial U_i}{\partial x_j}\frac{\partial u_j}{\partial x_i} + \frac{\partial u_i}{\partial x_j}\frac{\partial u_j}{\partial x_i} - \left\langle \frac{\partial u_i}{\partial x_j}\frac{\partial u_j}{\partial x_i} \right\rangle \quad .$$

If it is assumed that the rate of boundary layer growth is sufficiently slow for the mean velocity parallel to the boundary U_1 (in the x_1-direction) to be taken as a function only of the co-ordinate normal to the boundary, and that the interaction between the mean shear and the turbulence gives rise to the dominant term in the source function (see Kraichnan (1956a), and Lilley and Hodgson (1960)), then

$$q \simeq 2\frac{\partial U_1}{\partial x_2}\frac{\partial u_2}{\partial x_1} \quad , \qquad \ldots(2.6.1)$$

where u_2 is the fluctuating component of the velocity normal to the boundary. The corresponding approximation for the covariance of q is then taken directly from Equation (2.6.1) and it will be regarded as that

resulting from turbulence/mean-shear interaction. The terms consisting of the product of one mean shear term and a covariance formed from the product of three fluctuating terms which would otherwise arise in forming covariances of q from Equation (2.1.6), and which could also be regarded as arising from turbulence/mean-shear interaction, are ignored on the ground that third order correlations are usually very small. We therefore get

$$\langle q(\vec{y},t)q(\vec{z},t')\rangle \simeq 4\, M(y_2)\, M(z_2)\, \frac{\partial^2 \langle u_2(\vec{y},t)u_2(\vec{z},t')\rangle}{\partial y_1\, \partial z_1} \qquad \ldots(2.6.2)$$

where

$$M(x_2) = \frac{\partial U_1(x_2)}{\partial x_2} \quad .$$

With the assumption of statistical homogeneity in planes parallel to the boundary and stationarity in time, and using Equations (2.2.3), (2.3.4) and (2.6.2) we may write

$$F_{13}(y_2,z_2,\vec{x},\vec{x}',t,t') = F_{13}(y_2,z_2,\vec{\xi},\tau)$$

$$= \frac{M(y_2)\, M(z_2)}{\pi^2} \int_{-\infty}^{\infty} dy_1 \int_{-\infty}^{\infty} dy_3 \int_{-\infty}^{\infty} dz_1 \int_{-\infty}^{\infty} dz_3 \ldots$$

$$\ldots \frac{\partial^2 \langle u_2(\vec{y},t)u_2(\vec{z},t')\rangle}{\partial y_1\, \partial z_1} \frac{1}{|\vec{x}-\vec{y}|} \frac{1}{|\vec{x}'-\vec{z}|} \quad ,$$

$$\ldots(2.6.3)$$

where $\vec{\xi} = \vec{x}' - \vec{x}$ and $\tau = t' - t$. Integration of Equation (2.6.3) by parts leads to

$$F_{13}(y_2,z_2,\vec{\xi},\tau) = \frac{M(y_2)\, M(z_2)}{\pi^2} \int_{-\infty}^{\infty} dy_1 \int_{-\infty}^{\infty} dy_3 \int_{-\infty}^{\infty} dz_1 \int_{-\infty}^{\infty} dz_3 \langle u_2(\vec{y},t)u_2(\vec{z},t')\rangle \ldots$$

$$\ldots \quad \frac{\partial |\vec{x}-\vec{y}|^{-1}}{\partial y_1} \quad \frac{\partial |\vec{x}'-\vec{z}|^{-1}}{\partial z_1} \qquad \ldots(2.6.4)$$

On the basis of the assumptions made, we may also write

$$\langle u_2(\vec{y},t)\, u_2(\vec{z},t')\rangle = Q_{22}(y_2, z_2, \vec{r}) \quad , \qquad \ldots(2.6.5)$$

where $\vec{r} = \vec{z} - \vec{y}$.

Following Hodgson (1962) we then have

$$F_{13}(y_2, y_2+r_2, \vec{\xi}, \tau) = \frac{M(y_2)\, M(y_2+r_2)}{\pi^2} \int_{-\infty}^{\infty} dr_1 \int_{-\infty}^{\infty} dr_3\, Q_{22}(y_2, \vec{r}, \tau) \quad \ldots$$

$$\ldots \int_{-\infty}^{\infty} dy_1 \int_{-\infty}^{\infty} dy_3 \frac{\partial |\vec{x}-\vec{y}|^{-1}}{\partial y_1} \frac{\partial |\vec{x}'-\vec{y}-\vec{r}|^{-1}}{\partial r_1} \, . \qquad \ldots(2.6.6)$$

Hodgson showed that

$$\int_{-\infty}^{\infty} dy_1 \int_{-\infty}^{\infty} dy_3 \frac{\partial |\vec{x}-\vec{y}|^{-1}}{\partial y_1} \frac{\partial |\vec{x}'-\vec{y}-\vec{r}|^{-1}}{\partial r_1} = 2\pi g_{13}(y_2, \vec{\xi}, \vec{r}) \quad , \qquad \ldots(2.6.7)$$

where

$$g_{13}(y_2, \vec{\xi}, \vec{r}) = \left[1 - \frac{(\xi_1 - r_1)^2 (2y_2 + r_2 + 2m)}{m^2 (2y_2 + r_2 + m)} \right] \Big/ \left[m(2y_2 + r_2 + m) \right]$$

$$\ldots(2.6.8)$$

and

$$m^2 = (2y_2 + r_2)^2 + (\xi_1 - r_1)^2 + (\xi_3 - r_3)^2 \, . \qquad \ldots(2.6.9)$$

Hence Equation (2.6.6) becomes

$$F_{13}(y_2,z_2,\vec{\xi},\tau) = \frac{2M(y_2)M(z_2)}{\pi}\int_{-\infty}^{\infty} dr_1 \int_{-\infty}^{\infty} dr_3\, Q_{22}(y_2,z_2,r_1,r_3,\tau) \quad \ldots$$

$$\ldots \quad g_{13}(y_2,z_2,r_1,r_3,\vec{\xi}) \quad , \qquad \ldots(2.6.10)$$

where now

$$g_{13}(y_2,z_2,r_1,r_3,\vec{\xi}) = \left[1 - \frac{(\xi_1-r_1)^2(y_2+z_2+2m)}{m^2(y_2+z_2+m)}\right] \Big/ \left[m(y_2+z_2+m)\right] \qquad \ldots(2.6.11)$$

and

$$m^2 = (y_2+z_2)^2 + (\xi_1-r_1)^2 + (\xi_3-r_3)^2 \quad . \qquad \ldots(2.6.12)$$

Introducing a space-time correlation coefficient for the velocity fluctuations normal to the boundary, given by

$$R_{22} = \frac{\langle u_2(\vec{y},t)u_2(\vec{z},t')\rangle}{\langle u_2^2(\vec{y})\rangle^{\frac{1}{2}}\langle u_2^2(\vec{z})\rangle^{\frac{1}{2}}} \quad ,$$

we can write, for the present case,

$$R_{22}(y_2,\vec{r},\tau) = R_{22}(y_2,z_2,r_1,r_3,\tau) = \frac{Q_{22}(y_2,\vec{r},\tau)}{u_2'(y_2)\,u_2'(z_2)}$$

$$= \frac{Q_{22}(y_2,z_2,r_1,r_3,\tau)}{u_2'(y_2)\,u_2'(z_2)} \quad , \qquad \ldots(2.6.13)$$

where u_2' is the root mean square velocity fluctuation normal to the boundary. Equation (2.6.10) then becomes

$$F_{13}(y_2,z_2,\vec{\xi},\tau) = \frac{2}{\pi} M(y_2)M(z_2)u_2'(y_2)u_2'(z_2)I_{13}(y_2,z_2,\vec{\xi},\tau) \quad , \quad \ldots(2.6.14)$$

where

$$I_{13}(y_2,z_2,\vec{\xi},\tau) = \int_{-\infty}^{\infty} dr_1 \int_{-\infty}^{\infty} dr_3\, R_{22}(y_2,z_2,r_1,r_3,\tau)\, g_{13}(y_2,z_2,r_1,r_3,\vec{\xi}) \,. \qquad \ldots(2.6.15)$$

From Equation (2.3.3) we then have

$$G_{13}(y_2,z_2,\vec{\xi},\tau) = \frac{2}{\pi} M(y_2)M(z_2)u_2'(y_2)u_2'(z_2)\left[I_{13}(y_2,z_2,\vec{\xi},\tau)+I_{13}(z_2,y_2,\vec{\xi},\tau)\right]. \qquad \ldots(2.6.16)$$

3. CALCULATIONS FOR CONSTANT PRESSURE LAYERS.

3.1 Boundary Layer Model.

The space-time covariance of the wall pressure fluctuations is given by Equation (2.4.7) as

$$\langle p(\vec{x},t)p(\vec{x}',t')\rangle = \rho^2 \int_0^{\infty} dy_2 \int_0^{y_2} dz_2 \; G_{13}(y_2,z_2) \quad , \qquad \ldots(3.1.1)$$

where, from Section 2.6, it has been shown that under the assumption of the dominance of turbulence/mean-shear interaction in the generation of the pressure fluctuations and for a boundary layer which is slowly growing within which the turbulence exhibits statistical stationarity in time and homogeneity in planes parallel to the boundary, $G_{13}(y_2,z_2)$ (written in the abbreviated form here) is given in full by Equation (2.6.16). In the special case when $\vec{x} = \vec{x}'$ and $t = t'$, $\vec{\xi} = \tau = 0$, and R_{22} becomes a space correlation only. The mean square wall pressure fluctuations is then given by

$$\langle p^2 \rangle = \langle p(\vec{x},t)p(\vec{x},t)\rangle = \rho^2 \int_0^{\infty} dy_2 \int_0^{y_2} dz_2 \; G_{13}(y_2,z_2) \quad , \qquad \ldots(3.1.2)$$

where G_{13} is now understood to be evaluated at $\vec{\xi} = \tau = 0$.

The evaluation of Equation (3.1.1) or (3.1.2) requires the specification of the distributions across the boundary layer of the turbulence intensity u_2', the mean shear, and the spatial correlation

coefficient of the fluctuating velocity component u_2.

3.1.1 The Turbulence Intensity.

The values of u_2'/U_τ are based on the experimental measurements of Klebanoff (1955) which were made in a boundary layer with $Re_\delta^* \simeq 10^4$, together with those of Laufer (1954) which were made close to the wall in turbulent pipe flow, where Re_δ^* is the Reynolds number $\delta^* U_\infty/\nu$, δ^* is the boundary layer displacement thickness, U_∞ is the free stream velocity, ν is the kinematic viscosity, $U_\tau = (\tau_w/\rho)^{\frac{1}{2}}$ is the friction velocity at the wall pressure covariance datum point $\vec{x}$, τ_w is the wall shear stress and ρ is the fluid density. The two sets of data are shown in figure 1, and it can be seen that they are fairly consistent in the region in which they overlap. If we regard the distribution of u_2'/U_τ as a function of x_2^* ($x_2^* = x_2 U_\tau/\nu$) over the constant stress layer and a function of x_2/δ outside this layer, where δ represents the boundary layer thickness, then we can obtain the constant stress layer variation for $0 \leqslant x_2^* \leqslant$ about 600 and the outer layer variation for $0.2 \leqslant x_2/\delta \leqslant 1$ from figure 1 (since $x_2^* = 600$ is equivalent to $x_2/\delta = 0.2$ at the Reynolds number of Klebanoff's experiments). Experimental measurements of the mean velocity distribution show significant deviations from the logarithmic variation for values of x_2/δ greater than about 0.2, and it seems reasonable to define the outer edge of the constant stress layer as the point where this deviation has reached some chosen value. If we accept Coles's (1956) mean velocity profile, then the deviation of U_1/U_τ from the logarithmic variation is simply $\Pi w(x_2/\delta_c)/\kappa$, (where $w(x_2/\delta_c)$ is Coles's wake function, δ_c is the value of x_2 in the

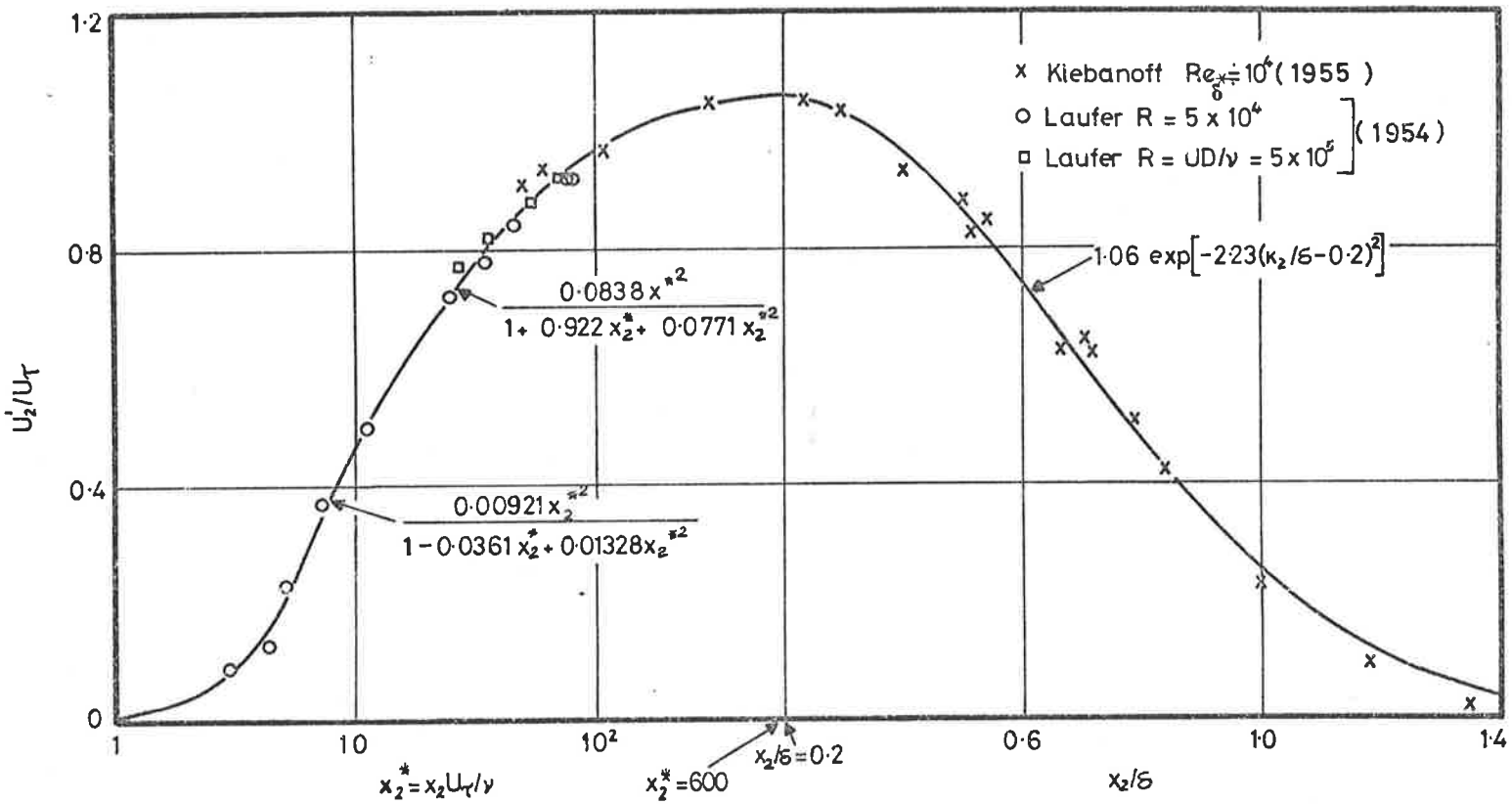

Fig.1 Distribution of Turbulence Intensity across the Boundary Layer.

outer part of the layer where $\partial(U_1/U_\tau)/\partial \ln(x_2/\delta_c) = 1/\kappa$, Π is Coles's profile parameter and κ is the von Karman constant. A given deviation will therefore occur at a particular value of x_2/δ at all Reynolds numbers. The outer edge of the constant stress layer will therefore be taken as $x_2/\delta = 0.2$ at all Reynolds numbers.

To obtain the u_2' distribution at Reynolds numbers higher than that of Klebanoff's measurements the variation for $0 \leq x_2^* \leq 600$ and $0.2 \leq x_2/\delta \leq 1$ will be taken from figure 1, but some assumption still has to be made for the region between $x_2^* = 600$ and $x_2/\delta = 0.2$. The assumption which has been made is that over this region u_2'/U_τ is constant and equal to the maximum value measured by Klebanoff. The resulting variation of the u_2'/U_τ distribution with Reynolds number is then as shown in figure 2, and the empirical expressions used to represent the data in the calculations are given as follows:

$$\frac{u_2'}{U_\tau} = \frac{0.00921 x_2^{*2}}{1 - 0.0361 x_2^* + 0.01328 x_2^{*2}} \qquad \text{for } 0 \leq x_2^* \leq 10 \ ,$$

$$= \frac{0.0838 x_2^{*2}}{1 + 0.922 x_2^* + 0.0771 x_2^{*2}} \qquad \text{for } 10 \leq x_2^* \leq 600 \ ,$$

$$= 1.06 \qquad \text{for } x_2^* \geq 600 \text{ and } x_2/\delta \leq 0.2 \ ,$$

$$= 1.06 \exp\left[-2.23(x_2/\delta - 0.2)^2\right] \qquad \text{for } x_2/\delta \geq 0.2 \ . \qquad \ldots(3.1.3)$$

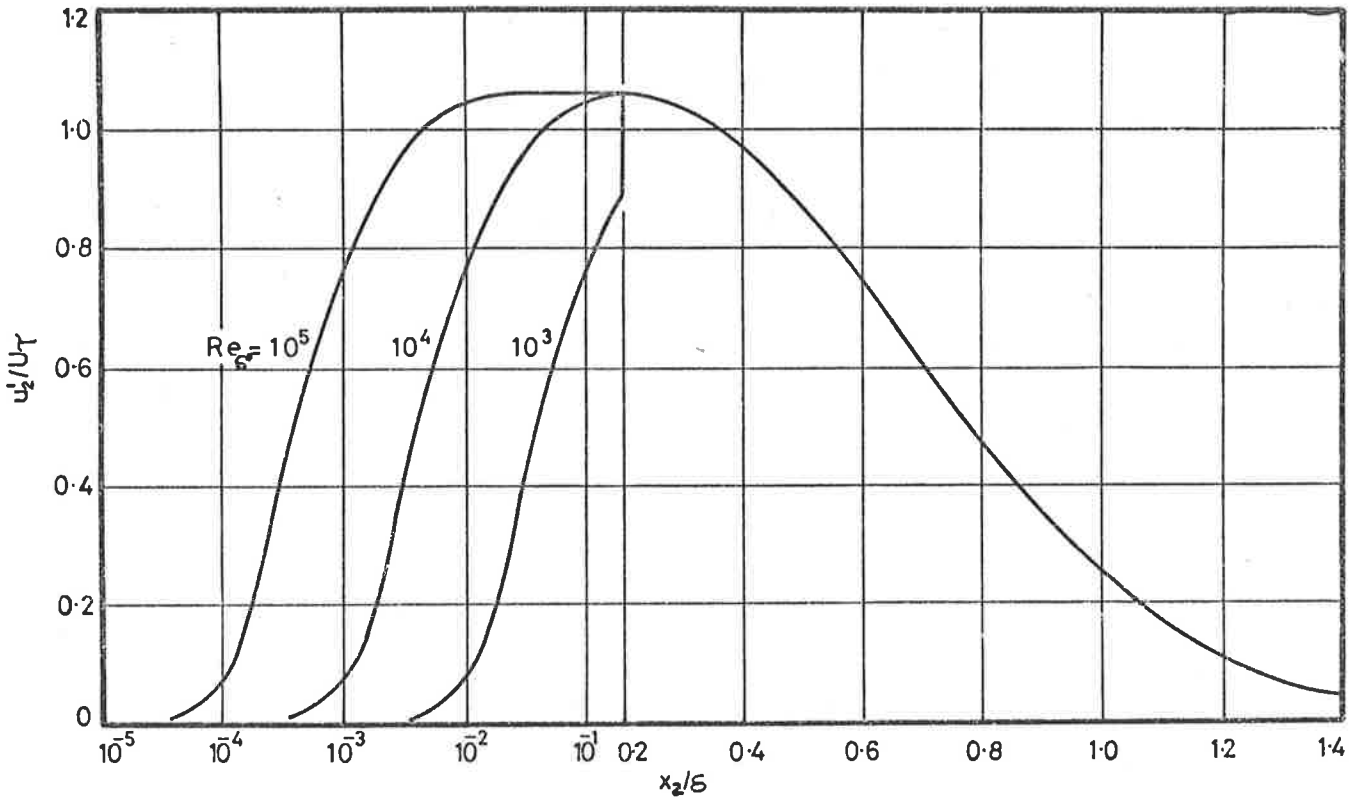

Fig. 2 Assumed Variation of Turbulence Intensity Distribution with Reynolds Number.

3.1.2 The Mean Shear.

The variation of the mean velocity U_1 with distance from the boundary in an incompressible, constant pressure, two-dimensional turbulent boundary layer, in the region of the boundary, is given by the law of the wall as

$$\frac{U_1}{U_\tau} = f(x_2^*) \quad .$$

Many proposals for the form of the function $f(x_2^*)$ have been made and it has been shown by Bull (1969b) that in the region $x_2^* \lesssim 33$, the mean shear which is given by the gradient of the mean velocity in the direction normal to the boundary can be taken as

$$\frac{\nu M(x_2^*)}{U_\tau^2} = \left[1 + \frac{x_2^*}{a} + \tfrac{1}{2}\left(\frac{x_2^*}{a}\right)^2 + \frac{1}{b}\left(\frac{x_2^*}{a}\right)^6 \right] \exp\left(-\frac{x_2^*}{a}\right) , \qquad \ldots(3.1.4)$$

with a = 4.0 and b = 1300. Further from the boundary than $x_2^* = 33$ and extending very nearly to the edge of the boundary layer, the mean velocity takes the form of the logarithmic distribution plus Coles's (1956) wake function. The mean shear for this region has been given by Bull as

$$\frac{\delta M(x_2)}{U_\tau} = \frac{1}{\kappa(x_2/\delta)} + \frac{\Pi}{c\kappa} w_\xi\left(\frac{x_2}{c\delta}\right) \qquad \ldots(3.1.5)$$

for $x_2^* \gtrsim 33$ and $x_2/\delta \lesssim 0.837$. Here c = 0.837, $w_\xi(\xi) = dw(\xi)/d\xi$ and $w(\xi)$ is Coles's wake function. Bull (1969a) suggested a form of the velocity distribution that eliminated the discontinuity which occurs near the edge of the layer when Coles's original wake function is used. He presented a power law for the mean velocity profile which matches Coles's profile at

the point in the wake region where the gradient of the profile is equal to that of the logarithmic region, and also satisfies the condition that $\partial U_1/\partial x_2 = 0$ at $x_2/\delta = 1$. With this representation, the mean shear in the region $0.837 \leq x_2/\delta \leq 1$ is given by

$$\frac{\delta M(x_2)}{U_\tau} = \frac{1}{c\kappa}\left[\frac{1 - x_2/\delta}{1 - c}\right]^{n-1} \qquad \ldots(3.1.6)$$

where $n = 1.67$. The variation with Reynolds number of the distribution of $\delta M(x_2)/U_\tau$ across the boundary layer, given by Equations (3.1.4), (3.1.5) and (3.1.6), is shown in figure 3.

3.1.3 The Correlation Function.

Particular values of the correlation coefficient $R_{22}(x_2,\vec{r})$ have been measured by Grant (1958) and more recently by Tritton (1967). We have information on $R_{22}(x_2;r_1,0,0)$, $R_{22}(x_2;0,r_2,0)$ and $R_{22}(x_2;0,0,r_3)$. Lilley and Hodgson (1960) in their calculation of p'/τ_w represented the boundary layer velocity field by a superposition of large and small eddies randomly distributed over all space. The large eddies were described by

$$v_1 = \frac{A}{\alpha_1}(1 - \alpha_3^2 r_3^2)\exp(-\alpha^2 r^2/2) \quad ,$$

$$v_2 = -\frac{A}{\alpha_2}\alpha_1 r_1(1 - \alpha_3^2 r_3^2)\exp(-\alpha^2 r^2/2) \quad ,$$

$$v_3 = \frac{A}{\alpha_3}\alpha_1\alpha_3 r_1 r_3(1 - \alpha_2 r_2)\exp(-\alpha^2 r^2/2) \quad ,$$

where v_1, v_2 and v_3 are the velocities in the x_1, x_2 and x_3 directions

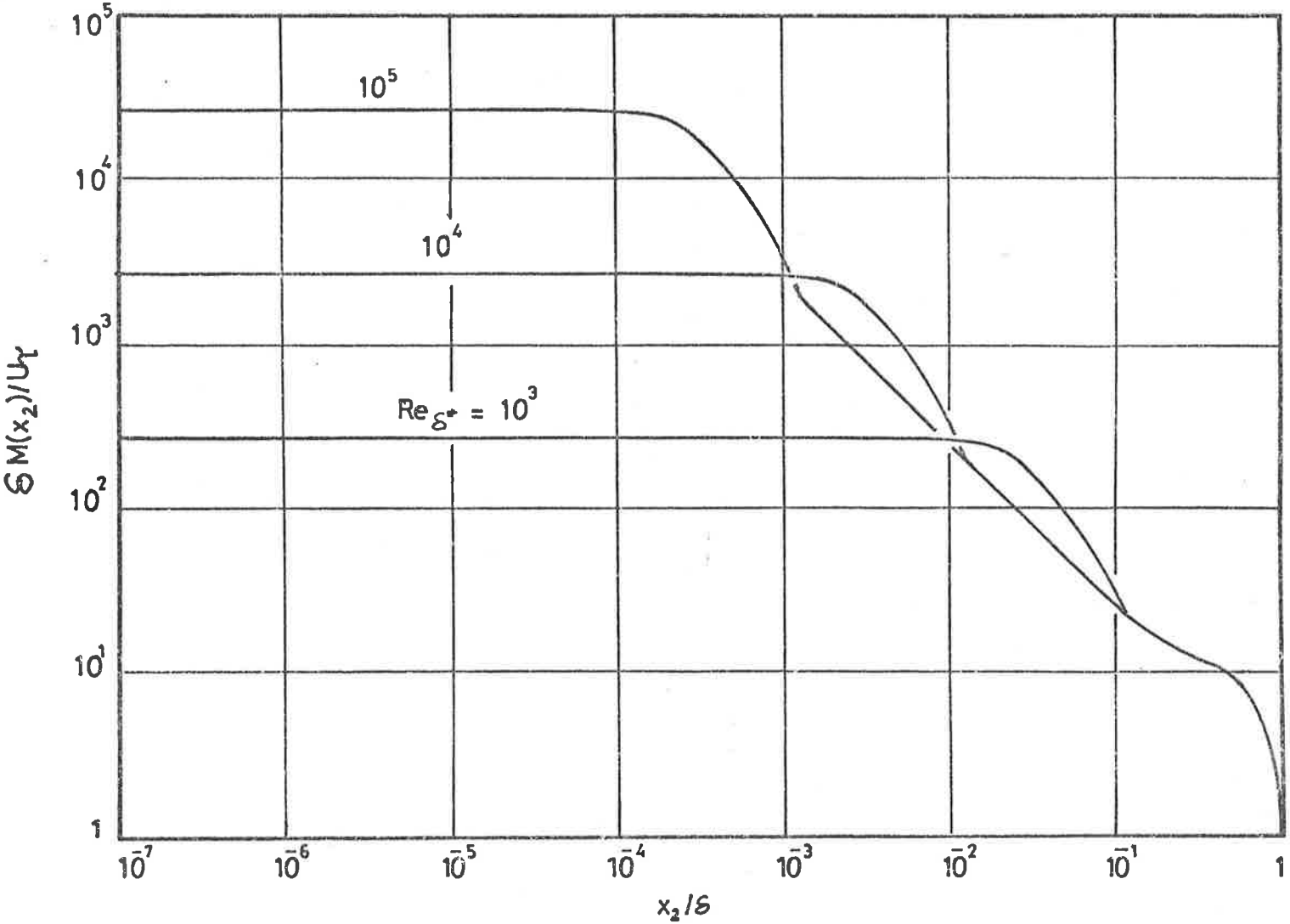

Fig. 3 Variation with Reynolds Number of the Mean Shear Distribution across the Boundary Layer. (After Bull 1969 (a) and (b).)

respectively, and,

$$\alpha^2 r^2 = \alpha_1^2 r_1^2 + \alpha_2^2 r_2^2 + \alpha_3^2 r_3^2 ,$$

and the small eddies being taken as isotropic.

The correlation functions are then,

$$R_{22}^s(x_2,\vec{r}) = (1 - \alpha_2)\left(f + \frac{\partial f}{\partial r}\frac{r_1^2 + r_3^2}{2r}\right) \qquad \ldots(3.1.7)$$

for the small eddies and

$$R_{22}^\ell(\vec{r}) = a_2\left(1 - \frac{\alpha_1^2 r_1^2}{2}\right)\left(1 - \alpha_3^2 r_3^2 + \frac{\alpha_3^4 r_3^4}{12}\right)\exp\left(-\frac{\alpha^2 r^2}{4}\right) , \qquad \ldots(3.1.8)$$

for the large eddies, where

$$r = (r_1^2 + r_2^2 + r_3^2)^{\frac{1}{2}} .$$

The resultant correlation function is then the sum of these two functions, that is,

$$R_{22}(x_2,\vec{r}) = R_{22}^s(x_2,\vec{r}) + R_{22}^\ell(\vec{r}) . \qquad \ldots(3.1.9)$$

The function f appearing in the small eddy correlation function gives a good representation of the experimental data if it is taken as exp(-r/s), where s is an appropriate length scale associated with these eddies. The correlation function due to the small eddies can then be written as

$$R_{22}^s(x_2,\vec{r}) = (1 - a_2)\left(1 - \frac{r}{2s} + \frac{r_2^2}{2rs}\right)\exp(-r/s) . \qquad \ldots(3.1.10)$$

Lilley and Hodgson represented the correlation throughout the layer

by the above function with values of constants chosen to suit Grant's measurements close to the boundary. The same representation has been used here, but an attempt has been made to represent the variation of the scale s with distance from the boundary in a manner which will be discussed in more detail later. For the large eddy contribution the values $\alpha_1\delta_0 = \alpha_2\delta_0 = 3.73$, $\alpha_3\delta_0 = 11.1$, as used by Lilley and Hodgson, and $a_2 = 0.085$ (somewhat less than used by Lilley and Hodgson) have been used for all values of x_2, where δ_0 is the value of x_2 at which $U_1 = U_\infty - U_\tau$. In the present work, δ_0/δ has been taken as 0.683 so $\alpha_1\delta = \alpha_2\delta = 5.46$ and $\alpha_3\delta = 16.26$.

It can be seen from the definition of R_{22} given in Section 2.6 that the calculation of the auto-covariance of the wall pressure fluctuations $\langle p(\vec{x},t)p(\vec{x},t')\rangle$ requires a knowledge of the values of the space-time correlation coefficient of the velocity fluctuations normal to the boundary at non-zero values of time delay, although the special case of the evaluation of the mean square pressure fluctuations requires only R_{22} values at $\tau = 0$.

As no extensive experimental data for R_{22} with non-zero time delay are available, this correlation coefficient has been evaluated by making use of the empirical formulation of R_{22} with zero time delay (the space correlation) which was developed for mean square pressure calculations. To do this the well known hypothesis due to Taylor (1938) is used, where, at least for time delays which are not large, the velocity fluctuations in any plane parallel to the boundary can be regarded as "frozen", and as being convected parallel to the boundary. In principle, it is then

possible to transform the space correlation function into the required space-time correlation function by means of the relationship

$$R_{22}(y_2,z_2,r_1,r_3,\tau) = R_{22}(y_2,z_2,r_1-U_c\tau,r_3,0) \quad , \qquad \ldots(3.1.11)$$

where U_c is the convection velocity of the velocity field in a plane at a distance z_2 from the boundary, if a point in the plane at distance y_2 is regarded as the datum point.

But, the convection velocity will vary with distance from the boundary and Equation (3.1.11) will give a different result depending on whether the datum point is taken to be that at y_2 or that at z_2. This is clearly at variance with reality. However, this inconsistency can be avoided by adopting the procedure detailed in Section 3.1.4. There, the scale of the R_{22} correlation is taken as that corresponding to the plane at a distance $(y_2 + z_2)/2$ from the boundary. Similarly, here, the convection velocity U_c is taken as the velocity for the plane at a distance $(y_2 + z_2)/2$ from the boundary.

Several previous investigations of the space-time correlations of the velocity fluctuations in turbulent boundary layer flows in planes parallel to the boundary - for example Favre, Gaviglio and Dumas (1957), Willmarth and Wooldridge (1963), Bull (1967) - have shown that the convection velocity of the velocity field is essentially equal to the local mean velocity, although Morrison (1969) has shown that this is no longer true for planes very close to the boundary (y_2^* less than about 20). In the calculations for the auto-covariance of the wall pressure

fluctuations, the convection velocity has therefore been taken as the mean flow velocity at a distance of $(y_2 + z_2)/2$ from the boundary; so that

$$U_c = U_1\left(\frac{y_2+z_2}{2}\right) . \qquad \ldots(3.1.12)$$

In the outer part of the boundary layer this value will not differ significantly from either $U_1(y_2)$ or $U_1(z_2)$. However, in the inner part of the layer, the convection velocity given by Equation (3.1.12) will give rise to values of U_c markedly different from $U_1(y_2)$ or $U_1(z_2)$, but in the light of Morrison's findings the errors will be less than might otherwise have been expected.

It should also be pointed out that, for the model used for these calculations, the maximum value of R_{22} for given values of y_2, z_2, and r_3 will in general occur for $\tau = r_1/U_c$ and in particular for $\tau = 0$ when $r_1 = 0$. This is not in accord with the experimental results of Favre, Gaviglio and Dumas (1957). The results from their investigations of the correlation of streamwise velocity fluctuations indicate that the maximum correlation occured at a value of τ somewhat different from r_1/U_c. However, scrutiny of the details of the calculations indicates that this discrepancy does not give rise to any significant error.

3.1.4 The Reciprocity Relationship and Eddy Scales.

It is important to note that Equations (3.1.8) and (3.1.10) correspond basically to turbulent flows in which the scale of the large eddies (as determined by α_1, α_2, and α_3), the scale of the small eddies s, and $\langle u_2^2 \rangle$

are all constant. However, in boundary layer flows $\overline{u_2^2}$ certainly varies with distance from the boundary surface, and even if the large eddy correlation is represented by Equation (3.1.8) (in which case its scale is not a function of the distance of the datum point from the boundary) the length scale s of the small eddies can be expected to be very small close to the wall and to increase with increasing distance from the boundary. It was therefore initially assumed that

$$s = s(x_2) \quad . \qquad \ldots(3.1.13)$$

A similar assumption has been made in previous work, for example in Hodgson's (1962) calculations based on $R_{22} = \exp(-r^2/x_2^2)$. Based on the data of Grant and Tritton, Equation (3.1.13) has been given the specific form

$$\left.\begin{aligned} s/x_2 &= 0.570 \quad \text{for } 0 \leqslant x_2/\delta \leqslant 0.2 \quad , \\ s/\delta &= 0.114 \quad \text{for } 0.2 \leqslant x_2/\delta \leqslant 1.0 \quad . \end{aligned}\right\} \qquad \ldots(3.1.14)$$

The correlation curves chosen as the best fits to Grant's and Tritton's data within the framework of Equations (3.1.8) and (3.1.10) are shown as dashed curves in figure 4. For these curves the abscissae are given in terms of δ and not δ_0 as used in the original presentations of the data. The variation of the scale is shown in figure 5.

However, any equation of the form of (3.1.13) leads to an inconsistency in the boundary layer model. The model chosen should satisfy the following reciprocal relationships:

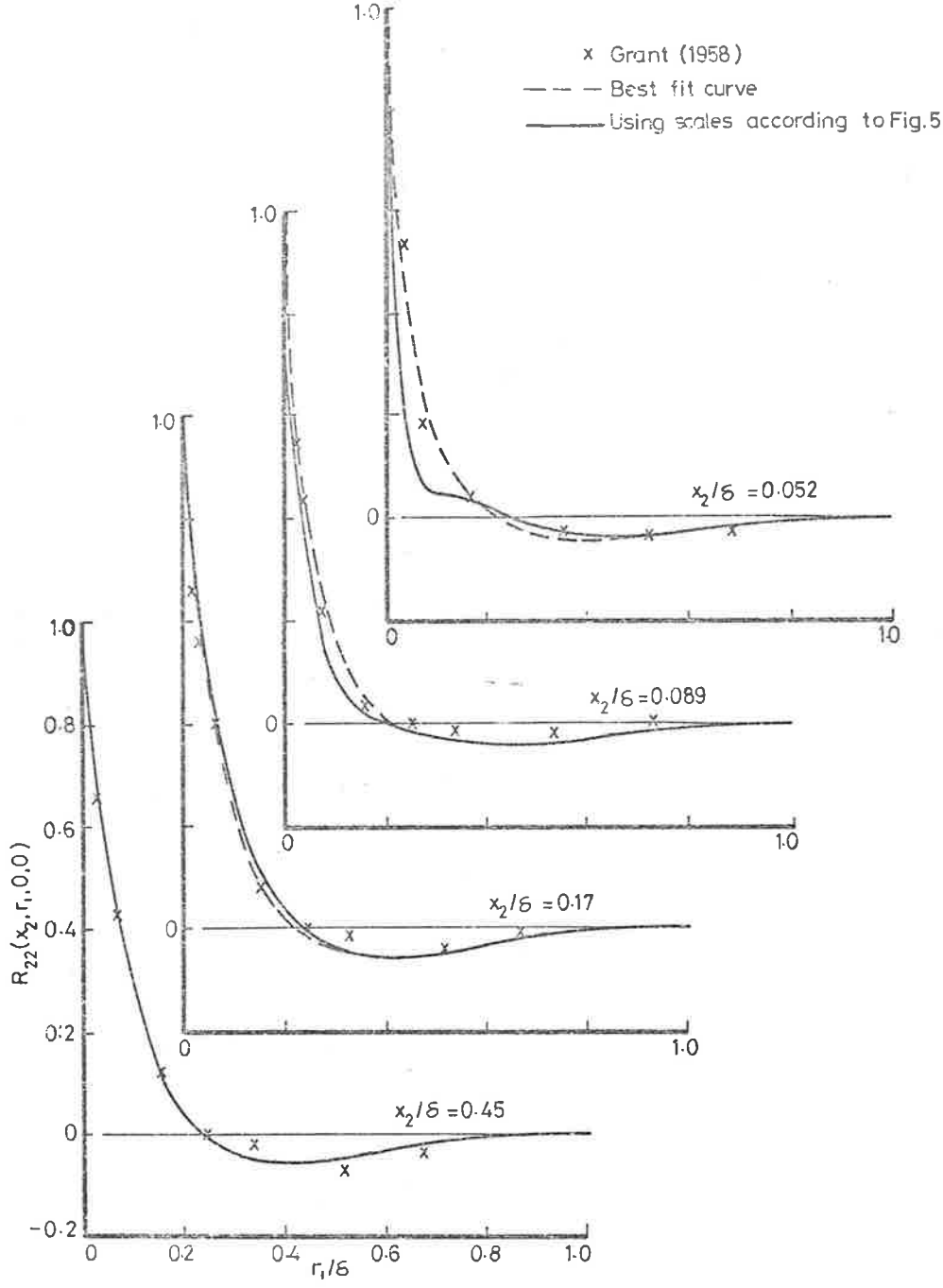
x Grant (1958)
— — — Best fit curve
——— Using scales according to Fig.5
x_2/δ =0·052
x_2/δ =0·089
x_2/δ =0·17
x_2/δ =0·45
$R_{22}(x_2, r_1, 0, 0)$
r_1/δ
1·0
0·8
0·6
0·4
0·2
0
-0·2
0·2
0·4
0·6
0·8

Fig.4 (a)

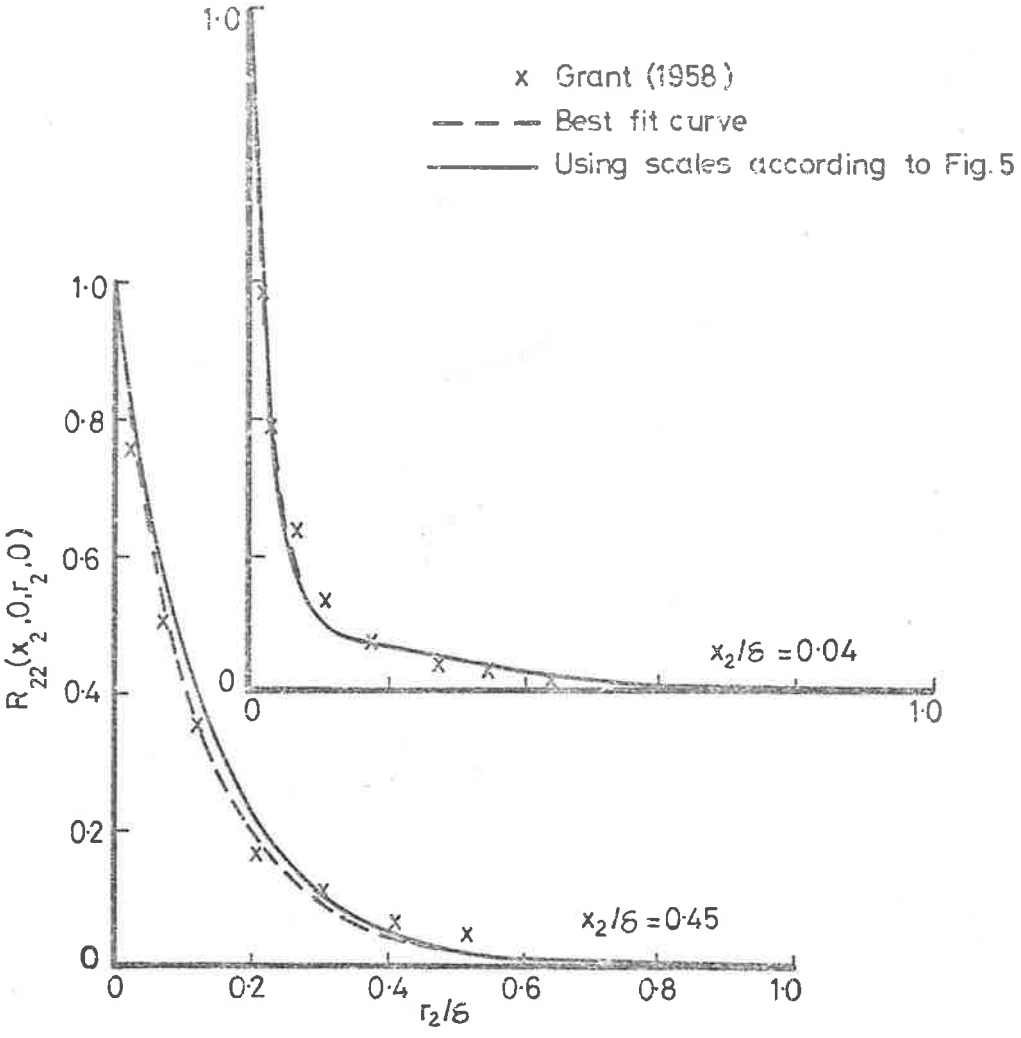

Fig. 4 (b)

Fig. 4 Comparison of Experimental and Assumed Velocity Correlations. ("Best Fit" curves are the best approximations obtainable within the framework of Equations (3·1·8) and (3·1·10)).

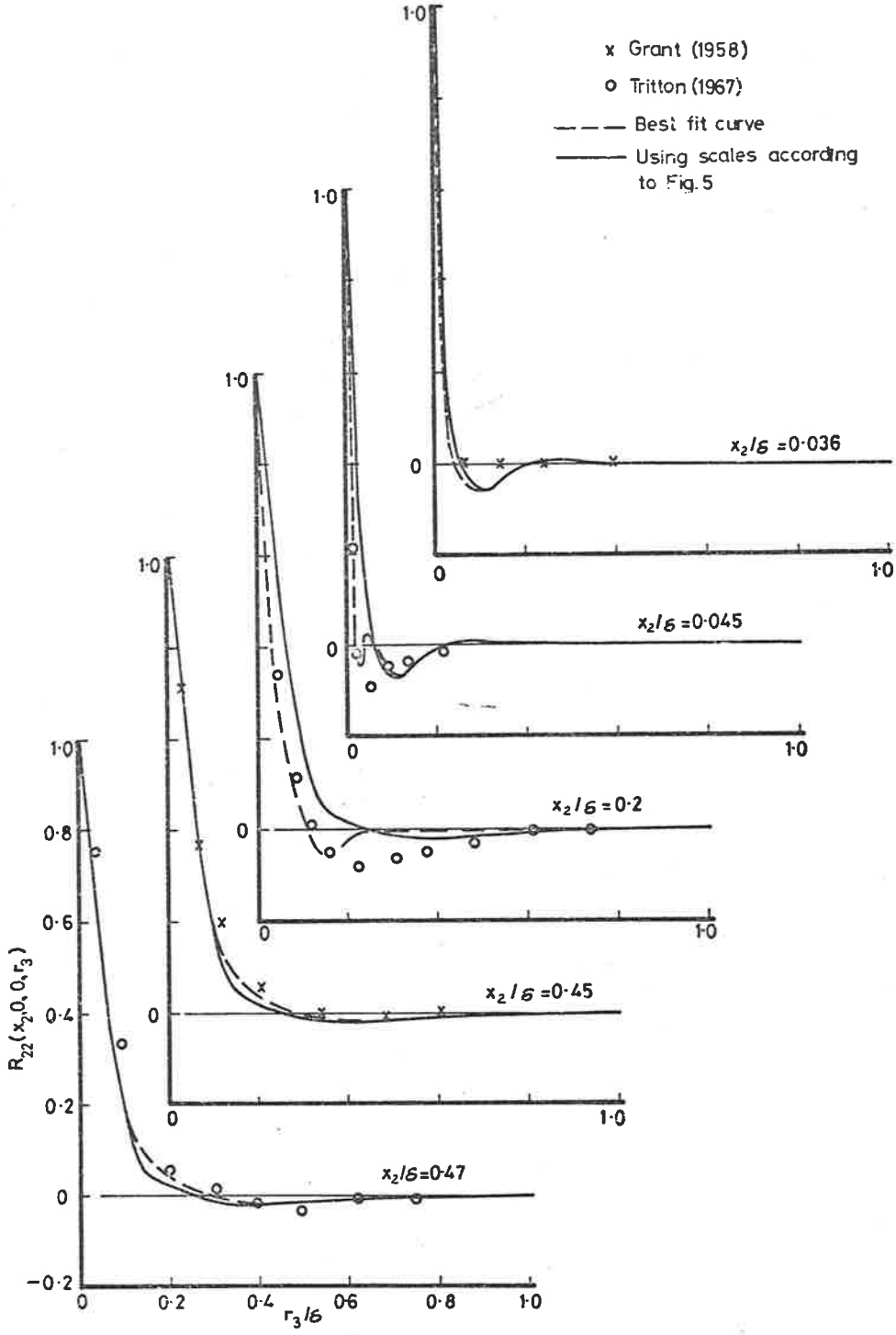
x Grant (1958)
o Tritton (1967)
Best fit curve
Using scales according to Fig. 5
x_2/δ =0·036
x_2/δ =0·045
x_2/δ = 0·2
x_2/δ =0·45
x_2/δ=0·47
$R_{22}(x_2,0,0,r_3)$
r_3/δ
1·0
0·8
0·6
0·4
0·2
0
−0·2
0·2
0·4
0·6
0·8

Fig. 4 (c)

o $R_{22}(x_2, r_1, 0, 0)$

Grant x $R_{22}(x_2, 0, r_2, 0)$ (1953)

□ $R_{22}(x_2, 0, 0, r_3)$

Tritton △ $R_{22}(x, 0\,0\, r_3)$ (1967)

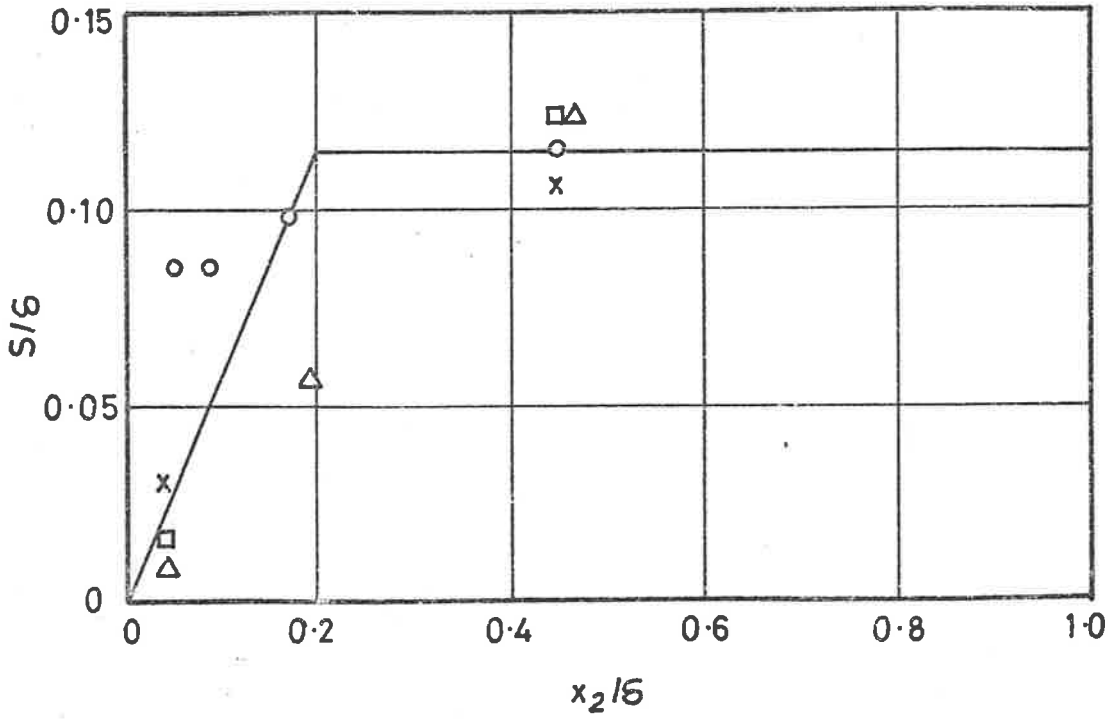

Fig. 5 Variation of Small Eddies across the Boundary Layer.

$$\langle u_2(\vec{y},t)u_2(\vec{z},t')\rangle = \langle u_2(\vec{z},t')u_2(\vec{y},t)\rangle \qquad \ldots(3.1.15)$$

or, equivalently,

$$u_2'(\vec{y})u_2'(\vec{z})\ R_{22}(\vec{y},\vec{z},t,t') = u_2'(\vec{y})u_2'(\vec{z})\ R_{22}(\vec{z},\vec{y},t',t), \quad \ldots(3.1.16)$$

and also

$$R_{22}(\vec{y},\vec{z},t,t') = R_{22}(\vec{z},\vec{y},t',t) \ . \qquad \ldots(3.1.17)$$

In these equations the expressions on the left hand side is the covariance for which $\vec{y}$ is understood to be the fixed datum point, and that on the right hand side a covariance for which $\vec{z}$ is the datum point. These reciprocal relations must be satisfied by the real flow; for the model, if the small eddy correlation is as given by Equation (3.1.10) when t = t', Equations (3.1.15), (3.1.16 and (3.1.17) will not be satisfied if the small eddies have a scale variation of the form given by Equation (3.1.13) (since the scale chosen will depend on whether $\vec{y}$ or $\vec{z}$ is regarded as the datum point). The lack of reciprocity resulting from a scale choice according to Equation (3.1.13) can be avoided by modifying the equation so that for correlation between two points $\vec{y}$ and $\vec{z}$ we take

$$s = s\left[\tfrac{1}{2}(y_2 + z_2)\right] \ . \qquad \ldots(3.1.18)$$

Equation (3.1.14) can then be modified to

$$\left.\begin{aligned} s/\left[\tfrac{1}{2}(y_2+z_2)\right] &= 0.570 \quad \text{for} \quad 0 \leq \tfrac{1}{2}(y_2+z_2)/\delta \leq 0.2 \ , \\ s/\delta &= 0.114 \quad \text{for} \quad 0.2 \leq \tfrac{1}{2}(y_2+z_2)/\delta \leq 1.0 \ . \end{aligned}\right\} \ldots(3.1.19)$$

Using Equation (3.1.18) or (3.1.19), the scale of the small eddies will

now be associated with the point midway between $\vec{y}$ and $\vec{z}$, and the model will satisfy Equations (3.1.15), (3.1.16) and (3.1.17). This also means that, while s is independent of the two co-ordinates parallel to the boundary, it will vary with the separation distance normal to the boundary between the two points considered, and for any given datum point this variation will not be symmetrical about the zero separation point - the scale will decrease with increasing separation distance on the boundary side of the datum point and increase on the side of the datum point remote from the boundary, a behaviour which seems to be acceptable from the physical point of view.

It should be noted, however, that the definition of R_{22} given above and in Section 2.6 is not the only possible one. For example, in presenting his experimental data, Grant (1958), for convenience, used an alternative form of the coefficient defined by

$$R_{22} = \frac{\langle u_2(\vec{y},t)u_2(\vec{z},t')\rangle}{\langle u_2^2(\vec{y})\rangle} \quad , \qquad \ldots(3.1.20)$$

where $\vec{y}$ is the datum point. If this procedure is followed, it is clear that, although the basic reciprocity relationship, Equation (3.1.15), should still be required to be satisfied, Equation (3.1.16) must be modified to

$$\langle u_2^2(\vec{y})\rangle \, R_{22}(\vec{y},\vec{z},t,t') = \langle u_2^2(\vec{z})\rangle \, R_{22}(\vec{z},\vec{y},t',t) \quad , \qquad \ldots(3.1.21)$$

and Equation (3.1.17) must be dispensed with. In this case, if the space correlation coefficient is still represented by Equations (3.1.8), (3.1.9)

and (3.1.10), Equations (3.1.15) and (3.1.21) will not be satisfied (as a result of the variations of ε and $\langle u_2^2 \rangle$ with the distance from the boundary), and the boundary layer model will not have the reciprocity property.

Figures 6(a) and 6(b) show the variation of the space correlation coefficient of the u_2 velocity fluctuations for the datum point at two distances from the boundary ($y_2/\delta = 0.040$ and 0.45 respectively), for both definitions of R_{22} - as in Section 2.6, and as in Equation (3.1.20) - with R_{22} expressed by Equations (3.1.8), (3.1.9) and (3.1.10) in each case, for seven angular directions from the datum point. Curves are shown for both forms of scale representation for the small eddies, Equations (3.1.14) and (3.1.19), and where possible the experimental data of Grant (1958) are also shown. When R_{22} is as defined in Section 2.6, the data of Grant have been modified so that they conform to this definition; the modification has been effected using the u_2'/U_τ distribution detailed in Section 3.1.1 for the Reynolds number corresponding to Grant's experiments ($Re_\delta{}^* \simeq 10^4$), and it has been assumed (as appears from Grant's paper to be the case) that in the experiments the second correlation point was always further away from the boundary than the datum point.

In concluding this section, we might note that the scale variation represented by Equation (3.1.14) is very slightly different from that chosen for the calculations previously presented by Bull and Lim (1968). A discussion of the choice of scale in that case and detailed comparisons with the data of Grant and Tritton are given in that paper.

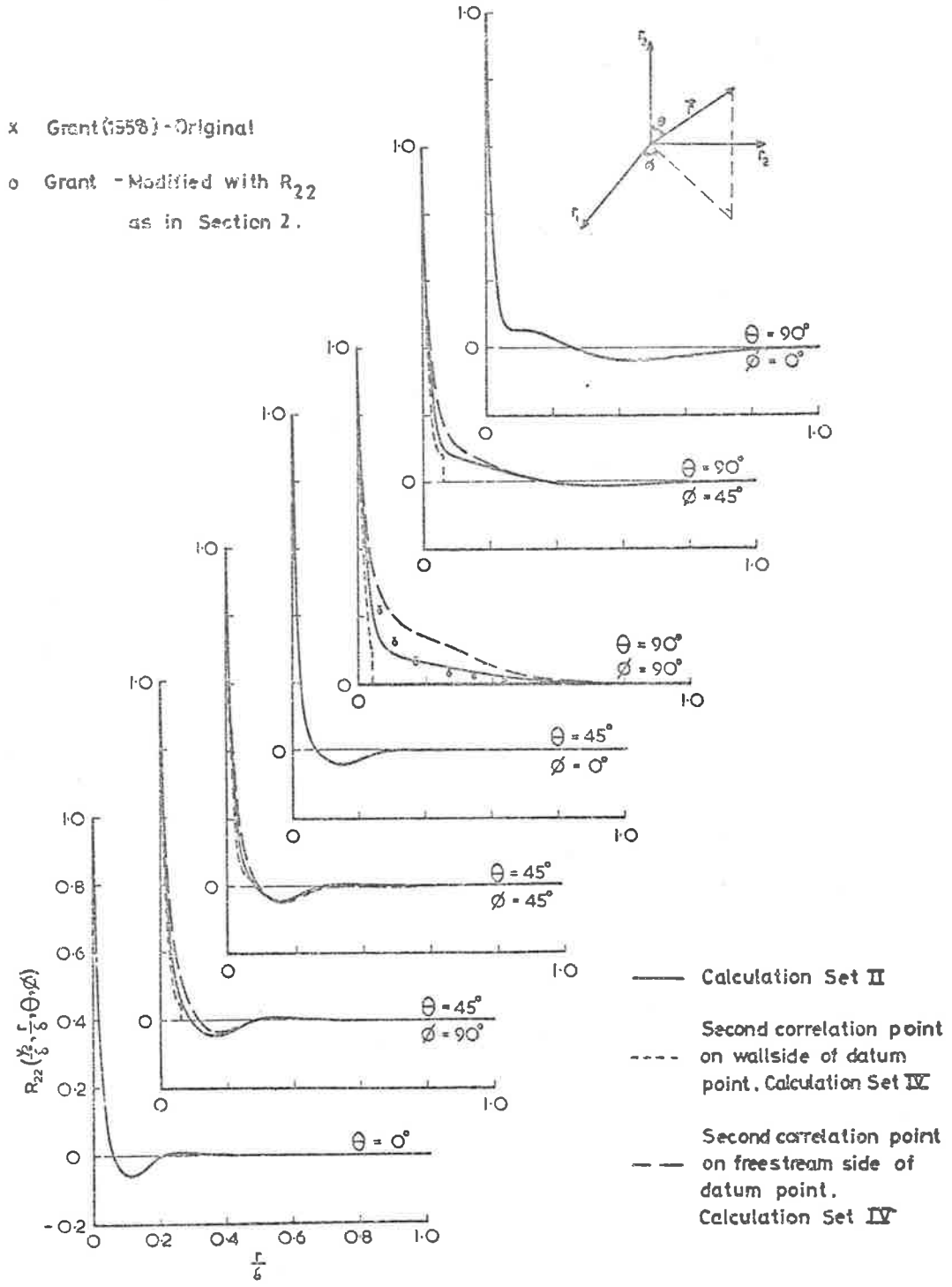

Fig. 6 (a) Variation of Space Correlation Coefficient R_{22} with Separation Distance in Various Directions from the Datum Point. $y_2/\delta = 0{\cdot}04$

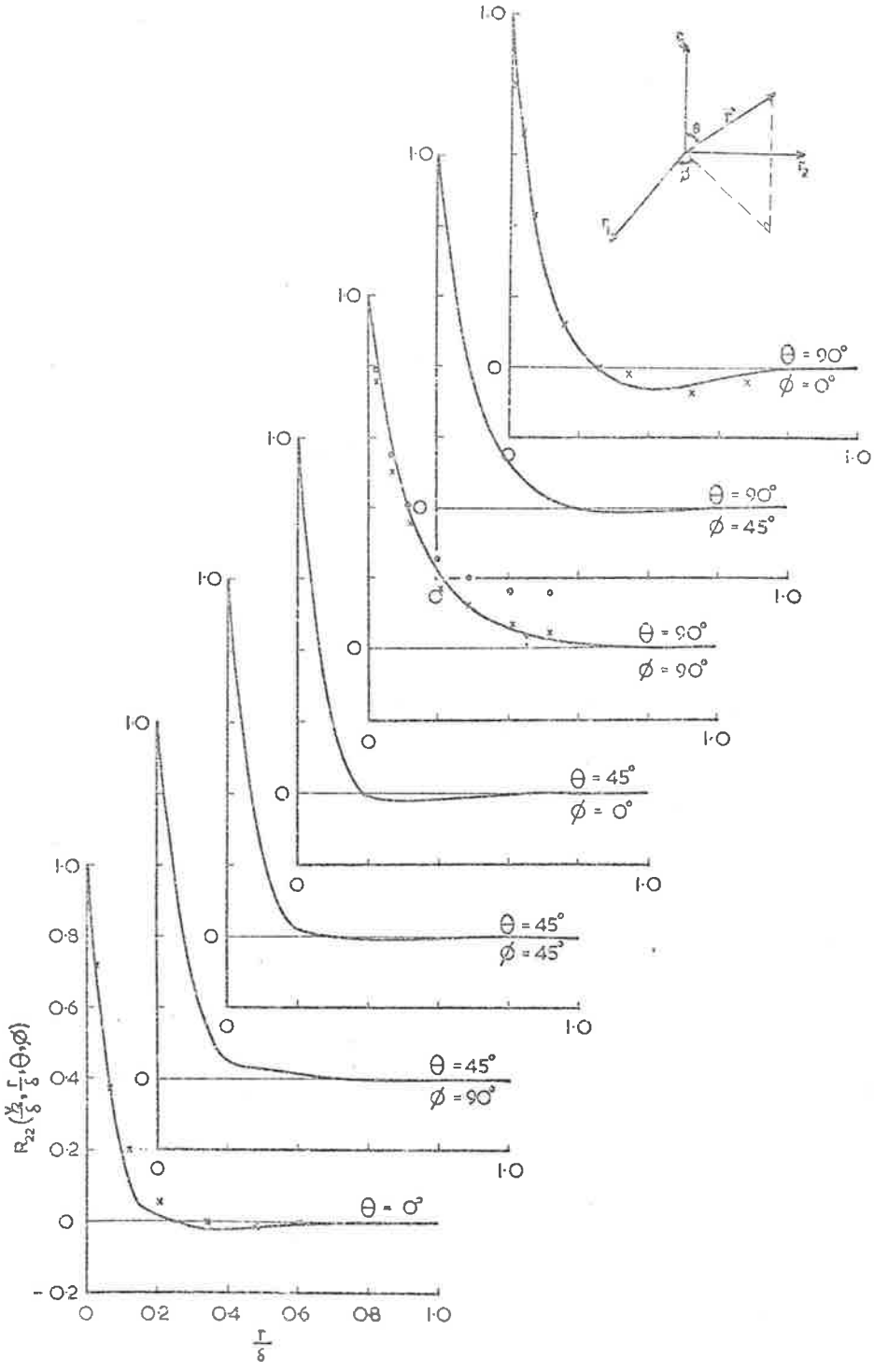

Fig. 6 (b) Variation of Space Correlation Coefficient R_{22} with Separation Distance in Various Directions from the Datum Point. $y_2/\delta = 0{\cdot}45$

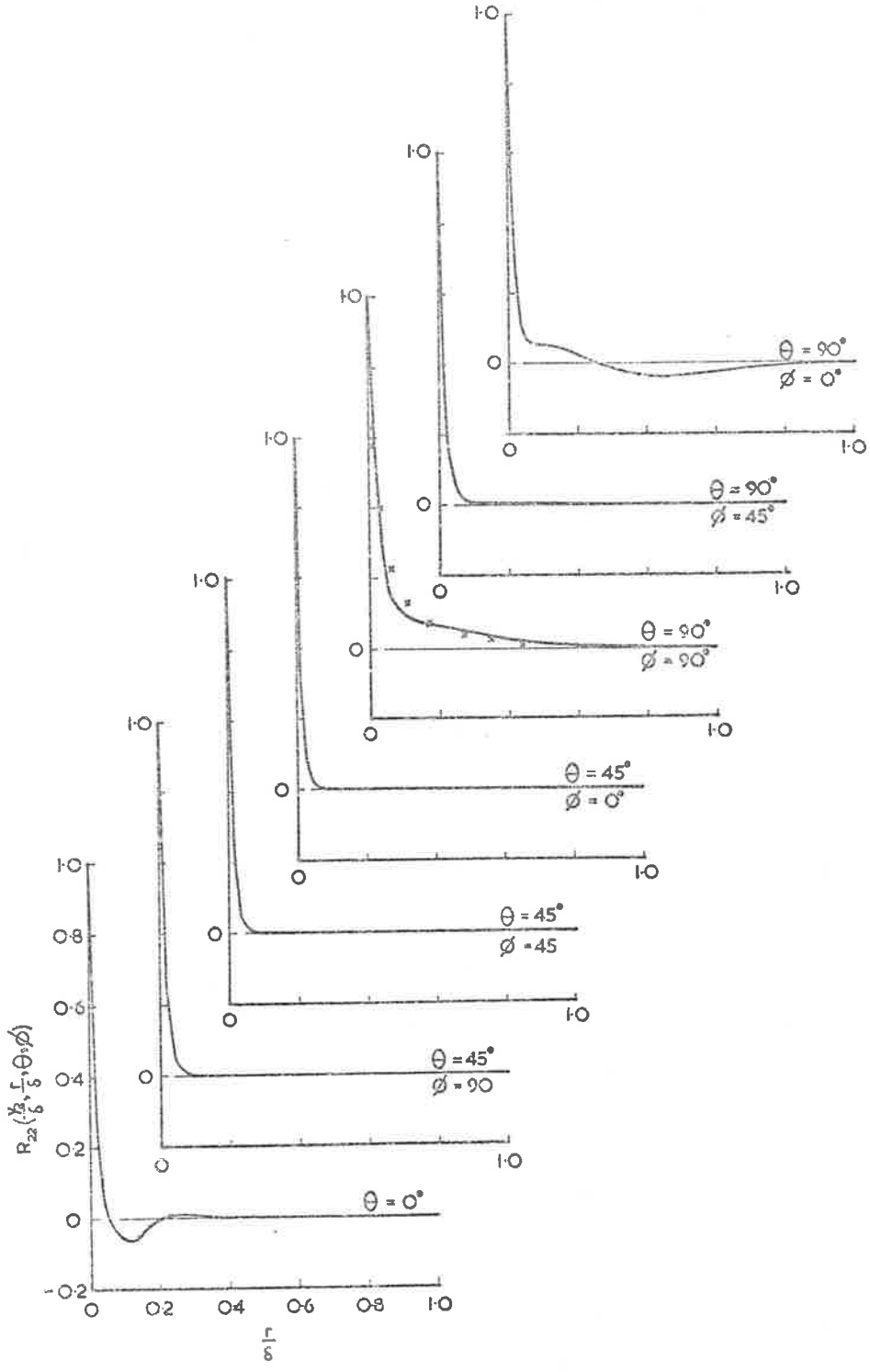

Fig. 6 (c) Variation of Space Correlation Coefficient R_{22} as given by Equation (3·2·4) with Separation Distance in Various Directions from the Datum Point. $y_2/\delta = 0{\cdot}04$

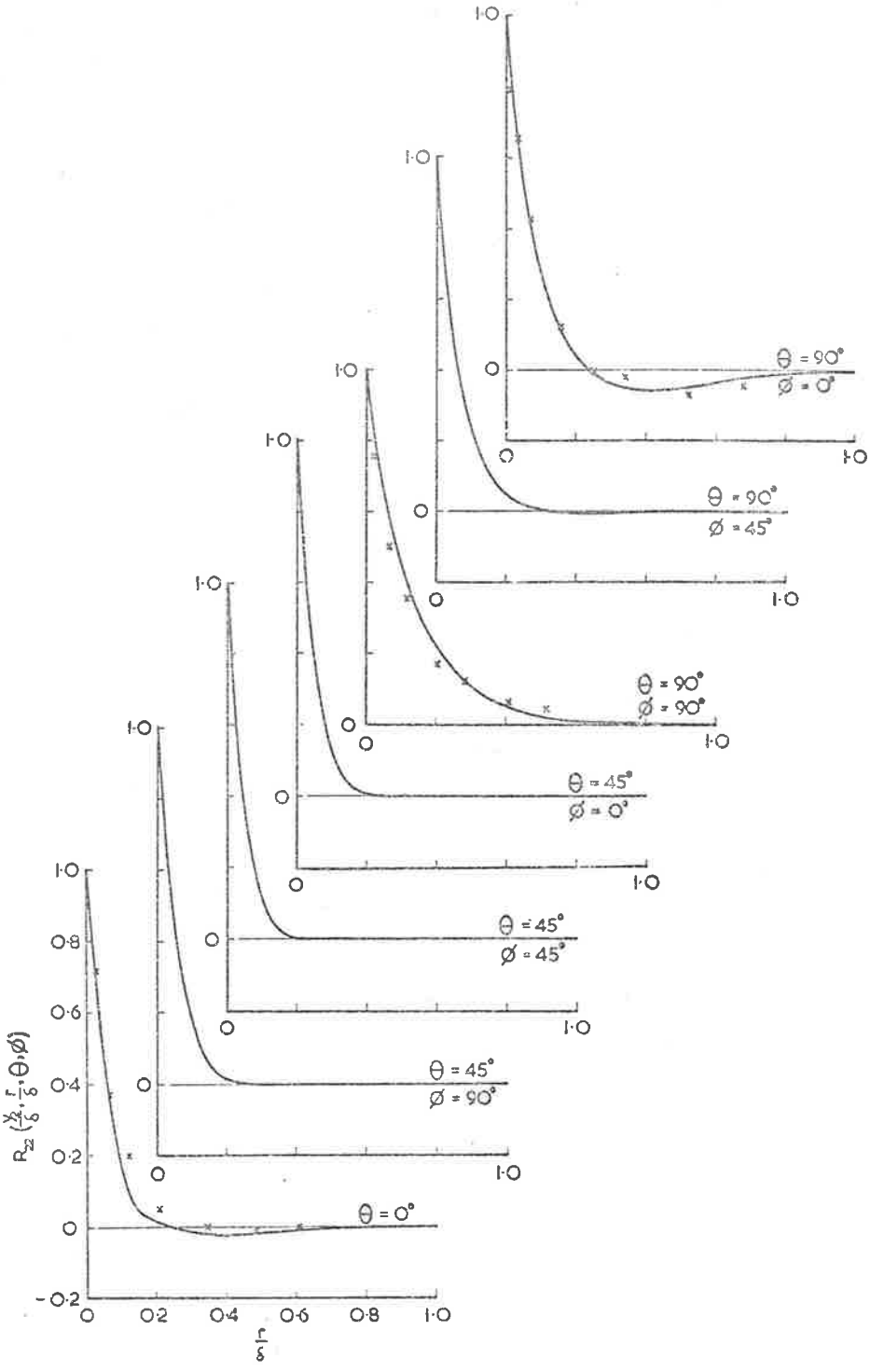

Fig. 6 (d) Variation of Space Correlation Coefficient R_{22} as given by Equation (3·2·4) with Separation Distance in Various Directions from the Datum Point. $y_2/\delta = 0{\cdot}45$

3.2 Calculation of the Auto-Covariance and the Mean Square of the Wall Pressure Fluctuations.

The equation of the covariance of the pressure fluctuations has been given in Section 2. In this section, we are primarily concerned with the calculation of the overall values of the auto-covariance and the mean square of the wall pressure fluctuations in a constant pressure turbulent boundary layer as given by Equations (3.1.1) and (3.1.2). The determination of the auto-covariance differ from that of the mean square value only in as much as in the former case $\vec{\xi} = 0$ and in the latter, $\vec{\xi} = \tau = 0$. Under normal circumstances, a general numerical procedure would have been devised for the evaluation of these values. However, due to the great extent of machine computing time otherwise required for the accurate evaluation of each of these values, the computational requirements have been broken down not only to a combination of machine and manual procedures but also to the extent of having separate optimised computer programmes.

3.2.1 Calculation Procedures.

The numerical evaluation was carried out on the C.D.C. 6400 digital computer in the University of Adelaide. To make possible a mutual check on consistency and accuracy of results, two different procedures were adopted, although, in fact, the check has been applied only to the calculations for the mean square pressure. The two methods are as follows.

Method 1: The computer programme which is described and given in

detail in Appendix A-I is designed to give the value of the three-fold integral

$$\frac{\partial P^*(y_2,\infty)}{\partial y_2} = \rho^2 \int_0^\infty dz_2 \, F_{13}(y_2,z_2) \quad , \qquad \ldots(3.2.1)$$

(F_{13} itself being, of course, a double-integral in (r_1,r_3) space as given by Equations (2.6.14) and (2.6.15), where, from Section 2.5, we define $P^*(y_2,z_2)$ as

$$P^*(y_2,z_2) = \rho^2 \int_0^{y_2} dy \int_0^{z_2} dz \, F_{13}(y,z) \quad . \qquad \ldots(3.2.2)$$

The final integration over y_2,

$$\langle p^2 \rangle = \int_0^\infty \left[\frac{\partial P^*(y_2,\infty)}{\partial y_2} \right] dy_2 \quad , \qquad \ldots(3.2.3)$$

is carried out manually.

Method 2: First, in the determination of the mean square wall pressure fluctuations, $I^s_{13}(y_2,z_2)$, the small eddy contribution to I_{13}, is calculated according to Equation (2.6.15), a process which requires only one machine integration, since, when R^s_{22} is represented by Equation (3.1.10), the double-integral of Equation (2.6.15) can be reduced to a single-integral (see Appendix B). The values of I^s_{13} obtained in this way are independent of Reynolds number, so that, for a particular boundary layer model, calculation of them has to be made only once. This is followed by the calculation of G^s_{13} as in Equation (2.6.16) and the machine

integration over z_2 to give $\partial P^s(y_2,\infty)/\partial y_2$, for the particular Reynolds number being considered. $\partial P^\ell(y_2,\infty)/\partial y_2$ corresponding to the large eddies is obtained by the same procedure as in Method 1 using Equations (2.6.14), (2.6.15), and (3.2.1). The computer programmes devised to perform these calculations are given in Appendix A-IV and A-V. The final integrations of $\partial P^s(y_2,\infty)/\partial y_2$ and $\partial P^\ell(y_2,\infty)/\partial y_2$ over y_2, as in Equation (3.2.3), are again done manually, resulting in the small and large eddy contributions to $\langle p^2 \rangle$ respectively. Summation gives the overall value of $\langle p^2 \rangle$.

3.2.2 Cases Considered.

(1) Mean Square Wall Pressure Fluctuations.

Four sets of calculations will be referred to; those previously given by Bull and Lim (1968) will be designated Set I, later calculations based on the same model will be designated Revised Set I, and two additional sets to be presented here will be designated as Set II and Set IV. The details of the boundary layer model and the calculation procedure for Set I can be found in the original paper; the conditions for the Revised Set I, Set II and Set IV calculations will now be detailed.

Revised Set I: The results presented by Bull and Lim (1968), which apparently gave overestimates of the mean square wall pressure fluctuations, has subsequently been found to suffer from certain defects (some of which were also inherent in earlier work). These are that the boundary layer model taken does not satisfy the reciprocity relationships discussed in Section 3.2; that in the numerical integration processes inadequate region

sizes were taken at the higher Reynolds numbers ($Re_\delta^* \geq 10^5$), a point discussed in greater detail in Section 3.2.3 below; and that the correlation coefficient, intended to be given by Equations (3.1.8), (3.1.9) and (3.1.10) as in the present work, was incorrectly represented in the computer programme. The form of the correlation coefficient actually used in the Set I calculations is

$$R_{22}(y_2,\vec{r}) = \left[a_2\left(1 - \frac{\alpha_1^2 r_1^2}{2}\right) \exp\left(-\frac{\alpha_1^2 r_1^2}{4}\right) + (1 - a_2)\left(1 - \frac{r_1}{2s}\right) \exp\left(-\frac{r_1}{s}\right)\right] \ldots$$

$$\ldots\left[a_2 \exp\left(-\frac{\alpha_2^2 r_2^2}{4}\right) + (1 - a_2) \exp\left(-\frac{r_2}{s}\right)\right] \ldots$$

$$\ldots\left[a_2\left(1 - \alpha_3^2 r_3^2 + \frac{\alpha_3^4 r_3^4}{12}\right) \exp\left(-\frac{\alpha_3^2 r_3^2}{4}\right) + (1 - a_2)\left(1 - \frac{r_3}{2s}\right) \exp\left(-\frac{r_3}{s}\right)\right] \quad \ldots(3.2.4)$$

It was felt that repeating the Set I calculations with the same boundary layer model, despite the fact that this did not correspond to that originally intended, but with adequate integration region sizes, would give an indication of the effect of the form of the correlation function on the calculated values of $\langle p^2 \rangle$. Hence, for the Revised Set I calculations, the boundary layer model is such that the turbulence intensity, mean shear and small eddy scale distributions are exactly the same as given by Bull and Lim (1968) and the correlation coefficient is as given by Equation (3.2.4). The turbulence intensity in this case is still described by Equation (3.1.3), and the variation with Reynolds number of the distribution of the mean shear in the form of $(\delta/U_\tau)(\partial U_1/\partial x_2)$ across the boundary layer is shown in figure 7. The machine integration for the

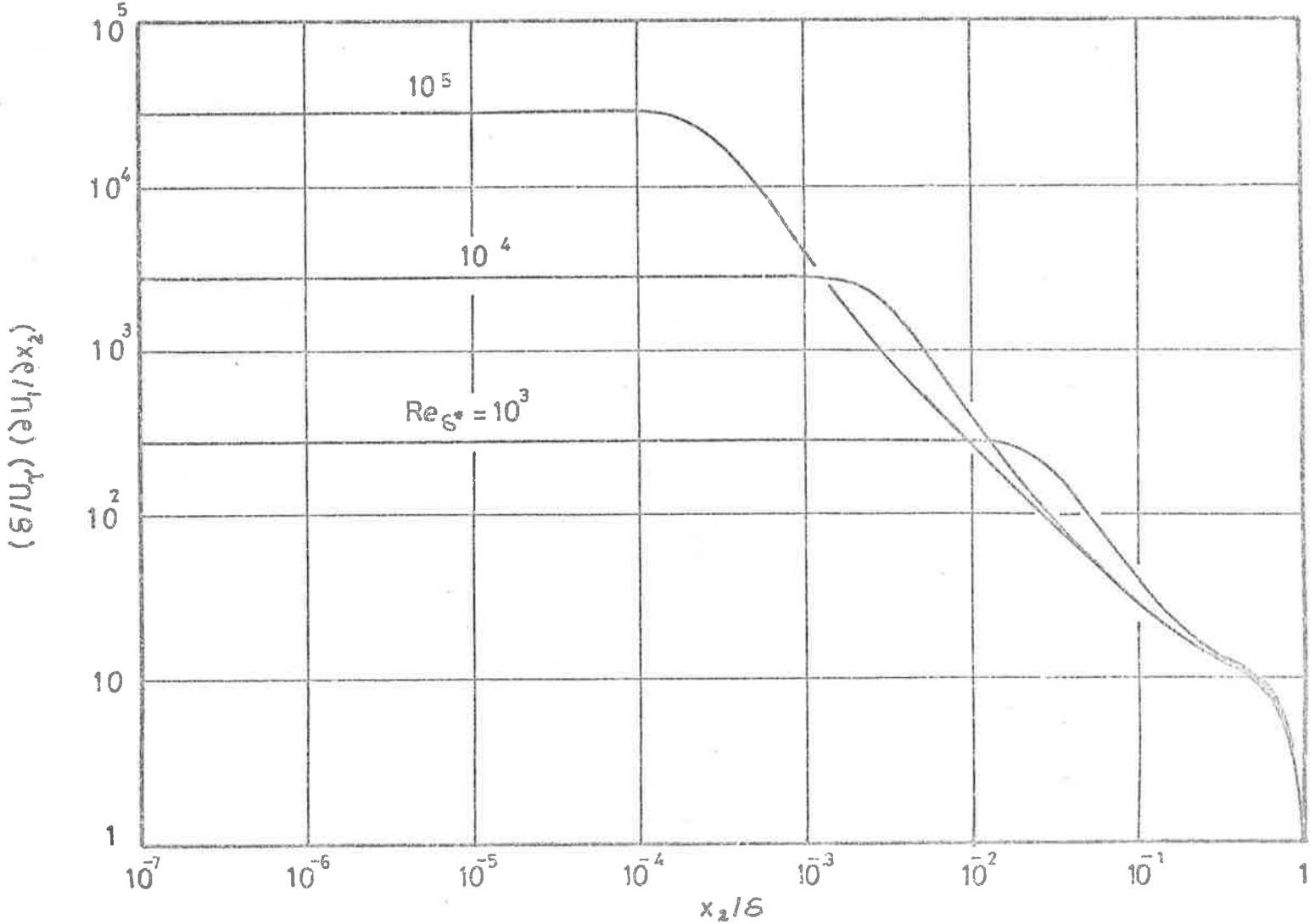

Fig.7 Variation of Mean Shear Distribution with Reynolds Number used in Revised Set.1 Calculations.

value of the triple-integral (Equation (3.2.1)) in this case was carried out by the method of Sag (1963) with prior inspection of the integrand to determine an adequate region size (see Section 3.2.3 below).

Set II: The distributions of the mean shear and the turbulence intensity are as detailed in Section 3.1. The space correlation coefficient of the u_2 velocity fluctuations is as defined by Grant (1958), Equation (3.1.20), with the small and large eddy contributions as given by Equations (3.1.10) and (3.1.8) respectively, and with the scale of the small eddies as given by Equation (3.1.14); so, for both the possibilities discussed in Section 3.1.4 the reciprocity relation is unsatisfied. For this set of calculations, because of the method of definition of the velocity correlation coefficient, the product $u_2'(y_2)u_2'(z_2)$ appearing in the expressions for F_{13} and G_{13} in Equations (2.6.14) and (2.6.16) respectively, is replaced by $\langle u_2^2(y_2)\rangle$.

Set IV: Again the distributions of the mean shear and the turbulence intensity are as in Section 3.1; the velocity correlation coefficient is as defined in Section 2 with the large and small eddy contributions given by Equations (3.1.8) and (3.1.10) respectively; the scale of the small eddies is as given by Equation (3.1.19). In this case, therefore, the reciprocity condition is satisfied.

For Revised Set I a Reynolds number range of $10^3 \leq Re_\delta{}^* \leq 10^6$ has been considered, and for Sets II and IV a range of $10^3 \leq Re_\delta{}^* \leq 10^7$.

(2) Auto-Covariance of the Wall Pressure Fluctuations.

In contrast to the calculation for the mean square value of the wall pressure fluctuations, and for reasons which will become obvious in the discussion, only one set of calculations was attempted for the auto-covariance. The boundary layer model is the same as that for the Set IV calculations for the mean square value except that the required space-time correlation function is obtained from the spatial correlation function by the use of Equations (3.1.11) and (3.1.12). The case considered has been for $Re_\delta^* = 10^4$ only.

3.2.3 Evaluation of the Required Multiple Integrals.

Basically, the calculation of the space-time covariance or the mean square value of the wall pressure fluctuations requires the evaluation of a six-fold (double space) integral. However, with the formulation adopted in the present case and subsequent analytical reduction, and by carrying out the final integration manually, the digital computer operation can be reduced to the evaluation of, at worst, a triple-integral. Although this is a large reduction in complexity, the accurate calculation of even this triple-integral presents considerable difficulties owing largely to the nature of the integrand.

Chronologically the evaluation of Equation (3.2.1) started with the use of a Monte Carlo method. A very poor convergence rate was obtained owing to the very peaky nature of the integrand (which, as can be seen from

Equations (2.6.14), (2.6.15) and (3.2.1), consists of a product of mean shears, turbulence intensities, the correlation coefficient R_{22} and the function g_{13}.), and the procedure was dropped when machine computation times required to produce satisfactory accuracy proved excessive.

This prompted a more detailed look at the integrand, and a three-fold application of Simpson's rule was introduced; this gave direct control of the subdivision of the region of integration and allowed the fineness of subdivision to be varied appropriately over the region. It was found that in order to reduce computation time, and increase accuracy to acceptable levels, a preliminary detailed print-out of the integrand was required so that a region of integration adequate but not excessively large could be selected. The computer programme written for this purpose is given in Appendix A-VI.

The importance of the study of the behaviour of the integrand before the overall computation is conducted cannot be over-stressed. The combined effect of the correlation coefficient, turbulence intensity, mean shear, and the g_{13} function is to create an integrand which has a distribution ill-suited to numerical evaluation - in general it has a very high value when the two points involved, $\vec{y}$ and $\vec{z}$, are close together, then falls off rapidly, oscillates and finally becomes insignificant as the separation between $\vec{y}$ and $\vec{z}$ increases. As an initial check on the computer programme and on the procedure outlined, the calculations of Hodgson (1962), using a correlation coefficient given by $\exp(-r^2/y_2^2)$, were repeated and it was found that for a given value of y_2, a region size in (r_1,r_3) space of

$3y_2.3y_2$ gave a numerical accuracy better than 0.1%.† (mesh size = $y_2/40$).

The calculations referred to as Set I (Bull and Lim (1968)) are also based on these region sizes, even though the correlation coefficient used in Set I does not have the same form as that in the calculations of Hodgson. Later work has shown that for the changed correlation coefficient the region sizes given above become inadequate for $Re_\delta^* \geq 10^5$, in which case regions where the correlation coefficient has significant negative values are excluded from the calculation, leading to an overestimation of p'/τ_w. For these region sizes, each evaluation of Equation (3.2.1) requires about 120 seconds of machine time. The later calculations also show that when the region size is increased sufficiently to include all significant values of correlation coefficient for $Re_\delta^* \geq 10^5$, the increasingly peaky character of the integrand with increasing Reynolds number again tends to lead to computation times which are excessively large, if accuracy comparable with that for the lower Reynolds numbers is to be obtained.

At this point the Simpson's rule procedure was replaced by the method of Sag (1963), which, by making appropriate transformation of the integrand, leads to a reduction of 50% or more in machine time for an equivalent accuracy. In all cases in this thesis where the results of an overall machine evaluation of a triple-integral are presented, they have been

---

† This check also indicated that the value of $p'/\tau_w = 2.56$ originally given for this case by Hodgson is too low, and that the correct value is about 4.5. This was confirmed by Dr. Hodgson in private communications.

obtained by Sag's method, with an integration region size determined by prior inspection of the integrand.

3.3 Results and Discussions.

3.3.1 G_{13} and Contributions to $\langle p^2 \rangle / \tau_w^2$.

It has been shown in Section 2 that the consideration of the function G_{13}, which represents the joint contribution of pairs of strata to the wall pressure fluctuations, is the most satisfactory method of characterising contributions from various regions of the boundary layer. The value of G_{13} resulting from the small eddies of the above boundary layer model is more readily calculated than that for the large eddies. For this reason the rather low Reynolds number of 10^3 had been chosen for the results given here, since at this Reynolds number the small eddies account for 90% of the mean square wall pressure fluctuations, and their contribution to G_{13} will serve quite adequately to illustrate the points made in Section 2. (The complete calculation for $Re_\delta^* = 10^3$ gives $\langle p^2 \rangle / \tau_w^2 = 1.204$ of which the small eddies contribute 1.083 in the Set IV series of calculations.)

The results of the calculations of G_{13} for the small eddies, according to Equation (2.6.16) with $\vec{\xi} = \tau = 0$, are shown in figure 8. The numerical procedures for the determination of G_{13} are given in Appendix A-VII. The values of G_{13} are given as sections at constant values of y_2 of the three-dimensional plot of the variation of the non-dimensional parameter $\delta^2 G_{13}(y_2, z_2)/U_\tau^4$ with y_2/δ and z_2/δ. (The discontinuities in the G_{13} curves

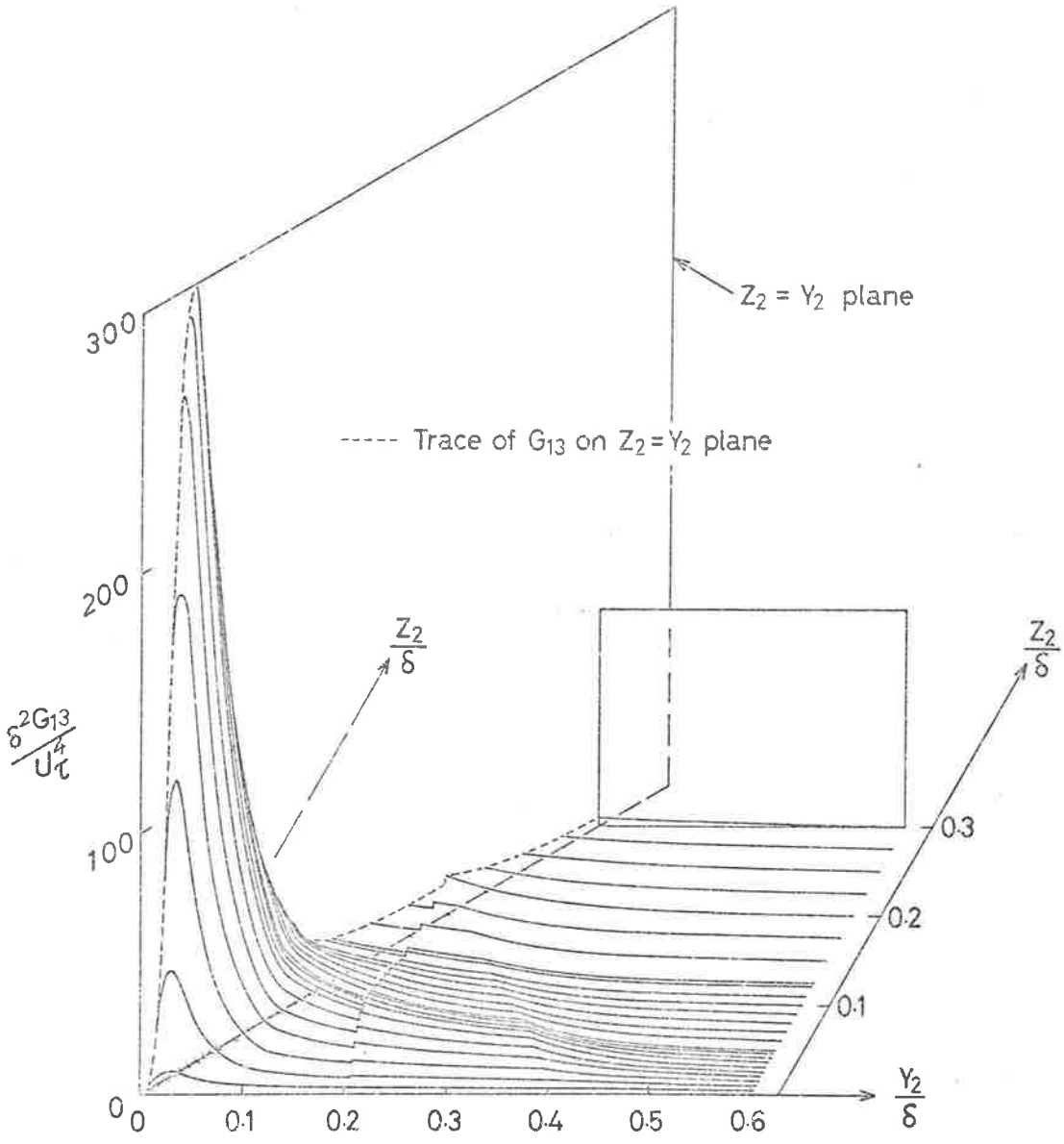

Fig. 8 Variation with y_2 and z_2 of the Joint Contribution Density Function, G_{13}, for the Small Eddy Contribution to the Mean Square Wall-Pressure at $Re_\delta^* = 10^3$.

result from the discontinuity in the assumed form of the $u_2'(z_2)$ versus z_2 curve (Section 3.1.1) at $z_2/\delta = 0.2$ for $Re_\delta^* = 10^3$; no discontinuities occur, for the assumed boundary layer model, for $Re_\delta^* \geq 10^4$. The discontinuities in slope of the G_{13} curves are due to the assumed form of the variation of the scale of the small eddies across the boundary layer; they occur in all cases at $(y_2+z_2)/2 = 0.2\delta$.)

It is clear from the figure that the values of G_{13} for which y_2 and z_2 are almost equal (even though the maxima of G_{13} do not occur at $y_2 = z_2$) make the major contribution to $\langle p^2 \rangle$, but the contribution from values for which y_2 and z_2 differ markedly is not negligible. It is also clear that the major part of the mean square pressure attributable to the small eddies comes, at this Reynolds number, from the inner region of the boundary layer for which both y_2/δ and z_2/δ are less than about 0.3 (y^* and $z^* <$ about 83, where the starred quantities are non-dimensionalised by the friction velocity $U_\tau = (\tau_w/\rho)^{\frac{1}{2}}$ and the fluid kinematic viscosity ν, and τ_w and ρ are the wall shear stress and the fluid density respectively); in fact this region accounts for about 80% of the small eddy contribution to $\langle p^2 \rangle$, that is, $C(0,0.3\delta) \simeq 0.8\, C(0,\infty)$.

Integration of the $\delta^2 G_{13}/U_\tau^4$ curves of figure 8 over z_2/δ yields the function

$$\frac{\delta}{U_\tau^4} \int_{z_2}^{\infty} dz_2 \; G_{13}(y_2, z_2) \quad ,$$

which can be expressed also in terms of the P and C functions used

previously (Section 2.4 and 2.5) as

$$\frac{\delta}{\tau_w^2}\,\frac{\partial}{\partial y_2}\left[P(y_2,\infty) - C(0,y_2)\right] = -\frac{\delta}{\tau_w^2}\,\frac{\partial C(y_2,\infty)}{\partial y_2}\ .$$

Its distribution is shown in figure 9. This figure also shows the non-dimensional form of the function "$\partial\langle p^2\rangle/\partial y_2$" of Equations (2.5.8) and (2.5.9), namely

$$\frac{\delta}{U_\tau^4}\int_{y_2}^{\infty} dz_2\, F_{13}(y_2,z_2) = \frac{\delta}{\tau_w^2}\,\frac{\partial P^*(y_2,\infty)}{\partial y_2}\ ,$$

F_{13} having been calculated from Equation (2.6.14) with $\vec{\xi} = \tau = 0$.

The integration of either curve over y_2/δ gives the small eddy contribution to $\langle p^2\rangle/\tau_w^2$. The difference between the two curves emphasises the possibility of error in deducing which regions of the boundary layer make the most important contributions to the mean square wall pressure fluctuations from curves, such as these, which represent first rather than second derivatives.

Further emphasis can be given to the point, by noting that if the curves in figure 9 were interpreted at their face value, it would, for example, be concluded from a further integration of the G_{13} curve that the region of the boundary layer between the boundary and $y_2/\delta = 0.13$ is responsible for 80% of the small eddy contribution to the mean square wall pressure fluctuations. On the other hand, the integration of the F_{13} curve would lead to the conclusion that the region between the boundary and $y_2/\delta = 0.23$ is responsible for the same contribution. However, the

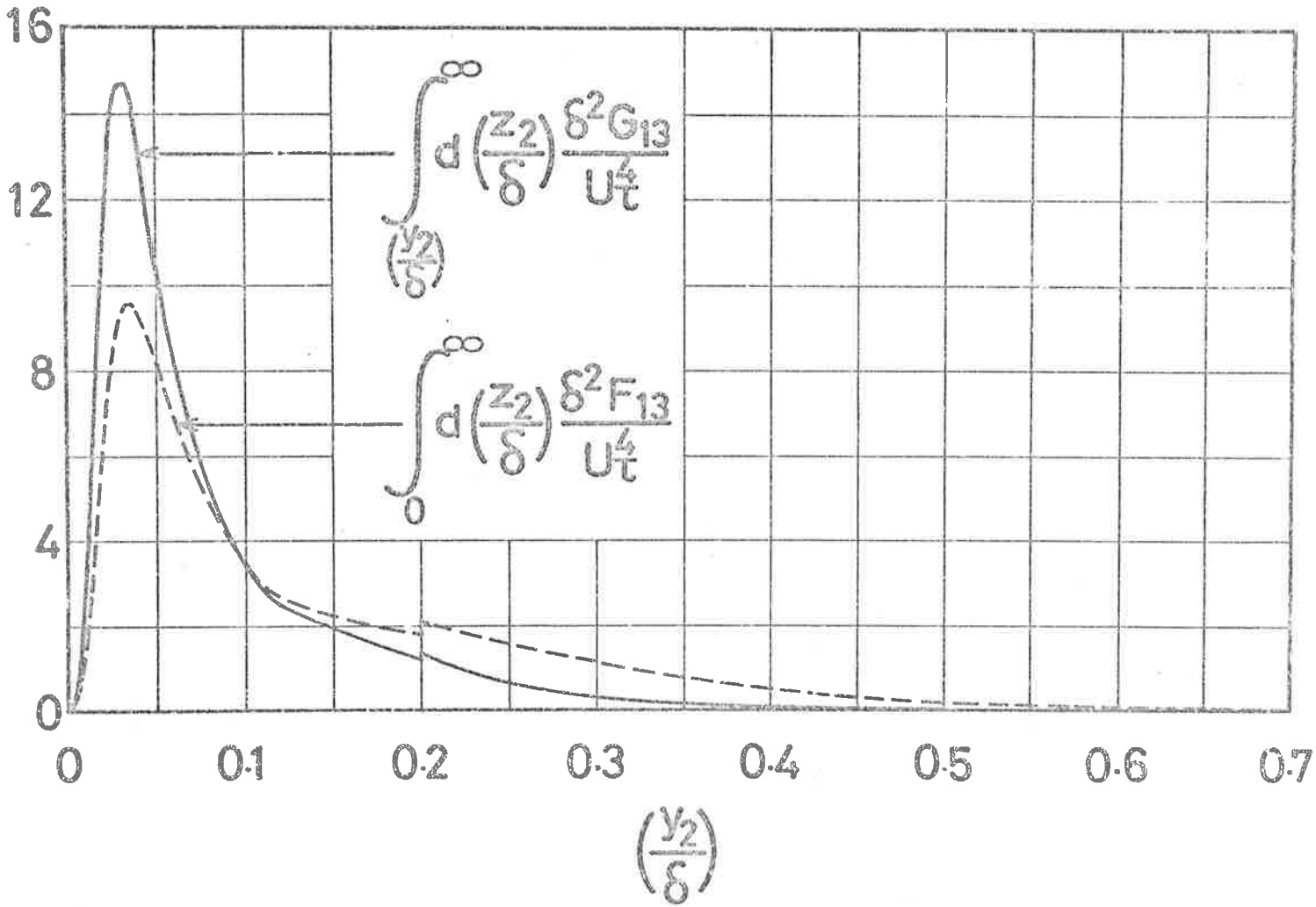

Fig. 9 Variation with Distance from the Wall of the F_{13} and G_{13} Functions Integrated only Once(with Respect to the Co-ordinate z_2 Normal to the Wall). $Re_{\delta^*} = 10^3$.

consideration of the function C which, since it includes only correlation of sources within the region considered, should be regarded as a superior indicator to either of the previous ones, indicates, as shown above, that the region between the boundary and the considerably larger value of $y_2/\delta = 0.3$ is required to produce the chosen contribution. This again points to the fact that for the correct deductions to be made, a carefully defined function such as C or, better still, the joint contribution density function C_{13} itself must be considered.

3.3.2 The Root Mean Square Wall Pressure Fluctuations.

The mean square wall pressure fluctuations arising from a two-dimensional, incompressible turbulent boundary layer on the assumption of the dominance of the turbulence/mean-shear interaction in the generation of the fluctuating pressure is given by Equation (3.1.2). In the past (see, for example, Hodgson (1962)) the solution of Equation (3.1.2) has been more in the nature of a calculated estimate with the use of gross assumptions on the nature of the properties of the turbulent boundary layer. The boundary layer model used here for the evaluation of $\langle p^2 \rangle$ has been detailed in Section 3.1 and as this represents the turbulent velocity field more closely than those used previously, it should be possible to regard the computed value for the fluctuating wall pressure with a higher degree of confidence.

As a consequence of the representation of the R_{22} correlation coefficient as the sum of two parts (Equation (3.1.9)) in the boundary

layer model used for the calculations, the mean square wall pressure fluctuations can also be represented in the same way, as the sum of small and large eddy contributions. In the calculations, with the exception of Revised Set I, these contributions have been considered separately throughout. For one or two Reynolds numbers in the case of Set II, a complete calculation of $\langle p^2 \rangle$ by Method 2 has not been carried out, only the large eddy contribution having been evaluated; however, in all such cases an overall value of $\langle p^2 \rangle$ has been obtained by Method 1, and the small eddy contribution obtained by difference. (See Table 3.1.)

The values of $I^s_{13}(y_2,z_2)$, according to Equations (2.6.15) and (3.1.10), which are required for calculations by Method 2 (see Section 3.2.1), are shown as a function of r_2/s in figure 10(a) for s given by Equation (3.1.14); the corresponding values for s given by Equation (3.1.19) are shown in figure 10(b). The two sets of curves of course become identical for $y_2/\delta \geq 0.4$. The joint contribution density function (Section 2) for the small eddies G^s_{13}, for any Reynolds number, can be obtained from these I^s_{13} values, which are independent of Reynolds number, by weighting them with the appropriate turbulence intensity and mean shear values, using Equation (2.6.16).

The total calculated root mean square wall pressure fluctuation values for Revised Set I, Sets II and IV are shown as a function of Reynolds number in figure 11 for $10^3 \lesssim Re_\delta^* \lesssim 10^7$, where the results of Bull (1967), Willmarth and Wooldridge (1963) and those from the present series of measurements in a constant pressure turbulent boundary layer have been

Table 3.1 Summary of $\langle p^2 \rangle$ Calculations for Constant Pressure Turbulent Boundary Layer (x indicates calculation carried out).

Reynolds number Re_δ^*		10^3	10^4	10^5	10^6	10^7
Revised Set I	Overall $\langle p^2 \rangle$ by Method 1.	x	x	x	x	
Set II	Small eddy contribution by Method 2.	x	x	(Obtained by difference between Method 1 & large eddy contribution.)		x
	Large eddy contribution by Method 2.	x	x	x	x	x
	Overall $\langle p^2 \rangle$ by Method 2.	x	x			x
	Overall $\langle p^2 \rangle$ by Method 1.		x	x	x	
Set IV	Small eddy contribution by Method 2.	x	x	x	x	x
	Large eddy contribution by Method 2.	x	x	x	x	x
	Overall $\langle p^2 \rangle$ by Method 2.	x	x	x	x	x
	Overall $\langle p^2 \rangle$ by Method 1.		x			

NOTE: For Set II, $Re_\delta^* = 10^4$, the calculation of the small eddy contribution by Method 2 was checked by a direct three-fold integration using the method of Sag (1963).

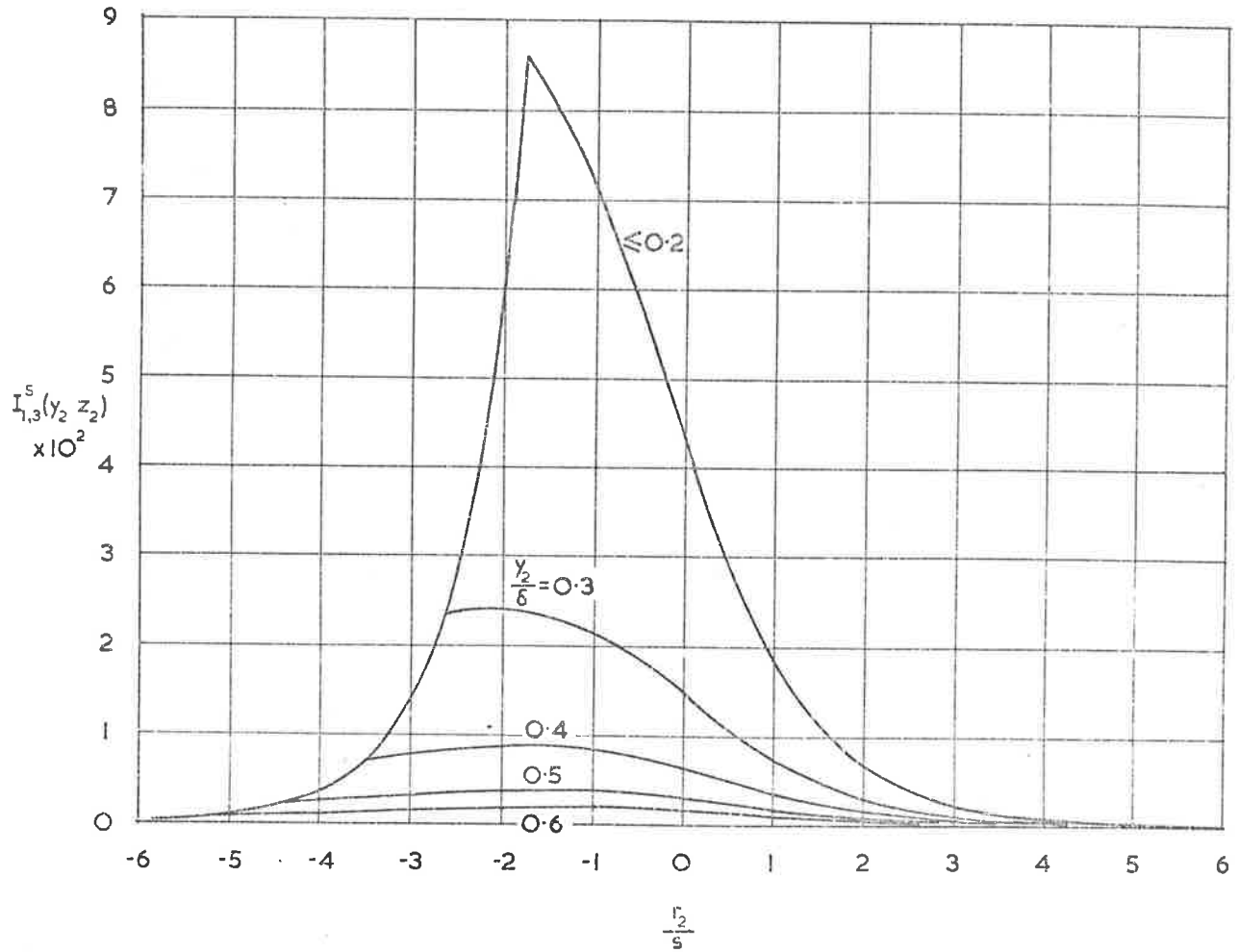

Fig. 10 (a) Variation of I_{13} with Separation Distance Normal to the Wall — Set II Calculations.

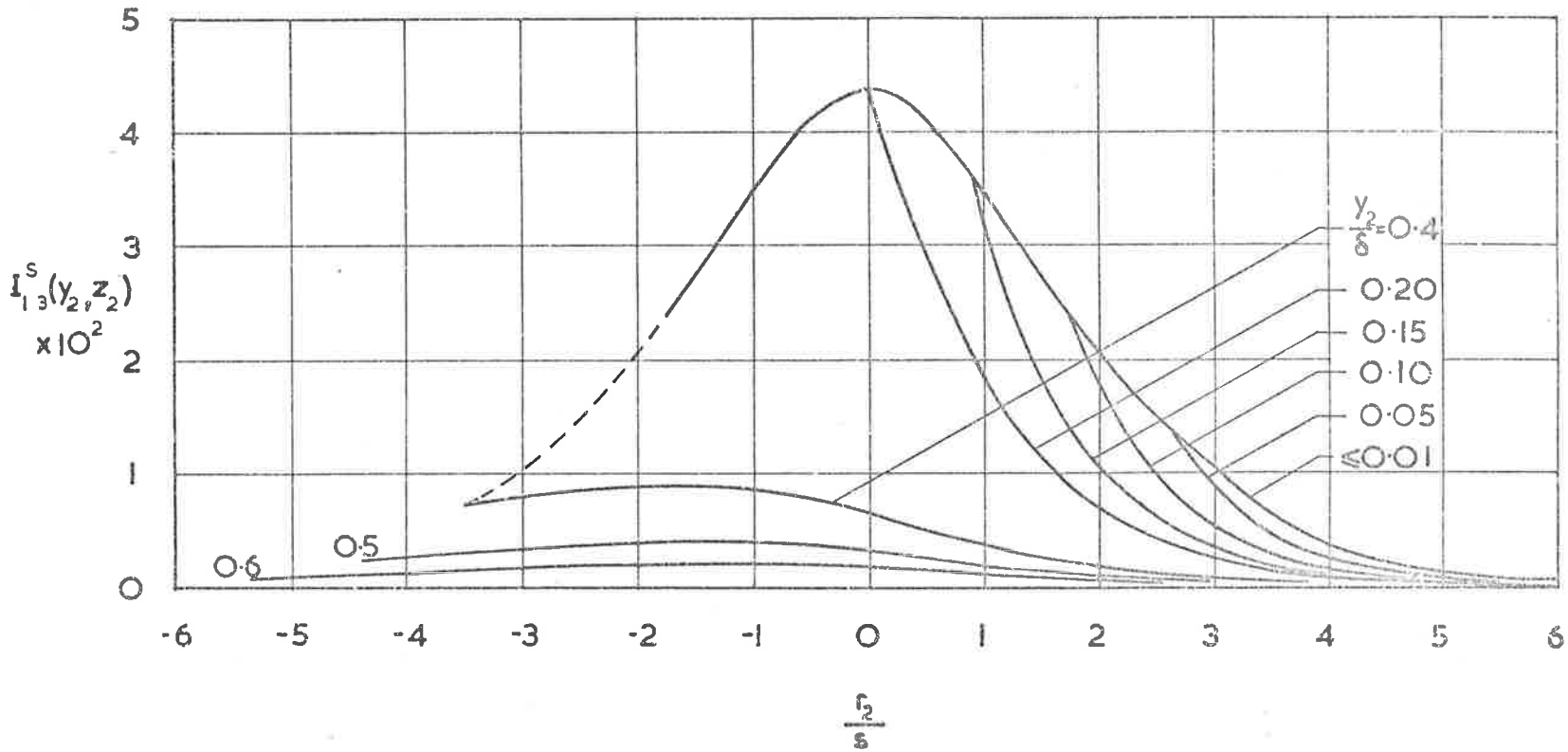

Fig. 10 (b) Variation of I_{13} with Separation Distance Normal to the Wall — Set IV Calculations.

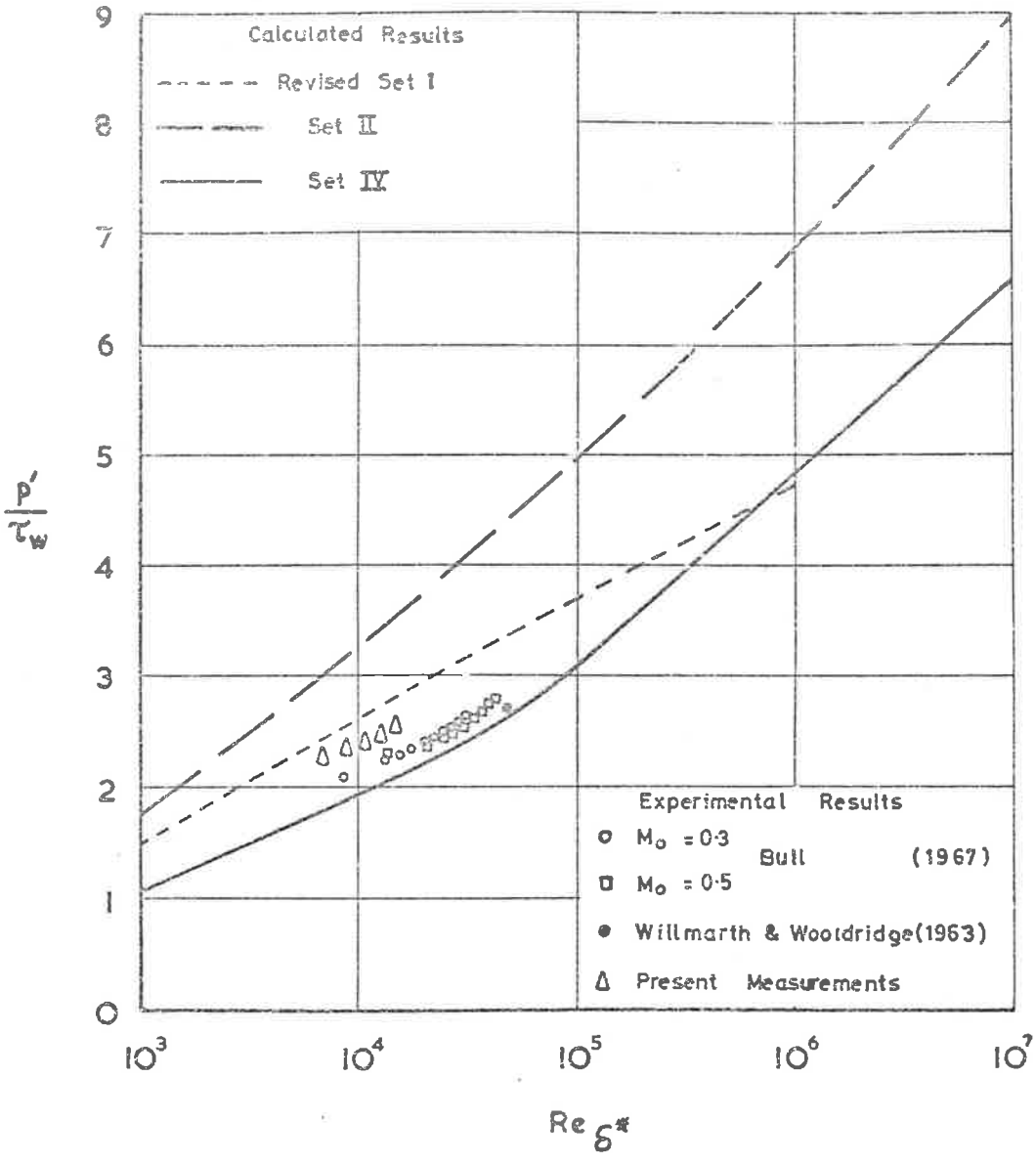

Fig.11 Effect of Reynolds Number on Root Mean Square Wall Pressure Fluctuations.

included for comparison.

The variation with Reynolds number of the separate contributions of the large and small eddies to the overall mean square pressure for Sets II and IV are shown in figures 12(a) and 12(b) respectively.

Table 3.1 summarises the calculations which were made to obtain the $\langle p^2 \rangle$ values, and also indicates the checks which have been made, by using Methods 1 and 2, on the accuracy and consistency of the computer programmes and the method of choosing region sizes for the integrations. The main checks were made for $Re_\delta^* = 10^4$ (although less extensive checks were made for other Reynolds numbers). For Set II the check on the calculation of the small eddy contribution by Method 2 referred to in Table 3.1 gave agreement within 0.1%, and the machine calculated values of $\partial P^*(y_2,\infty)/\partial y_2$ (required for the final manual integration giving $\langle p^2 \rangle$) agreed within 0.1%. In the case of Set IV the agreement between the values of $\partial P^*(y_2,\infty)/\partial y_2$ obtained by Methods 1 and 2 was not as good as for Set II; this difference led to a difference of about 0.8% in the resultant values of $\langle p^2 \rangle$. The source of the error was traced to the fact that, for Set IV, the scale representation of the small eddies leads to an integrand which would require the integration region for Method 1 to be subdivided slightly more finely than in the computer programme used for Set II to achieve the same numerical accuracy. The check can therefore still be regarded as satisfactory, and the results given for Set IV are those obtained by Method 2 which avoids this problem.

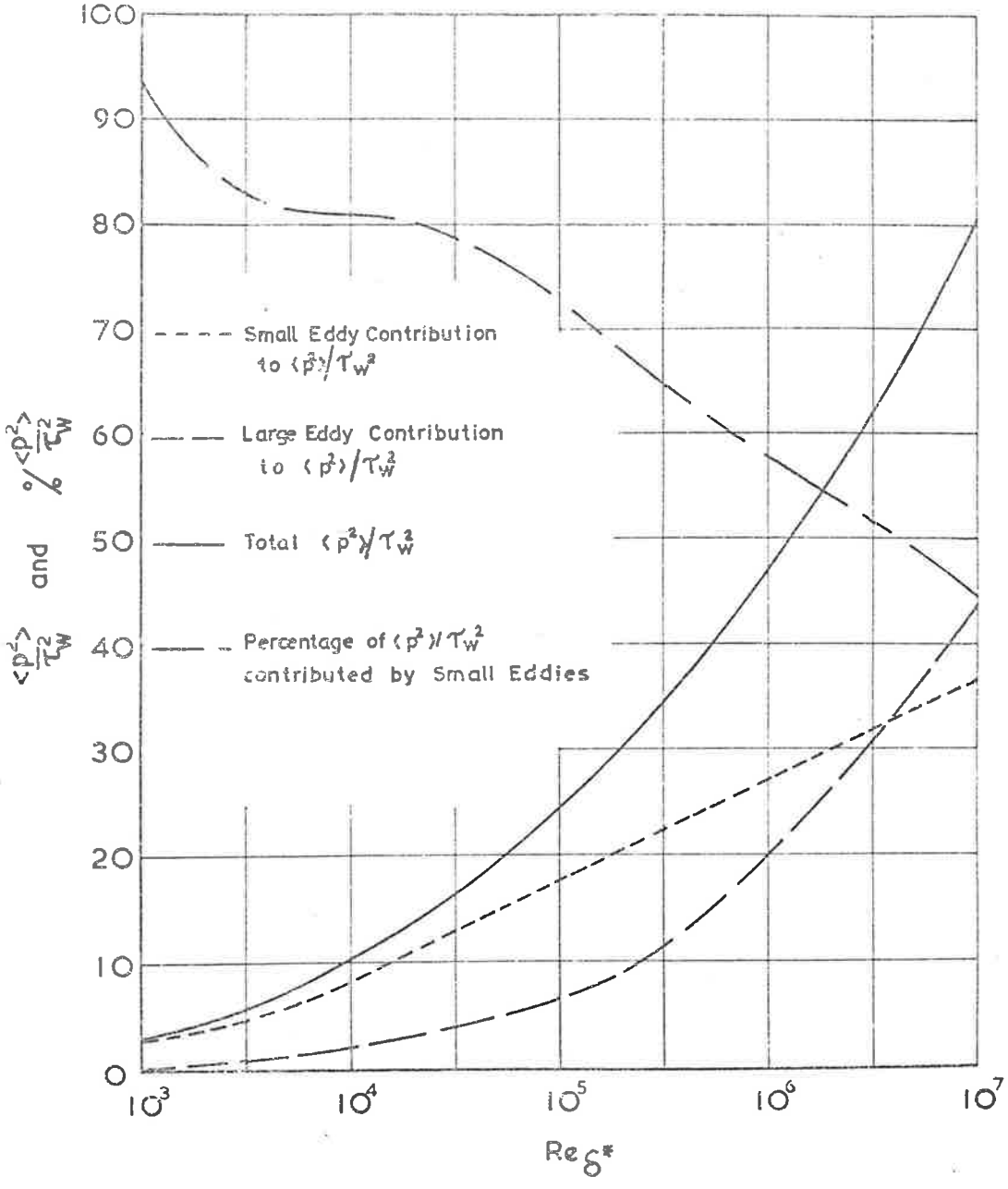

Fig. 12 (a) Effect of Reynolds Number on Calculated Small and Large Eddy Contributions to the Mean Square Wall Pressure Fluctuations. Set II

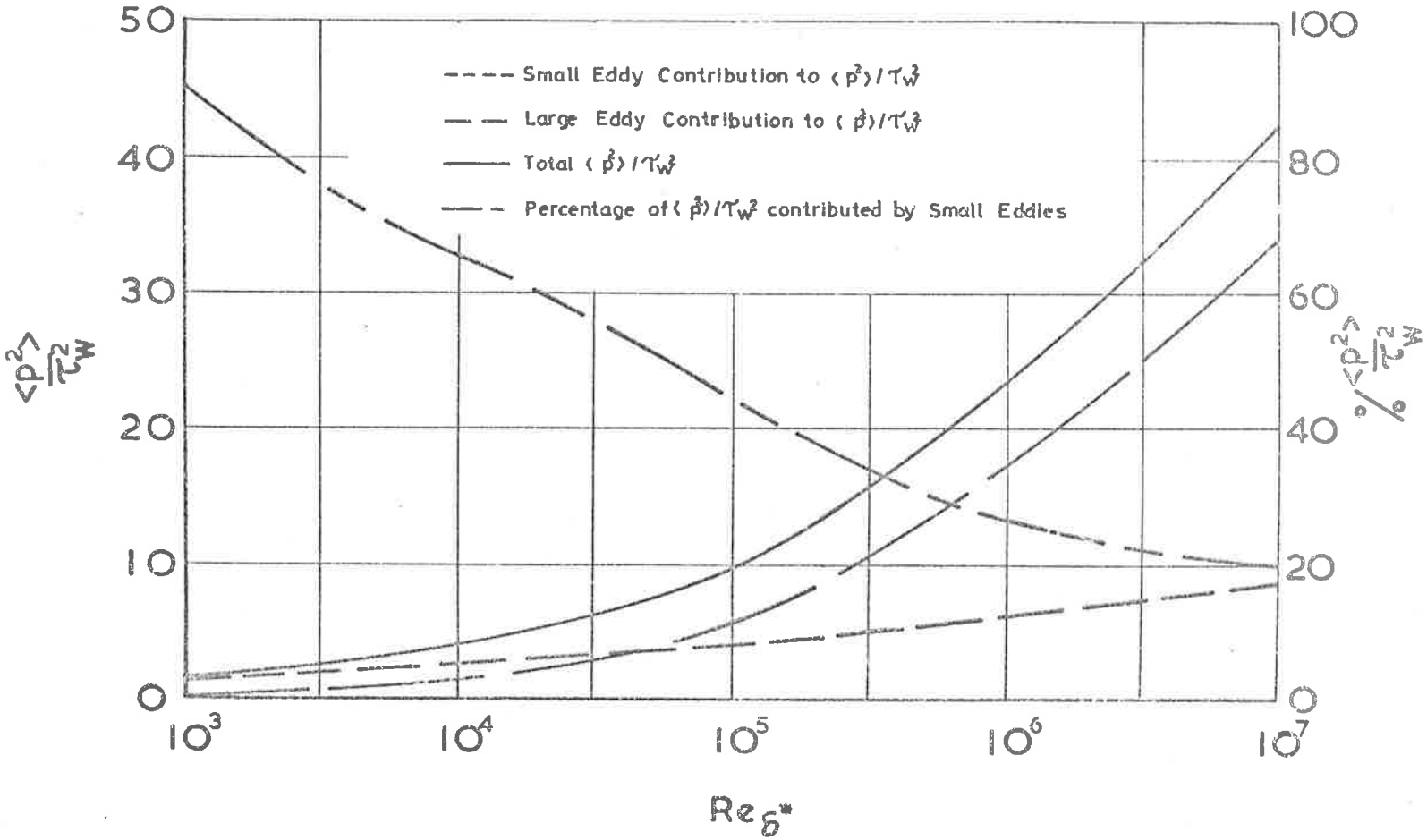

Fig. 12(b) Effect of Reynolds Number on Calculated Small and Large Eddy Contributions to the Mean Square Wall Pressure Fluctuations. Set. IV.

It will by now have become obvious that the characteristics of the boundary layer models assumed in the various sets of calculations, and the calculation procedures, have been given in considerable detail. This has been done intentionally, so that there should be no doubt or ambiguity concerning the assumptions on which any particular set of results is based; it is further justified by the conclusion reached in the discussion to follow, that the numerical values obtained for $\langle p^2 \rangle$ depend quite critically on the details of the representation of the turbulent velocity field, and it therefore seems highly desirable that this detailed information should be readily available to assist anyone to make a considered assessment of the results.

Before considering the $\langle p^2 \rangle$ values themselves, it is perhaps worth noting that the integrand in the double-space integral for the space-time covariance of the wall pressure fluctuations, Equation (2.1.9), contains the product of $|\vec{x}-\vec{y}|$ and $|\vec{x}'-\vec{z}|$ in the denominator, and therefore tends to infinity as the two field points, $\vec{y}$ and $\vec{z}$, approach the boundary surface points $\vec{x}$ and $\vec{x}'$ respectively (in the corresponding expression for $\langle p^2 \rangle$, $\vec{x}$ and $\vec{x}'$ are of course coincident). In the reductions and modifications of Equation (2.1.9) which have been made, this property of the integrand is transferred to the function g_{13} which, in the case of $\langle p^2 \rangle$, tends to infinity as y_2, z_2, r_1 and r_3 all approach zero. However, this characteristic of g_{13} is offset by the behaviour of R_{22} near the boundary, and the integration of this product, as in Equation (2.6.15), leads to values of $I_{13}(y_2,z_2)$ which are finite for all y_2 and z_2 including $y_2 = z_2 = 0$. The behaviour of $I^s_{13}(y_2,z_2)$ as y_2 and z_2 approach zero can

be seen in figures 10(a) and 10(b).

The results of the three sets of calculations of p'/τ_w given in figure 11 show two important effects. Firstly, the difference between the results of Revised Set I and Set II is essentially the result of a change in specification of the correlation coefficient R_{22} (check calculations indicate that the small difference between the two cases in specification of the scale of the small eddies, and the difference in the assumed mean shear distribution near the boundary, have only minor effects). The difference between the assumed values of R_{22} for the two calculations can be seen by comparing figures 6(a) and 6(b) with figures 6(c) and 6(d). For a given datum point, the two specifications of R_{22}, Equation (3.2.4) with the small eddy scale s as given by Bull and Lim (1968), and Equations (3.1.8), (3.1.9) and (3.1.10) with s given by Equation (3.1.14), respectively, give almost identical values provided that the second correlation point is located on a line through the datum point parallel to one of the three main cartesian co-ordinate directions; but, for other directions, the correlation coefficient for Revised Set I falls off to zero more rapidly with increasing separation distance than that for Set II. This leads to lower values of $\langle p^2 \rangle/\tau_w^2$ for Revised Set I than for Set II. The amount of the reduction increases with Reynolds number from about 27% at $Re_\delta^* = 10^3$ to about 52% at $Re_\delta^* = 10^6$ (with corresponding reductions in p'/τ_w of about 15% and 31% respectively). Secondly, the difference between the values of p'/τ_w obtained in Sets II and IV results only from a change in the form of specification of the scale of the small eddies; only in the latter case is the reciprocity relationship, which must be satisfied in

the real physical flow, satisfied by the model used for the calculations. The effect of the scale specification on the correlation coefficient R_{22} can be seen in figures 6(a) and 6(b), the former for the region where the scale is varying with distance from the boundary, the latter for a region where the scale is constant. Again the change produces large reductions in the value of $\langle p^2 \rangle / \tau_w^2$, although in this case, in the main, the amount of the reduction falls with increasing Reynolds number, being about 60% at $Re_\delta^* = 10^3$ and about 47% at $Re_\delta^* = 10^7$ (or about 37% and 27% respectively in p'/τ_w).

The solution of the equations of motion for the mean square wall pressure fluctuations is obtained as a six-fold integral of the whole of the turbulent velocity field in the boundary layer; as such its value might be thought to be insensitive to the details of the particular boundary layer model on which calculations are based, as a result of blurring of the details by the multiple integration process. The two effects just discussed indicate quite clearly that this is not so, and that the calculated values of $\langle p^2 \rangle$ are very much dependent on the detailed assumptions made about the turbulent velocity field.

Of the three boundary layer models for which the mean square wall pressure fluctuations have been calculated, that for Set IV must be regarded as the most physically realistic. Figure 11 also shows a comparison of the experimental results of Bull (1967) which have been corrected for lack of resolution of the pressure transducers with which they were obtained, and the value obtained by Willmarth and Wooldridge

(1963) by extrapolation to zero transducer size of measurements made with several sizes of transducers. The results obtained from the present series of measurements made in the constant pressure turbulent boundary layer have also been included. It does seem to be significant that, while the two models which are less acceptable physically (those for Revised Set I and Set II) lead to overestimates of $\langle p^2 \rangle$ compared with the experimental results, the model for Set IV yields values of $\langle p^2 \rangle$ which are less than the experimental values. Considered physically, the latter is a more acceptable result, since the values of $\langle p^2 \rangle$ have been calculated on the assumption of dominance of turbulence/mean-shear interaction, and the difference between the calculated and experimental values can be ascribed to the combined effect of pressure source terms which have been ignored (it is of course conceivable that the neglected terms make a negative contribution to $\langle p^2 \rangle$, but the situation just referred to seems the more plausible).

From the results obtained the indications are quite definitely that, for a two-dimensional incompressible turbulent boundary layer, turbulence/mean-shear interaction is the dominant process in producing wall pressure fluctuations, and, from the comparison of the Set IV results with experiment, that it is responsible for the generation of roughly 80% of the mean square wall pressure fluctuation.

Although the experimental data cover a more limited Reynolds number range than the calculations, the Set IV results appear to reproduce the experimental variation over this limited range very well (figure 11). The

calculations also indicate that for large variations in Reynolds number the value of p'/τ_w can be expected to vary considerably; the Set IV results indicate a rise in the contribution of turbulence/mean-shear interaction to p'/τ_w from 1.10 at $Re_\delta^* = 10^3$ to 6.51 at $Re_\delta^* = 10^7$. It would therefore appear that the single representative value of p'/τ_w obtained in previous calculations (for example, Lilley and Hodgson's (1960) value of about 3.0) is typical only of the limited range of Reynolds number which has so far been explored experimentally. It might be noted that the corresponding variation of p'/q_∞ with Reynolds number is less marked being from 4.9×10^{-3} to 6.8×10^{-3}, where $q_\infty = \frac{1}{2}\rho U_\infty^2$.

Figures 12(a) and 12(b), for Set II and Set IV respectively, show that at a low Reynolds number the small eddies make the dominant contribution to $\langle p^2 \rangle$ (over 90% at $Re_\delta^* = 10^3$), but that the proportion of $\langle p^2 \rangle$ contributed by them falls off as the Reynolds number increases - for Set II the proportion falls off to about 45% at $Re_\delta^* = 10^7$, while for the physically more realistic Set IV the fall-off rate with increasing Reynolds number is even more rapid, the proportion being down to about 20% at $Re_\delta^* = 10^7$. This implies, as can be seen from inspection of figures 12(a) and 12(b), that the variation of the total value of $\langle p^2 \rangle$ with Reynolds number is predominantly a reflection of the variation of the absolute value of the large eddy contribution with Reynolds number.

The effects of the Reynolds number on the distributions of the turbulence intensity and the mean shear have been described in Section 3.1 and shown in figures 2 and 3 respectively. It can be seen that the effect

of an increase in the Reynolds number is not only to increase the value of the turbulence/mean-shear product for $y_2/\delta < 0.2$ but also to extend towards the wall the region over which the turbulence intensity has its maximum value. The mean square pressure has been given by Equation (3.1.2) which contains the product of the mean shear, the turbulence intensity, the correlation coefficient and the geometric term g_{13} as the integrand. For the boundary layer model used, the last two terms have no Reynolds number dependency so it would appear that the variation of the large or small eddy contribution comes about only as a result of the Reynolds number effect on the turbulence/mean-shear product. However, this would only be so if the correlation coefficient associated with the small eddies were exactly the same as that for the large eddies, since the contributions to the mean square pressure also result from integral effects of the correlation functions. The small eddies are correlated only over small distances, and their scale variation (see figure 5) is such that the correlation coefficient approaches a delta function near the boundary. Since the Reynolds number effect on the boundary layer model is to increase the turbulence/mean-shear product near the boundary the increase in the small scale contribution to the mean square pressure comes from the summation of mainly localised increases in the value of the integrand of Equation (2.6.16). On the other hand, the slow fall-off of the large scale correlation coefficient results in the summation of the increases over a considerably larger region of the boundary layer and, it is the difference between "localised" summation of increases and region summation which accounts for the dissimilar variation of the small scale and large scale contributions with Reynolds number. So, the variation of the mean square wall pressure fluctuations with Reynolds number is due not only to

the variation of the turbulence/mean-shear product, as would initially appear, but also to the correlation scales associated with the turbulence.

3.3.3 The Auto-Covariance of the Fluctuating Wall Pressure and Its Frequency Power Spectrum.

The general equation of the space-time covariance of the pressure fluctuations in turbulent shear flow has been derived in Section 2.1. Under the assumption of the dominance of the turbulence/mean-shear interaction in the generation of the fluctuating pressure, the equation of the pressure covariance for the case of a slowly growing boundary layer in which the turbulence can be regarded as statistically stationary in time and homogeneous in planes parallel to the boundary has been given by Equation (3.1.1). When $\vec{x}' = \vec{x}$, $\vec{\xi} = 0$ and the space-time covariance becomes the auto-covariance which is given by

$$\langle p(\vec{x},t)p(\vec{x},t')\rangle = \rho^2 \int_0^\infty dy_2 \int_0^\infty dz_2 \; G_{13}(y_2,z_2,0,\tau) \quad , \qquad \ldots(3.3.1)$$

where $G_{13}(y_2,z_2,0,\tau)$ and associated expressions can be derived from those given in Section 2.6 by subtituting $\vec{\xi} = 0$ in each of the expressions. As has been pointed out in Section 3.1, the solution of Equation (3.3.1) requires a knowledge of the space-time correlation coefficient distribution of the fluctuating component of the velocity normal to the boundary. Available data for non-zero time delays are not sufficiently comprehensive to be of use. However, if use is made of Taylor's (1938) hypothesis for a "frozen" turbulence pattern, we can write

$$R_{22}(y_2,z_2,r_1,r_3,\tau) = R_{22}(y_2,z_2,r_1-U_c\tau,r_3,0) \quad , \qquad \ldots(3.3.2)$$

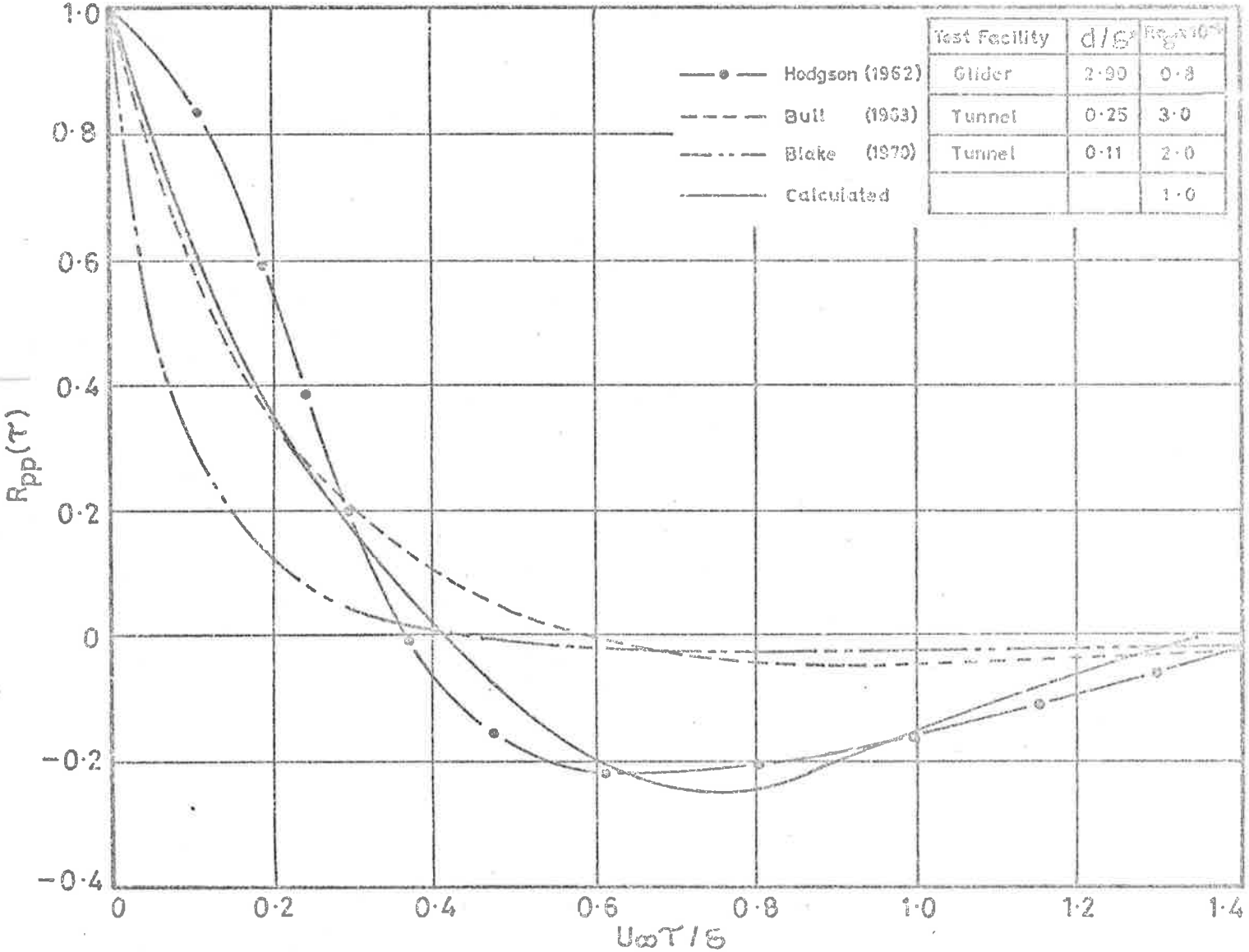

Fig. 13 Calculated Autocorrelation $Re_{\delta^*}=10^4$ with corresponding Experimental Results.

where y_2 is the distance of the datum point from the boundary surface and U_c is the convection velocity of the velocity field at a distance z_2 from the boundary. The required space-time correlation function is then easily obtained from the space correlation. The detail of the transformation has been given in Section 3.1.3.

The calculated auto-covariance of the wall pressure fluctuations in a constant pressure turbulent boundary layer is shown in figure 13 where $Re_\delta^* = 10^4$, and the boundary layer model which has been detailed in Section 3 satisfies the reciprocity relationship and is the most physically realistic of the models considered to date. The auto-covariance is given in the form of the correlation coefficient defined as

$$R_{pp}(\tau) = \frac{Q_{pp}(\tau)}{\langle p^2 \rangle} \quad , \qquad \ldots(3.3.3)$$

$$Q_{pp}(\tau) = \langle p(\vec{x},t)\, p(\vec{x},t+\tau) \rangle \quad , \text{ and}$$

$$\langle p^2 \rangle = Q_{pp}(0) \quad .$$

The computer programme for the selection of the region over which the numerical integration is to be carried out is given in Appendix A-VIII and that for the numerical evaluation of the auto-covariance using the procedure of Sag (1963) is given in Appendix A-IX.

The experimental results derived from the mean experimental curves of $R_{pp}(0,0,0,\tau)$ versus ξ_1/δ^* obtained by Hodgson (1962), Bull (1967) and Blake (1970) have been included for comparison. Hodgson's results were obtained from the measurements made on the wing of a glider in flight, the

corresponding Reynolds number Re_δ^* has been estimated to be 0.8×10^4. The results from Bull and from Blake were from measurements in wind tunnels with $Re_\delta^* \simeq 3 \times 10^4$ in the former case and $Re_\delta^* \simeq 2 \times 10^4$ for the latter. In each of the three cases, the abscissa has been converted to the form $\tau U_\infty/\delta$ from ξ_1/δ^* ($= \tau U_c/\delta^*$) with the assumption that $U_c/U_\infty = 0.8$.

It can be seen from figure 13 that the calculated results of R_{pp} for close separations has the form taken by the results of Bull for which $0.15 < d/\delta^* < 0.5$, where d is the diameter of the transducer sensing element. Blake's results which were for $0.101 < d/\delta^* < 0.113$ has a higher rate of decay indicating that the better resolution of the transducers which have been used is significant. At larger separations, the calculated values give a curve which has a form similar to that obtained by Hodgson whose measurements were made with a relatively large transducer giving $d/\delta^* = 2.93$. It can be noted that the longitudinal integral scale and the integral time scale defined by Equations (1.2.10) and (1.2.11) respectively, are zero.

The Fourier transform of the auto-covariance $Q_{pp}(\tau)$ with respect to time gives the spectral function

$$\phi_{pp}(\omega) = \frac{1}{2\pi} \int_{-\infty}^{\infty} Q_{pp}(\tau)\, e^{-i\omega\tau}\, d\tau \quad , \qquad \ldots(3.3.4)$$

the inverse relationship being

$$Q_{pp}(\tau) = \int_{-\infty}^{\infty} \phi_{pp}(\omega)\, e^{i\omega\tau}\, d\omega \quad . \qquad \ldots(3.3.5)$$

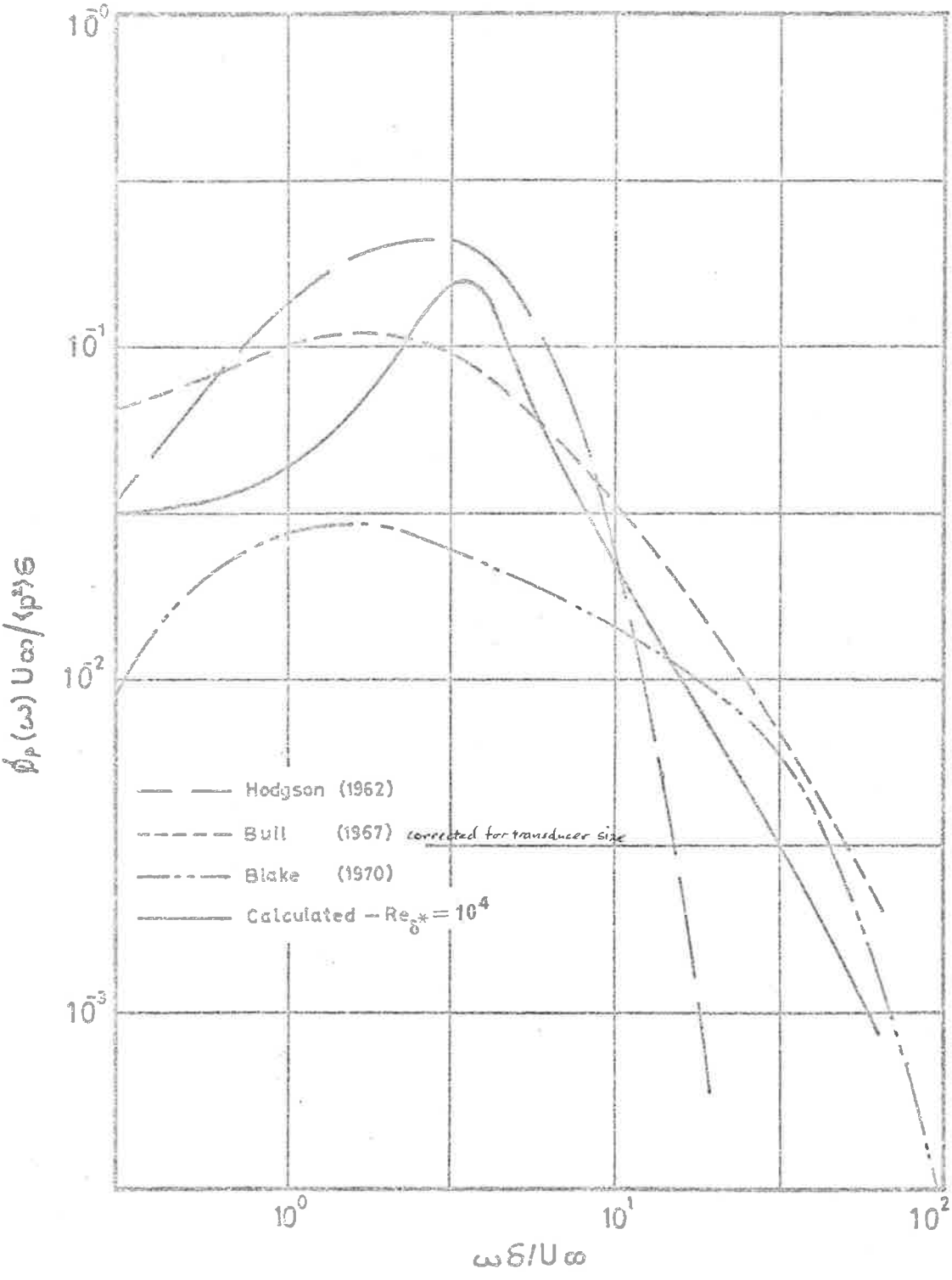

Fig. 14a Frequency Spectra of Wall-Pressure Fluctuations.

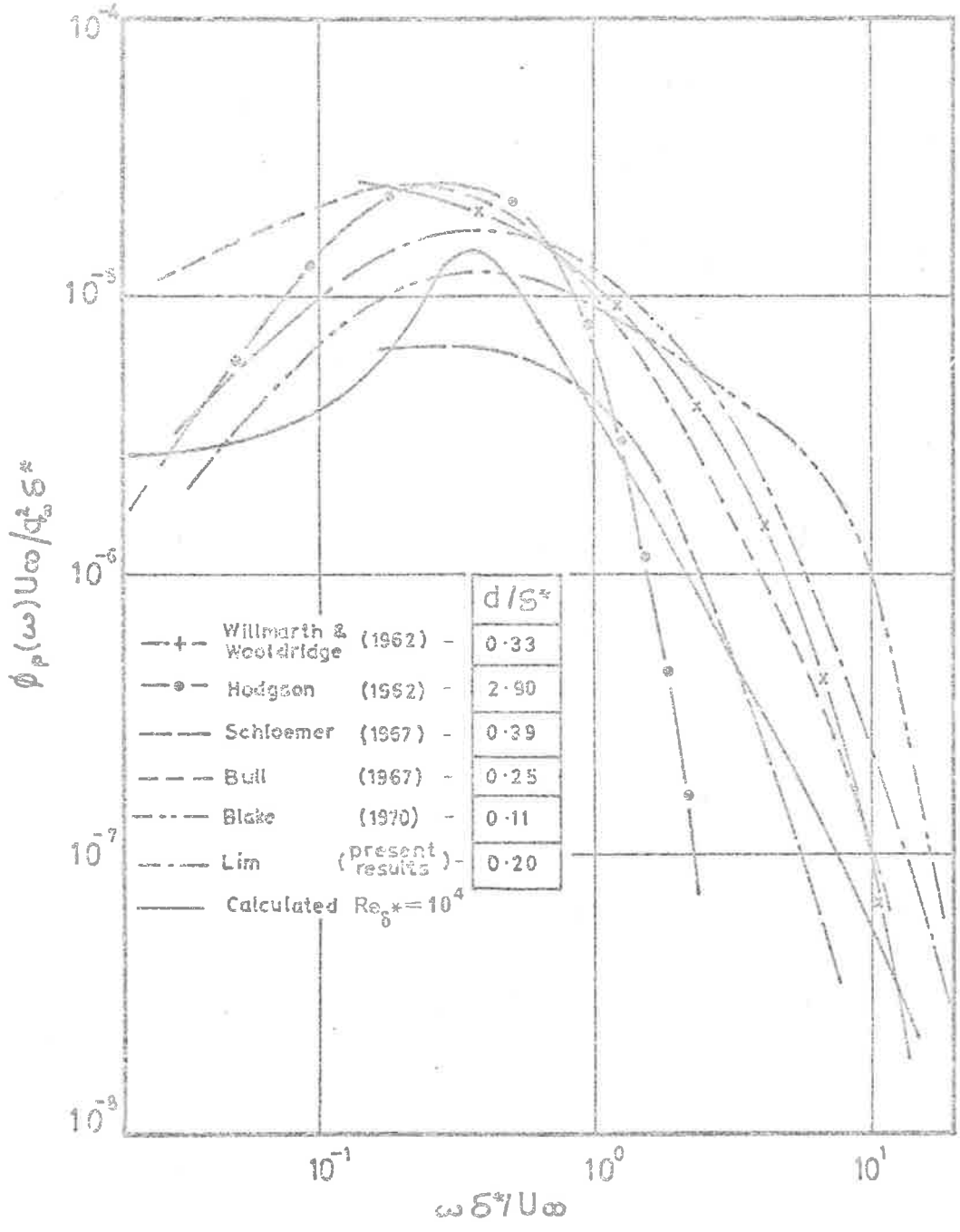

Fig. 14 b Frequency Spectra of Wall-Pressure Fluctuations.

The frequency power spectral density $\phi_p(\omega)$ of the pressure fluctuations as measured by a wave analyser is given by

$$\phi_p(\omega) = \frac{2}{\pi} \int_0^\infty Q_{pp}(\tau) \cos \omega\tau \, d\tau \quad . \qquad \ldots(3.3.6)$$

In the determination of $\phi_p(\omega)$ with the use of Equation (3.3.6), the fitted curve to the calculated distribution of $R_{pp}(\tau)$ shown in figure 13 was used to represent $Q_{pp}(\tau)$. The resultant distribution of $\phi_p(\omega)$ for the constant pressure turbulent boundary layer for which $Re_\delta{}^* = 10^4$ is shown in figures 14(a) and 14(b).

Bull (1967) has used the form of the spectral distribution plotted as $\phi_p(\omega)U_\infty/\langle p^2\rangle\delta$ versus $\omega\delta/U_\infty$ as shown in figure 14(a) in an effort to obtain a collapse of the spectral values, and to determine from the mean distribution of the data interpolated values at high frequencies not obtainable in the thinner boundary layers due to limitations in the measuring equipment. The curve obtained for the boundary layer model is compared with those representing the mean experimentally determined distributions of Hodgson (1962), Bull (1967) and Blake (1970). The different characteristics of the distribution indicate markedly different frequency characteristics, a condition which is better shown in figure 14(b) where the values have been plotted in the non-dimensional form $\phi_p(\omega)U_\infty/q_\infty^2\delta^*$ versus $\omega\delta^*/U_\infty$, with $q_\infty = \frac{1}{2}\rho U_\infty^2$ representing the dynamic head of the free stream. In addition to the results of Hodgson, Bull and Blake, the mean experimental curves of Willmarth and Wooldridge (1962), Schloemer (1967) and that from the present series of measurements for which $0.14 < d/\delta^* < 0.3$ have been included in the plot for comparison. Each of

the pressure spectra shows a peak in the region $\omega\delta^*/U_\infty = 0.3$, and the distribution of the spectral density calculated from the boundary layer model described in Section 3 can be seen to fall within the range covered by the various experimental curves. Although Hodgson's results were for a relatively large transducer, his results for the low frequencies can be expected to suffer less from the effect of a low signal to noise ratio than those obtained in wind tunnels, and his values of $\phi_p(\omega)U_\infty/q_\infty^2\delta^*$ for $\omega\delta^*/U_\infty$ less than about 1.0 can be regarded with greater confidence. At frequencies higher than for $\omega\delta^*/U_\infty = 1.0$, the results of Blake for which $d/\delta^* \simeq 0.1$ can be expected to be more representative of the actual pressure field due to the better transducer resolution at the higher frequencies. Certain points can now be made on the comparison of the calculated values with the experimental ones. On the basis that Hodgson's results can be taken as representative of the actual distribution of the spectral density of the wall pressure fluctuations at the lower frequencies and that those of Blake as that at the higher frequencies, the calculated values of the spectral density are low at all frequencies (even when it is remembered that the calculated value represents only about 80% of the total mean square pressure - see p. 88). For frequencies in the range $0.3 < \omega\delta^*/U_\infty < 3.0$, that is, beyond the frequency at which the spectral distribution shows a peak and below the frequency at which transducer resolution might affect Blake's data, the calculated values fall off much more rapidly than the experimental results. This may indicate that the small scale or the high frequency characteristics of the theoretical model are not representative of those in the boundary layer. A similar comment can be made on the low frequency nature of the model, although in this case the discrepancy is perhaps not quite so important since the errors introduced by inaccuracies in the low frequency characteristics of the

boundary layer model have very much less effect on the overall mean square pressure than those at the higher frequencies; the neglect of contributions for which $\omega\delta^*/U_\infty$ is less than 0.1 results in, at worst, a 3% deficiency in the mean square value, or 1.5% in the value of p'/τ_w.

The auto-covariance given by Equation (3.3.1) is the result of the integral effect of the overall boundary layer characteristics. It has been shown in Section 3.3.2 that the overall value of the mean square wall pressure fluctuations is very sensitive not only to the specification of the correlation function as seen by the difference in the values of Revised Set I from those of Set II but also to the specification of the small eddy scale which directly affects the shape of the correlation curve for points near to the boundary. In the same way, the auto-covariance and the frequency power spectral density can be expected to be sensitive to the choice of eddy scales and the correlation function. A further factor of influence in the case of the auto-covariance would be the effective convection velocity that has been used in the present model for the conversion of the space correlation function to that of the space-time correlation function using Taylor's hypothesis for frozen eddy patterns.

3.4 Conclusions.

The theoretical calculations for the wall pressure fluctuations in a turbulent boundary layer developed in a flow with zero mean pressure gradient have been based on the assumptions that

(1) turbulence/mean-shear interaction gives rise to the dominant contribution to the pressure fluctuations,

(2) the boundary layer exhibits statistical stationarity in time and homogeneity in planes parallel to the boundary,

(3) the boundary layer grows sufficiently slowly so that the mean velocity parallel to the boundary, and the root mean square velocity fluctuation normal to the boundary are functions only of the co-ordinate normal to the boundary.

The boundary layer models which have been employed allow an examination of the effects of the changes of the specification of the mean shear, the eddy scales, and the correlation coefficient on the overall values of the mean square wall pressure fluctuations. The variation of these pressures with Reynolds number was also examined.

From the results which have been obtained, and from the comparison of calculated and experimental values, the following conclusions can be drawn.

(1) The computational procedures for the determination of the wall pressure fluctuations have been found to be reliable, and checks on the accuracy of the computer programmes have shown the results to be consistent to within 0.8% for the worst case.

(2) The detailed consideration of the mathematical formulation for the fluctuating pressure shows that the use of the "joint contribution density function" is the most meaningful way of presenting the contributions of the various regions of the turbulent boundary layer to the space-time covariance of the wall pressure fluctuations.

(3) The consideration of the joint contribution density function for $Re_\delta{}^* = 10^3$ indicates that in this case the region of the boundary layer

close to the boundary is responsible for the major contribution to the wall pressure fluctuations, the region between the boundary surface and $y_2/\delta = 0.3$ accounting for about 70% of the overall mean square pressure. Consideration of the boundary layer model indicates that the inner part of the layer will produce an increasing proportion of the total mean square pressure as the Reynolds number is increased.

(4) The value of the mean square pressure is sensitive to the choice of the eddy scales and the correlation function, and the slight variation in the specification of the mean shear in the transition region gives rise to insignificant effects on the overall value.

(5) A single representative value of p'/τ_w obtained in previous calculations is typical of only a limited range of Reynolds number, and over the Reynolds number range $10^3 \leq Re_\delta^* \leq 10^7$, the variation in contribution of the turbulence/mean-shear interaction to p'/τ_w is from 1.10 to 6.51. Over the limited Reynolds number range for which experimental results are available, the variation of the calculated values of p'/τ_w is in accord with that of the experimental results.

(6) At the low Reynolds numbers, the small eddies make a dominant contribution to $\langle p^2 \rangle$ (over 90% at $Re_\delta^* = 10^3$). The proportion of the contribution falls off with the increase in Reynolds number to a value of about 20% at $Re_\delta^* = 10^7$.

(7) The variation of the total value of $\langle p^2 \rangle$ with Reynolds number is predominantly a reflection of the variation of the value of the large eddy contribution with Reynolds number. It is a function also of the correlation scales assigned to the eddy structure of the turbulence.

(8) For a two-dimensional incompressible turbulent boundary layer, turbulence/mean-shear interaction is the dominant process in the generation

of the wall pressure fluctuations, and accounts for about 80% of the overall mean square value.

(9) Comparison of the calculated auto-correlation and the frequency power spectral density distribution with experimental results shows that the calculated values fall within the range covered by the experimental curves. This lends further weight to the credibility of the assumption that turbulence/mean-shear interaction plays a dominant role in the generation of the wall pressure fluctuations.

(10) The experimental results for which good transducer resolution at the higher frequencies is claimed indicate that the high frequency characteristics of the theoretical model may not be representative of that in the actual boundary layer. This could be due to a deficiency of the model and/or the neglect of the other pressure source terms which provide relatively small but not negligible contributions to the pressures.

Before leaving the constant pressure layer and considering briefly the extension of the calculation to layers with non-zero pressure gradients, two comments on the boundary layer model should perhaps be made. The first concerns the scale variation of the small eddy structure which has been taken as a function only of the boundary layer thickness. For regions close to the wall, the effect of the wall on the flow can be expected to be very strong (as shown by the variation of the mean velocity distribution). Thus, it is highly probable that in the constant stress layer the scale variation of the small eddies might depend on wall parameters rather than on δ, as has been used. Secondly, although the turbulence intensity distribution has been taken as that given by Equation

(3.1.3) it should be noted here that there is a degree of uncertainty in the form of the distribution in the region of the outer edge of the constant stress layer (where $y_2 U_\tau/\nu \geq 600$ and $y_2/\delta \leq 0.2$). Here, in the absence of experimental data, u_2'/U_τ has been taken as constant.

Calculations for the fluctuating wall pressure in a boundary layer under the influence of a mean streamwise pressure gradient have yet to be attempted. However, it should be acceptable for such calculations to be carried out using a model similar to that for the constant pressure layer (suitably modified to account for the effects of the imposed pressure gradient). Coles's (1956) form for the mean velocity distribution in a boundary layer is known to be satisfactory for a wide range of pressure gradients. Hence, the formulation for the mean shear used in the case of the constant pressure layer can also be used when the mean pressure gradient is not zero. The only modification required to Equations (3.1.5) and (3.1.6), apart from the use of a different value of the pressure gradient parameter Π, would be in the values of δ_c/δ and U_c/U_∞, where U_c is the mean velocity at a point δ_c from the wall. In the case of the constant pressure layer all other parameters on which the wall pressure fluctuations depend were assumed to be functions of y_2/δ for y_2 outside the constant stress layer. The outer edge of the constant stress layer was taken as the y_2 value at which a chosen deviation of U_1/U_τ from logarithmic variation occurs, and it was argued that if the velocity distribution proposed by Coles is accepted then this value of y_2/δ is independent of Reynolds number. Since Coles's form for the velocity distribution is known to be applicable to boundary layers in non-zero mean

pressure gradients, the same argument can be applied to this case and it should again be acceptable to represent all relevant parameters as functions of $\zeta_c = y_2/\delta_c$ for all $\zeta_c \geq \zeta_c'$, where $\zeta_c' = 1 - 0.1057/\Pi_{pg}$ and Π_{pg} is Coles's pressure gradient parameter for a pressure gradient layer. The constant stress layer would therefore become thinner as the pressure gradient increased. For points within the constant stress layer ($y_2/\delta_c \leq \zeta_c'$), since there are few, if any, data for u_2' and the correlation coefficient R_{22} for self preserving layers with non-zero mean pressure gradients in the first instance, the best which could be done would be to assume variations similar to those taken for the constant pressure layer. Thus the specification of u_2' might become

$$\frac{u_2'}{U_\tau} = \frac{0.0092 1 y_2^{*2}}{1 - 0.036 1 y_2^{*} + 0.01328 y_2^{*2}} \qquad \text{for } 0 \leq y_2^{*} \leq 10,$$

$$= \frac{0.0838 y_2^{*2}}{1 + 0.922 y_2^{*} + 0.077 1 y_2^{*2}} \qquad \text{for } 10 \leq y_2^{*} \leq 600,$$

$$= 1.06 \qquad \text{for } y_2^{*} \geq 600 \text{ and } y_2/\delta_c \leq \zeta_c'$$

$$= 1.06 \exp\left[-2.23(y_2/\delta_c - \zeta_c')^2\right] \qquad \text{for } y_2/\delta_c \geq \zeta_c', \qquad \ldots(3.4.1)$$

and that for R_{22} might be according to Equations (3.1.8), (3.1.9) and (3.1.10) with the variation of the length scale s given by

$$\left.\begin{aligned} s/y_2 &= 0.570 \qquad \text{for } 0 \leq y_2/\delta_c \leq \zeta_c', \\ s/\delta &= 0.114 \qquad \text{for } \zeta_c' \leq y_2/\delta_c \leq \delta/\delta_c. \end{aligned}\right\} \qquad \ldots(3.4.2)$$

Clearly an improvement in the credibility of the calculations would

require systematic measurements of these properties of the boundary layer and this in itself implies a quite extensive and demanding experimental programme.

On the basis of a model similar to that used for the constant pressure layer it might be expected that the value of p'/τ_w would increase with increasing adverse pressure gradient at a given Reynolds number since the effect of the adverse pressure gradient is to decrease the thickness of the constant stress layer, an effect similar to that brought about by the increase in the Reynolds number.

4. THE EXPERIMENTAL EQUIPMENT.

4.1 The Variable Working Section Boundary Layer Tunnel.

4.1.1 Design Considerations.

The boundary layer which exists on the surface of a solid body in relative motion to a fluid is, very frequently, of a turbulent nature even though the turbulence level in the main body of the fluid is very low. Boundary layers of interest and of engineering concern are often developed over curved surfaces such that a mean pressure gradient in the streamwise direction is imposed on them. It is for the purpose of extending experimental investigations of the turbulent boundary layer into the realm where mean pressure gradients are significant that a variable working section boundary layer tunnel becomes desirable.

A number of important factors must be considered so that the fluid properties as well as the environmental characteristics are within acceptable limits when the tunnel is in operation. Such requirements are:

(1) that the test section of the tunnel be provided with the facility for the variation of the mean pressure gradient in the direction of mean flow;

(2) that the acoustic level in the test section due to the external sound field be kept at a sufficiently low level so as not to interfere with wall pressure measurements;

(3) that the mechanical vibration of the test section be sufficiently

small so as not to affect instruments sensitive to acceleration;

(4) that the free stream turbulence level should be insignificant compared to the turbulence level in the boundary layer;

(5) that the turbulent boundary layer in the test section be developed through natural transition from the laminar state;

(6) that the drive mechanism should provide for prolonged operation of the wind tunnel with the provision for an easy and accurate flow speed control.

4.1.2 Description of the Boundary Layer Tunnel.

The general arrangement of the variable working section boundary layer wind tunnel is depicted in figure 15. It is an open circuit system with the centrifugal compressor situated downstream of the working section. The principal dimensions of the tunnel are given in Table 4.1. The overall length of the wind tunnel from the inlet to the end of the acoustically lined exhaust ducting is about 27 m. The drive unit and the working section are placed in the same laboratory. Figure 16 is a view of the working section of the wind tunnel showing the instrumentation used in the Pitot traverse of the boundary layer and in the determination of the spectral density of the wall pressure fluctuations. Port holes are provided on the top (horizontal) wall of the working section at 0.3 m (1 ft) intervals. These have been accurately machined to take interchangeable instrumentation or dummy plugs and to ensure no significant discontinuity of the surface over which the boundary layer is developed. Air is drawn in at the bell-mouth through two sets of honeycombs and a

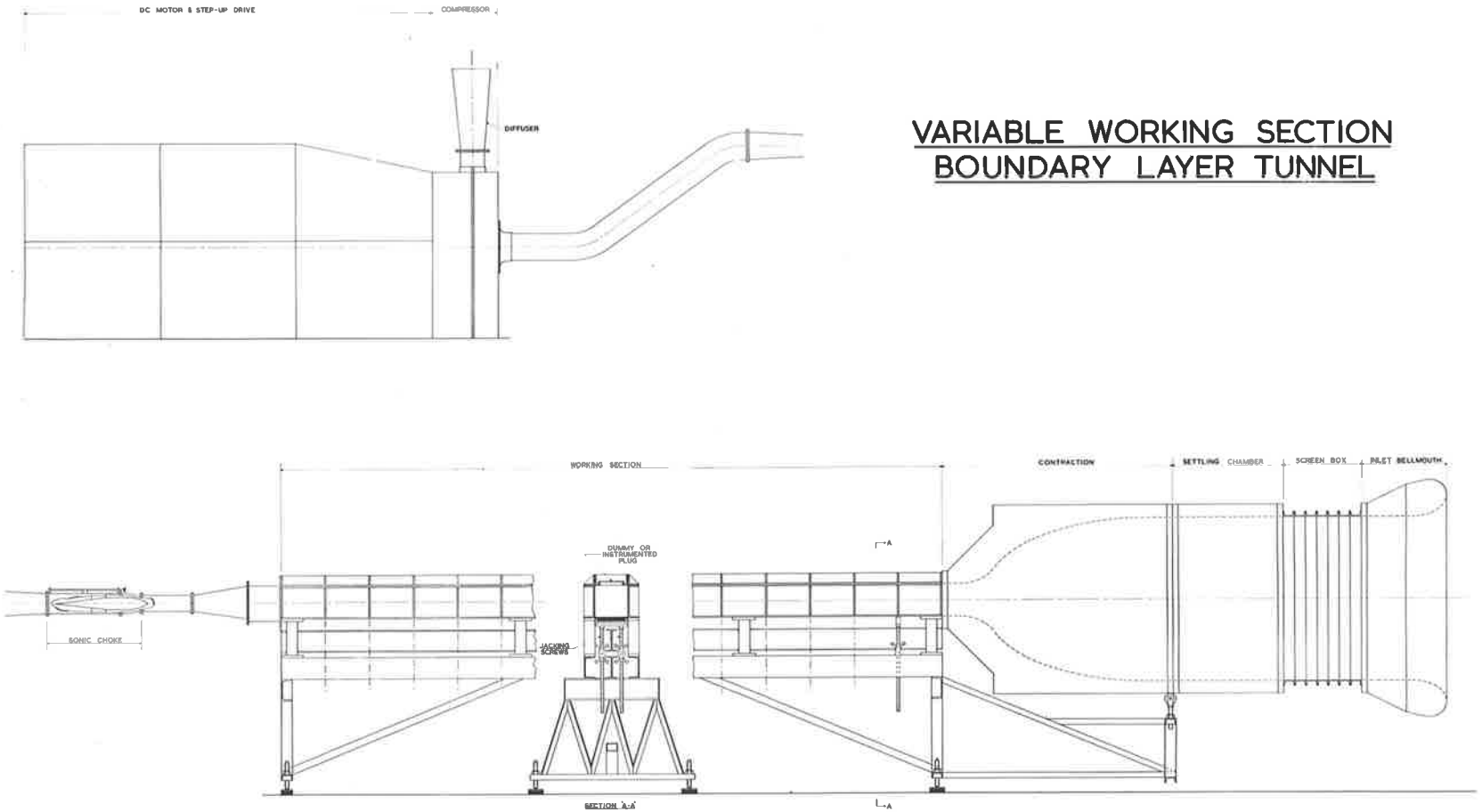

Fig. 15 General Arrangement.

Table 4.1 Principal Dimensions of Boundary Layer Tunnel.

Inlet	
Internal dimension of Bell-mouth	1.15 m sq.
Honeycombs:	
Number	2
Thickness	100 mm
Cell Size	6.5 mm
Separation	Variable
Gauze Screens:	
Number	6
Number of Mesh per cm	13
Wire Diameter	0.32 mm
Separation	76 mm
Settling Chamber	
Internal Dimension	1.15 m sq.
Length	1.7 m
Contraction	
Internal Dimension at Upstream End	1.15 m sq.
Internal Dimension at Downstream End	230 mm sq.
Contraction Ratio	25 : 1
Length	1.4 m
Working Section	
Height - variable	230 mm max.
Width	230 mm
Length	4.5 m

overlay fig.16

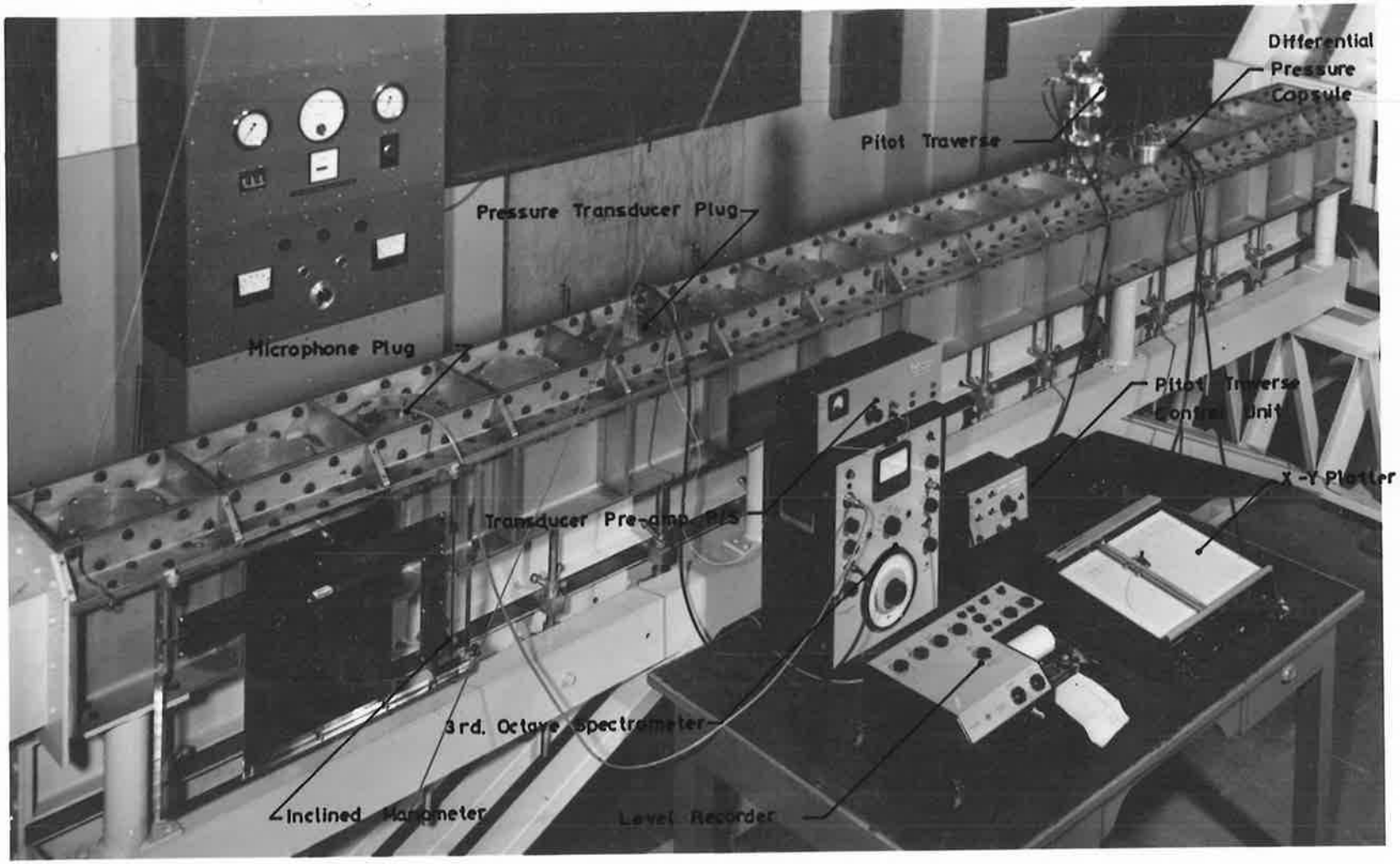

Fig.16 General View of Tunnel Working Section. Simulation Set-up for both Pitot and Wall Pressure Measurements.

series of wire screens before entering the working section after the contraction. It then enters the centrifugal compressor and is expelled through the diffuser and the exhaust ducting. The contour of the bell-mouth is given in figure 17 along with details of the inlet section.

4.1.3 The Drive Mechanism.

The measurements to be made in the wind tunnel are for the properties of the turbulent boundary layer in a steady state. Although it is possible to conduct such measurements in intermittently running tunnels, such as the blow-down tunnels, a continuously running tunnel offers great advantages. It facilitates prolonged measurements similar to those required in the setting up of the test section for an equilibrium boundary layer over the full length or over a considerable portion of the working section of the wind tunnel.

The prime-mover chosen for the drive unit of the tunnel is a DC motor with a rating of 60 kW continuous running. Its rated maximum rotational speed is 790 rpm. It is coupled to the centrifugal compressor through two stages of step-up gear-boxes which provide an overall ratio of about 19 : 1.

A rectified three-phase power supply was constructed to provide the necessary power to the DC motor. It embodies thyristors and firing circuits which regulate the conducting of the three-phase supply. A full wave bridge then provides the DC to the motor armature. Power for

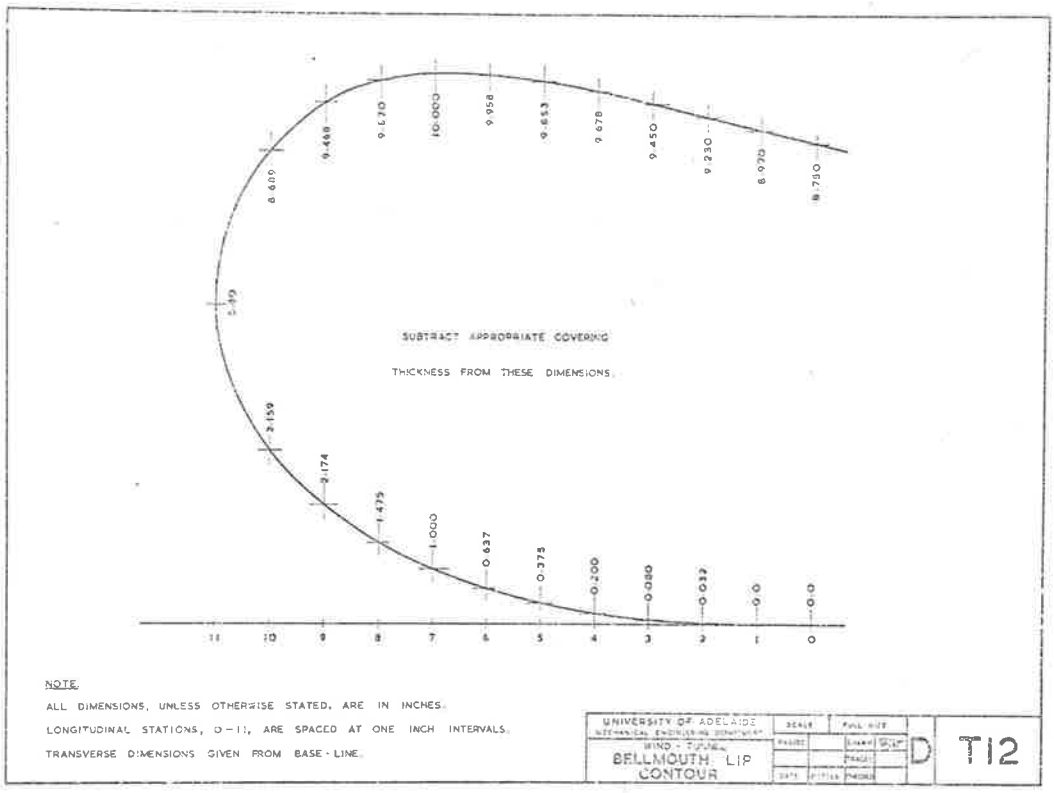

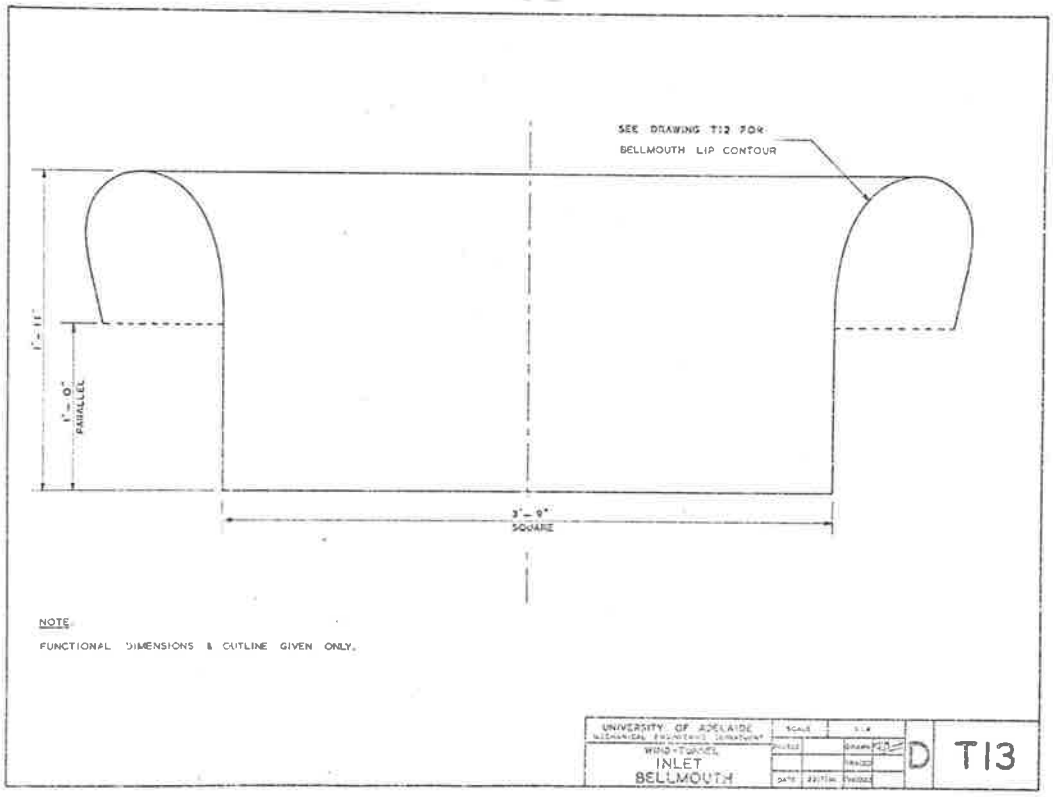

Fig.17 Dimensions of Inlet Section.

the field coils comes from the rectification of one of the phases. The range of the supply voltage is from 0 to 540 V DC with a maximum current rating of 150 A. The details of the power supply are given in Appendix C.

The maximum flow rate in the wind tunnel is 1.7 kg per second. The tunnel has a sonic choke downstream of the working section and the compressor speed is maintained such that sonic conditions exist in the choke at all times.

4.1.4 Boundary Layer Transition.

Because of space limitations, it was not possible to design the tunnel to obtain natural transition of the boundary layer. A boundary layer trip was resorted to to promote the early transition of the boundary layer to the turbulent state, and it was felt that the added advantage of the boundary layer trip would be the prevention of a wandering transition.

For a flow under zero pressure gradient conditions and low free stream turbulence, the transition of a boundary layer over a smooth surface from the laminar to the turbulent state occurs at a critical Reynolds number given by (see, for example, Schlichting (1960))

$$Re_t = U_\infty x_t/\nu = 2.8\times10^6 \quad , \qquad \ldots(4.1.1)$$

where x_t is the distance along the surface from the leading edge. The critical Reynolds number at which transition is likely to occur is reduced

in the presence of free stream turbulence, and in the case of a wind tunnel where the honeycombs and the gauze screens act as turbulence generators, the Reynolds number at transition may be as low as

$$Re_t = 3.2 \times 10^5 \quad . \qquad \ldots(4.1.2)$$

The velocity in the inlet section of the wind tunnel before the contraction is 1 m/s. The length of the parallel section required to ensure that transition of the boundary layer to the turbulent state occurs before the contraction can then be estimated using Equation (4.1.2), and x_t was found to be about 4 m. As the available space cannot accommodate such a length, a boundary layer trip has to be used.

Dryden (1963), on the analysis of the data of Tani and Hama (1945) on boundary layer transition under the effects of a two-dimensional cylindrical surface roughness element, showed that a collapse could be obtained if Re_t is plotted against k/δ_k^*, where k is the height of the roughness element and δ_k^* is the displacement thickness of the boundary layer at the roughness location. A strip of 6.35 mm (0.25 inch) square section is used as a trip, and using the method of Tani (1961) the point of transition is estimated to be about 3.1 m from the inlet when the trip is placed 1 m downstream of the inlet. As a compromise between the required length and the available space, the length of the parallel section at the inlet of the tunnel, which includes the settling chamber, has, in fact, a total of 2.9 m. Measurements of the velocity profile of the boundary layer in the test section indicate that satisfactory transition has been achieved under these conditions.

4.1.5 The Turbulence Level.

It is desirable that the turbulence level in the free stream be kept as low as possible. To this end, a series of gauze screens in conjunction with two sets of honeycombs and a high contraction ratio are employed - a technique which has been tried and proven over the years. (See, for example, Pope and Harper (1966), or Pankhurst and Holder (1952).) The distance between the honeycombs can be varied to allow an optimum separation to be obtained whereby any large scale eddy motion occuring at the inlet can be broken up. Figure 18 gives the details of the contour of the contraction as obtained from Bull (1963).

The main mechanism employed in the effort to reduce the level of turbulence in the free stream in the test section is the use of fine wire screens or gauze screens. It has been shown (see Collar (1939), Batchelor (1945), and MacPhail (1939)), in general, that where a gauze screen is to be used for reducing the turbulence level in the free stream in a tunnel, the pressure drop coefficient $K = (p_1 - p_2)/\frac{1}{2}\rho U_\infty^2$ should be of the order of 2, where p_1 and p_2 are the pressures upstream and downstream of the gauze screen respectively, ρ is the fluid density and U_∞ is the velocity over the screen. The specifications of the gauze screens are given in Table 4.1 and the results of Simmons (1945) show that under the conditions of maximum flow velocity through the tunnel, the pressure drop coefficient has a value of about 1.8. Taylor (1935 Pt. II) has shown that the turbulence generated by a wire grid decays in a manner given by

$$\frac{U_\infty}{u} = 8.9 + 1.035 \frac{x}{M} , \qquad \ldots(4.1.3)$$

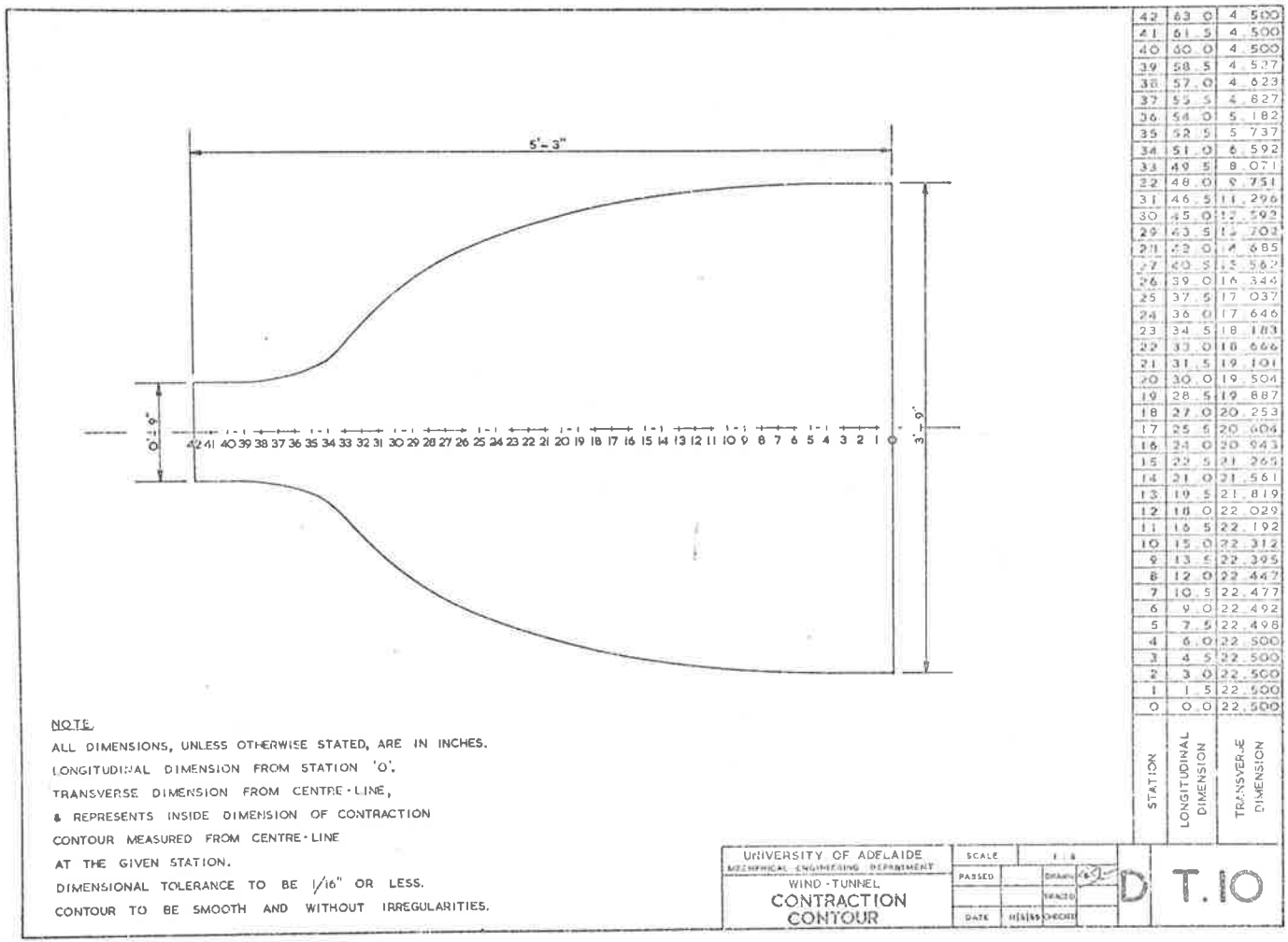

STATION	LONGITUDINAL DIMENSION	TRANSVERSE DIMENSION
42	63.0	4.500
41	61.5	4.500
40	60.0	4.500
39	58.5	4.537
38	57.0	4.623
37	55.5	4.827
36	54.0	5.182
35	52.5	5.737
34	51.0	6.592
33	49.5	8.071
32	48.0	9.751
31	46.5	11.296
30	45.0	13.592
29	43.5	14.702
28	42.0	15.685
27	40.5	15.582
26	39.0	16.344
25	37.5	17.037
24	36.0	17.646
23	34.5	18.183
22	33.0	18.666
21	31.5	19.101
20	30.0	19.504
19	28.5	19.887
18	27.0	20.253
17	25.5	20.604
16	24.0	20.943
15	22.5	21.269
14	21.0	21.561
13	19.5	21.819
12	18.0	22.029
11	16.5	22.192
10	15.0	22.312
9	13.5	22.395
8	12.0	22.447
7	10.5	22.477
6	9.0	22.492
5	7.5	22.498
4	6.0	22.500
3	4.5	22.500
2	3.0	22.500
1	1.5	22.500
0	0.0	22.500

Fig. 18 Contour of Contraction.

where u' is the fluctuating component of the velocity, x is the distance downstream of the turbulence producing grid, and M is the centre distance between the wires forming the grid. On this basis, the separation distance between the individual gauze screens has been chosen to be 76 mm (3.0 inch) giving the value of u'/U_∞ of about 1% at this distance. The value of the turbulence intensity in the free stream at the entry to the test section has been found to be about 0.04%.

4.1.6 The Test Section.

Extruded aluminium channels and angles were used in the construction of the three fixed sides of the test section. These have been heavily ribbed to increase the stiffness of the structure. The rims of the ports taking the dummy or instrumentation plugs have also been stiffened by rings. The remaining side of the test section (the floor) has been made of a 1.6 mm (16 S.W.G.) stainless steel sheet. Soft sponge rubber has been glued to the edges of the sheet so that an effective seal is achieved to prevent the leakage of air into the test section. Hand operated screw-jacks have been provided at intervals of 304 mm (1 ft) to raise or lower the floor in order to change the flow cross-sectional area and hence the velocity and static pressure along the test section. The screw-jacks act on rubber blocks which have been vulcanised on the stainless steel sheet. The hardness of the rubber has been measured to be about 40 on the Durometer. The rubber attachment blocks have been used to avoid the possibility of flat regions which could occur along the sheet if a non-elastic attachment were used. Figure 19 shows the cross-sectional

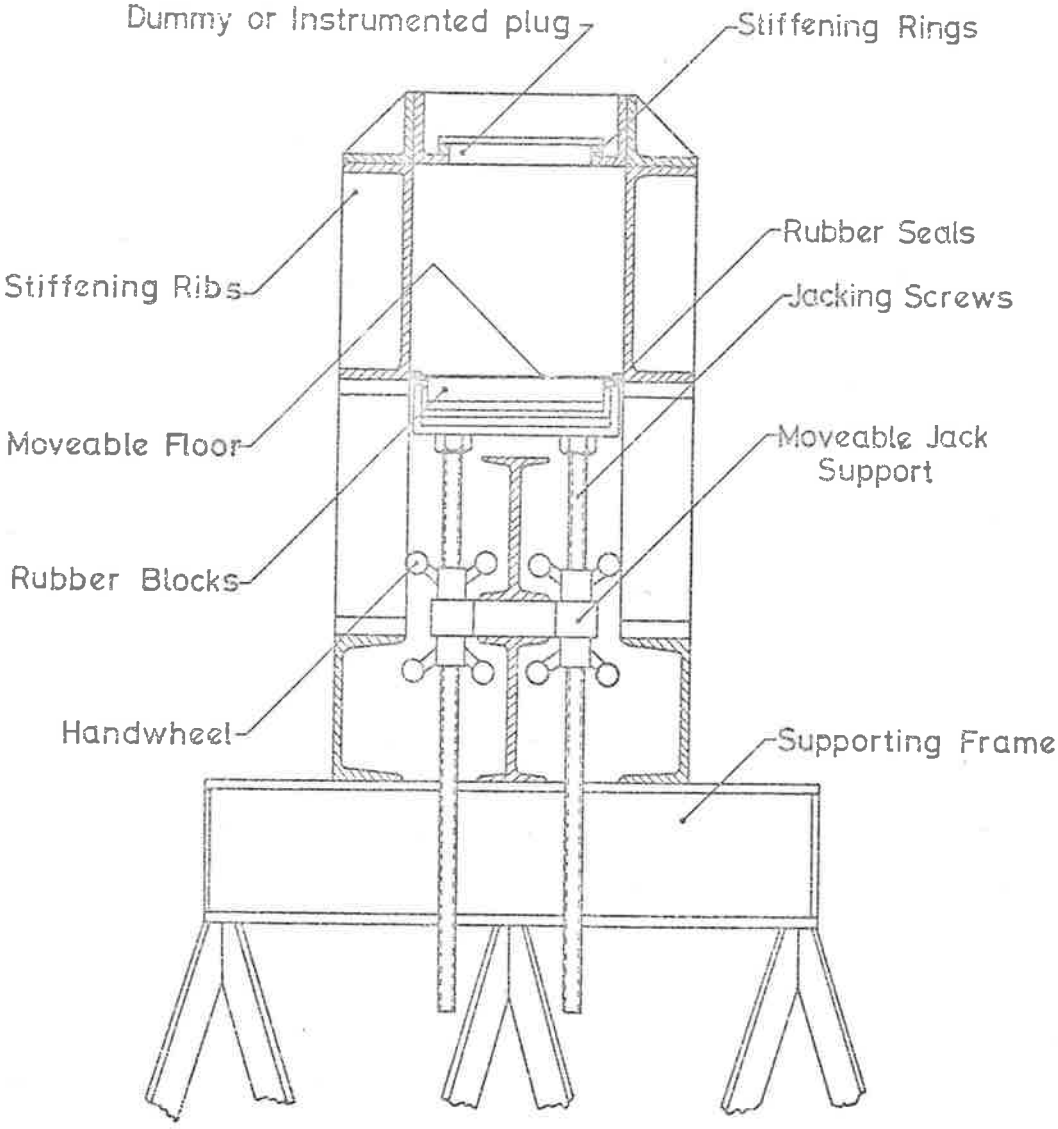

Fig. 19 Tunnel Cross-Section.

details of the test section.

The stainless steel sheet is rigidly anchored at the upstream end of the test section. At the downstream end it is secured at the clamping plate section, where the free end of the stainless steel sheet is sandwiched between the outer wall of the clamping section and a chamferred plate in the tunnel. Wing nuts have been provided for the ease of securing the free end of the sheet after positional adjustment of the floor of the test section.

4.1.7 Noise in the Test Section.

With certain types of instrumentation, and with piezo-electric pressure transducers in particular, in addition to electric circuit noise extraneous signals can arise from any acoustic field in the test section or from vibration of the tunnel structure.

The main source of acoustic noise in the boundary layer tunnel is the centrifugal compressor and its drive. Sound from it can propagate into the test section directly along the airstream or along an indirect path around the laboratory and into the intake of the tunnel. An effective means of suppressing the direct propagation of the noise from the compressor is the use of a sonic choke between the compressor and the test section (although some noise can still propagate through the boundary layer on the test section walls). The indirect propagation of acoustic noise has been suppressed by a sound-proof cover over the compressor and its

drive. The cover relies on both mass and damping to reduce the transmission of sound into the room. It consists of a heavy shell of steel plate lined on the inside with a thick layer of heavy sound absorption material. It was also found necessary to lag the exhaust and diffuser ducting as these became sources of significant sound intensities after the acoustic suppression treatment had been applied to the compressor and its drive.

Reduction to an acceptable level of tunnel vibration and the consequent effect of acceleration on the piezo-electric transducers to be used for the pressure fluctuation measurements has been achieved by (a) using a heavy stiff test section to minimise vibration excited by ambient sound field, and (b) isolating the tunnel test section from sources of mechanical vibration. Two flexible couplings in the form of soft rubber collars are used to isolate the test section from the compressor, one being placed just downstream of the test section and the other just upstream of the compressor. The test section is mounted on a heavy frame-work and the feet of the supporting frame-work rest on four anti-vibration pads made from vulcanised rubber whose hardness is about 40 on the Durometer. These resilient mounts coupled with the mass of the heavy frame-work give a low natural frequency of vibration of the test section (actually about 2 Hz).

4.1.8 The Sonic Choke.

Figure 20 shows the layout of the sonic shoke and the overall

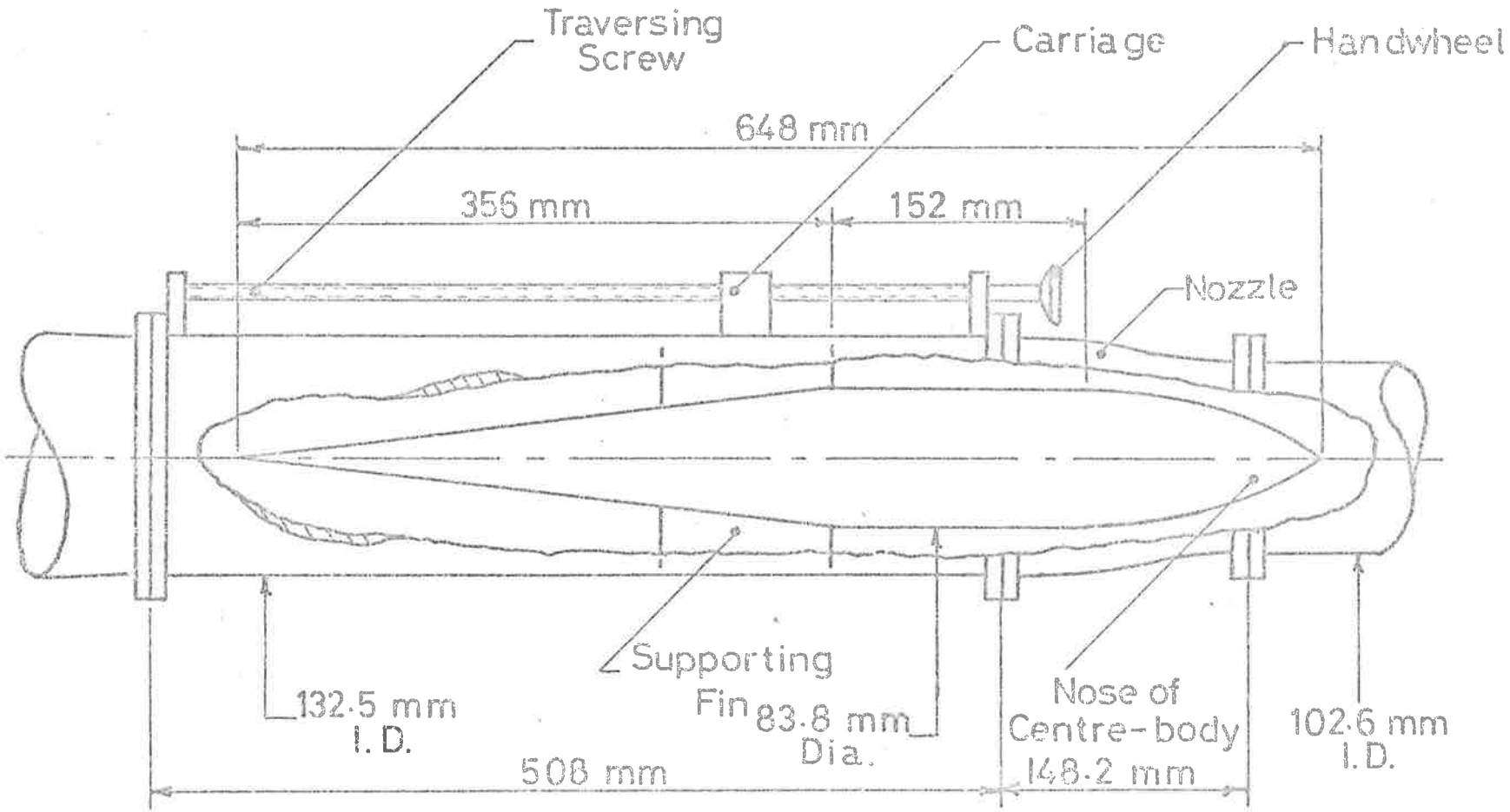

Fig. 20 Sonic Choke - General Arrangement and Overall Dimensions.

dimensions of the components. Detailed dimensions of the centre-body and of the nozzle are given in Appendix D.

The function of the choke in preventing excessive internal transmission of the fluid borne noise into the working section has already been referred to in Section 4.1.7. The flow cross-sectional area of the choke can be varied to allow variation of the mass flow in the tunnel, and this has the added advantage that it provides a good regulation of the flow - static or total head readings can be set to and maintained at better than 0.05 mm water gauge.

The overall effectiveness of the acoustic and the mechanical isolation of the test section is such that the signal to noise ratio from the piezo-electric pressure transducer measurements in the constant pressure turbulent boundary layer has a maximum value of 40 db at about 5 kHz and falls off on either side of this frequency to 5 db at about 200 Hz and about 25 kHz.

4.2 The Pressure Transducers.

4.2.1 Choice of Type to be Used.

The measurements of fluctuating pressures can be effected by the use of either the condenser microphone or the piezo-electric pressure transducer. The choice of one type over the other in any measurement to be made is usually decided through the consideration of a number of factors.

The principal advantages of a piezo-electric pressure transducer over the conventional condenser microphone are

(1) that a greater range of frequency can be measured as the sensing area can be made sufficiently small to decrease spatial attenuation at the higher frequencies.

(2) that the reduction of the size of the sensing element allows the reduction of the overall size of the transducer. This feature is particularly important in measurements of the space correlations where very close separations are often required.

(3) that the calibration of the transducer is insensitive to changes in the mean ambient pressure.

(4) that the piezo-electric pressure transducer face is infinitely more robust than the diaphragm of a condenser microphone designed for use over a similar frequency range.

(5) that the operation of the piezo-electric transducer is not affected greatly by the dust particles or moisture in the environment.

A great disadvantage of the piezo-electric pressure transducer is its relatively lower sensitivity. Electrical noise in the amplification system can become troublesome in that it can give rise to an output with a low signal to noise ratio. Extreme care must be taken in the design of the amplification equipment with emphasis on the use of low noise components. The piezo-electric transducer is also more sensitive to vibration than the condenser microphone, and the accelerometer effects can result in very high noise levels. Particular attention must then be paid to the isolation of its mounting from vibration sources.

The choice of the piezo-electric transducer for the measurement of the wall pressure fluctuations has been made mainly on the bases of the higher frequency response attainable, the smaller overall size, and the stability of its calibration with changes in the mean ambient pressure.

The piezo-electric effect is a property of many crystalline materials. A piezo-electric material, when compressed in certain directions, develops a potential difference, and conversely, the application of an electrical voltage creates mechanical distortions. It has been found that certain polycrystaline ceramic materials which are not piezo-electric in nature will behave as a piezo-electric body after being polarised. The polarising process subjects the material to a high polarising electric field which results in the alignment of the dipole moments in the material. This alignment and hence the polarised state is not a permanent property. The application of heat that will raise the temperature of the material beyond a certain value will destroy the polarisation and the material on cooling, assuming that the temperature encountered has not been excessive, will revert to its natural state. The Curie point is the temperature at which this reversal is precipitated.

4.2.2 Choice of Material and Element Size.

Of the polycrystaline materials available, barium titanate and lead zirconate-titanate are two of the more widely used examples. Both give good sensitivity although lead zirconate-titanate has the better sensitivity of the two with the added advantage of a higher Curie point.

This advantage is of particular significance when the construction of the transducer calls for the soldering of conductors to the electrodes on the element. Of the crystalline materials, quartz is the more widely used. However, the transducers employing quartz as the sensing elements provide a sensitivity which is only about one-hundredth to one-fiftieth of those which employ barium titanate or lead zirconate-titanate elements. The quartz transducers are also affected more by changes in the mean temperature. This makes quartz a useful material only in an environment where the drift in the calibration due to a change in temperature can either be taken as insignificant or be corrected for. An example of the possible use of quartz transducers is in the measurement of relatively high pressure changes. As the amplitude of the pressure fluctuations in boundary layer flow is only of the order of 10^{-4} atmosphere, the choice of the material for the piezo-electric transducer elements is narrowed to that of either barium titanate or lead zirconate-titanate. The latter has been chosen because of its inherently higher sensitivity and higher Curie point.

It has been shown by Bull (1963) that for a particular material used for the element, the signal to noise ratio of a piezo-electric pressure transducer is a function only of the cross-sectional area of the sensing element although the sensitivity is dependent on the thickness. However, it was also pointed out that the resonant frequency of the element itself is also a function of the thickness and decreases with the increase in thickness. The procedure in the choice of the thickness of the element is, usually, to use the thickest possible while at the same time ensuring that the resonant frequency would be high enough so that the response of the

transducer is flat to the highest frequency of interest.

4.2.3 Construction of Transducers.

Although a double screened transducer has been shown by Bull (1963) to give maximum sensitivity for a given element, the simple construction indicated in the cross-sectional drawing of the piezo-electric pressure transducer given in figure 21 has been employed. This type of construction has been decided on after the consideration of the number of transducers which will eventually be required when correlation measurements are to be made.

The transducer has a brass shell with an outside diameter of 6.35 mm (0.25 inch). The thickness of the cylindrical shell is 0.76 mm (0.030 inch). The insulating material between the central stem and the shell is silicon loaded ebonite which possesses a good insulating property as well as being able to provide a good surface for the adhesion of Araldite which is used to form the diaphragm. The central stem is made from a 12 B.A. threaded rod and the internal diameter of the body is made as large as practicable to reduce the inherent capacitance of the body. The transducer element is a lead zirconate-titanate disc with the nominal dimensions of 0.76 mm (0.030 inch) diameter and 0.76 mm (0.030 inch) thickness. It is a product of the Brush Clevite Company of Southampton, England. The designation of the lead zirconate-titanate element used for the transducer is PZT-5H. The transducer elements were not obtained in the size mentioned above but were cut from a much larger disc of the specified thickness. A clearance is

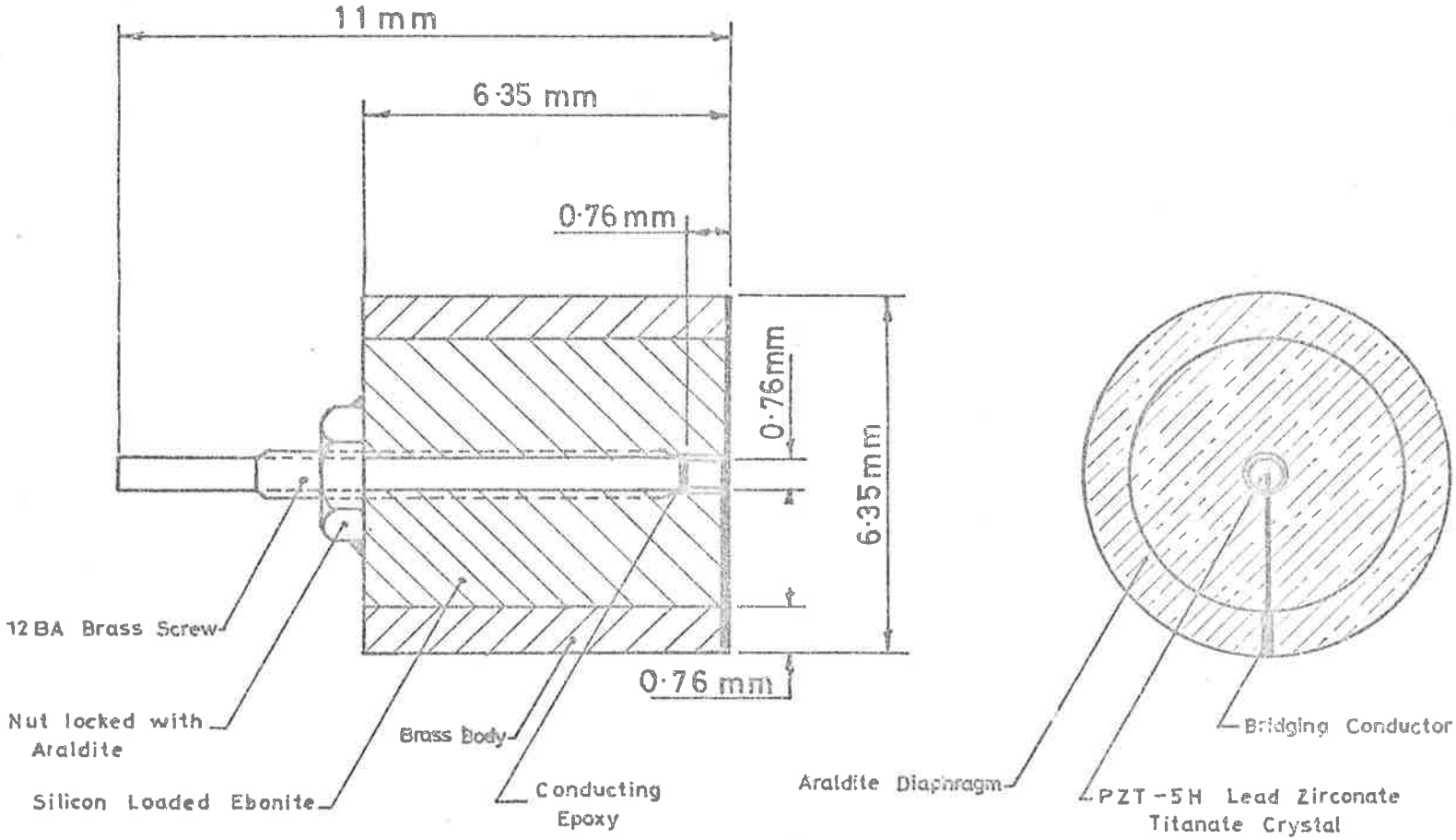

Fig. 21 Details of Piezo-electric Pressure Transducer.

provided between the transducer element and the insulation to prevent the transmission of mechanical stress from the surrounding material to the side of the element. This ensures that the pressure signals act only on the face of the element. The clearance has been made small (about 25 μm (0.001 inch)) so that the diaphragm material would have little likelihood of flowing into it and affecting the performance of the transducer. The Epirez type 614 conducting epoxy made by Indelab Proprietory of Granville, New South Wales is used for the mounting of the element on the central stem. The conductor bridging the circuit between the element and the transducer body is made of 25 μm (0.001 inch) diameter copper wire and is attached to the element and the transducer body with the use of the conducting epoxy.

Before commencing the construction of the transducer, it is particularly important to ensure that the transducer element has a proper set of electrodes. The procedure that is employed is to clean the element with concentrated nitric acid containing 3% hydrofluoric acid. This is done so that any contamination including any old and oxidised electrode material would be removed leaving a clean surface. After washing and drying, a coating of thermosetting silver preparation, type FSP 36 (002) made by Johnson Matthey of Hatton Garden, England, is applied in turn to each end of the element to form the electrodes, care being taken to ensure that the full area is coated without allowing any of the silver preparation to flow down the side of the element. When the electrodes have been formed and set, the transducer element is attached to the central stem with the aid of the conducting epoxy. After the epoxy has set, the central stem is

screwed into position so that the surface of the transducer element is flush with that of the transducer body. The locknut is then tightened and secured with Araldite adhesive. At this stage, the copper bridging conductor is attached to the body and the transducer element by means of the conducting epoxy. The diaphragm on the face of the transducer is formed by first spreading Araldite on the face of the transducer to ensure that the epoxy adheres to the body and the element. The transducer assembly is then placed face down on a piece of polythene on a flat surface and left to stand. When the Araldite has set, the transducer is ready for use after trimming off the excess epoxy around the perimeter of the body.

The typical value of the capacitance of the transducer elements is about 10 pF and that for the completed transducers is about 11 pF. The resistance across the central stem and the body for the completed transducer is higher than 1000 MΩ. Figure 22 shows two completed transducers and a pre-amplifier, the latter will be described in detail below.

4.2.4 Transducer Pre-amplifier.

Since the piezo-electric element has the characteristic of a very high input impedance, a cathode follower or a pre-amplifier serving the function of an impedance matching device is usually required before the signal from the transducer can be analysed.

A cathode follower was used initially in the development of the

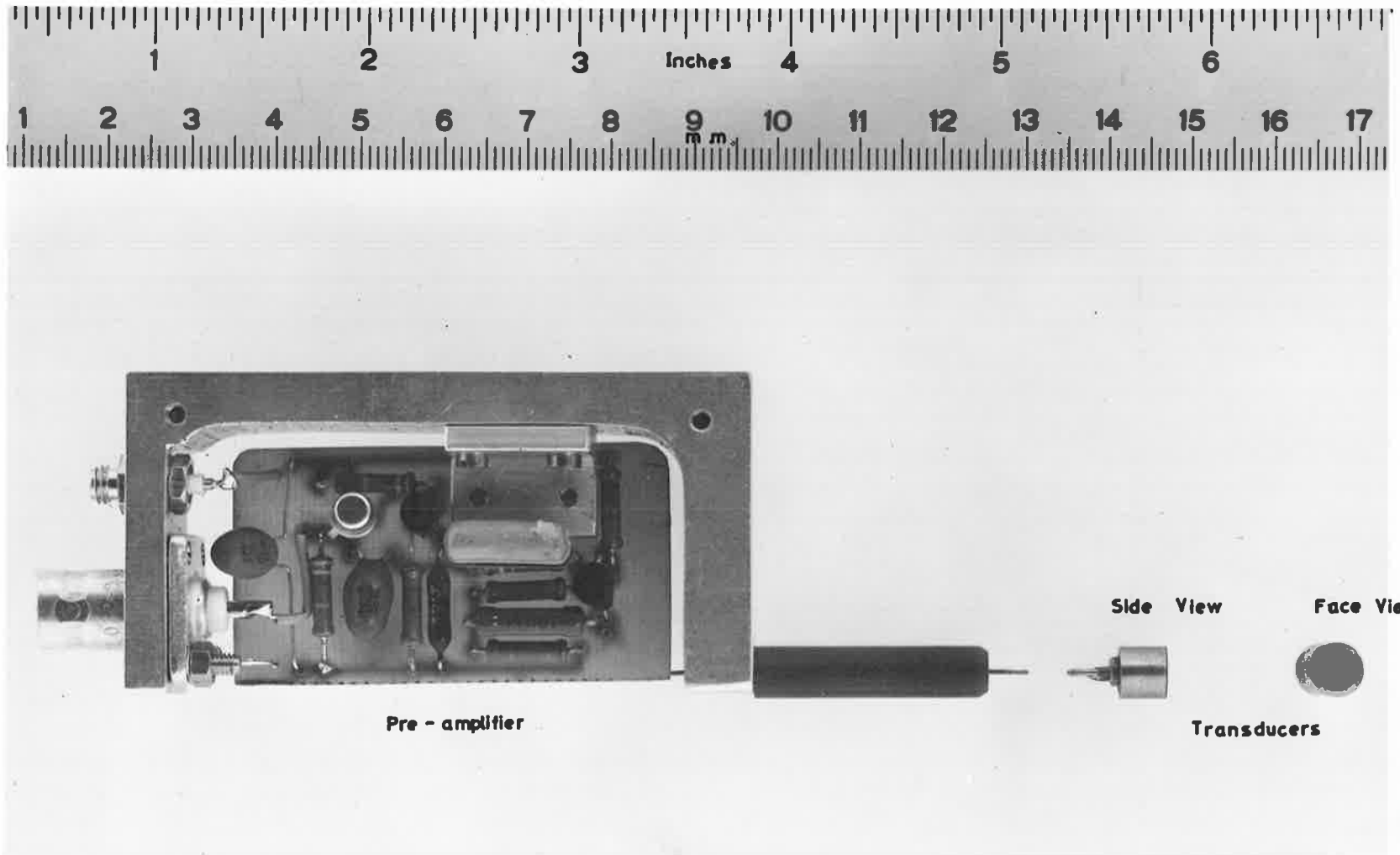

overlay fig. 22

Fig. 22 Piezo-electric Transducers and Pre-amplifier.

piezo-electric pressure transducers. However, it was found that the high level of the acoustic field in the laboratory induced vibration in the components of the cathode follower and resulted in an output with a high degree of noise. It was found that the shielding of the cable between the transducer and the cathode follower was also a critical factor with regard to the noise in the output of the cathode follower. The decision was then made to use a low noise, solid state pre-amplifier which would be compact enough to be placed very close to the transducer itself. This has the advantage in that not only is the use of a lead which is liable to be noisy dispensed with but also in that, as the capacitance of the lead has been disposed of, the effective sensitivity of the transducer/pre-amplifier combination is increased.

The general arrangement of the transducer/pre-amplifier combination in an instrumentation plug is shown in figure 23. Figure 24 shows the circuit diagram of the low noise pre-amplifier. The pre-amplifier is a two stage device using low noise field effect transistors and an emitter follower output. The output is boot-strapped to give a gate resistor multiplication factor of about 10. The principal low noise components are the Texas 2N5245 field effect transistors and the 100 MΩ gate resistor from Bruel and Kjoer.

The frequency response of the pre-amplifier is shown in figure 25 using the apparatus set up as illustrated in figure 26. It can be seen that the response is flat from about 100 Hz to about 1 MHz, a range which adequately covers the low frequency requirements of pressure transducer

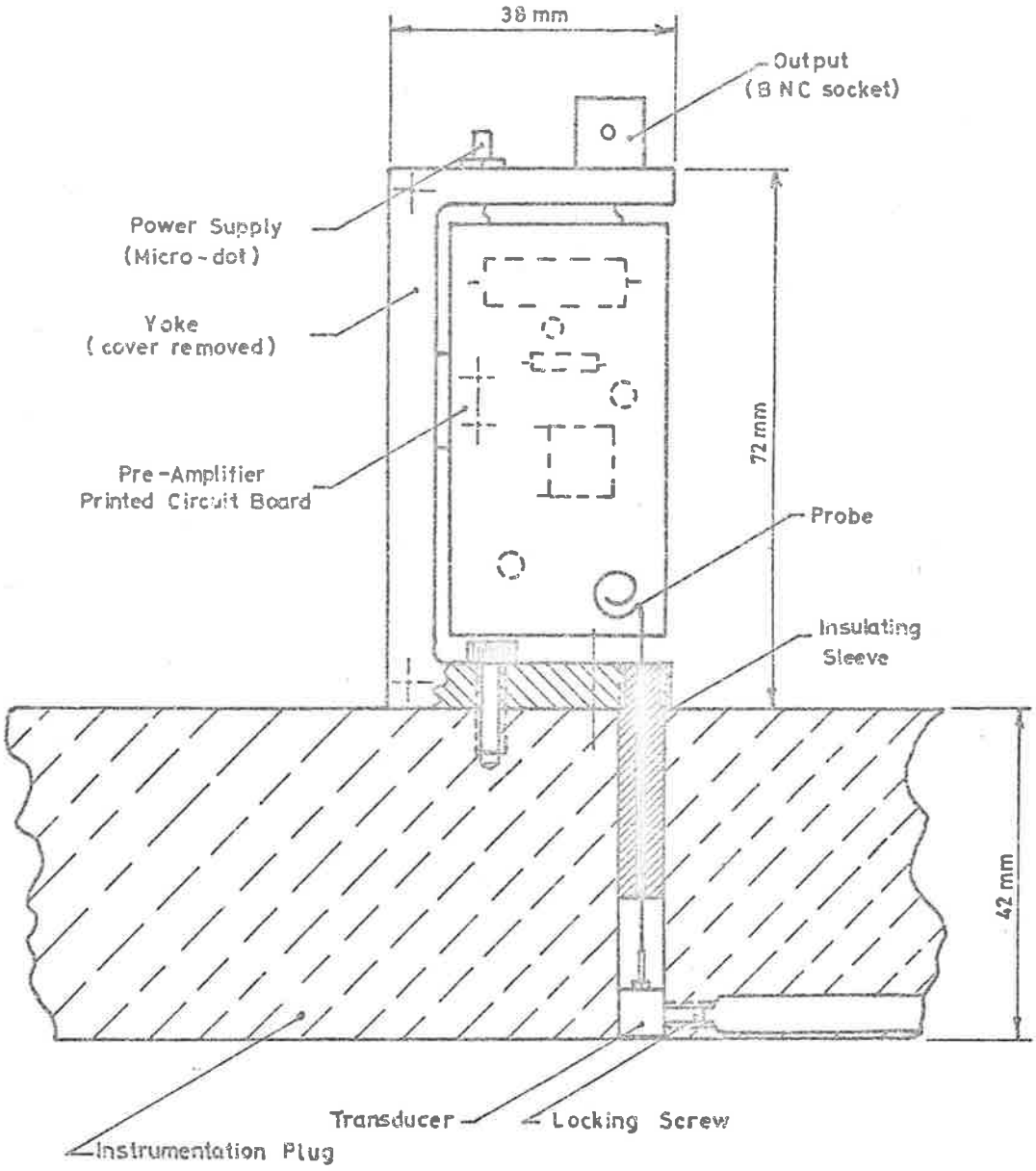

Fig. 23 General Arrangement of Transducer/Pre-Amp. Combination in Instrumentation Plug.

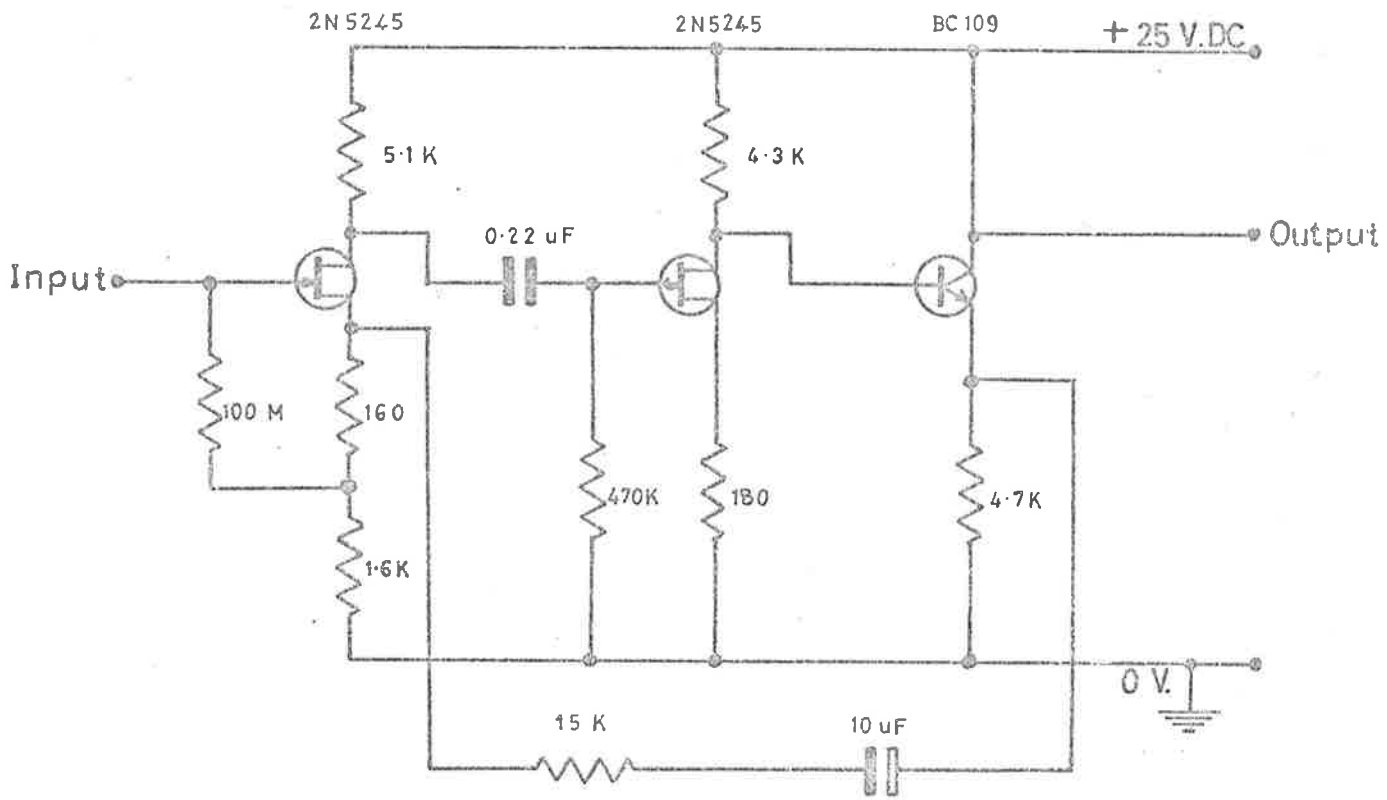

Fig. 24 Low Noise F.E.T. Transducer Pre-Amplifier Circuit.

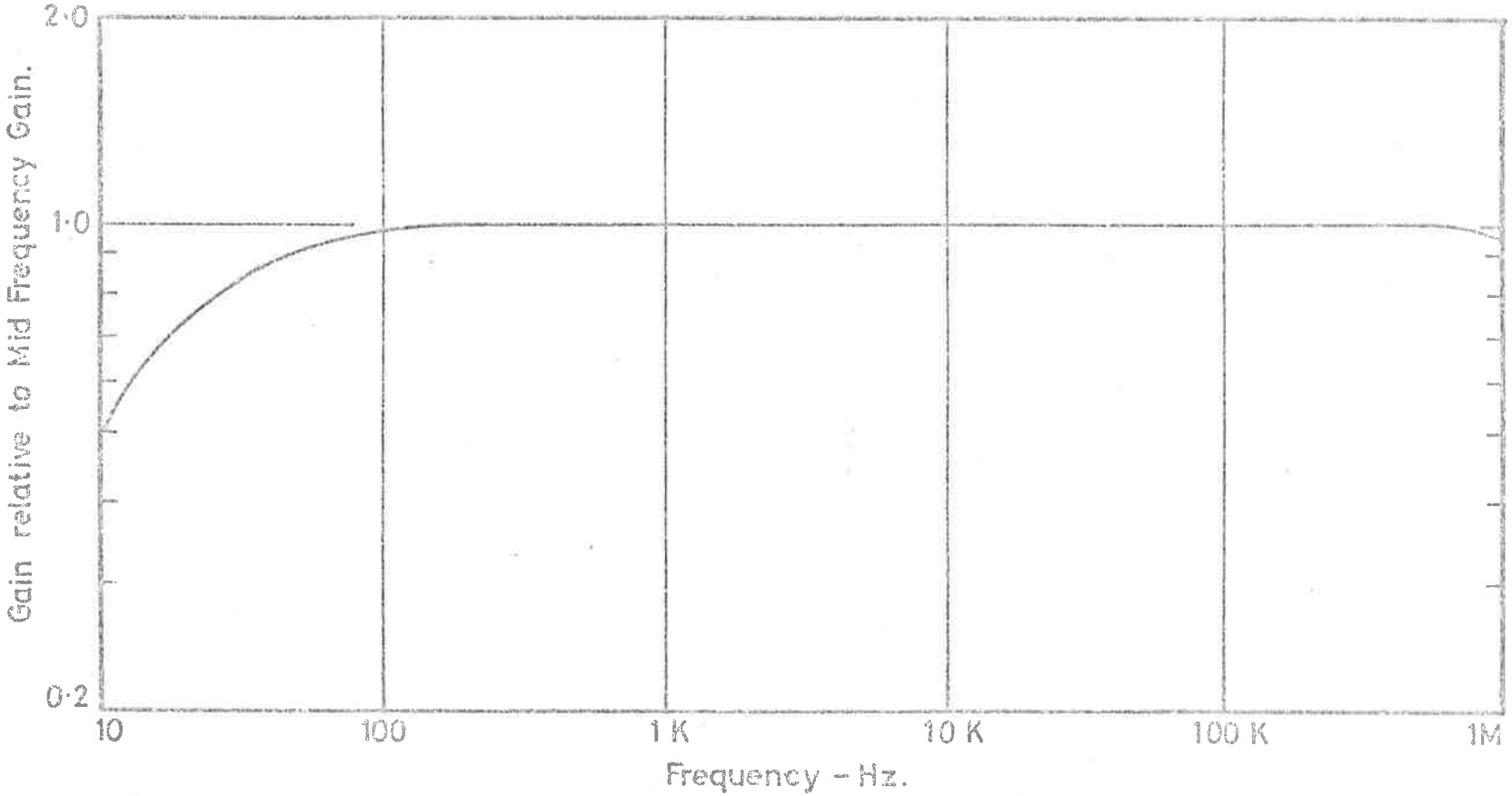

Fig.25 Frequency Response of Transducer/Pre-Amplifier Combination.

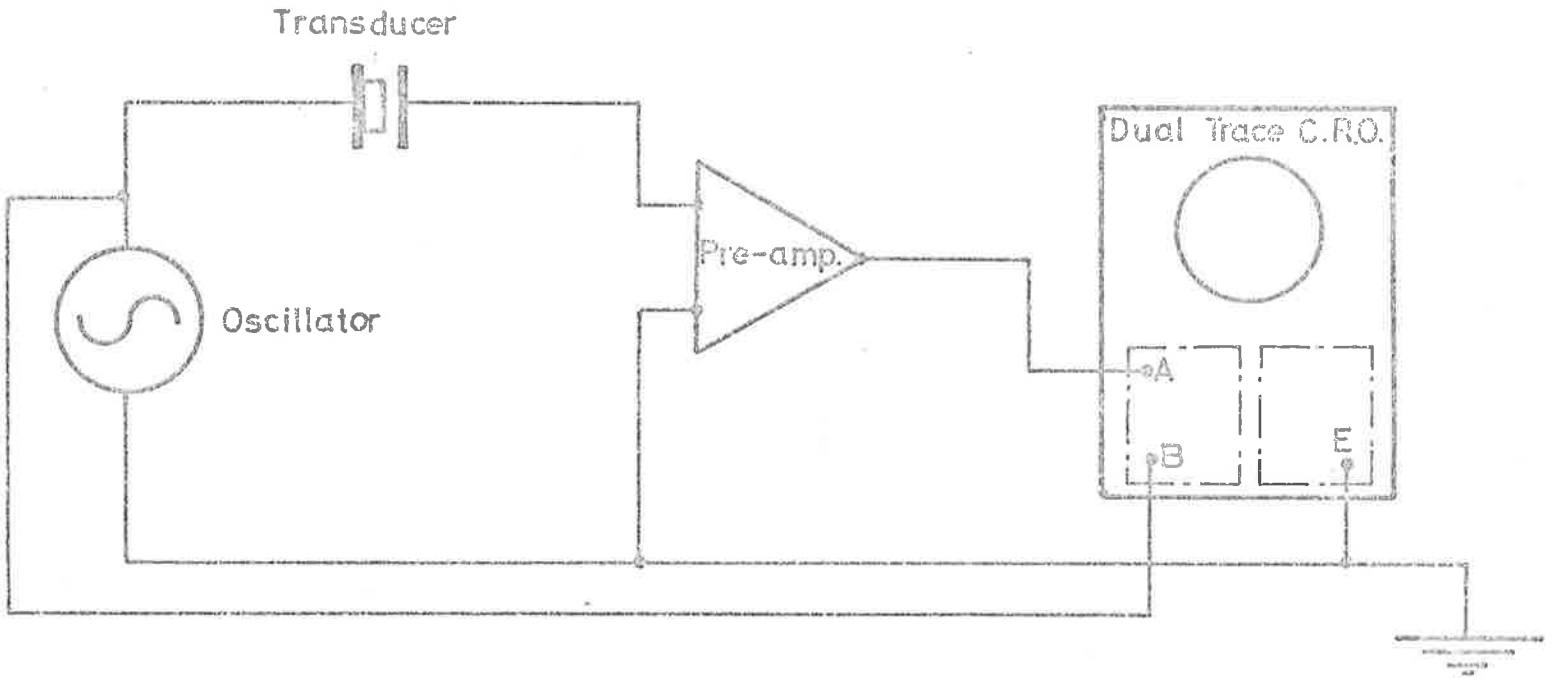

Fig. 26 Diagram of Apparatus for the determination of Transducer / Pre-Amplifier Frequency Response.

work in boundary layer measurements. The high frequency limit of the response is far in excess of the present requirements, and the useful upper limit is usually imposed by associated equipment and the transducer itself. The voltage gain of the pre-amplifier is about 5.

4.2.5 Transducer Amplifier.

The output of the piezo-electric transducers constructed for the measurement of pressure fluctuations in the turbulent boundary layer is expected to be of the order of 10^{-5} volts for the flow conditions which can be set up in the boundary layer tunnel. In order that correlation measurements may be made using a commercial correlator, it is necessary to amplify the signal. A variable gain high gain amplifier has been constructed to serve this purpose. Figure 27 shows the circuit of the amplifier which features solid state components, low noise, low output impedance, high frequency response and calibrated gain settings. The frequency response of the amplifier is shown in figure 28.

4.2.6 Transducer Calibration.

Two basic principles were employed in the methods used for the calibration of the pressure transducers. In the first case the transducer was mounted with its face flush with the surface of an instrumentation plug which was then placed in a shock tube extension made so that the surface of the instrumentation plug was itself flush with the internal surface of the shock tube extension. Measurement was then made of the

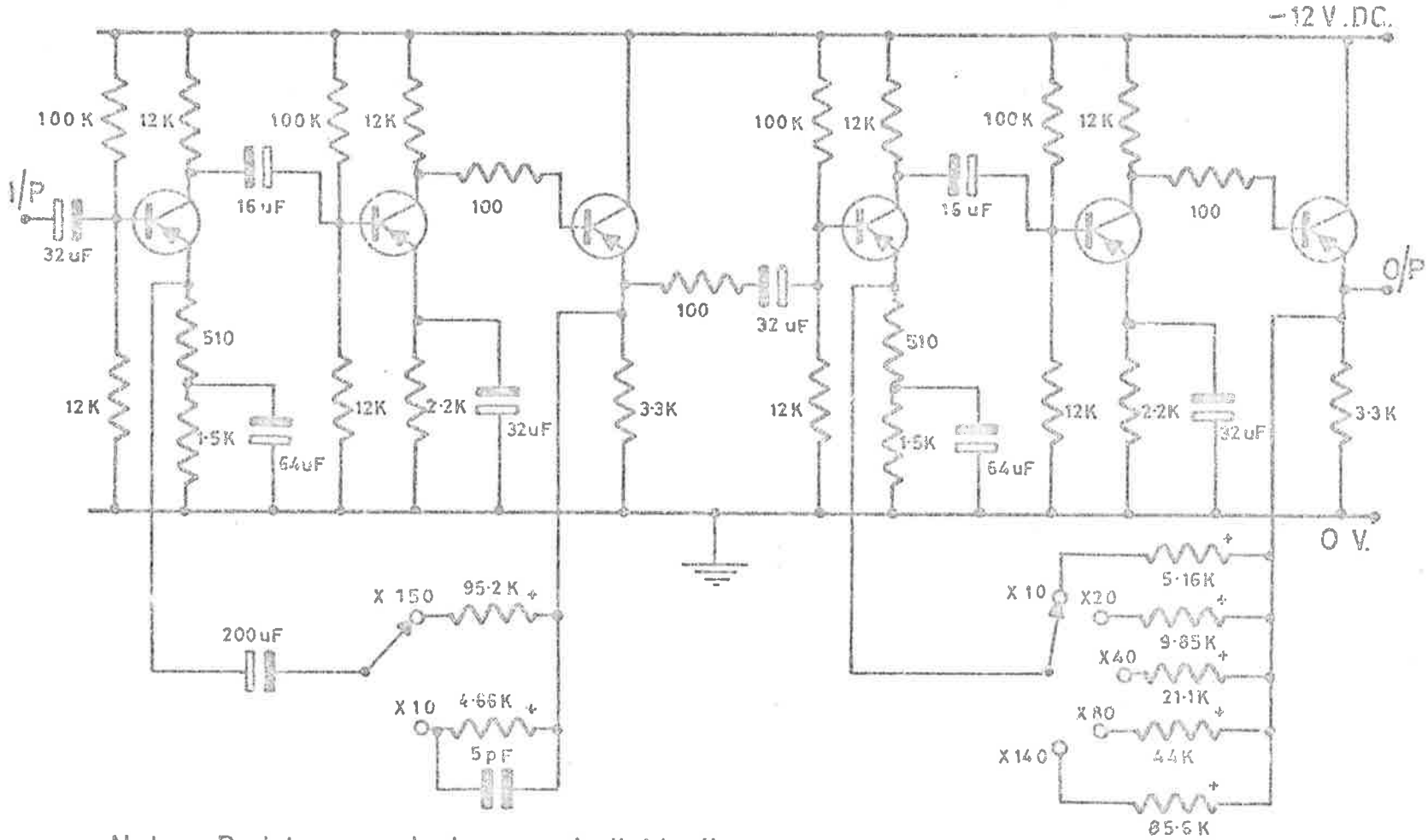

Note :- Resistors marked + are individually selected to gains as indicated.
All transistors 2N4250.

Fig. 27 Circuit Diagram of Transducer Amplifier (High gain).

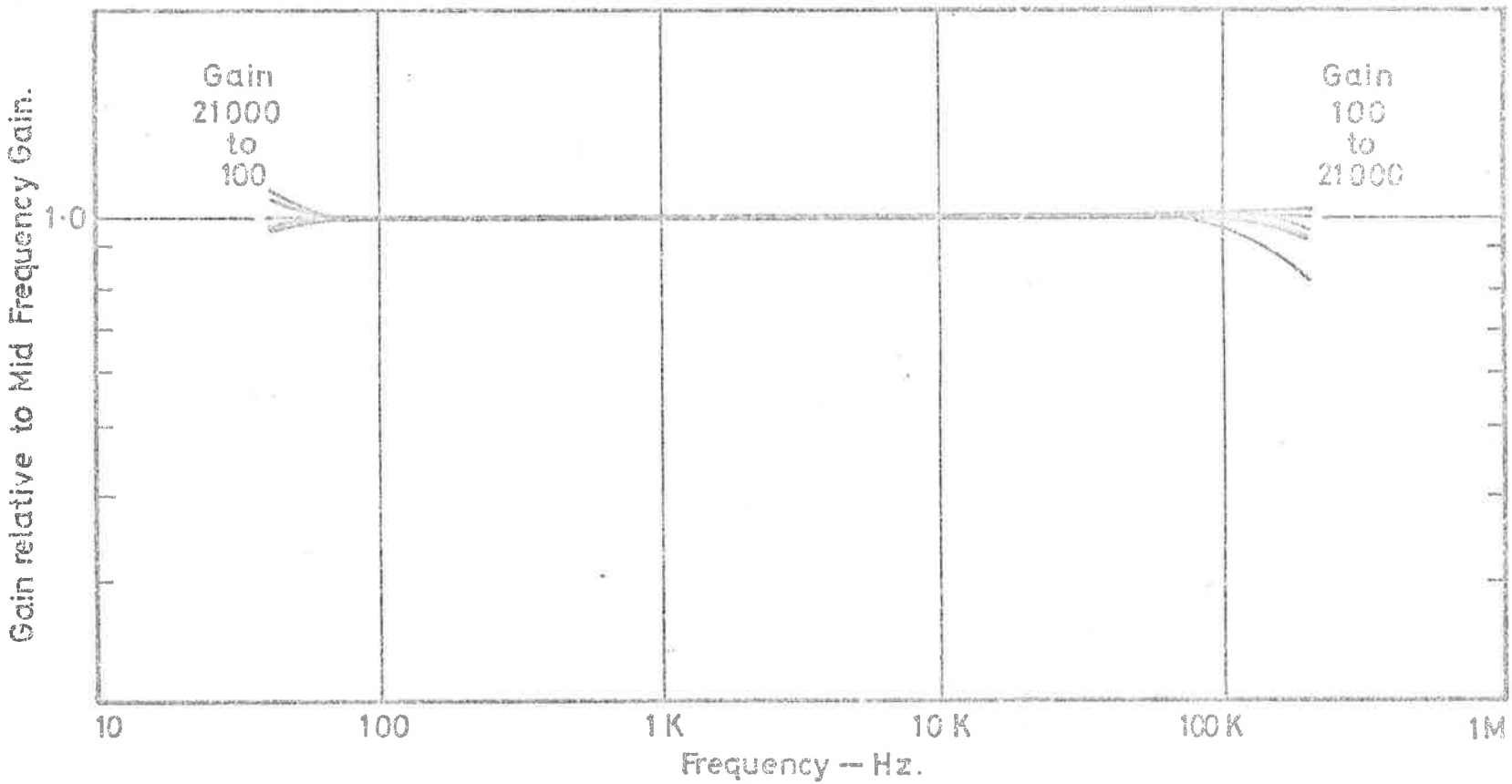

Fig.28 Frequency Response of Transducer Amplifier.

voltage step at the output of the pre-amplifier generated by the transducer in response to the application of a known pressure step associated with the passage of a shock front across its face. In the second case the transducer was calibrated against a standard condenser microphone in a situation where both the transducer and the standard microphone together with an exciter were mounted in the walls of a small air cavity.

In the case of the shock tube calibration, the magnitude of the pressure step applied to the transducer can be obtained from the expression

$$\frac{\Delta p}{p_1} = \frac{2\gamma}{\gamma-1}(M_s^2-1) \quad , \qquad \ldots(4.2.1)$$

where p_1 is the static pressure ahead of the shock (which is atmospheric pressure in an open ended shock tube),

γ is the ratio of the specific heat of the gas in the low pressure chamber of the shock tube at constant pressure to the specific heat at constant volume,

$M_s = U_s/a_1$ is the shock Mach number,

U_s is the speed of progression of the shock front,

$a_1 = \sqrt{\gamma RT_1}$ is the speed of sound in the gas ahead of the shock front,

R is the gas constant, and

T_1 is the temperature of the gas ahead of the shock front. The speed of progression of the shock front U_s can be obtained from the relationship

$$U_s = \frac{\ell}{\Delta t} \quad , \qquad \ldots(4.2.2)$$

if the facilities are available for the determination of the time Δt taken by the shock front to traverse a distance ℓ.

The magnitude of the applied pressure step can also be given by (see Bannister and Mucklow (1948))

$$\left(\frac{p_2}{p_1}\right)^{1/7} = \frac{2}{1 + (p_1/p_4)^{1/7}} \quad , \qquad \ldots(4.2.3)$$

where $p_2 = p_1 + \Delta p$ is the magnitude of the pressure directly behind the shock front, and

p_4 is the pressure in the high pressure chamber of the shock tube.

The experimental set-up is shown in figure 29. The oscilloscope comprises the Tektronix 564B storage oscilloscope main frame, the 3B3 time base, and the 3A9 differential amplifier. The output from the pre-amplifier of the triggering transducer is connected to the external triggering terminal of the time base unit after amplification by the high gain amplifier. The transducer which is to be calibrated has its pre-amplifier output connected to the input terminals of the differential amplifier of the oscilloscope. The values of the pressures p_1 and p_4 are read off from mercury manometers.

Although the construction of the apparatus has a provision for two timing transducers so that the pressure step may be determined by the use of Equations (4.2.1) and (4.2.2), this facility has not been used. Instead, the triggering transducer has been used in conjunction with the transducer which is to be calibrated. The accurate determination of the value of Δt and hence the shock Mach number requires a pair of identical timing transducers and an accurate chronometer. The time delay facility in the 3B3 time base has been used for the latter purpose since the sweep

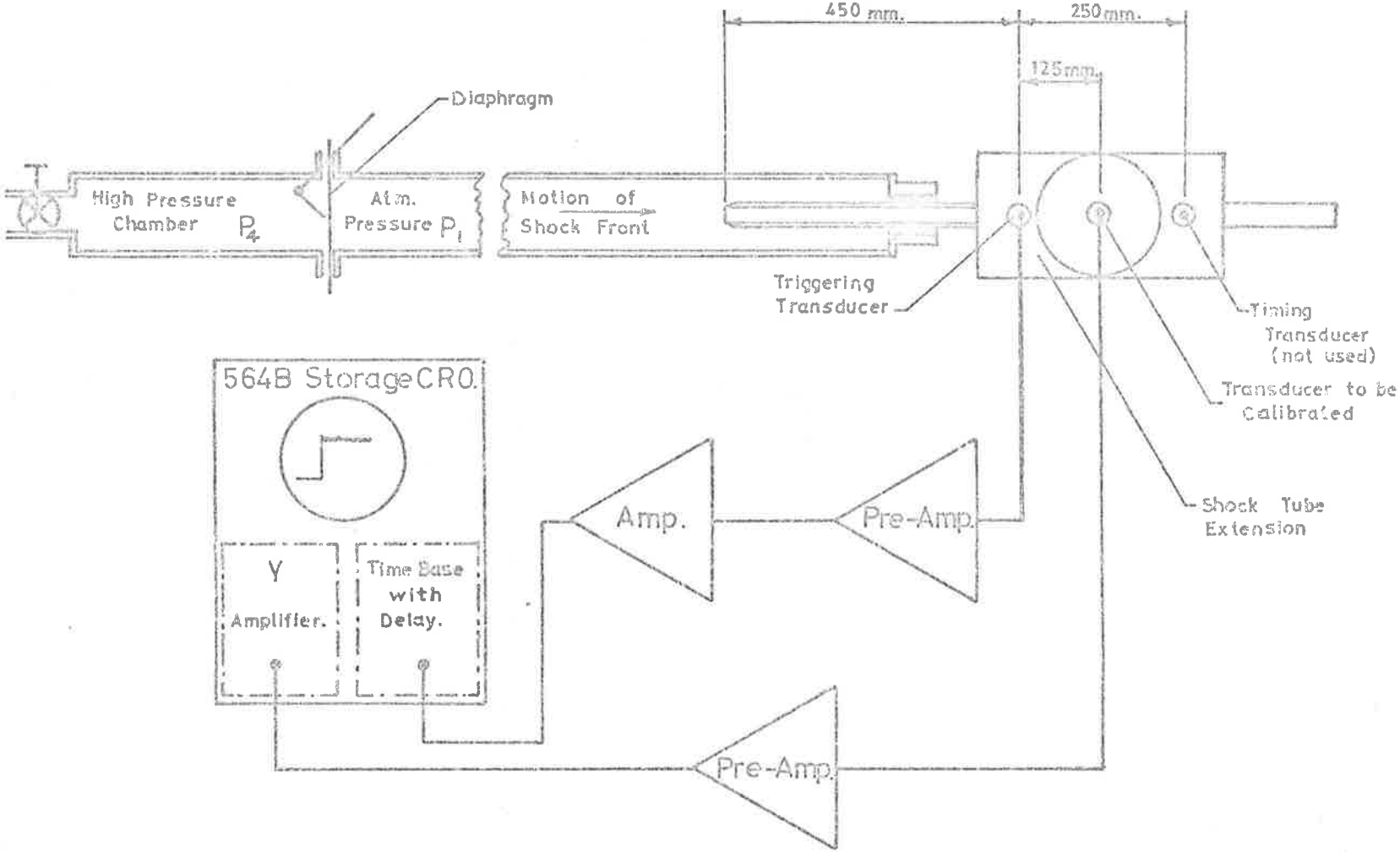

Fig.29 Apparatus for Shock Tube Calibration of Pressure Transducers.

rate can be coupled with the time delay so that only relatively small values have to be read off the oscilloscope photographs to determine the time taken by the shock front to travel the distance between the triggering transducer and the transducer to be calibrated. The voltage step generated by the transducer at the output of its pre-amplifier is also read from the oscilloscope photographs.

Equation (4.2.3) gives the alternative means for the determination of the applied pressure step directly from the values of the absolute pressure on the two sides of the diaphragm. The transducer output voltage is still determined from the oscilloscope photograph.

The typical response of the transducer to a pressure step is shown in figure 30. The progressive fall off of the output voltage of the transducer after the initial rise (due to the passage of the pressure step) is a function of the low frequency response of the transducer/pre-amplifier combination, the fall off being more rapid the higher the frequency at which the -3 db point occurs. It can be seen from figure 25 that the -3 db point for the transducer/pre-amplifier combination is about 20 Hz. The fall in output voltage of 10% will then occur after a time lapse of about 800 μ-seconds, a condition which is shown up in figure 30(a).

However, in the interval of time from a few μ-seconds to about 100 μ-seconds after the initial rise in output voltage, any deviations from a constant voltage output can be attributed to the effects of the frequency response function of the transducer itself. An example of this is the

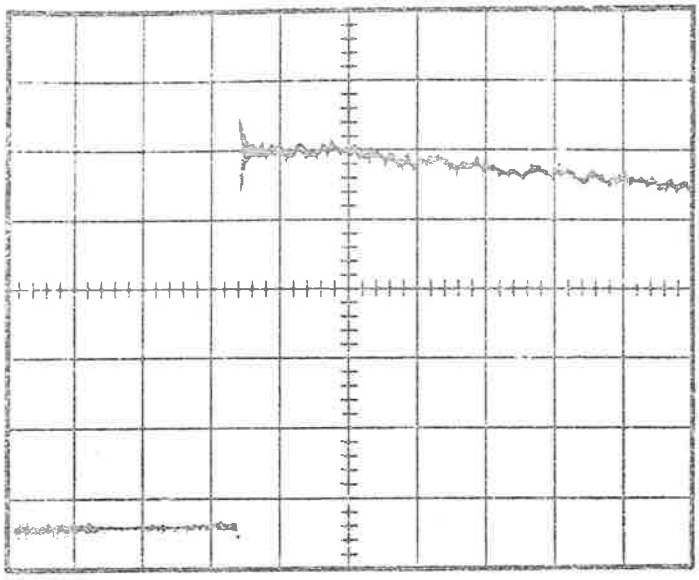

(a) Horizontal Scale : 100 μsec/div.

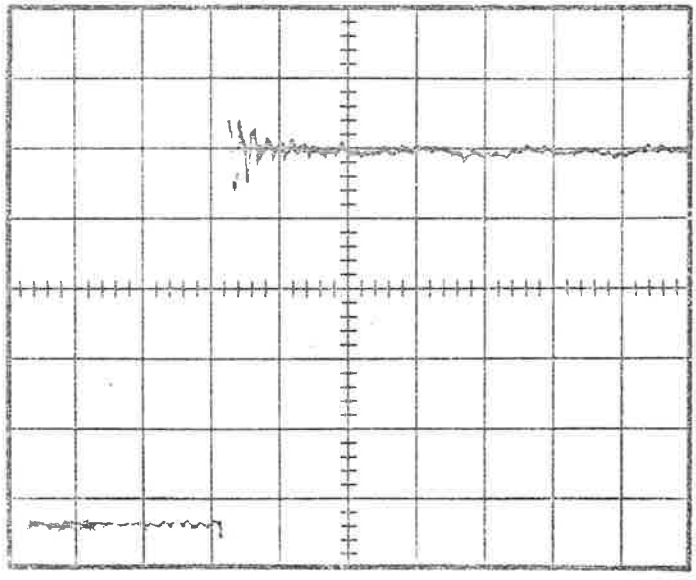

(b) Horizontal Scale : 20 μsec/div.

Fig. 30 Typical Oscilloscope Traces showing Response of the Pressure Transducer to the Passage of a Shock Wave. Vertical Scale : 0·2 Volt/div.

appearance of oscillations superimposed on the output trace which indicate the presence of mechanical resonances in the transducer. Even when particular care has been taken to ensure that the transducer is free of resonance at all frequencies in its working range, the output trace may still show a high frequency oscillation immediately following the passage of the shock front. The high frequency oscillation usually persists for about 15 μ-seconds and appears to correspond to the resonant vibration of the crystal itself in its fundamental thickness mode. This effect can be seen in figure 30(b).

The bursting of the diaphragm invariably excites vibration in the shock tube. Care must be taken to mechanically isolate the transducer from the shock tube vibration as the result of poor isolation will be the appearance of oscillations on the output trace of the transducer. However, the vibration in the walls of the shock tube will also affect the transducer before the shock arrives since it travels at a much higher speed than the shock front. Hence it is usually fairly easily identified and is not particularly troublesome provided the induced oscillations are not large in amplitude.

The shock tube calibration of the transducers relies on the assumption that the sensitivity is the same at all frequencies over the working range. It can be seen that this is a fair assumption provided that the frequency response of the associated pre-amplifier is also constant over this range and provided that the shock pressure step is reproduced without superimposed oscillations resulting from resonances in the mechanical

structure of the transducers.

The typical calibration curves for the pressure transducers are shown in figures 31 and 32 where the magnitude of the shock pressure step has been derived from the use of Equations (4.2.1) and (4.2.3) respectively. The calibrations shown are for the same transducer.

The second procedure for the calibration of the piezo-electric pressure transducers makes use of a coupler which is constructed so that the transducer and the condenser microphone are both mounted facing a small cavity into which the acoustic oscillations of an exciter are directed. The Bruel and Kjoer 6.35 mm (0.25 inch) diameter condenser microphone is used as the standard against which the transducer is calibrated, and the exciter is an earpiece driven by an oscillator. The arrangement for the calibration of a transducer is shown in figure 33. The upper limit of the frequency range over which the coupler is of use is a function of the cavity dimension. The pressure generated in the cavity is uniform so long as the cavity dimension is small compared with the acoustic wavelength corresponding to the frequency of the excitation. If the maximum dimension of the cavity is d, a uniform pressure can be expected for a wavelength λ at least as small as that for which $\lambda/10 \simeq d$. For the coupler which has been constructed, $d \simeq 8$ mm. Hence the frequency range can be expected to extend to about 4 kHz. This has been confirmed by a simple test where the transducer was replaced by another condenser microphone. By keeping the output of one microphone constant at a series of exciter frequencies and noting the output of the other, the useful limit of the range of the

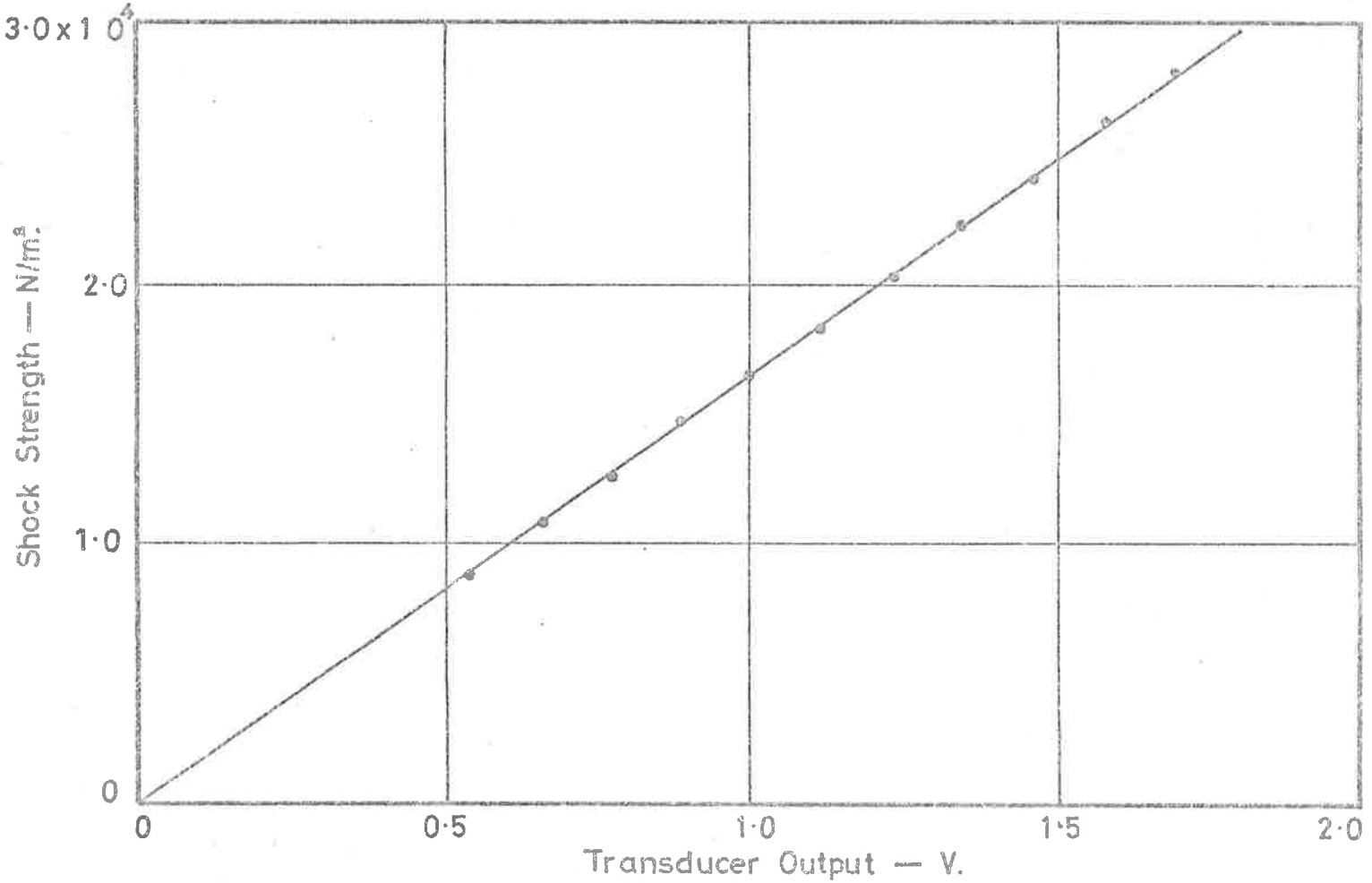

Fig. 31 Typical Curve of Shock Tube Calibration of Pressure Transducers — Shock Velocity Method.

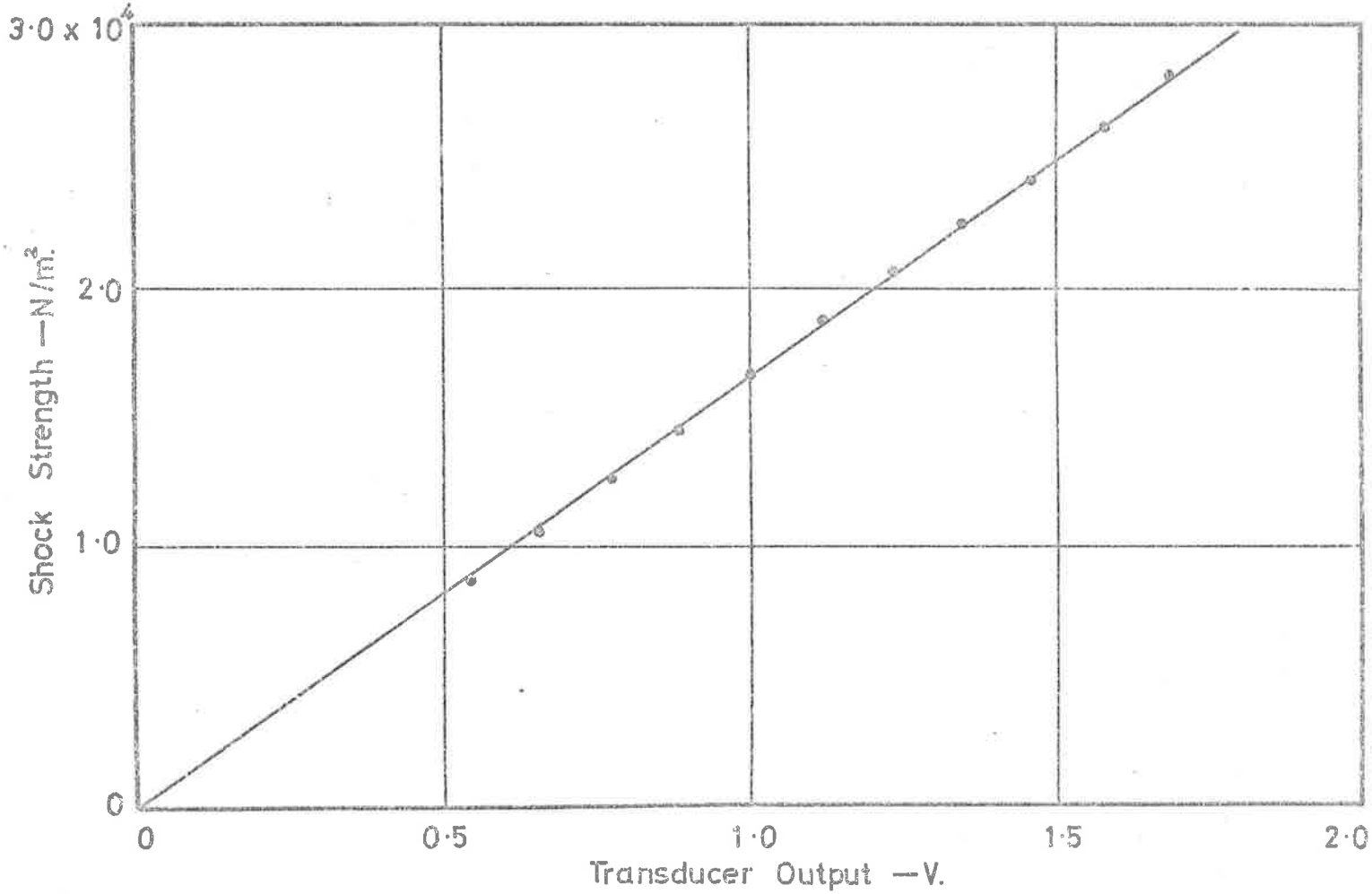

Fig.32 Typical Curve of Shock Tube Calibration of Pressure Transducers — Diaphragm Pressure Method.

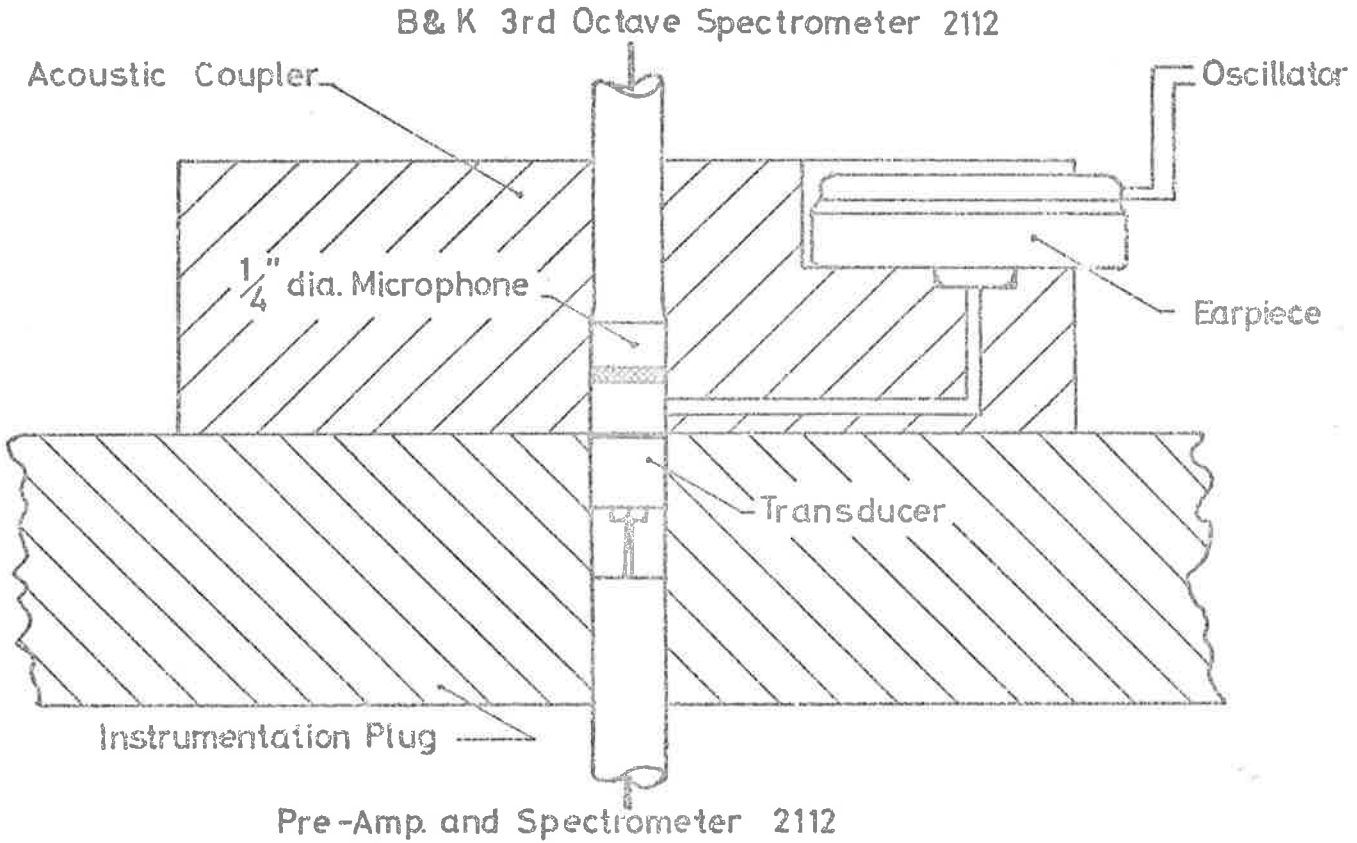

Fig. 33 Cross Section of Apparatus for Acoustic Calibration of Pressure Transducers.

coupler can then be estimated as the point where the output of the second microphone starts to show marked variations. Figure 34 shows the results of the test which indicate that the upper frequency limit is about 2.5 kHz.

A typical calibration curve for the pressure transducers obtained by the use of the acoustic coupler is shown in figure 35. The transducer used is the same as that whose calibration has been given in figure 31 and 32. Since the agreement between the results obtained from the two different methods (shock tube, and acoustic coupler) is good and has been found to be consistent to 2% or better, the procedure which has been adopted for the calibration of a newly constructed transducer is to initially check the flatness of the overall response of the transducer using the shock tube method. The acoustic method is then used to check the calibration directly before and after each tunnel run.

4.3 Differential Pressure Capsule and Pitot Traverse.

4.3.1 The Differential Pressure Capsule.

The boundary layer mean velocity distributions were obtained using a Pitot tube. The results allowed the determination of the displacement thickness δ^*, the momentum thickness θ, the shape parameter H, the Clauser (1954) thickness Δ, the family parameter G, and the pressure gradient parameter β, which, for an incompressible boundary layer, are defined as follows;

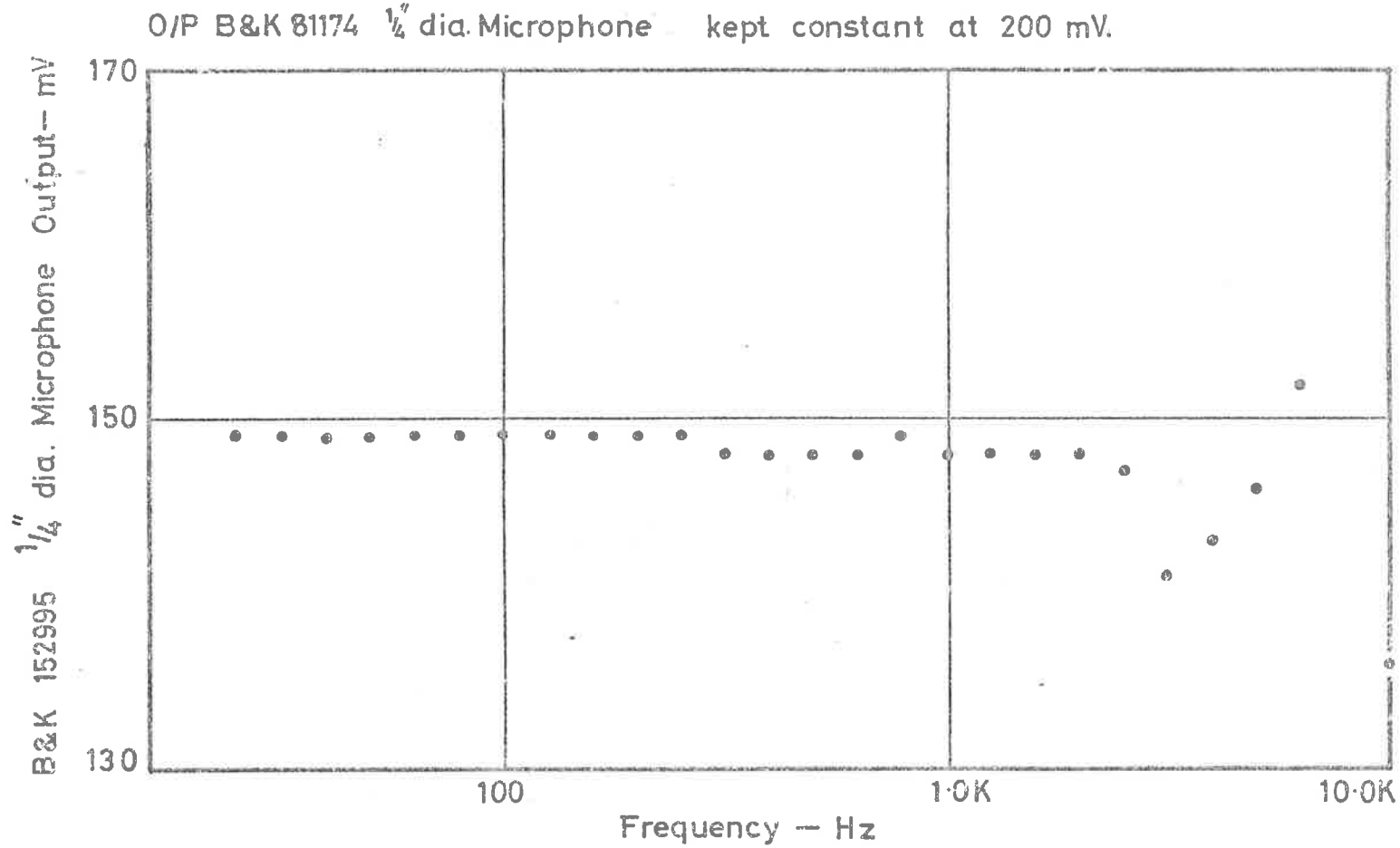

Fig. 34 Behaviour of Acoustic Coupler using Two Known Microphones.

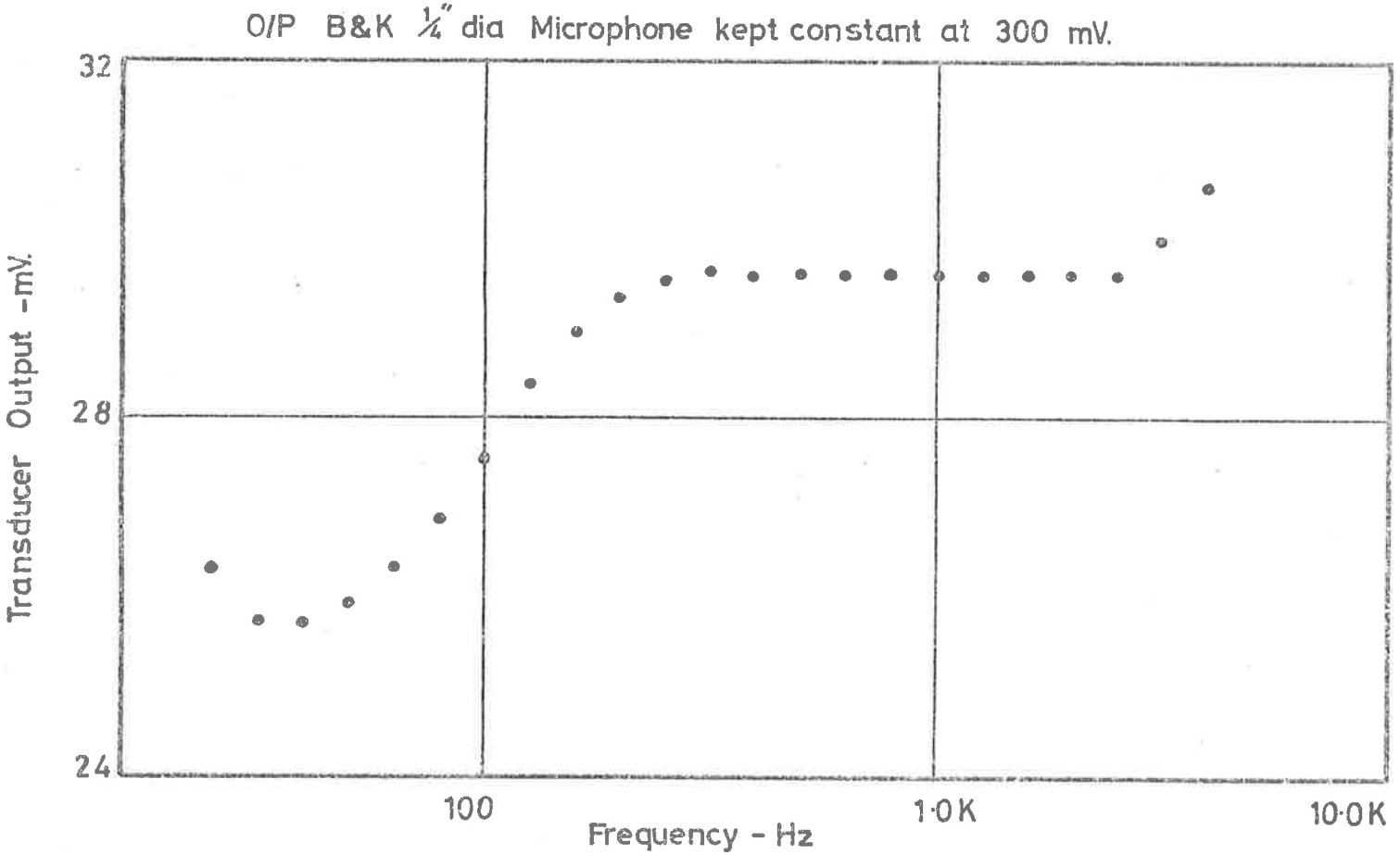

Fig. 35 Typical Curve for Acoustic Calibration of Pressure Transducers.

$$\delta^* = \int_0^\infty \left(1 - \frac{U_1}{U_\infty}\right) dy \quad , \qquad \ldots(4.3.1)$$

$$\theta = \int_0^\infty \frac{U_1}{U_\infty}\left(1 - \frac{U_1}{U_\infty}\right) dy \quad , \qquad \ldots(4.3.2)$$

$$H = \frac{\delta^*}{\theta} \quad , \qquad \ldots(4.3.3)$$

$$\Delta = \int_0^\infty \left(\frac{U_\infty - U_1}{U_\tau}\right) dy \quad , \qquad \ldots(4.3.4)$$

$$G = \frac{C_2}{\Delta} \quad , \qquad \ldots(4.3.5)$$

$$\beta = \frac{\delta^*}{\tau_w}\left(\frac{dp}{dx}\right) \quad , \qquad \ldots(4.3.6)$$

where

$$C_2 = \int_0^\infty \left(\frac{U_\infty - U_1}{U_\tau}\right)^2 dy \quad , \qquad \ldots(4.3.7)$$

τ_w is the wall shear stress, U_τ is the friction velocity, and y is the distance from the boundary surface.

The Pitot traverses when manually carried out are time consuming. A relatively cheap and simple device has been constructed to perform the traverses automatically when used in conjunction with a recorder or an X-Y plotter. This device is called the "differential pressure capsule" and is shown in figure 36. It consists of a cantilever which is acted upon by

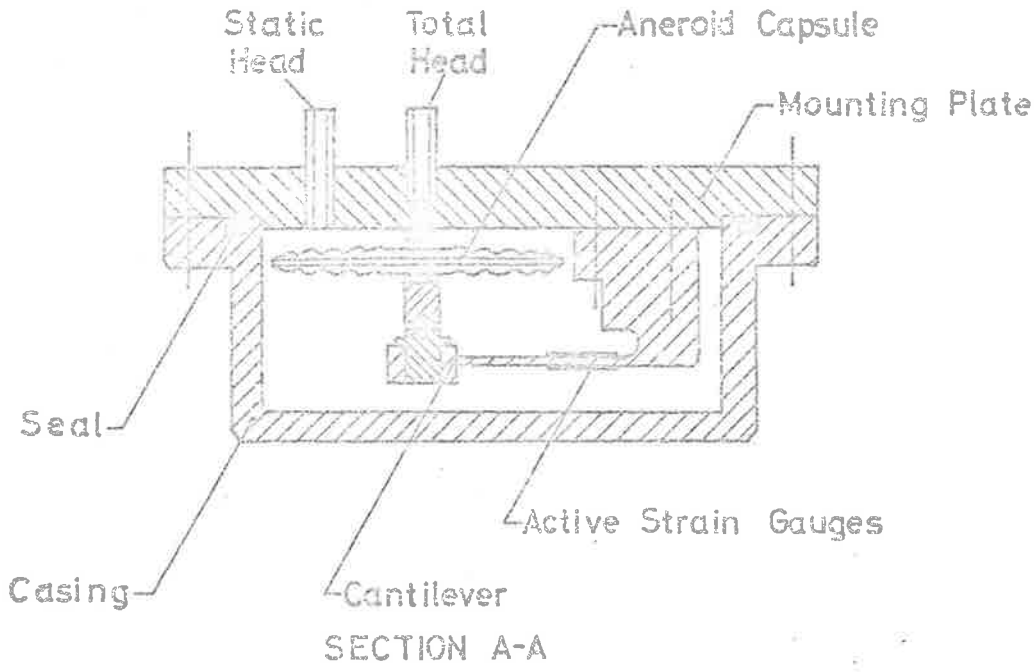

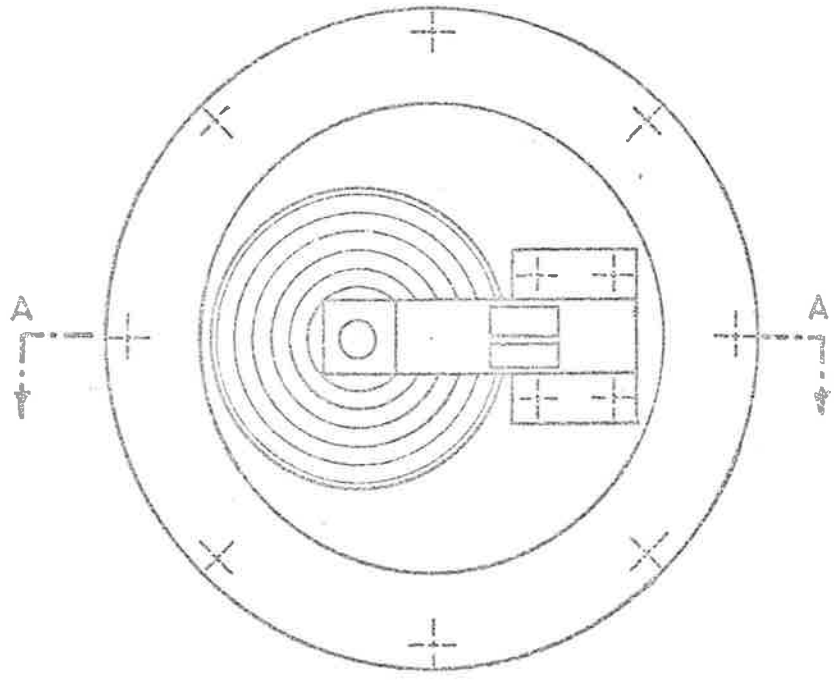

Bottom View — Casing removed.

Fig. 36 Differential Pressure Capsule. -General Arrangement.

an aneroid capsule, and the combination is placed in a container so that the wall static pressure is made to act on the outside of the aneroid capsule while the total pressure from the Pitot tube acts on the inside. The difference in pressure forces on the aneroid capsule results in strain in the cantilever arm. The strain is sensed by a strain gauge bridge cemented on the cantilever, and the output of the bridge is amplified and recorded. The circuit diagram of the strain gauge bridge and its amplifier is shown in figure 37. The amplifier is constructed on a patch board and is enclosed in the differential pressure capsule to ensure temperature stability.

The frequency response of the differential pressure capsule is found to be about 3 Hz. An excellent linearity is indicated by the calibration curve shown in figure 38. The sensitivity of the unit at the output of the strain gauge amplifier is about 8 mV per mm of water gauge or about 60 $\mu V/(N/m^2)$. Hysterisis effects are insignificant for measurements extending to as high as 130 mm of water gauge. There has been no drift in the calibration due to changes of the mean ambient temperature encountered in any tunnel run.

4.3.2 The Traversing Mechanism.

The traversing mechanism for the Pitot tube is shown in figure 39. The spindle of a linear precision potentiometer is attached to the carriage on to which is clamped the stem of the Pitot tube. A regulated voltage supply is applied across the potentiometer, and the location of the Pitot

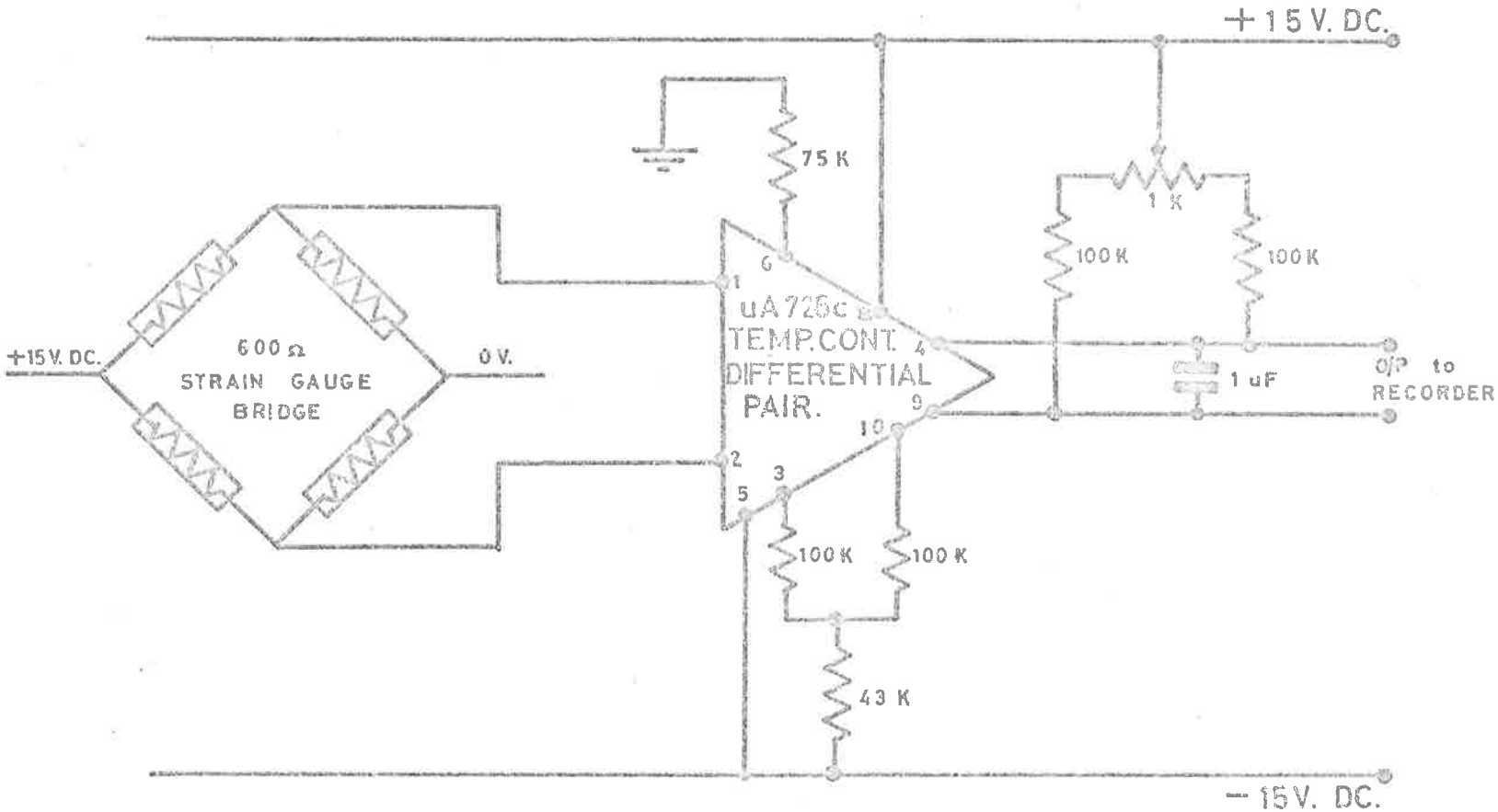

Fig. 37 Strain Gauge Bridge and Bridge Amplifier.

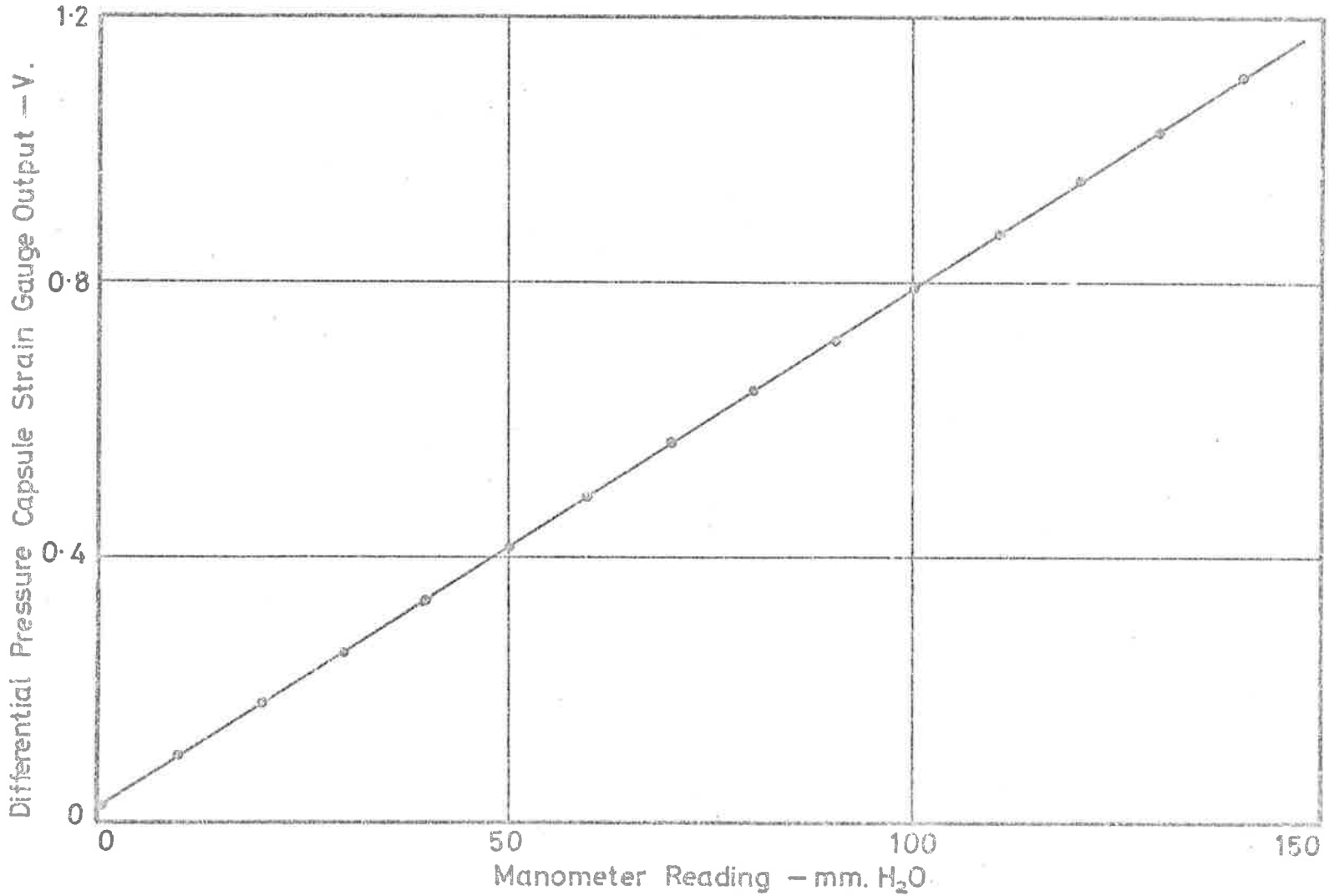

Fig.38 Calibration Curve for Differential Pressure Capsule.

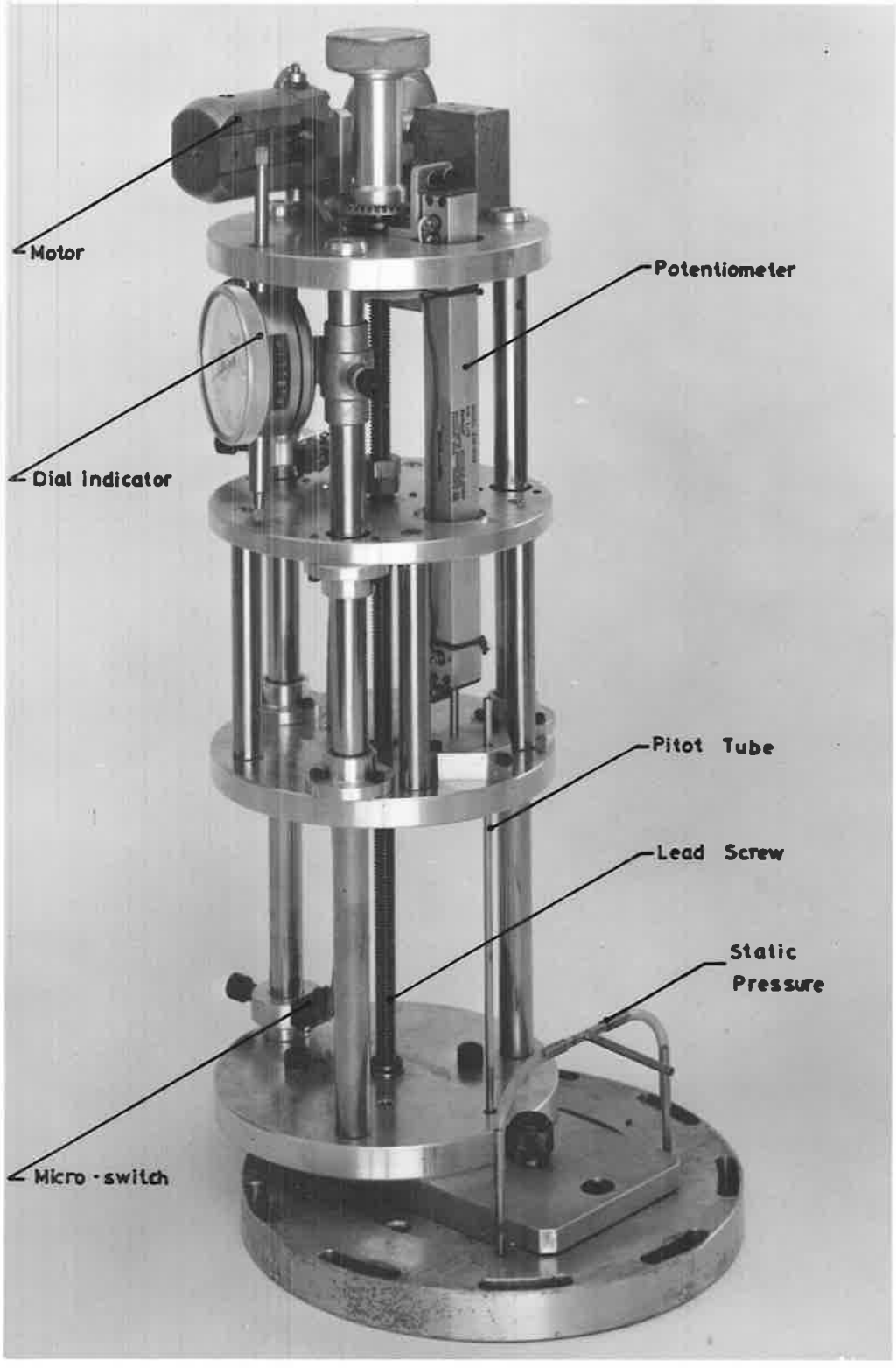

Fig. 39 Pitot Traversing Mechanism.

overlay fig. 39

tube is sensed as a voltage from the wiper of the potentiometer. The resolution of the potentiometer is essentially infinite, and positional accuracy is better than 5 μm. The linearity of the potentiometer is shown in figure 40. The carriage of the traversing mechanism is moved with the aid of a screw driven by a small electric motor which has the facility of directional as well as speed control. The circuit diagram of the power supply to the potentiometer and the variable low voltage supply to the drive of the traversing mechanism is shown in figure 41. A dial indicator is provided to facilitate the positioning of the Pitot tube and to allow the determination of its travel to an accuracy of at least 13 μm (0.0005 inch).

The initial set-up of the Pitot tube in the instrumentation plug to determine its wall position is achieved by observing through a microscope the reflection of the Pitot tube on the highly polished plug surface. The Pitot tube is racked towards the plug surface until the Pitot and its reflection just meet. The dial indicator is then set to zero to indicate the wall position of the Pitot tube. This procedure is adopted before each set of tunnel runs and the readings checked after the conclusion of the runs to ensure that the Pitot tube has not moved in relation to the carriage and the dial indicator.

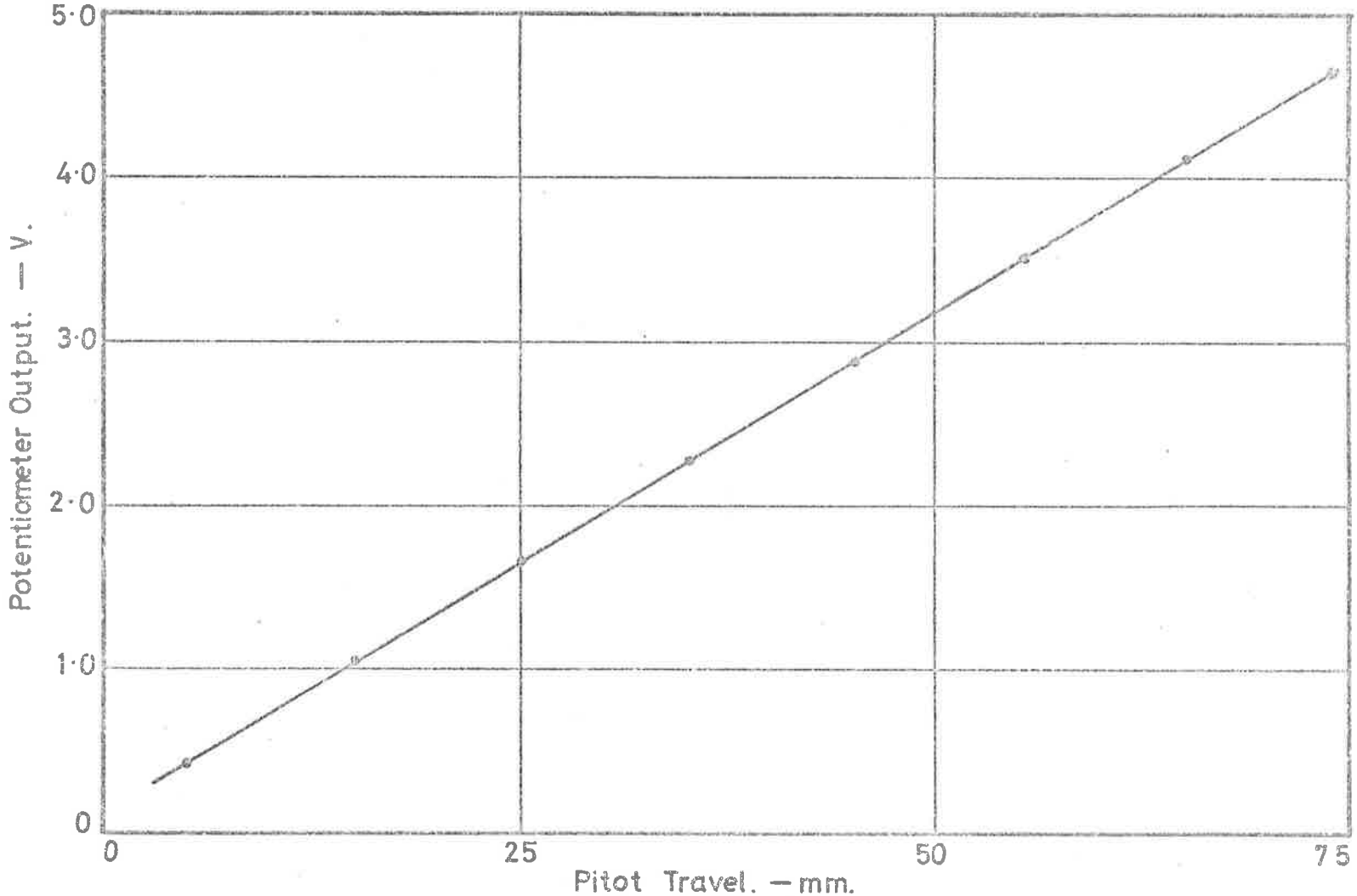

Fig. 40 Calibration Curve for Potentiometer Output.

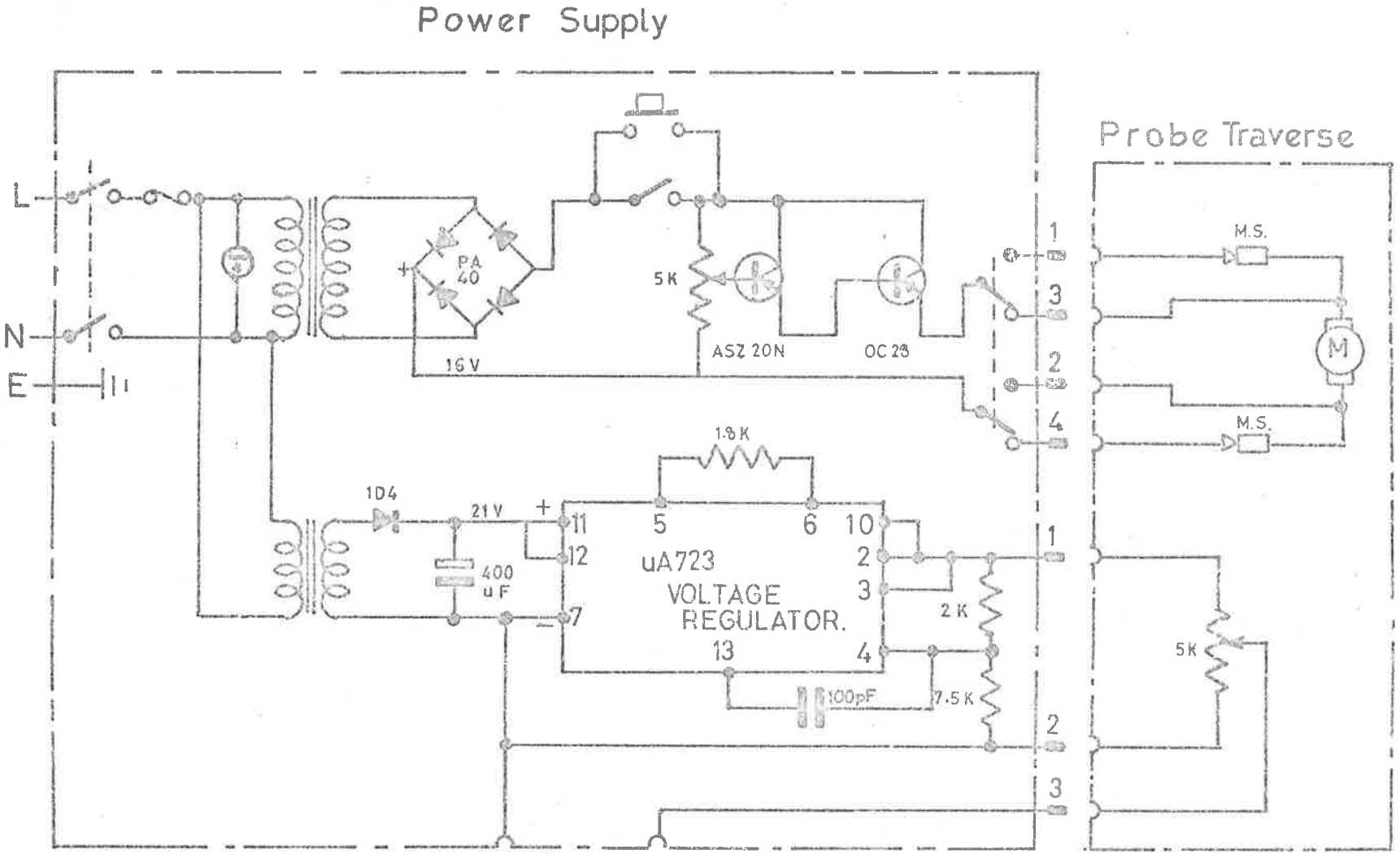

Fig. 41 Circuit Diagram for Pitot Traversing Mechanism.

5. THE EXPERIMENTAL WORK.

5.1 Constant Pressure Boundary Layer Measurements.

A constant pressure turbulent boundary layer was developed in the boundary layer tunnel which has been described in Section 4.1. Measurements of the wall static pressure, the total pressure across the boundary layer, the acoustic field intensity, and the power spectral densities of the fluctuating wall pressures were made in the test section of the tunnel. This work, although very limited in scope, has been conducted mainly with the aim of proving the experimental equipment and supplementing available data regarding the variation of the wall pressure fluctuations with Reynolds number, although it was envisaged that the experience which would be gathered in the exercise would prove to be of help in later measurements in layers developed under the effects of mean pressure gradients.

5.1.1 Mean Flow Properties.

The experimental set-up for the determination of the total pressure distribution in the boundary layer is shown diagrammatically in figure 42. The wall static pressure and the Pitot tube total pressure tappings are connected to the appropriate points in the differential pressure capsule which has been described in Section 4.3. The output of the strain gauge amplifier is connected to a set of terminals on an X-Y plotter while the output of the precision potentiometer indicating the position of the Pitot

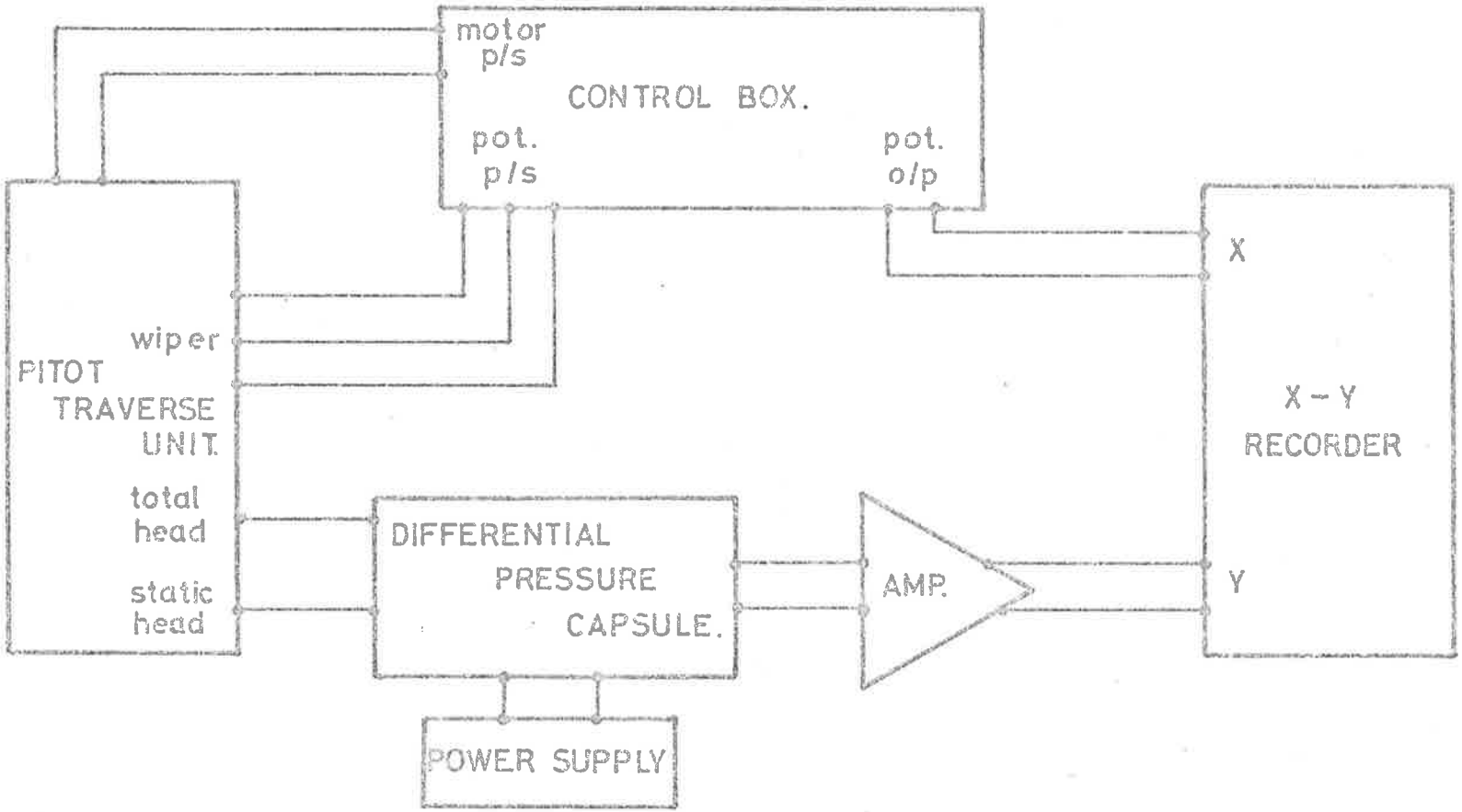

Fig. 42 Schematic Diagram of Experimental Set-up for Boundary Layer Traverse.

tube is connected to the other set of terminals of the plotter. The sensitivity of the plotter is adjusted so that the largest possible trace is obtained. The scaling of the axes is determined by comparing the deflection of the pen in the appropriate direction with the readings of a micro-manometer (for the pressure axis) or the dial indicator (for the Pitot tube travel). A typical trace of the Pitot traverse of the boundary layer is shown in figure 43. The variation of the total pressure across the boundary layer is extracted from the trace with the aid of a curve reader, and the values together with those for the wall static pressure and the total pressure in the free stream are then reduced to give the values required for the determination of the various boundary layer parameters defined in Section 4.3. Patel's calibration for a round Pitot tube was used to compute the wall skin friction C_f and the associated values of the wall shear stress τ_w and friction velocity U_τ. (see Patel (1965)).

It has been shown by the wealth of experimental results that provided the Reynolds number based on the inside diameter of the tube exceeds about 200, the Pitot tube gives accurate measurements of the total pressure in a uniform, non turbulent and subsonic flow independent of the Mach number. However, errors in the total pressures can arise when the Pitot tube is used in a turbulent flow with transverse total pressure gradient (shear flow) and in close proximity to a boundary surface. It is generally accepted that if the flow is turbulent the reading of the Pitot tube is increased by a quantity of the order of $\frac{1}{2}\rho(u^2+v^2+w^2)$, where u, v and w represent the turbulent velocity components. However, as pointed out by

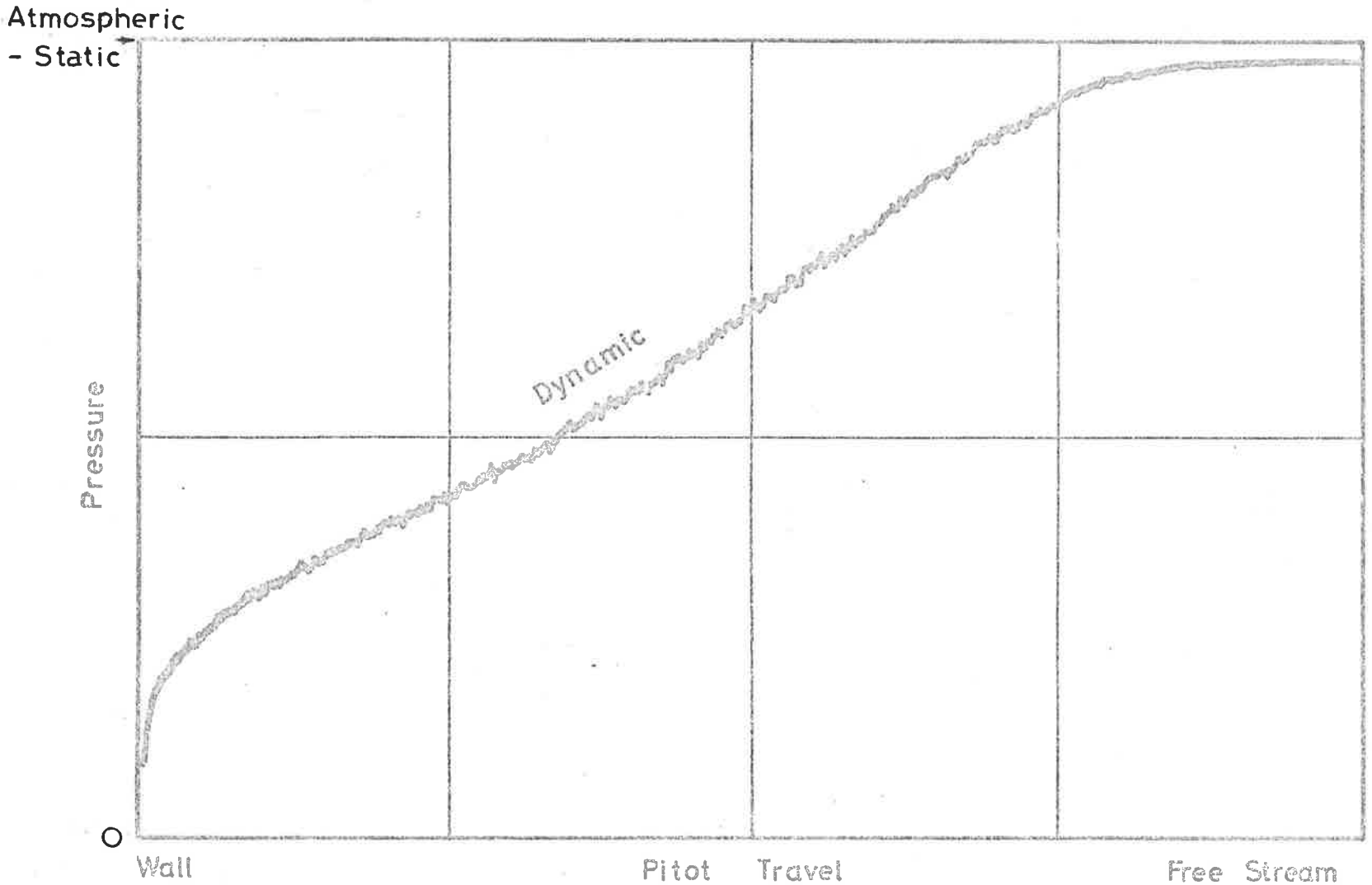

Fig. 43 Typical trace of Pitot traverse across a Turbulent Boundary Layer.

Hinze (1959) there is no universal agreement on the magnitude of the correction to be applied. MacMillan (1956) has shown that the pressure in a Pitot tube in a shear layer is equal to the total pressure at a point displaced about $0.15D_o$ from the centre of the tube in the direction of increasing velocity, where D_o is the outside diameter of the tube. In the case where the Pitot tube is used in the presence of a solid surface so that the centre-line of the tube is located at $y/D_o < 2$, where y is the distance from the surface, the displacement is reduced by the wall effect, and for the tube touching the surface, the displacement is from $0.09D_o$ to $0.11D_o$. Owing to the uncertainty of the corrections to be applied, and since the effect in any case is small, no attempt has been made to correct for the Pitot tube readings in the experimental work reported here.

5.1.2 The Wall Pressure Fluctuations.

The measurements which were made in the experimental investigation of the wall pressure fluctuations beneath a zero pressure gradient turbulent boundary layer are limited to the determination of the frequency power spectral density and the mean square value of the fluctuating pressures. The apparatus is shown diagrammatically in figure 44. The wind tunnel used in the experiment has been described in Section 4.1. The output of the transducer pre-amplifier is connected to the input of the third octave spectrometer whose output is fed into the level recorder. The signal from the transducer pre-amplifier is monitored on the screen of the oscilloscope. The piezo-electric transducers used are set rigidly into the wall of the wind tunnel and flush with its surface with the aid of the removeable

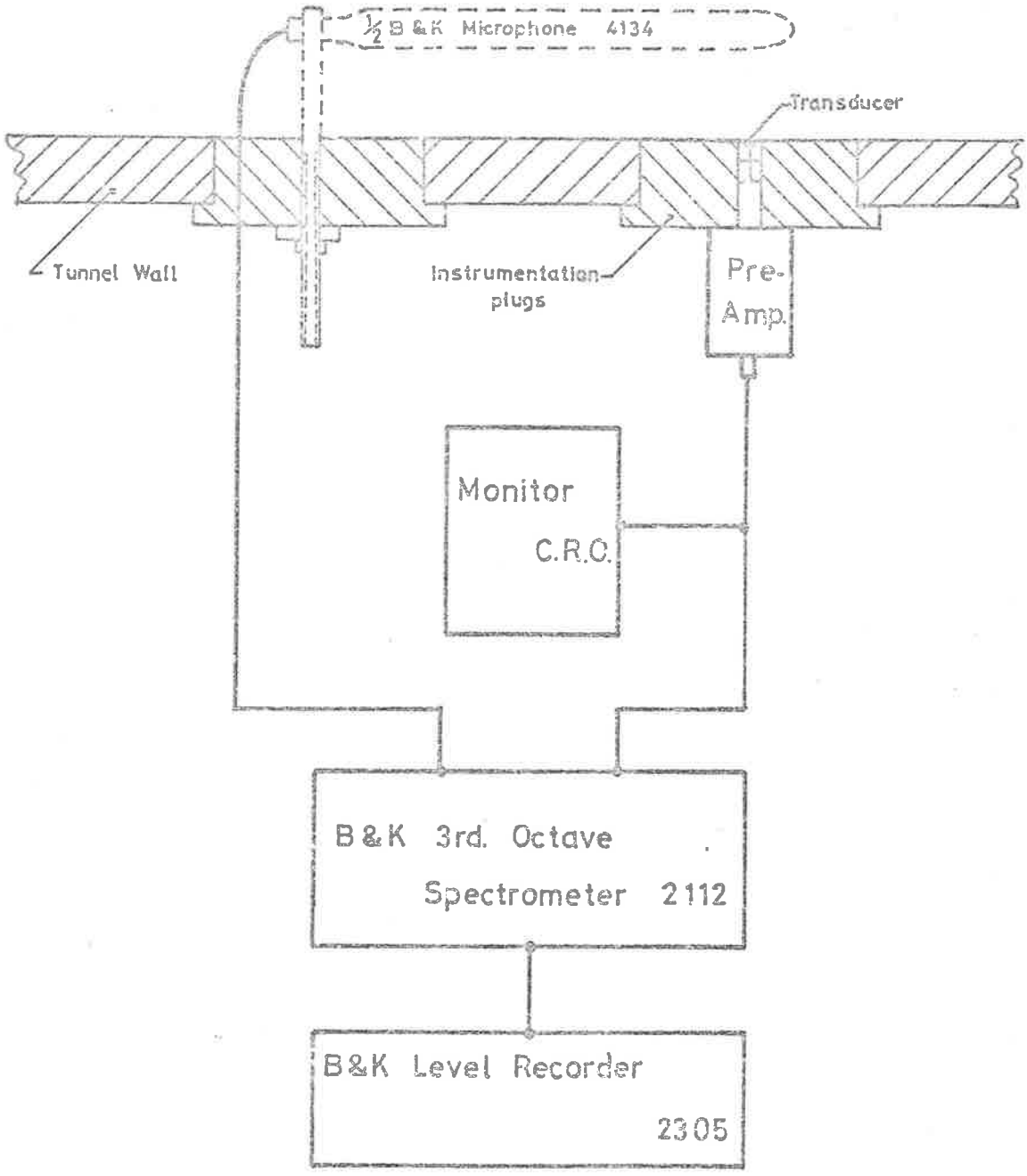

Fig. 44 Block Diagram of Apparatus for Measuring Spectral Density of Wall Pressure Fluctuations.

instrumentation plugs. These transducers have 0.76 mm diameter sensing elements and give, for the present results, values of the ratio of the diameter d of the sensing element to the boundary layer displacement thickness δ^* in the range $0.14 \leq d/\delta^* \leq 0.30$. The construction and calibration of the transducers have been described in Section 4.2. A condenser microphone fitted with a nose cone is placed in the free stream in the test section at a point corresponding to the location of the piezo-electric transducer. Its output is amplified and filtered by the third octave spectrometer before being fed into the level recorder. The recording of the overall spectral levels from the piezo-electric transducers is done after the recording of the acoustic spectral distribution and the removal of the microphone from within the test section.

The signal from the piezo-electric transducer at the output of its pre-amplifier may have in it extraneous contributions due to

(1) electronic noise in the amplification system,

(2) vibration of the transducer whereby the inertial forces generate a signal independent of the boundary layer flow, and

(3) acoustic field in the environment of the transducer.

The extraneous contribution due to the presence of electronic noise accounts for less than 0.5% of the mean square pressure in all measurements. The level of the spectral density of the noise falls off very rapidly with increasing frequency to negligible proportions compared to that of the wall pressure fluctuations. However, at low frequencies, the power spectral

density of this noise can become quite significant and has been found to rise to a level of about 20% of the overall spectral density at 200 Hz. Although the total effect of the noise is small, the procedure adopted is to correct for it at frequencies where it is significant, and to neglect measurements where it is dominant.

The efforts taken to minimise vibration in the test section have been described in Section 4.1. The effect of the precautions and hence the success of the measures were checked by first obtaining the third octave spectral density distribution from the piezo-electric transducer with the tunnel drive stationary, and then repeating the measurements with the tunnel running and the transducer blanked off from the influence of the flow in the test section. The blanking off of the transducer was achieved by retracting the transducer from the surface and inserting a blanking plug to shield the transducer from the effects of the airstream. No significant difference was found in the two spectra except at the centre-band frequency of 160 Hz or 200 Hz depending on the rotational speed of the wind tunnel drive where an increase of the spectral density due to the extraneous disturbance of up to about 6 db was noted. This low frequency excitation appears to be a resonant frequency and has a very narrow band of influence, and its effects soon become negligible with increasing frequency. Hence, at frequencies greater than 250 Hz, the effect of the vibration in the test section can be ignored. In fact, care was taken to ensure that the experimental measurements were made with the speed of the tunnel drive restricted so that the resonant mode at 200 Hz was not excited.

The acoustic field in the environment of the transducer results from the propagation of noise into the test section and from boundary layer noise. The frequency power spectral density distribution of the extraneous contributions due to the acoustic field is shown in figure 45. The spectra from various positions in the working section of the tunnel have been plotted, and it can be seen, by comparison with the spectra of the wall pressure fluctuations shown in figure 53, that the acoustic field makes significant contributions at the low and high frequency ends of the spectrum. The proportion of the extraneous contributions from the acoustic field falls rapidly to negligible values with the increase in the frequency starting with about 25% of the overall power spectral density at 200 Hz. However, this proportion rises again to about the same value at 25 kHz. It is necessary then to correct the overall measurements for acoustic contributions whose sum effect is to account for up to 12% of the mean square value of the wall pressure fluctuations obtained without correcting the spectral distributions for the effects of transducer resolution.

The procedure adopted is to fit a mean curve to each of the third octave spectral density plots for the electronic noise, the extraneous contributions due to the acoustic field, and the output from the piezo-electric pressure transducer obtained from the level recorder. The third octave spectral density distributions are then read off from the fitted curves and reduced to give the frequency power spectral density distribution of the wall pressure fluctuations.

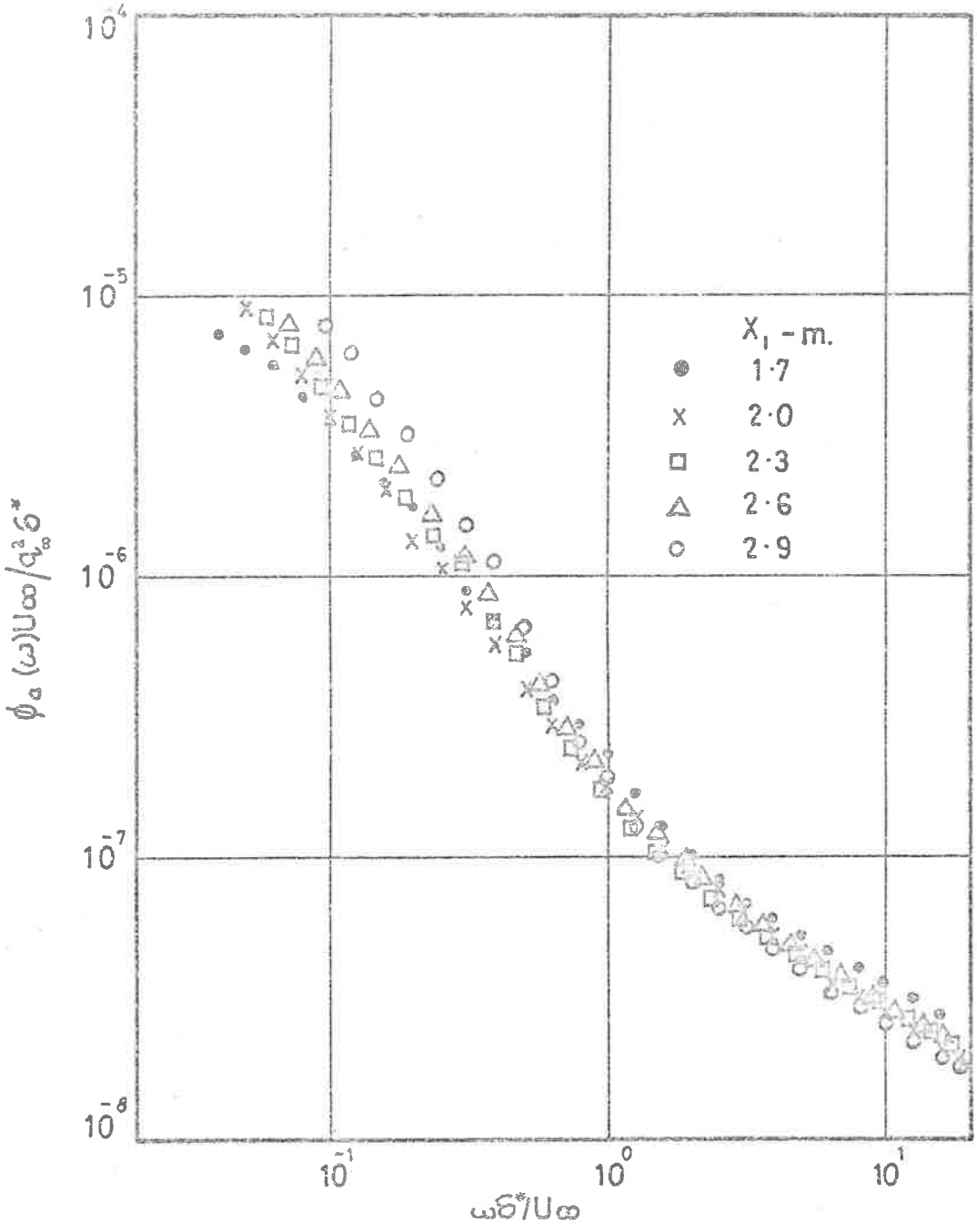

Fig.45 Spectra of Sound Field in Wind Tunnel Working Section.

5.1.3 Results and Discussions.

The variation of the free stream dynamic pressure q_∞ along the full length of the wind tunnel test section is shown in figure 46 in conjunction with the variation of the free stream velocity U_∞ along a section of the tunnel. It can be seen that over the distance of 1.3 m to about 3.1 m from the start of the test section, an essentially constant pressure flow region has been achieved.

The mean velocity profiles at 5 streamwise stations are shown in figure 47. The variations of δ^*, θ, and H (determined according to Equations (4.3.1), (4.3.2), and (4.3.3)) with distance from the start of the wind tunnel test section are shown in figure 48, and the variations of the Reynolds numbers Re_{δ^*} and Re_θ, based on the boundary layer displacement thickness and the momentum thickness respectively, are shown in figure 49.

Clauser (1954) has shown that for an equilibrium turbulent boundary layer

$$\frac{\delta^*}{\delta} = C_1 \frac{U_\tau}{U_\infty} \quad , \qquad \ldots(5.1.1)$$

where δ is the geometrical thickness of the boundary layer, U_τ is the friction velocity,

$$C_1 = \int_0^\infty \left(\frac{U_\infty - U_1}{U_\tau} \right) d(y/\delta) \quad , \text{ and}$$

y is the distance from the boundary surface. Coles (1956) has given the

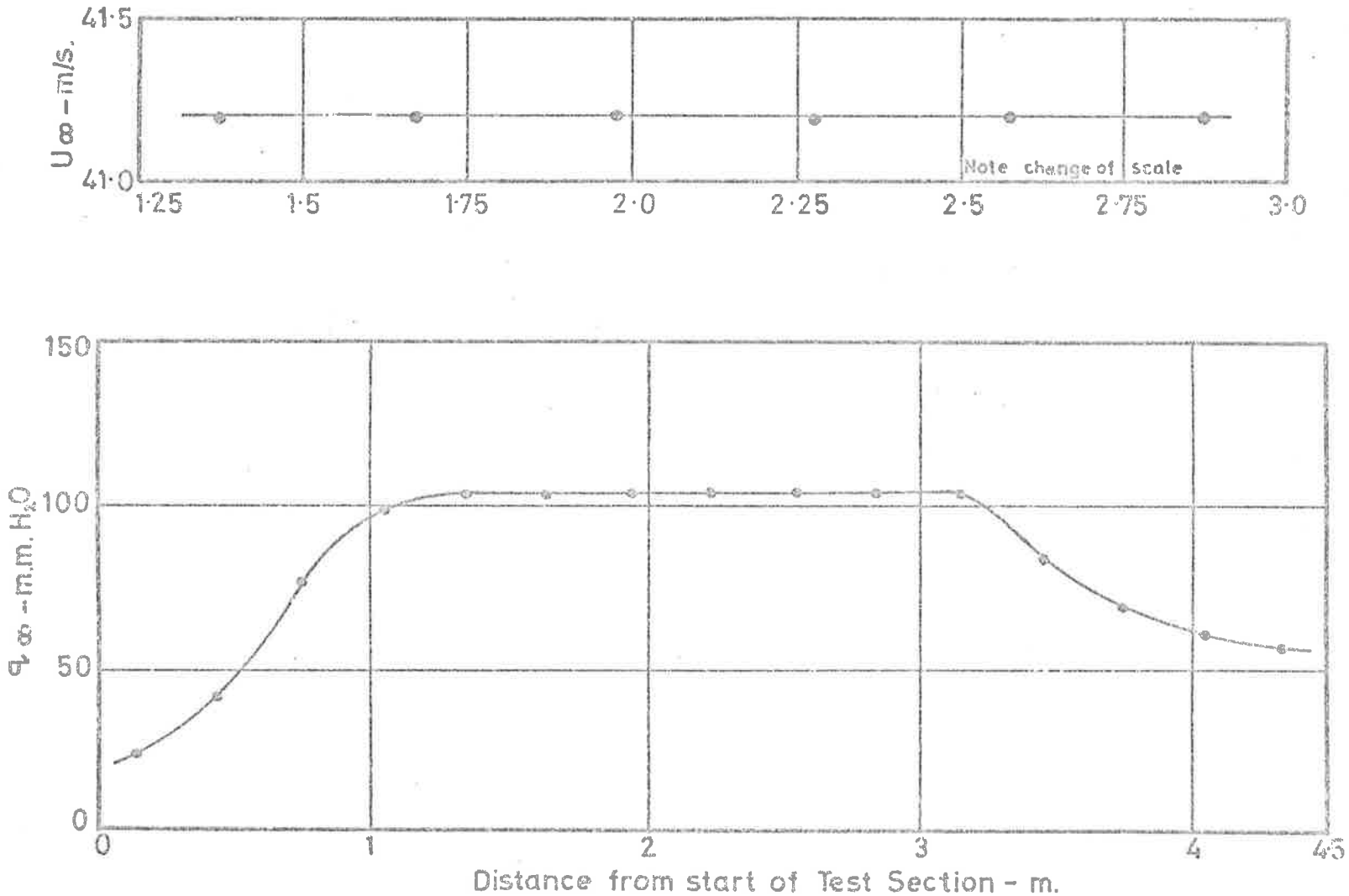

Fig. 46 Variation of Dynamic Pressure and Free Stream Velocity along Test Section.

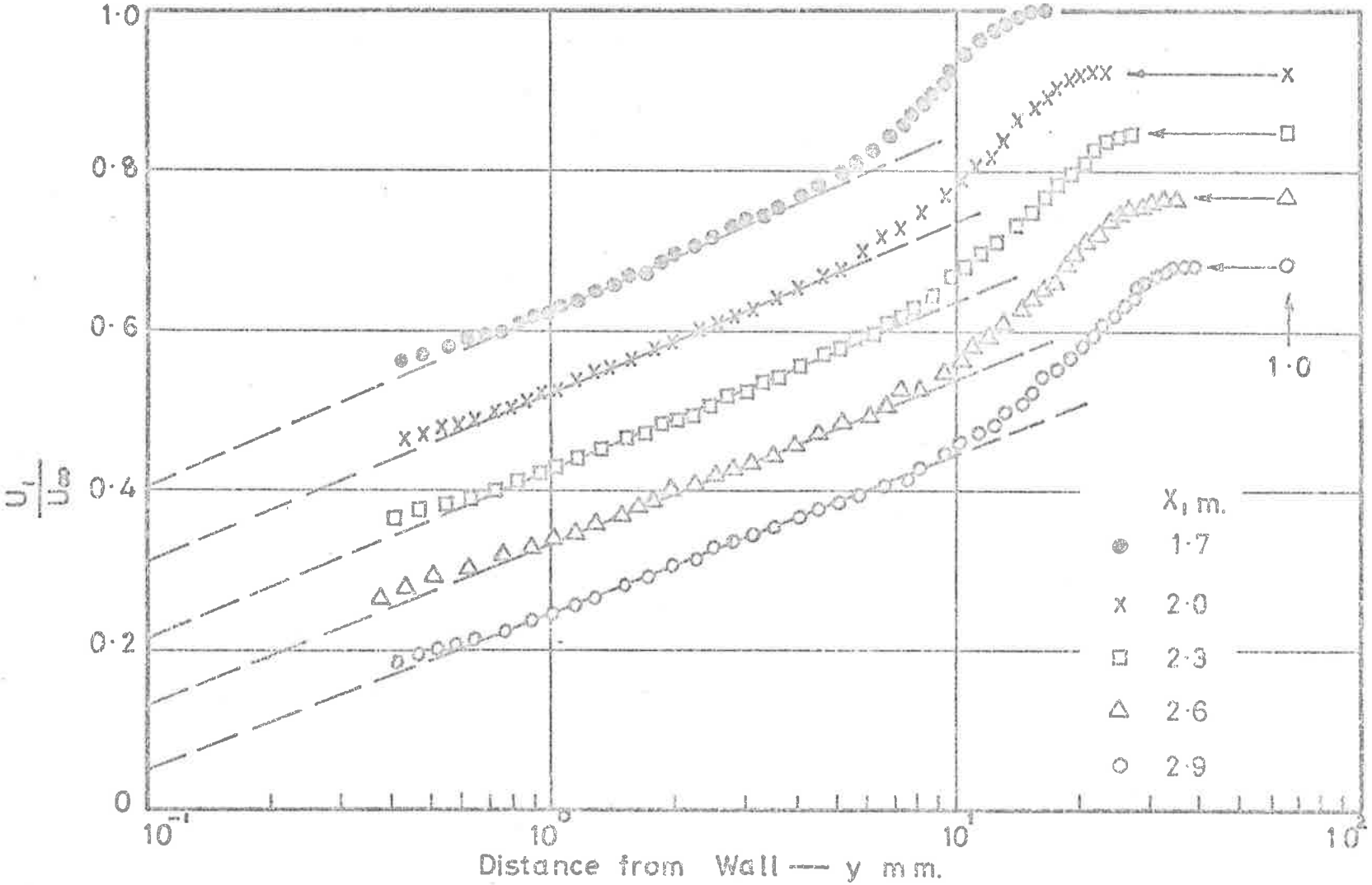

Fig. 4'7 Boundary Layer Mean Velocity Profiles.

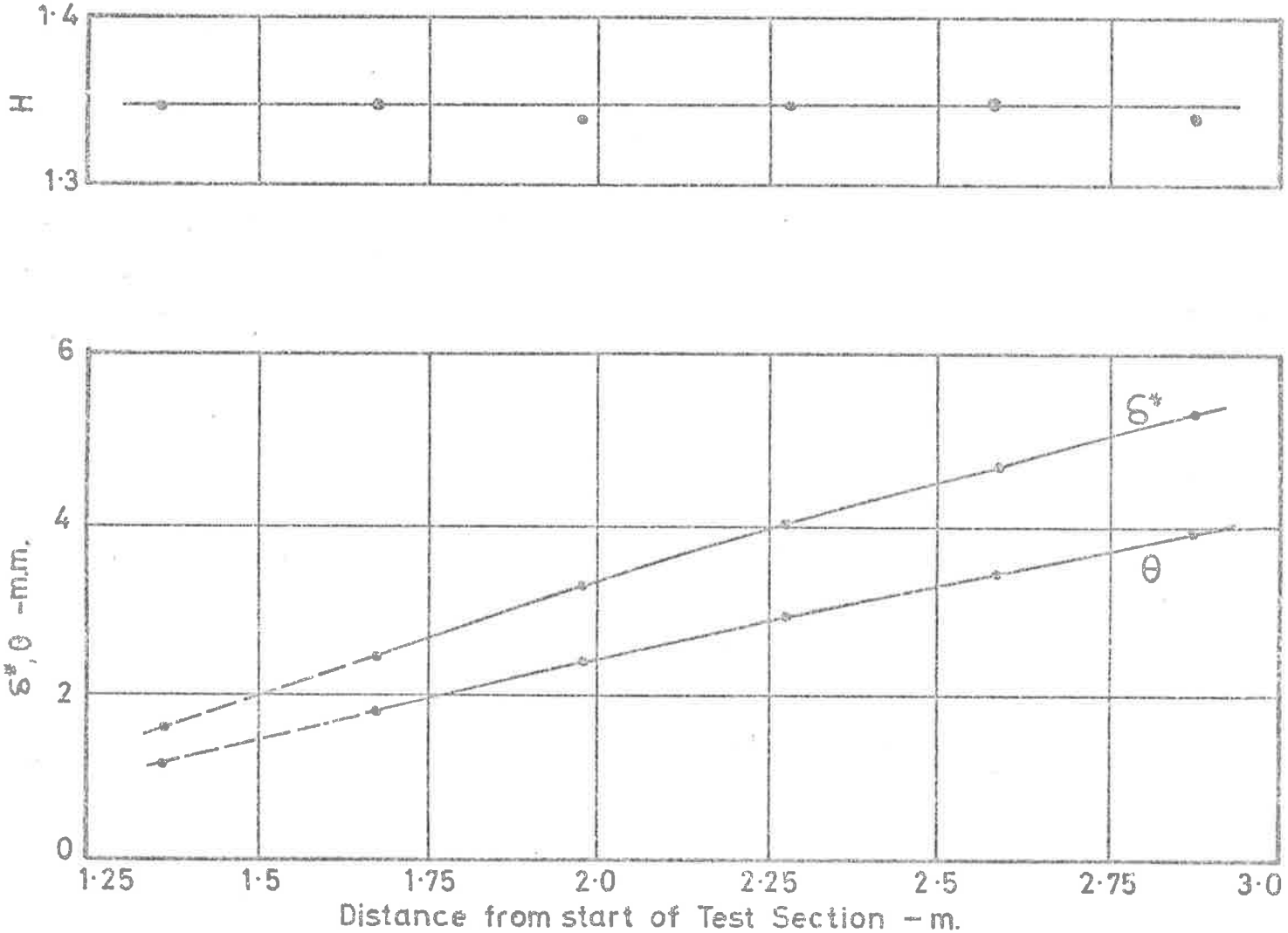

Fig. 48 Variation of δ^*, θ and H along Test Section.

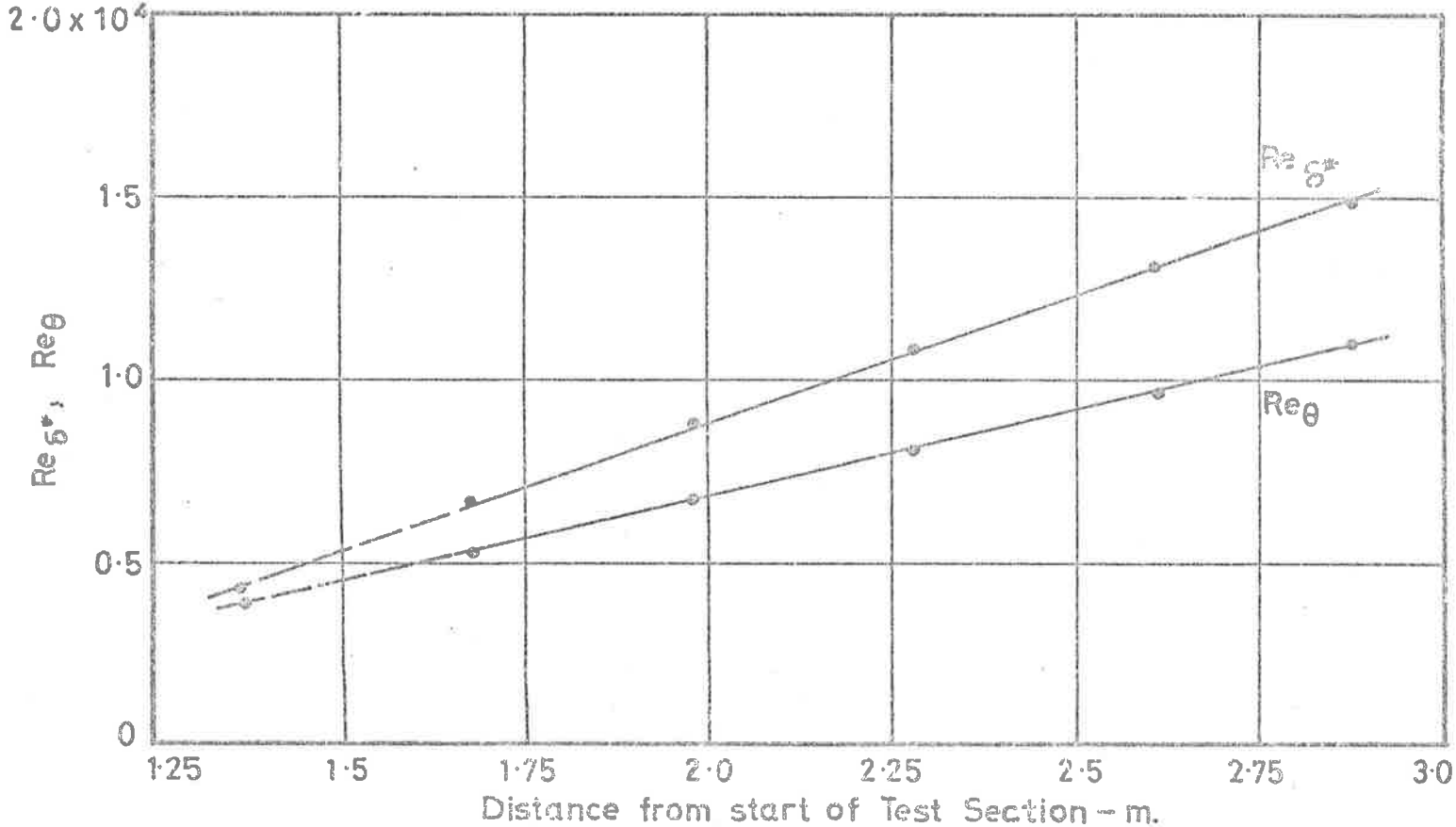

Fig. 49 Variation of Re_{δ^*}, Re_θ along Test Section.

value of C_1 as 3.88. The value of δ can then be obtained by the use of Equation (5.1.1) and its variation along the wind tunnel test section is shown in figure 50 along with that of the Reynolds number Re_δ based on this geometrical thickness of the boundary layer.

It has been recognised for quite some time that certain regions may be distinguished in a boundary layer. In the region of the fluid immediately adjacent to the boundary, the flow must be mainly viscous as all velocities, including turbulence fluctuations, become zero at the boundary, and so does the Reynolds number expressed in terms of the local velocity and distance from the boundary. This predominantly viscous region is called the viscous sublayer. Outside this region the effect of viscosity on the flow will decrease gradually with increasing distance from the boundary until, ultimately, a region is reached where the flow is completely turbulent and viscosity effects are negligibly small. The intermediate region where the flow is neither completely viscous nor completely turbulent is called the transition region. In the fully turbulent region near the boundary surface, the mean velocity profile is given by the "law of the wall" as

$$\frac{U_1}{U_\tau} = \frac{1}{\kappa}\left[\ln\left(\frac{yU_\tau}{\nu}\right) + A\right], \qquad \ldots(5.1.2)$$

where A and κ are constants. The wall skin friction can then be determined using the method of Clauser (1954), and the values obtained are shown in figure 51 along with the values of the wall shear stress and the friction velocity. These values are in general agreement with the values obtained using Patel's (1965) calibration for the round Pitot tube, the discrepencies

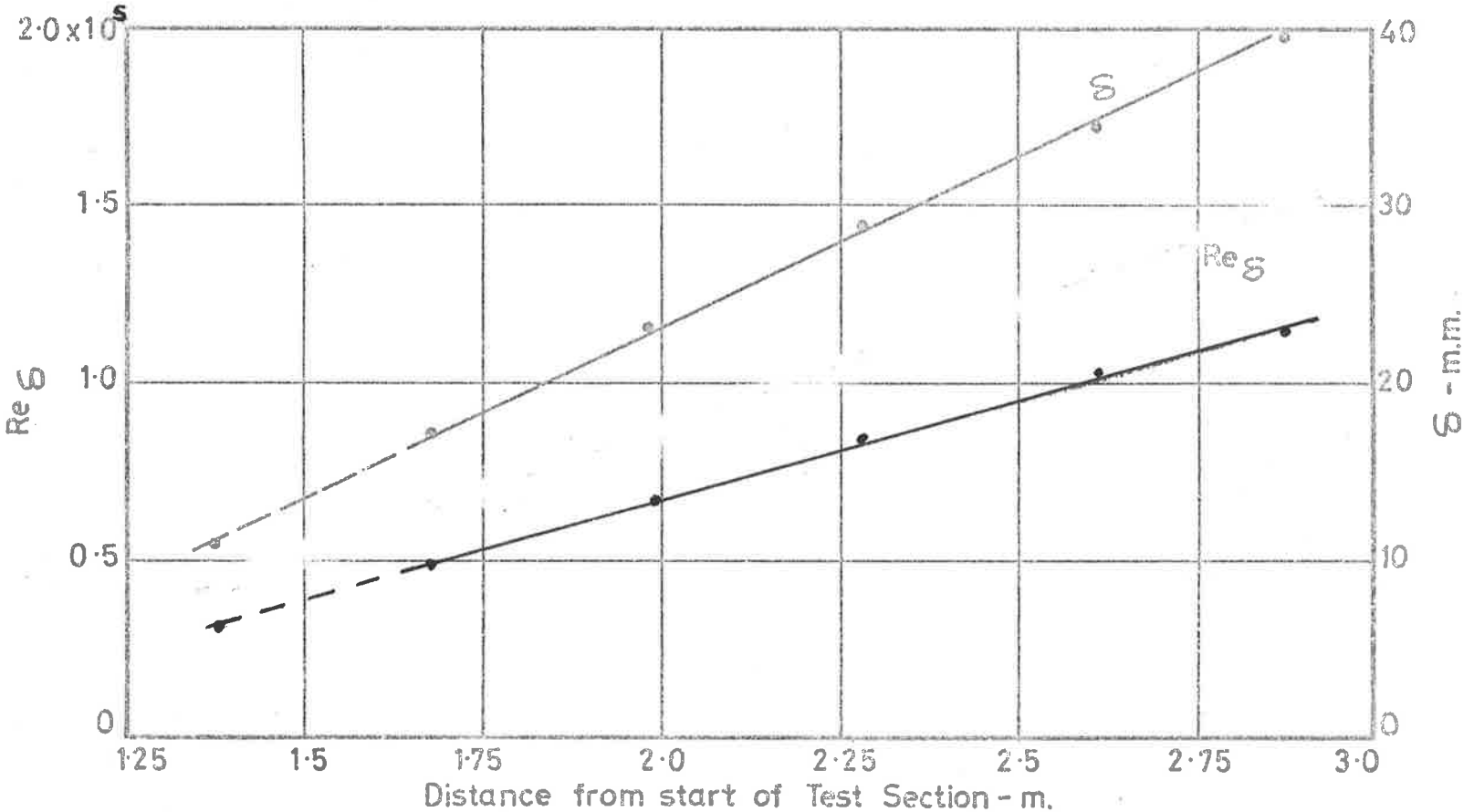

Fig. 50 Variation of δ and Re_δ along Test Section.

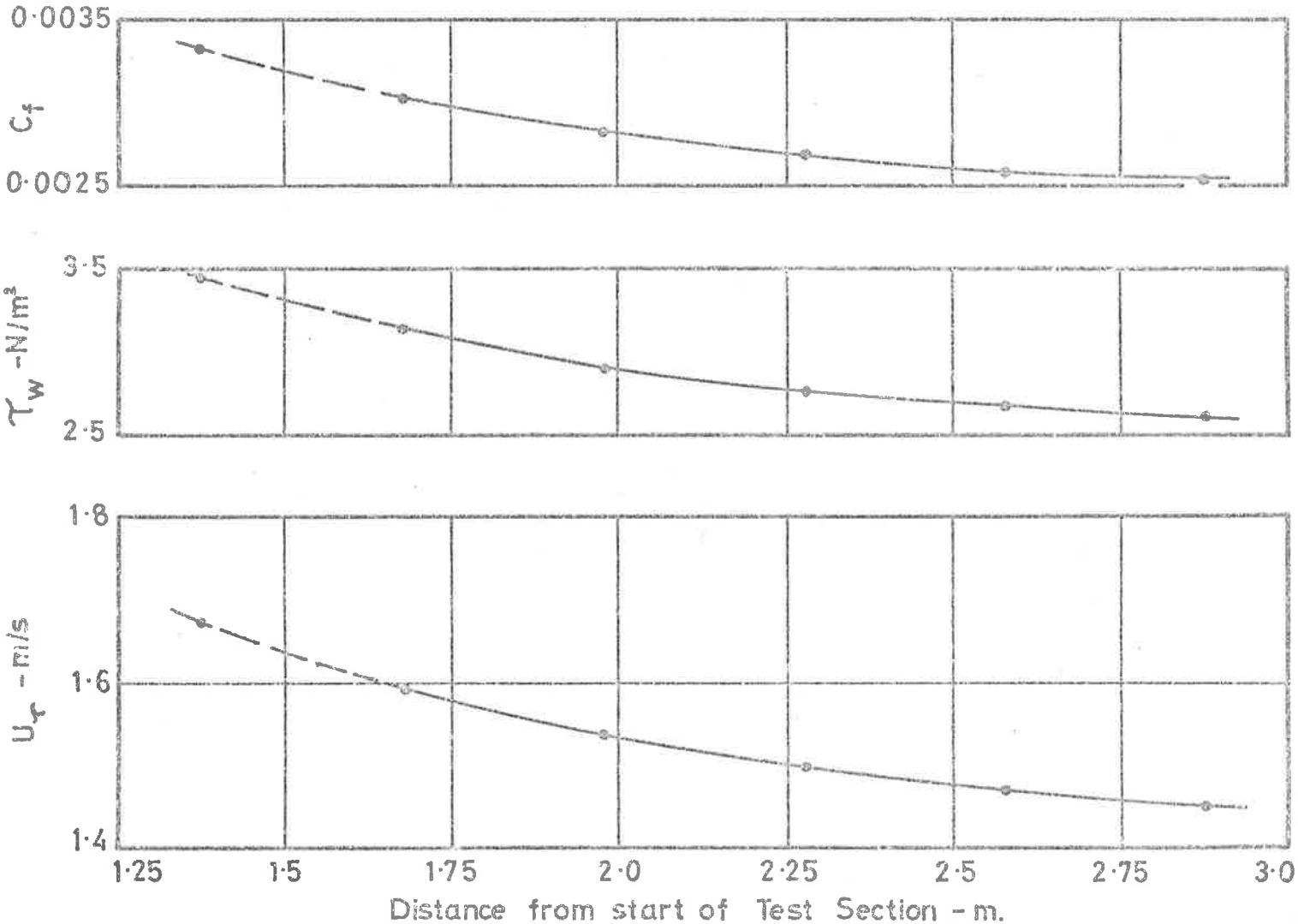

Fig. 51 Variation of C_f, U_τ and τ_w along Test Section.

being only, at worst, 5%.

The velocity profiles, replotted in the form $(U_\infty - U_1)/U_\tau$ against y/δ, are shown in figure 52. The experimental profiles give a mean curve which is in excellent agreement with Coles's (1956) profile but is different from the one suggested by Bull (1969a) and which has been used in the boundary layer model described in Section 3.1, although the differences are not great. However, the results do show that in the outer region and in a portion of the inner region the boundary layer is obeying the velocity defect law.

The distribution of the frequency power spectral density $\phi_p(\omega)$ of the wall pressure fluctuations corrected for both acoustic and amplifier electronic noise is shown in figure 53 along with the mean experimental curves obtained by Willmarth and Wooldridge (1962), Hodgson (1962), Schloemer (1967), Bull (1967), and Blake (1970). Due to the low signal to noise ratio at the low and high frequencies, measurements below the frequency of 200 Hz and those above 25 kHz have been rejected, and the results which have been presented cover the range $0.075 \leq \omega\delta^*/U_\infty \leq 20$. The results are in good agreement (to within 2 db over the major portion of the frequency range) with measurements which have similar d/δ^* values.

The mean square value of the wall pressure fluctuations $\langle p^2 \rangle$ is determined by the integration of the power spectral density which has been corrected for electronic and acoustic noise, that is,

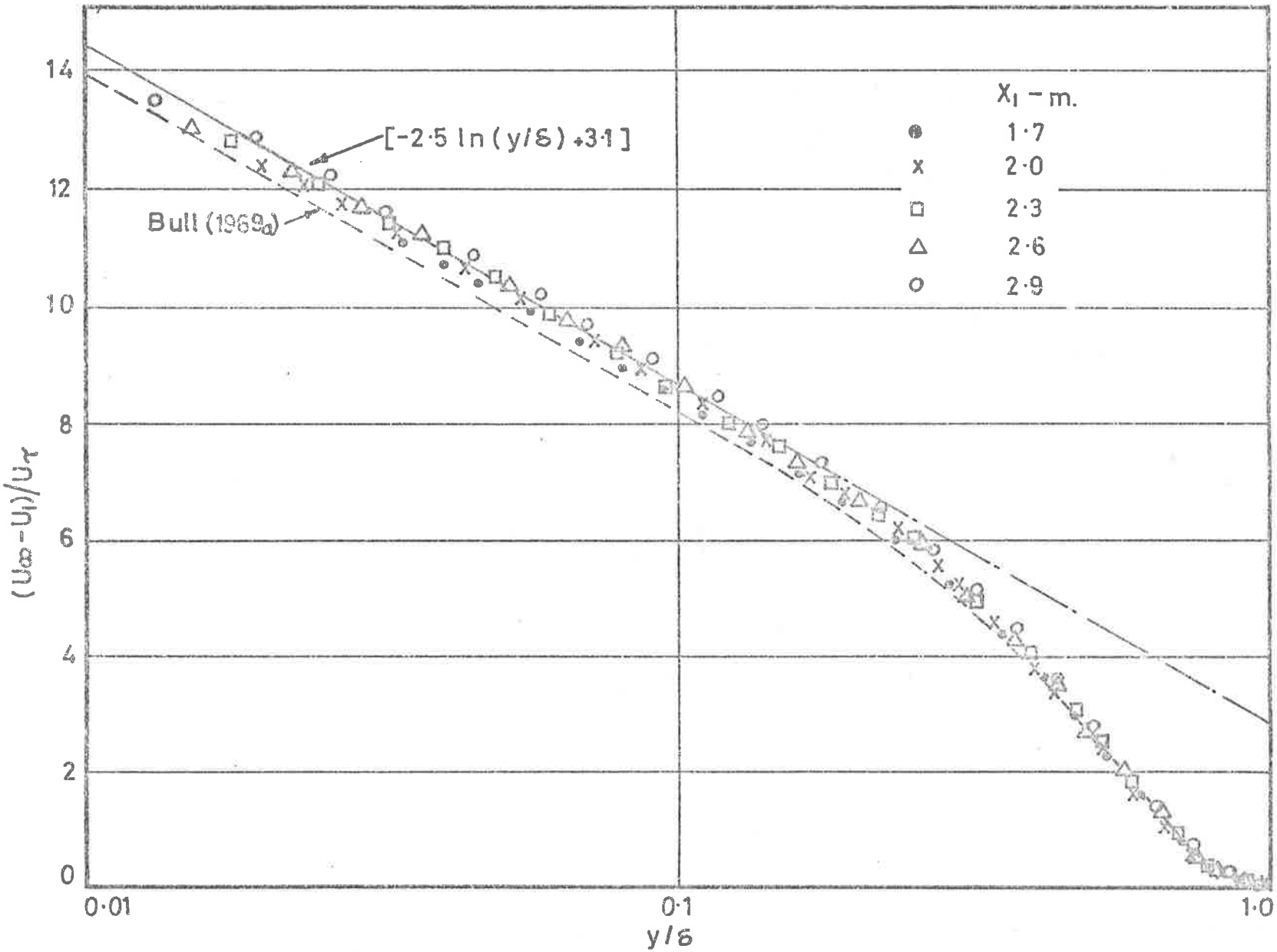

Fig. 52 Boundary Layer Velocity Profiles.

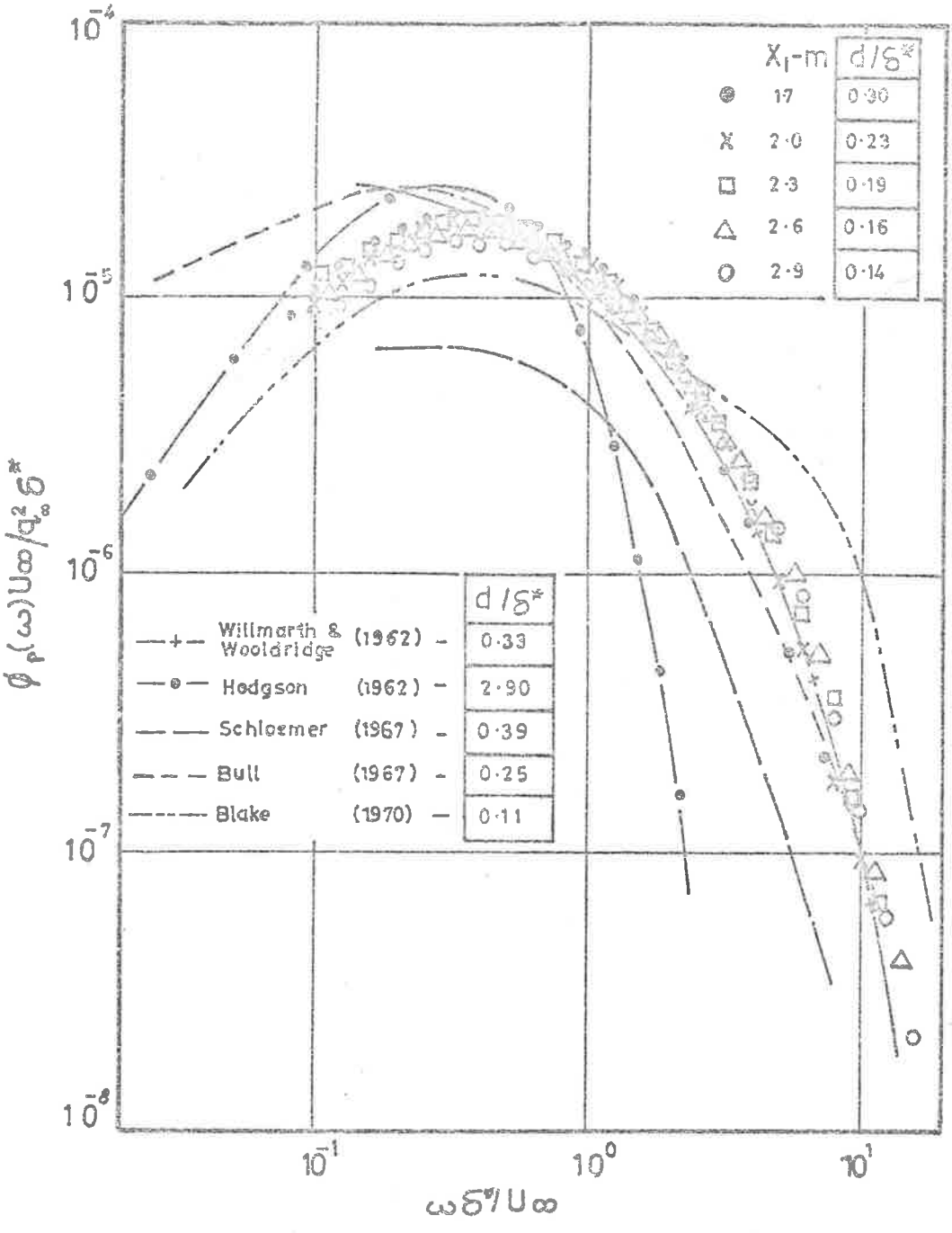

Fig.53 Frequency Spectra of Wall Pressure Fluctuations not corrected for Transducer size.

$$\langle p^2 \rangle = \int_0^\infty \phi_p(\omega)\, d\omega \quad . \qquad \ldots(5.1.3)$$

Corcos (1963) has shown that the effects of transducer resolution and, hence, the correction that has to be applied to the measured values can be quite considerable at the higher frequencies. The correction to the measured spectral density relies on the representation of the cross-spectral density or the narrow frequency band correlations as a function of $\omega\xi_1/U_c(\omega)$ and $\omega\xi_3/U_c(\omega)$ (where ξ_1 and ξ_3 are the separation distances in the x_1 and x_3 directions respectively and $U_c(\omega)$ is the frequency dependent convection velocity) and is a function of $\omega r/U_c(\omega)$, where r is the radius of the circular transducer element. One of the aims of the experimental work was to achieve a small d/δ^* so that little or no corrections of the measured values would be required. However, although the ratio of d/δ^* is relatively small for the present case, the corrections at the higher frequencies are still large and certainly cannot be ignored. The results of Bull (1967) are used to give the require values of $U_c(\omega)$, and the corrections to the measured spectral density distributions are applied according to the values calculated by Corcos and given in figure 54. The results of the corrected spectra are shown in figures 55, 56 and 57. Good collapse of the experimental data can be seen in each of the three figures although it must be kept in mind that the range of experimental conditions is rather limited. Figure 56 indicates that the frequency distributions of the various spectra are similar, and the comparison of figure 55 with figure 57 indicates that the free stream dynamic pressure would be a more useful non-dimensionalising parameter than the wall shear stress as the

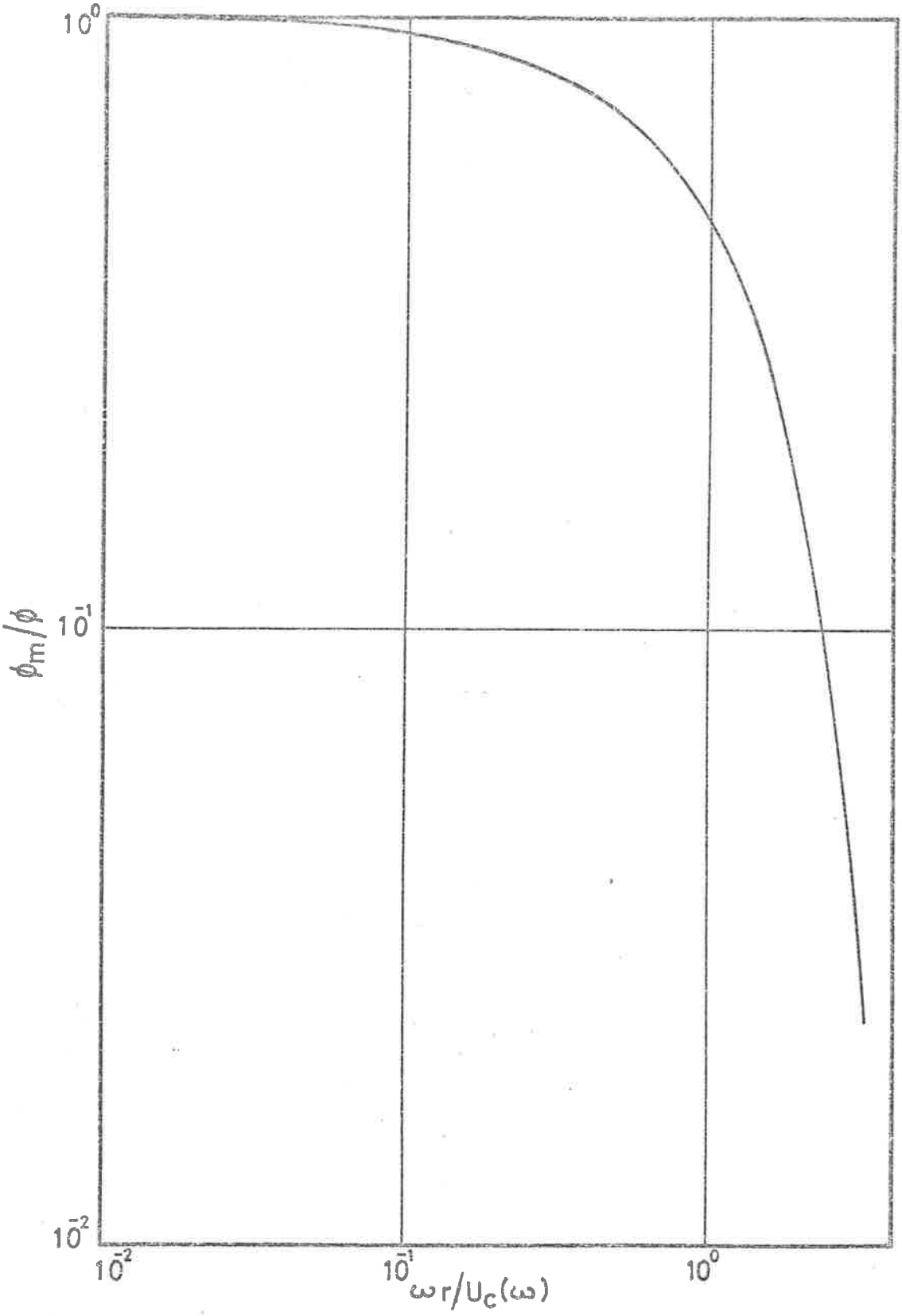

Fig.54 Attenuation of the Frequency Power Spectral Density by a Circular Pressure Transducer. (After Corcos 1963.)

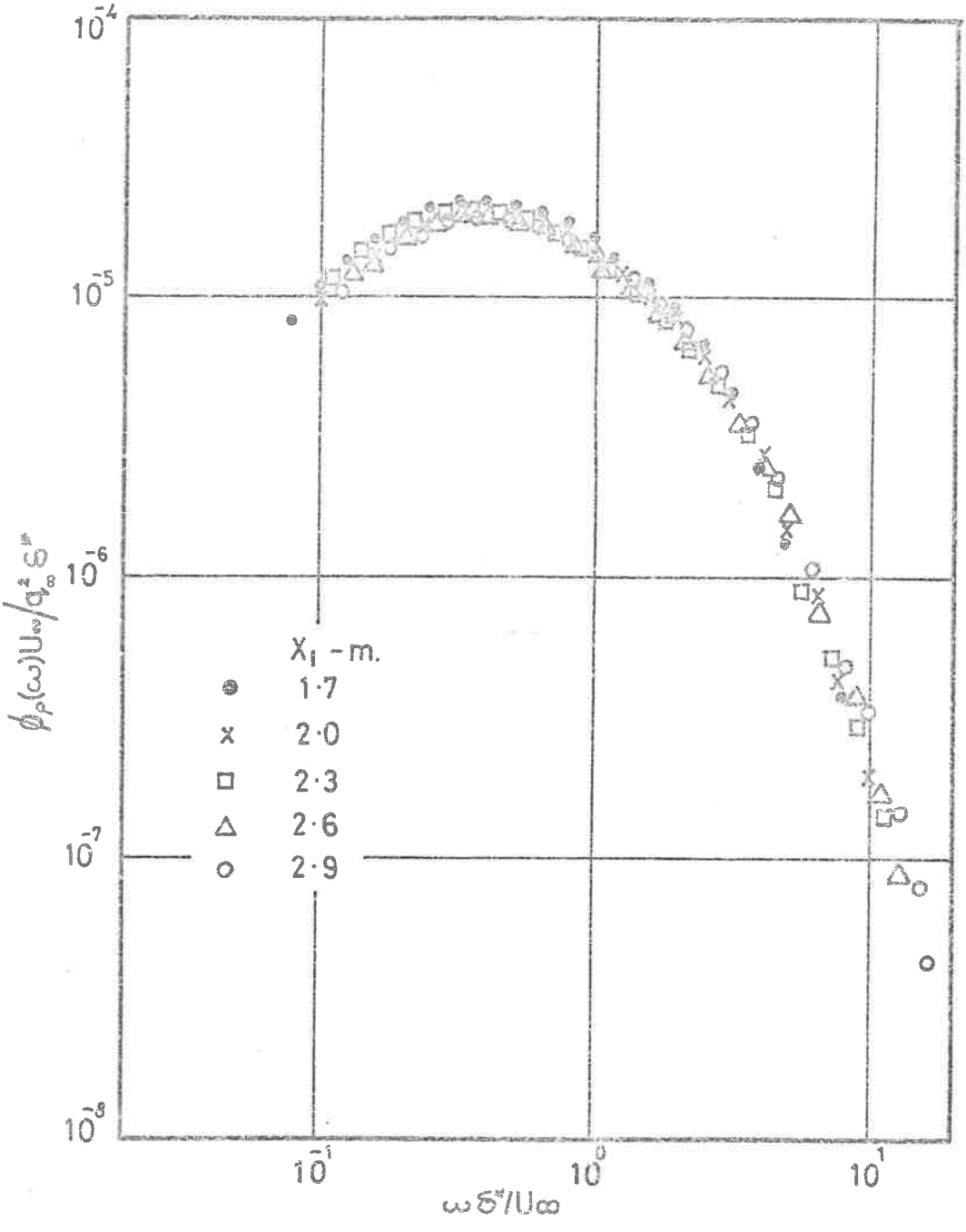

Fig.55 Frequency Spectra of Wall Pressure Fluctuations corrected for Transducer size.

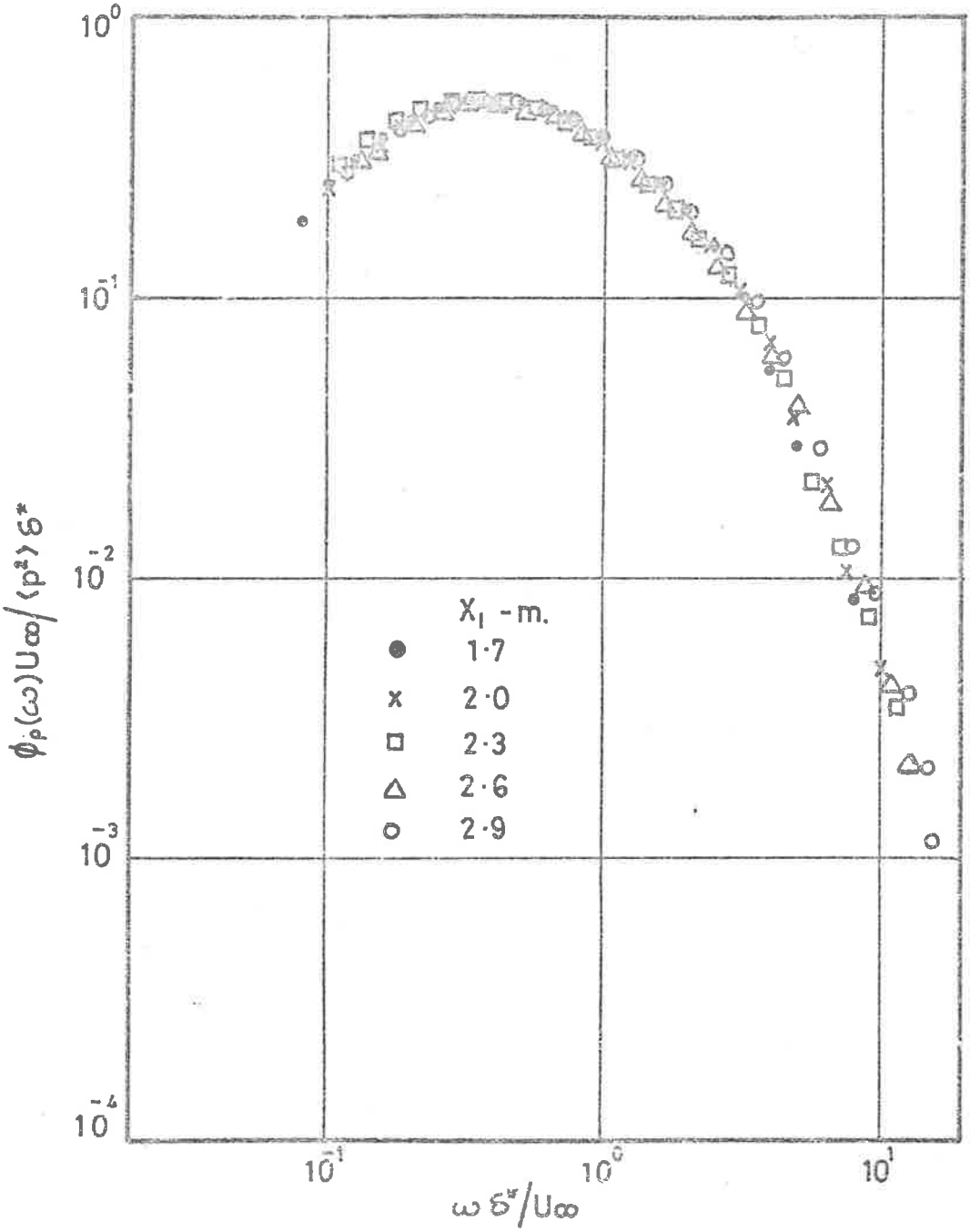

Fig.56 Frequency Spectra of Wall Pressure Fluctuations corrected for Transducer size.

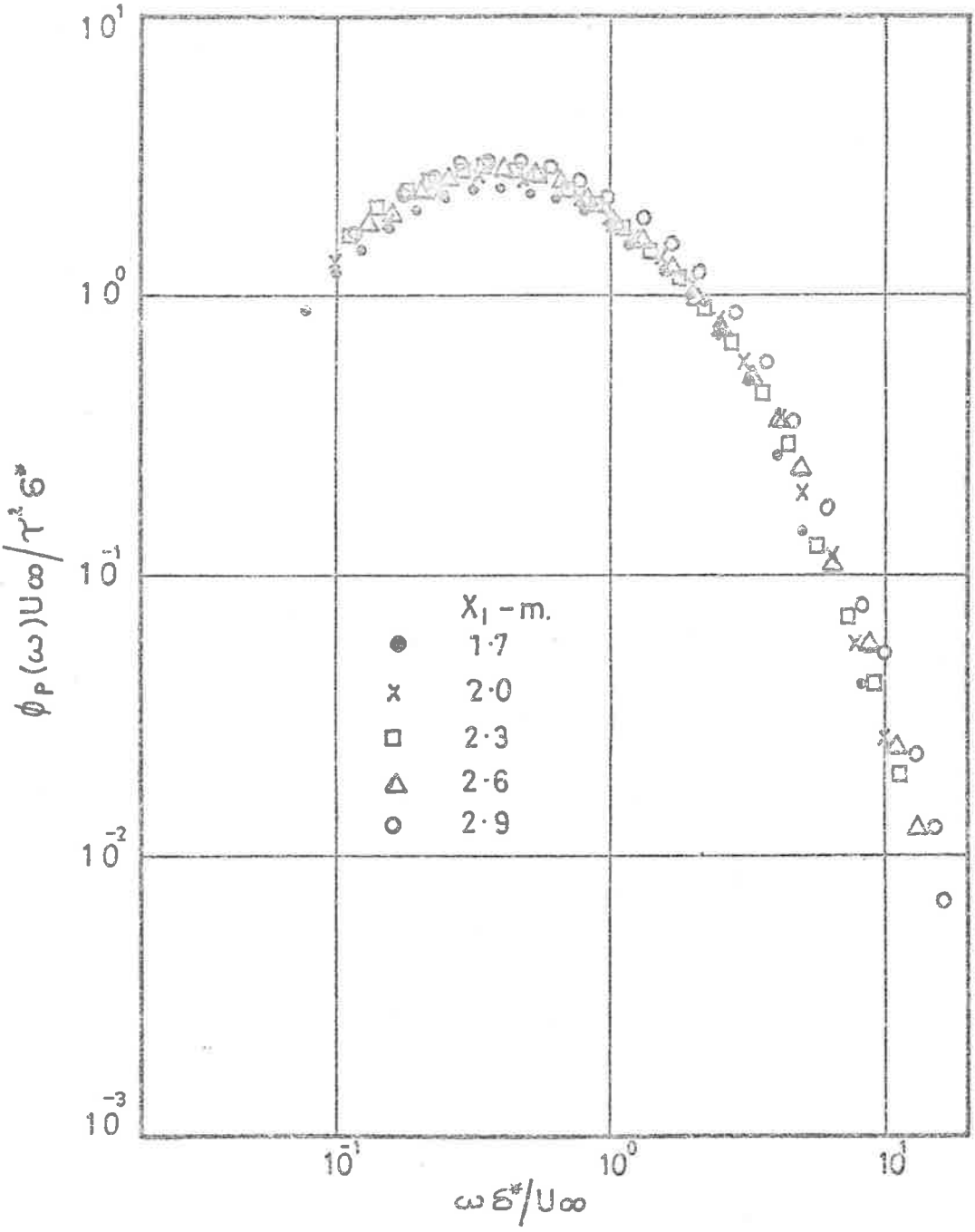

Fig.57 Frequency Spectra of Wall Pressure Fluctuations corrected for Transducer size.

variation between the spectra is less in figure 55 than that in figure 57, thus indicating that p'/q_∞ may have a value which can be regarded as constant and independent of the Reynolds number for most engineering purposes at least for $7\times10^3 \leq Re_\delta^* \leq 1.5\times10^4$ where p'/q_∞ is from 6.8×10^{-3} to 6.3×10^{-3}.

The mean square value of the wall pressure fluctuations corrected for transducer size effects is obtained from the frequency power spectral density distribution which has been corrected for transducer size effects. The variation of the root mean square value of the pressure fluctuations in the wind tunnel test section for the values as measured and for values corrected for transducer size effects is shown in figure 58. The ratio of the corrected to the uncorrected values p'/p'_m is shown in figure 59 where the results of Bull (1967) have been included for comparison. Bull's results were originally plotted against δ, and the assumption used here in the re-presentation of his results is that $\delta/\delta^* = 7.84$, a value representing the mean obtained from his measurements. The variation of the root mean square wall pressure fluctuations as a function of the Reynolds number is shown in figure 60. Bull's results have also been plotted in figure 60(b) for comparison. Over the Reynolds number range $7\times10^3 \leq Re_\delta^* \leq 1.5\times10^4$, p'/τ_w when determined from the measured spectral density curves varies from 2.1 to 2.4. After the application of the correction for transducer size, p'/τ_w varies from 2.3 to 2.5 over the same Reynolds number range. Although the Reynolds number covered by the present experimental results is rather limited, the variation of p'/τ_w with Reynolds number as reported by Bull is again evident. The present results give values of p'/τ_w which are higher than those of Bull, but the differences can be classified as small being at worst only about 6%.

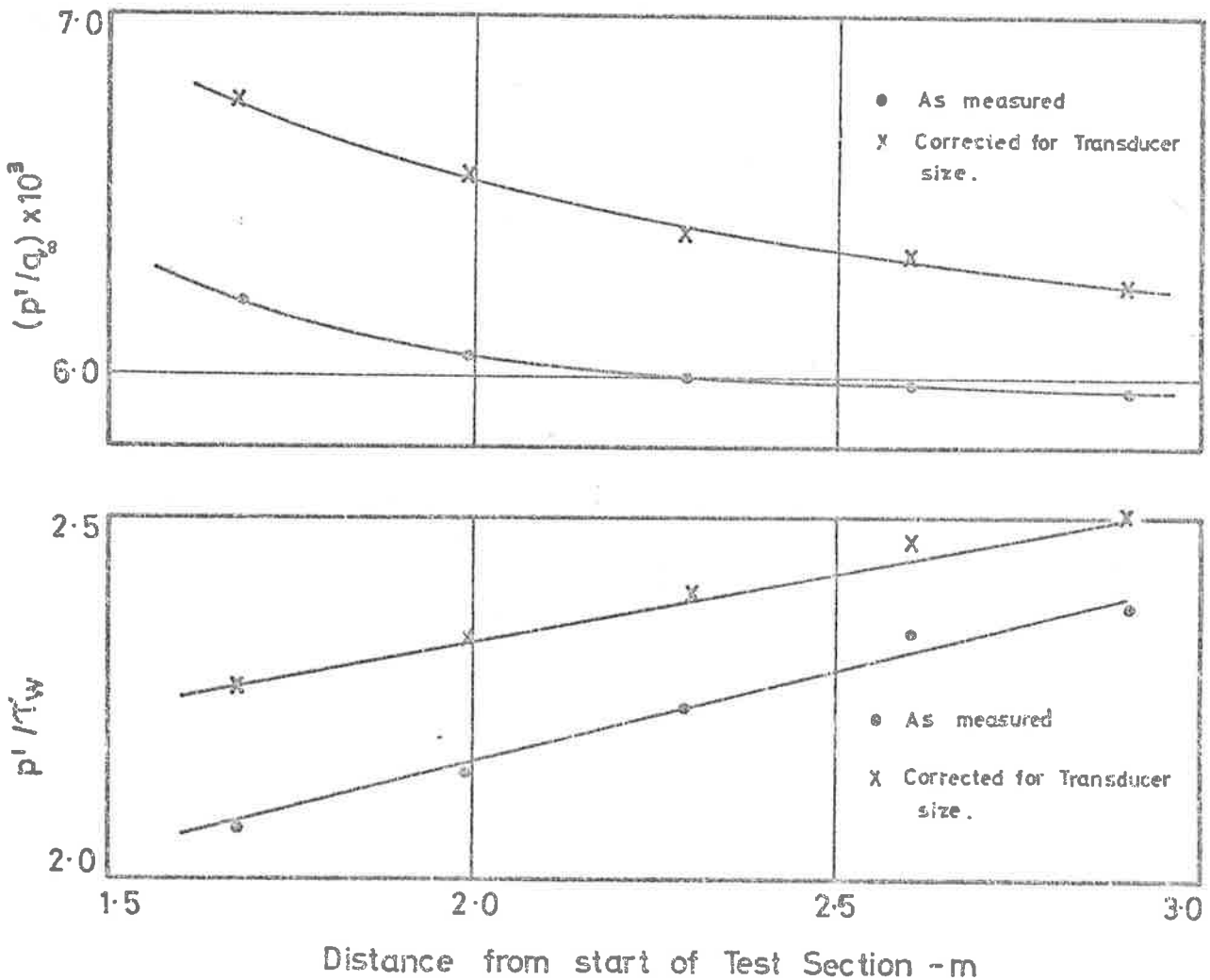

Fig. 58 Variations of R.M.S. Wall Pressure Fluctuations along Tunnel Test Section.

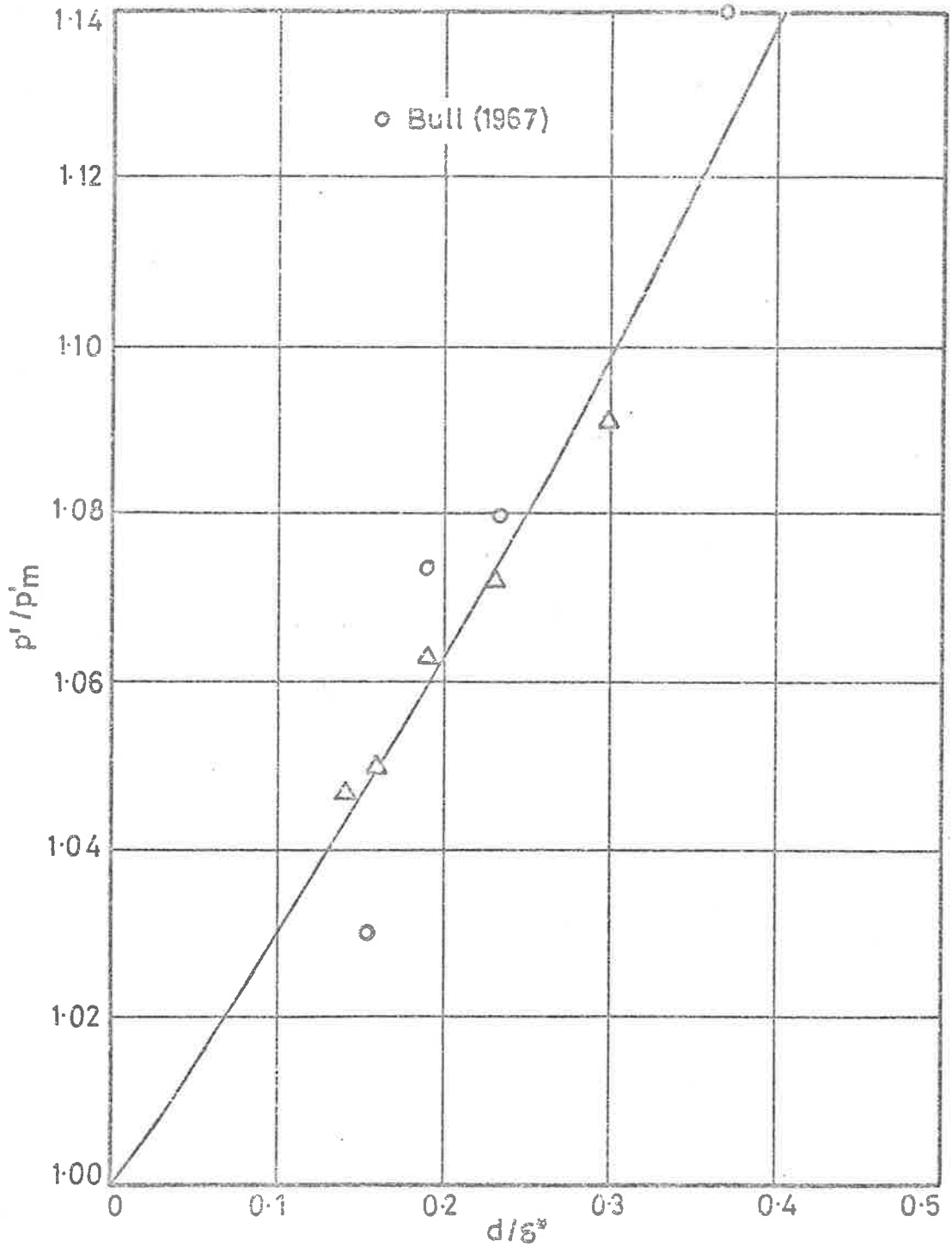

Fig.59 Correction to measured R.M.S. Pressure Fluctuation as a function of Transducer size, (Determined from Corrected Spectral Density Curves.)

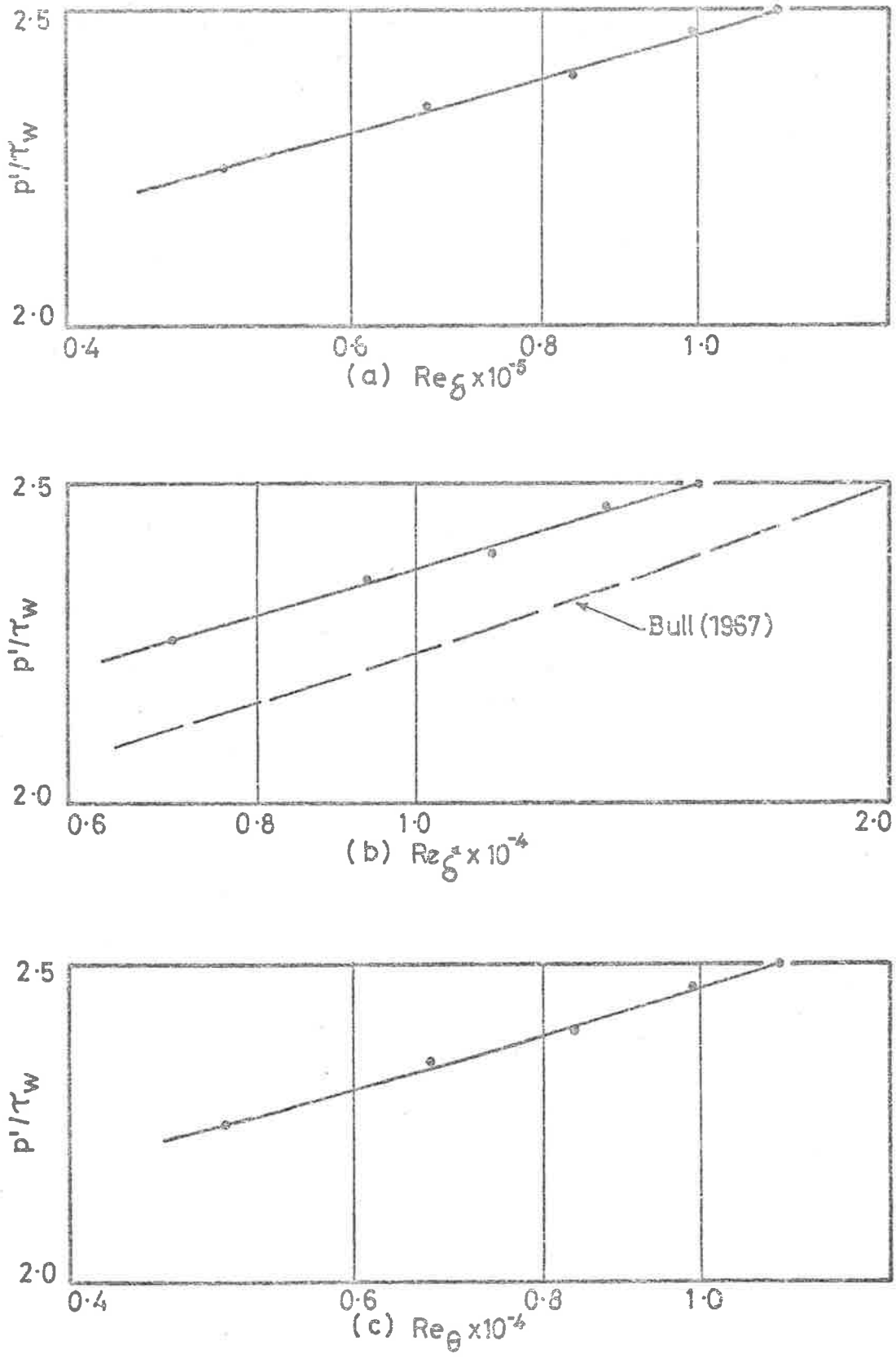

Fig. 60 Variation of the Root Mean Square Wall Pressure Fluctuations with Reynolds Number.

The evidence, though not overwhelming, is then that p'/τ_w in a constant pressure turbulent boundary layer is a function of Reynolds number and increases with increasing Reynolds number. As the scope of the present results is limited in the range of Reynolds number, no attempt is made to specify the form of the variation except to note that the trend of the increase is similar to that observed by Bull (1967).

5.1.4 Conclusions.

Spectral density measurements of the wall pressure fluctuations under a constant pressure turbulent boundary layer conducted only for a limited range of experimental conditions indicate that:-

(1) The agreement obtained between the present results and those of previous investigators confirms the validity of the results and proves the proper functioning of the experimental equipment.

(2) Over the Reynolds number range $7\times10^3 \leq Re_\delta^* \leq 1.5\times10^4$, p'/τ_w varies from 2.3 to 2.5. The variation of p'/τ_w with Re_δ^* is similar to that observed by Bull (1967) although the present values are about 6% higher.

(3) The effect of the transducer size on its resolution at the high frequencies is not negligible for the present series of measurements for which $0.14 \leq d/\delta^* \leq 0.30$. Correction of the spectral density distributions for the effect of transducer size results in better overall collapse of the frequency power spectral density $\phi_p(\omega)$ in terms of $\phi_p(\omega)U_\infty/q_\infty^2\delta^*$ compared with $\phi_p(\omega)U_\infty/\tau_w^2\delta^*$.

(4) Because of the slightly better collapse of the data when non-dimensionalised by q_∞ rather than τ_w, it is tempting to conclude that sources in the outer part of the boundary layer are responsible for the

greater portion of the overall pressure fluctuations (contrary to the conclusion based on the theoretical work of Section 3). However, as Laufer and Narayanan (1971) have shown, it is possible for events in the inner part of the layer to scale on outer layer parameters, and therefore, in the absence of other evidence, such a conclusion would appear to be premature.

5.2 Pressure Gradient Boundary Layer Measurements.

The constant pressure or zero mean pressure gradient turbulent boundary layer is a special case of the more general type of boundary layers. In most instances, boundary layers of interest are those developed under the effects of finite pressure gradients. Some measurements of the wall pressure fluctuations in this case have been reported by Schloemer (1967). His measurements were obtained, however, for a somewhat arbitrary pressure gradient only, that is, on the surface of a flat plate where the variation of the free stream velocity was provided by the insertion of an aerofoil section in the test section of a wind tunnel.

Clauser (1956) has pointed out the "black box" nature of the problem of the turbulent boundary layer and has suggested that the response of the boundary layer is best studied by limiting the factors affecting the development and the characteristics of the boundary layer. It has been realised for some time that the behaviour of a boundary layer depends not only on the local effects of pressure gradient, wall shear stress, boundary layer thickness, etc., but also on the history of the layer far upstream of

---

Laufer, J. and Narayanan, M.A.B. 1971 Mean Period of the Turbulent Production Mechanism in a Boundary Layer. Physics of Fluids, vol 14, Res. Notes, p182-3.

the point of interest. The gross forces acting on the boundary layer are those due to the pressure gradient dp/dx and the wall shear stress τ_w, and Clauser (1954) argued that a simple, well defined pressure history would exist if the pressure gradient parameter β, given by

$$\beta = (\delta'/\tau_w)(dp/dx) \quad , \qquad \ldots(5.2.1)$$

is a constant throughout, where δ' is the effective face area of the layer per unit depth. He termed such layers "equilibrium" layers and went on to show (Clauser (1956)) that they are characterised by

$$\beta = (\delta^*/\tau_w)(dp/dx) = \text{constant} \quad , \qquad \ldots(5.2.2)$$

where δ^* is the boundary layer displacement thickness.

The equilibrium condition where β is a constant is an attractive and most reasonable basis for the study of the turbulent boundary layer, and the measurements presented in this section are those of the mean flow properties and the spectral density distributions of the wall pressure fluctuations in an adverse pressure gradient equilibrium turbulent boundary layer. It is believed that the wall pressure measurements presented are the first to be made in an equilibrium turbulent boundary layer existing under the effects of a finite mean streamwise pressure gradient.

5.2.1 Mean Flow Properties.

The apparatus and the experimental set-up for the determination of the total head distribution across the boundary layer have been described in

Sections 4.3 and 5.1.

The procedure adopted in the setting up of the boundary layer in the wind tunnel test section was to initially estimate the wall shear stress τ_w from the Pitot tube reading (used as a Preston tube) and the boundary layer displacement thickness δ^* from an appropriate relationship to the boundary layer thickness. The mean streamwise pressure gradient dp/dx was obtained from the static pressure distribution along the tunnel test section, and the value of β was determined using Equation (5.2.2). The procedure was repeated until the estimated value of β along the test section was within 10% of the mean. The boundary layer traverse was then conducted using the Pitot tube and the differential pressure capsule to obtain more accurate values of δ^* and to give better estimates of τ_w by the comparison of the mean velocity profiles with the law of the wall. Invariably, the first estimates of δ^* were found to be different from those obtained from the Pitot traverses of the boundary layer and the use of Equation (4.3.1). However, the latter values serve as guides to better estimates of δ^* in subsequent re-adjustments of the flow in the test section provided that the changes in the mean flow have not been too drastic. The agreement between the value of the wall shear stress obtained by the fit of the mean velocity profile to the law of the wall and that estimated from the Pitot tube wall reading was found to be better than 5%, and indicated that any three-dimensional effects were probably negligible. Due to the interdependence of the variables which make up the pressure gradient parameter, a number of tunnel adjustments were made before a satisfactory equilibrium layer could be obtained. The resultant configuration of the tunnel floor is shown in

figure 61.

5.2.2 The Wall Pressure Fluctuations.

The equipment used in the measurements of the wall pressure fluctuations in the equilibrium turbulent boundary layer developed under the effects of an adverse pressure gradient was the same as that used in the constant pressure layer measurements and has been described in Section 5.1.2. The spectral density measurements of the wall pressures were made at two points along the wind tunnel test section.

5.2.3 Results and Discussions.

An equilibrium turbulent boundary layer was developed over a short distance of the working section of the wind tunnel. The variation of the static pressure along the relevant section of the tunnel is shown in figure 62, and variations of the mean streamwise pressure gradient, the wall shear stress and the boundary layer displacement thickness are shown in figures 63, 64 and 65 respectively. The corresponding variation of β, derived from these results is shown in figure 66. In figures 63 to 66, the two upstream test results have been included and are joined by a broken line to indicate the history of the layer prior to the section where the equilibrium boundary layer exists.

It can be seen from the distribution of β along the boundary layer that an equilibrium boundary layer exists between x_1 = 2.9 m and 3.2 m from

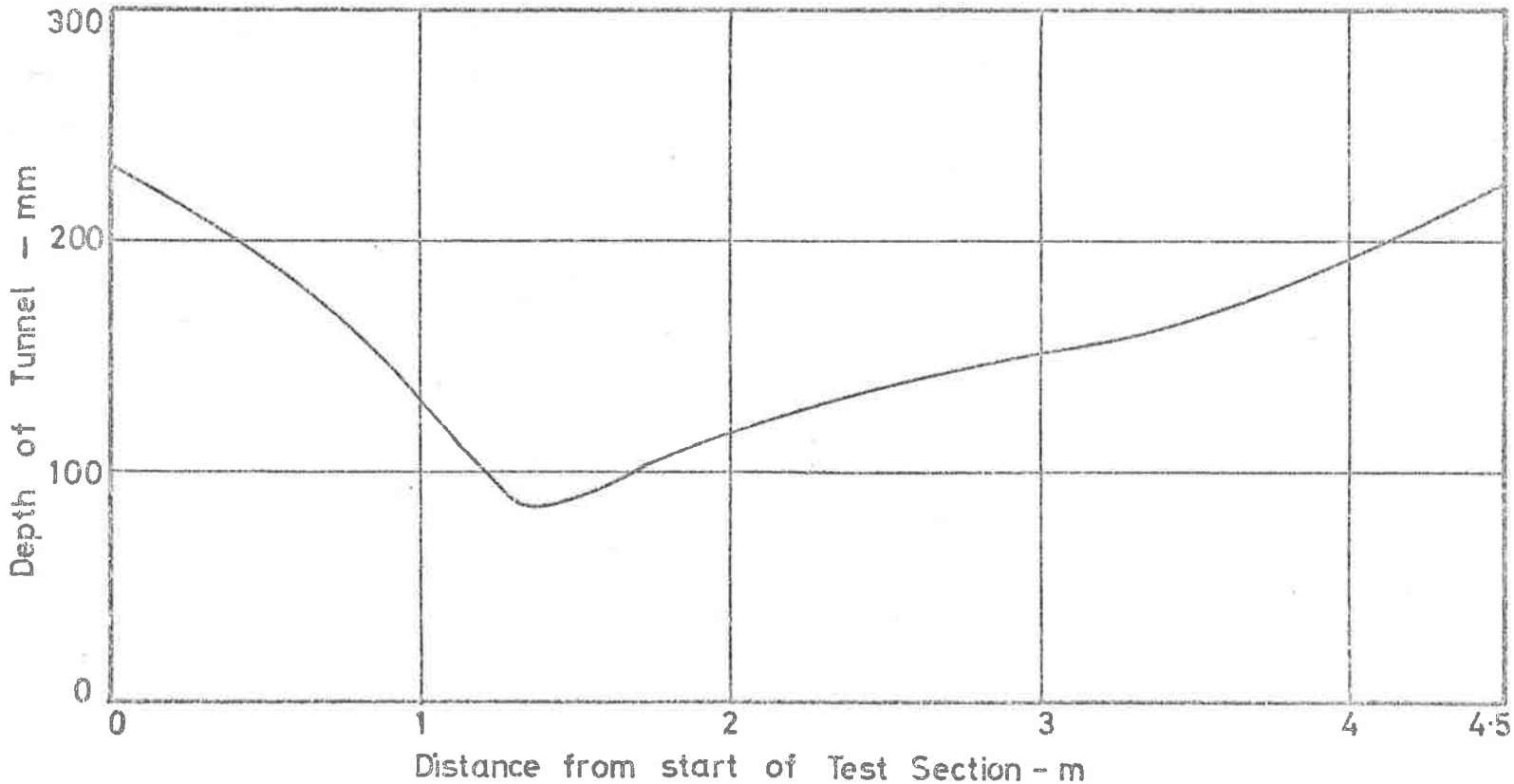

Fig. 61 Tunnel Floor Position for Adverse Pressure Gradient Turbulent Boundary Layer.

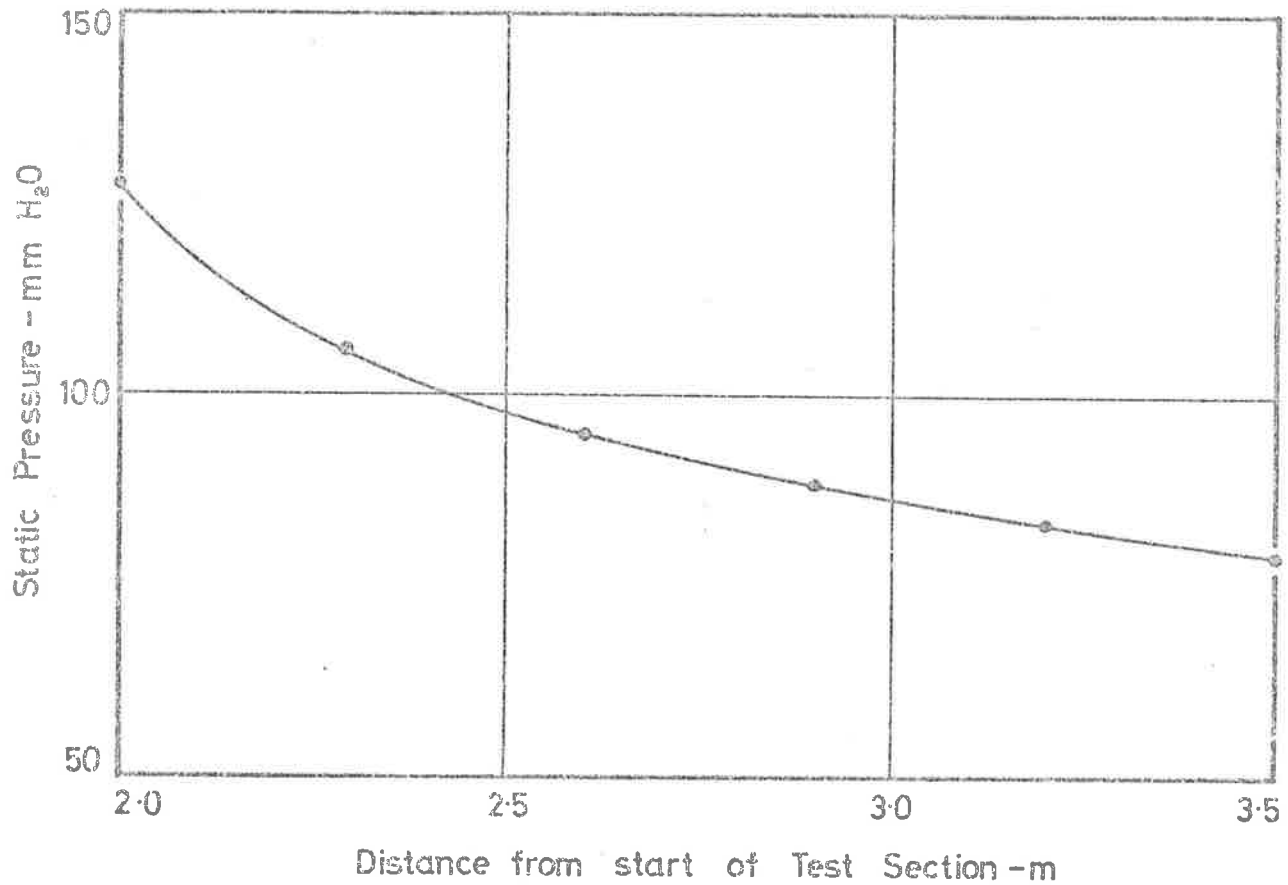

Fig. 62 Static Pressure Distribution along Test Section.

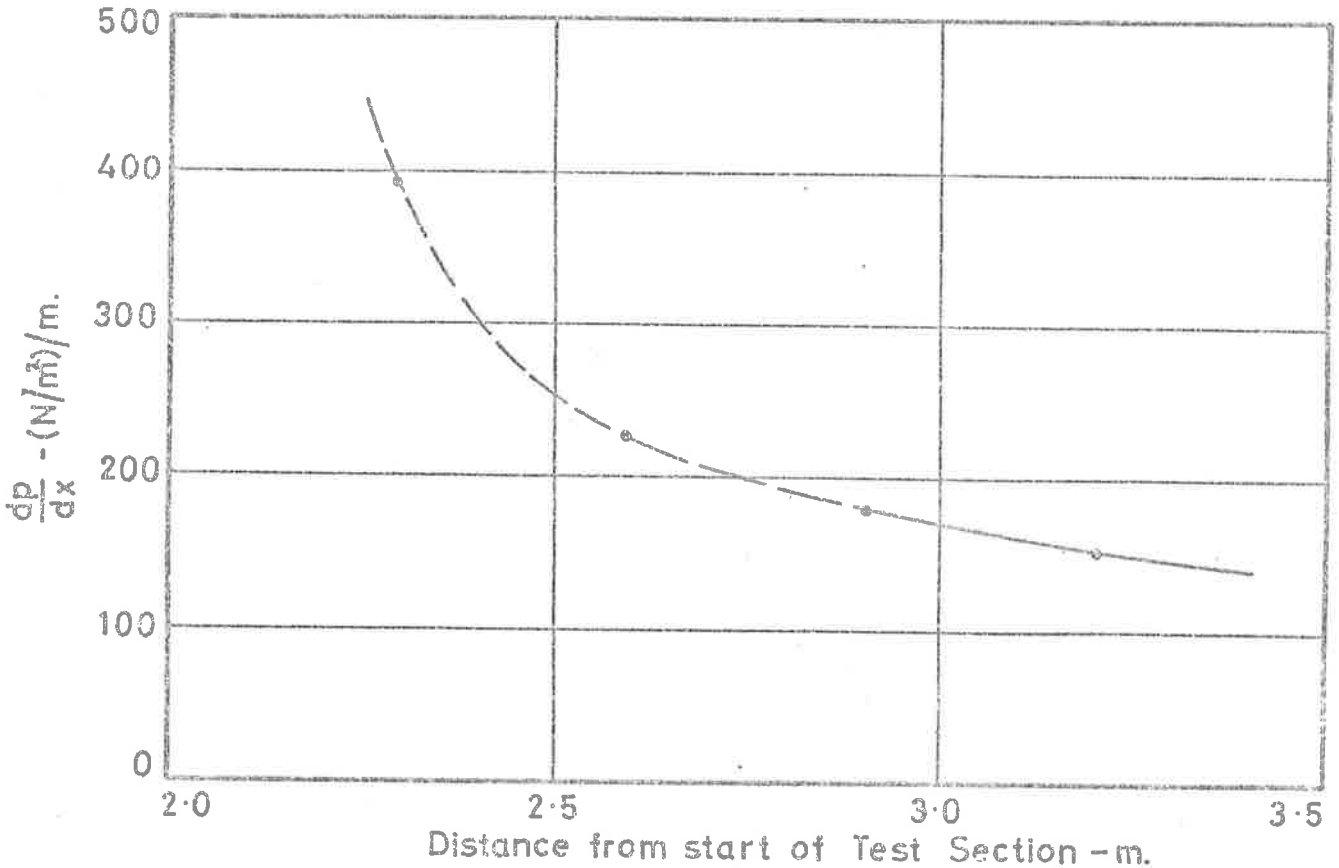

Fig. 63 Variation of Mean Streamwise Pressure Gradient along Test Section.

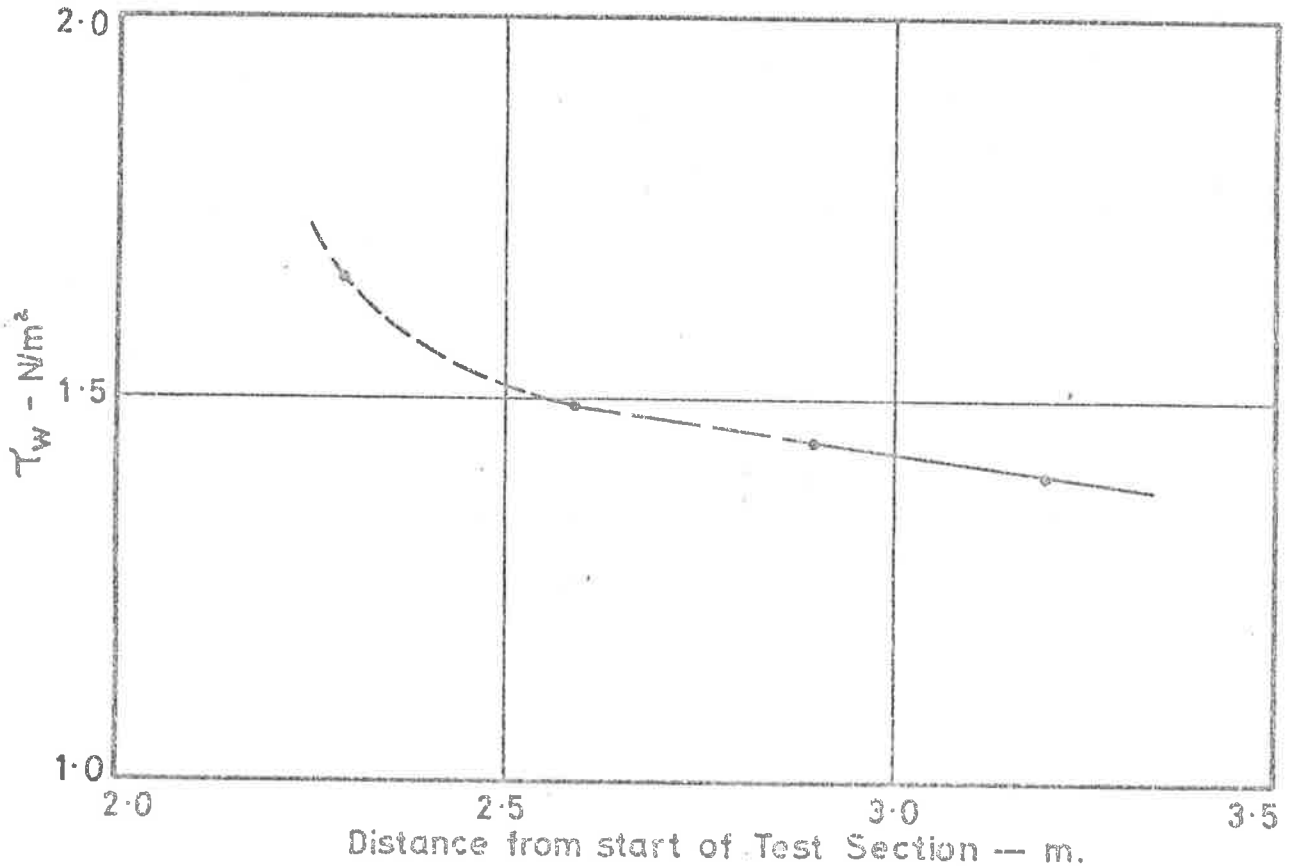

Fig. 64 Variation of Wall Shear Stress along Test Section.

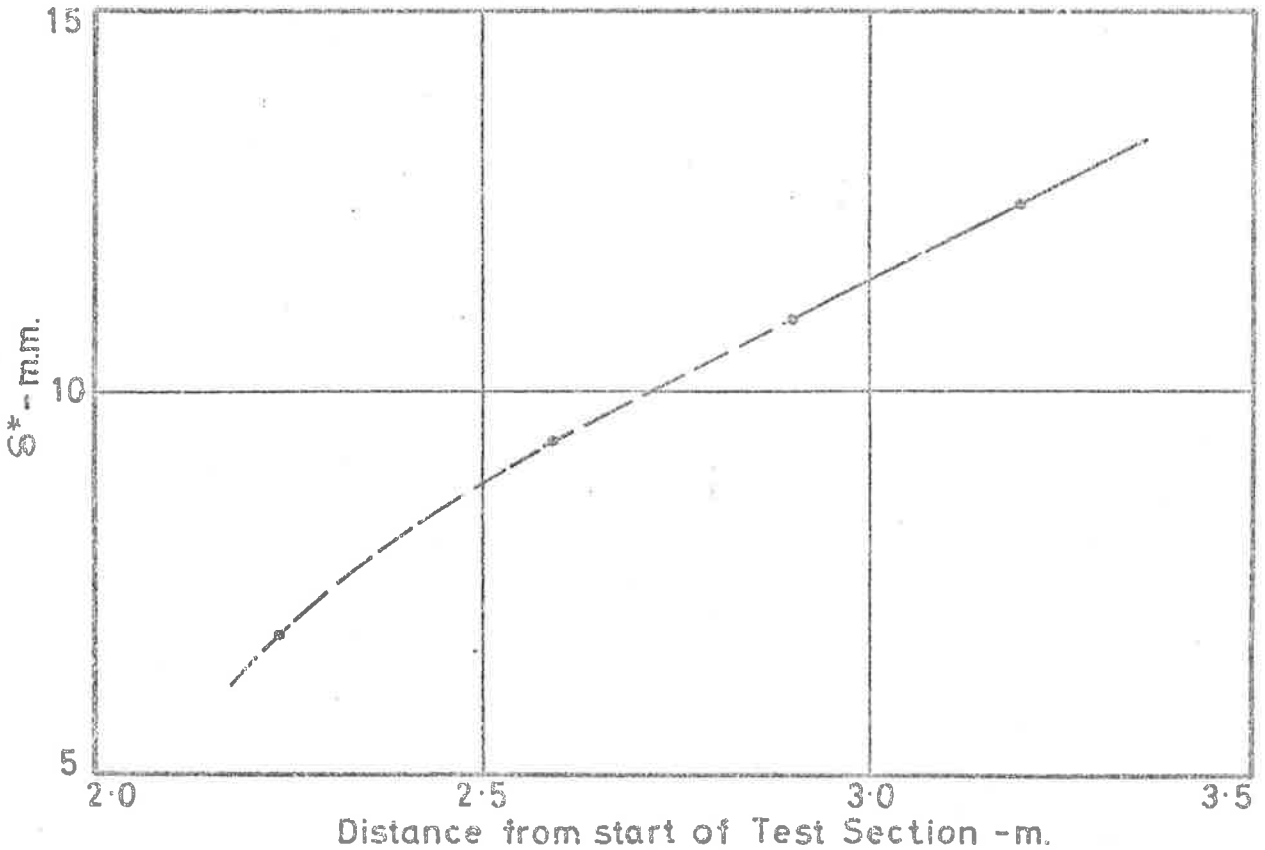

Fig. 65 Variation of Boundary Layer Displacement Thickness along Test Section.

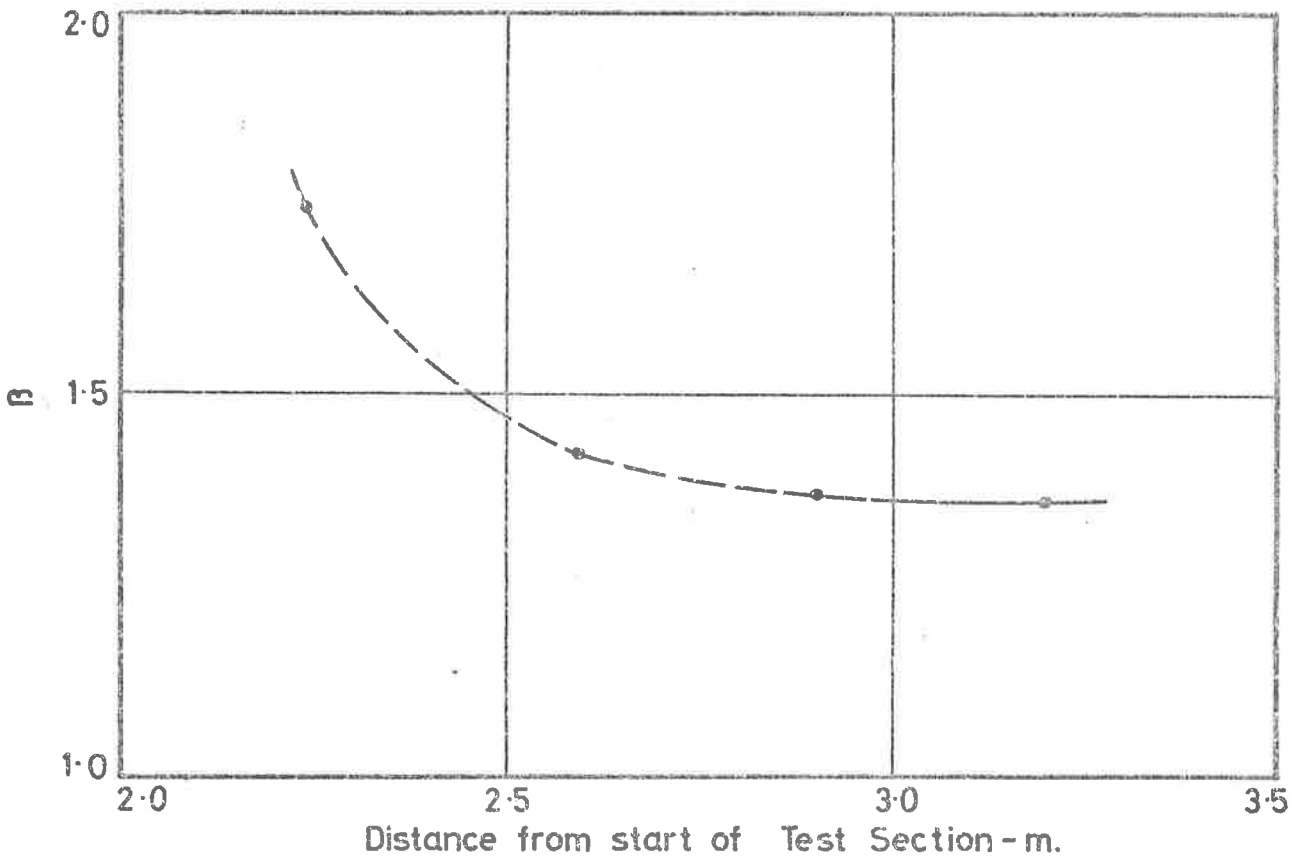

Fig. 66 Variation of Pressure Gradient Parameter with distance along Tunnel Test Section.

the start of the working section. This is confirmed by the variation of Clauser's family parameter G which is shown in figure 67, where

$$G = \frac{\int_0^\infty \left(\frac{U_\infty - U_1}{U_\tau}\right)^2 dy}{\Delta}, \qquad \ldots(5.2.3)$$

and

$$\Delta = \int_0^\infty \left(\frac{U_\infty - U_1}{U_\tau}\right) dy, \qquad \ldots(5.2.4)$$

is the Clauser universal thickness. The mean velocity profiles at the two downstream points (x_1 = 2.9 m and 3.2 m) plotted to show the wall influence are shown in figure 68. Similarity of the profiles can be seen for yU_τ/ν up to about 500. The law of the wall has been included for comparison. The profiles replotted in the form of the velocity defect are shown in figure 69 where the results of Clauser (1954) for a similar value of the family parameter have been included for comparison. Similarity of the profiles is again evident. These results indicate that an equilibrium layer does exist at least over the length of the tunnel test section for which 2.9 m $\leq x_1 \leq$ 3.2 m. The pressure gradient parameter for the layer is taken as β = 1.37. The free stream velocities at the two points are 37.2 m/s and 36.2 m/s, and the boundary layer displacement thicknessess are 11 mm and 12.5 mm, where in each case the second value is that for the point furthest downstream.

The spectral density distributions of the acoustic field and of the fluctuating wall pressure which have been corrected for acoustic and

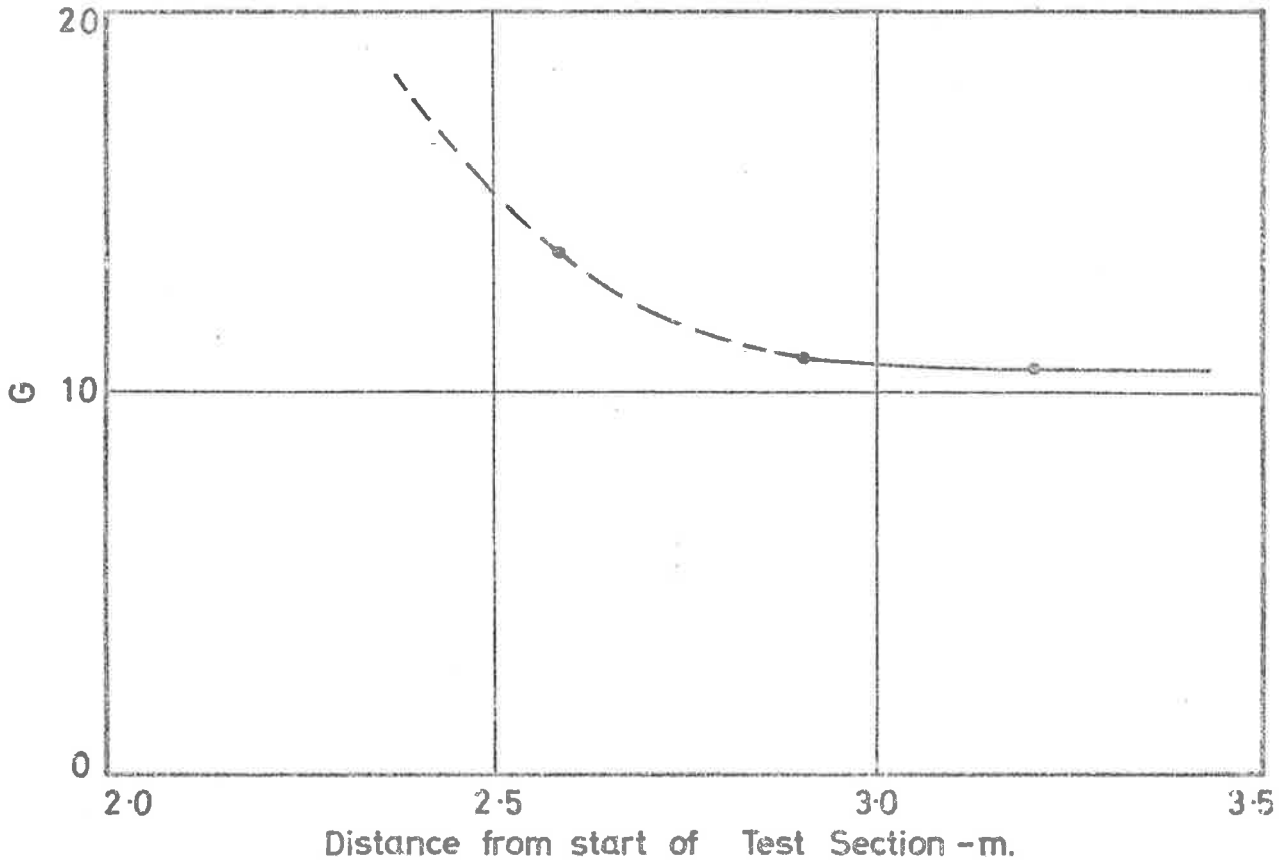

Fig. 67 Variation of Clauser's Family Parameter with distance along Tunnel Test Section.

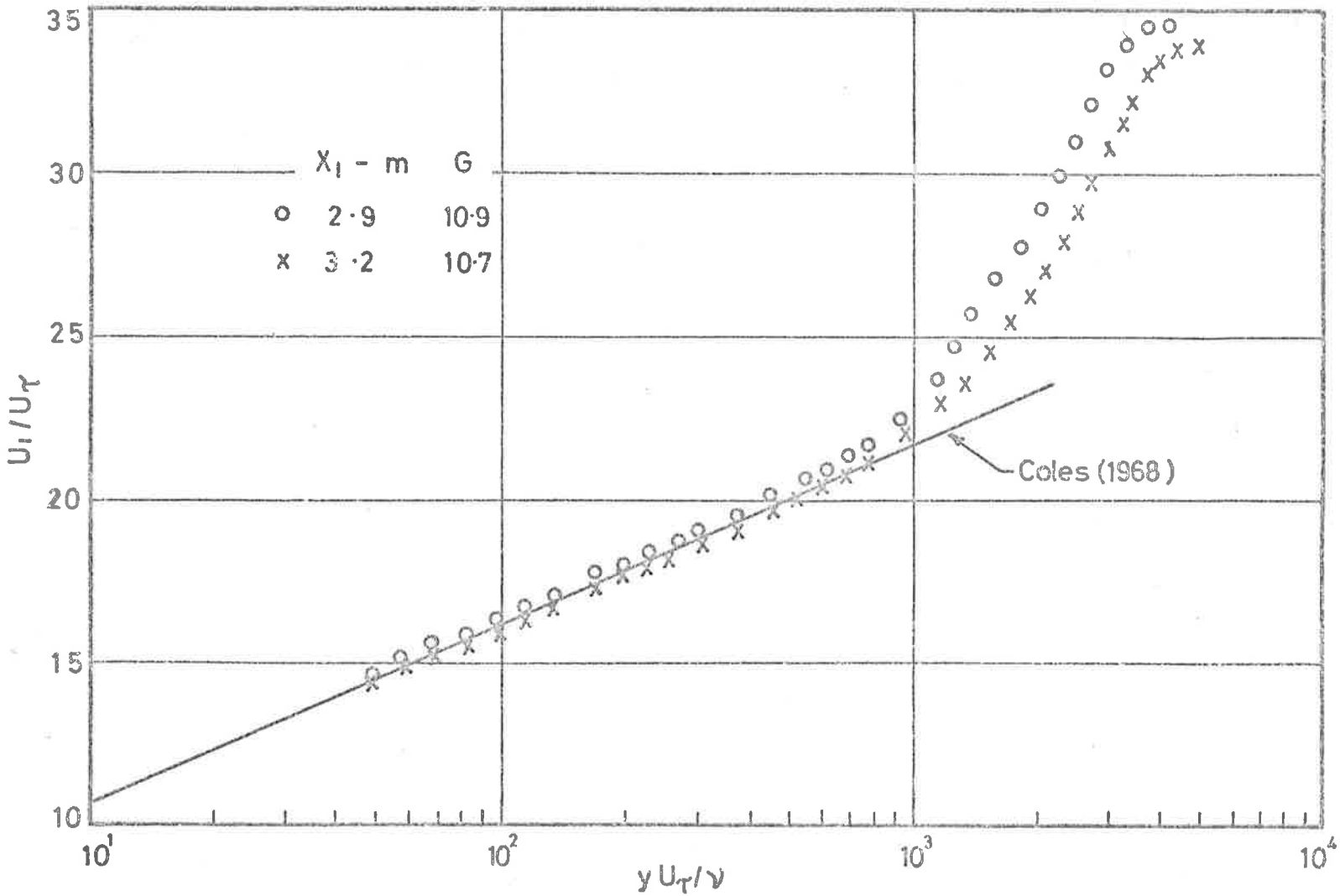

Fig. 68 Boundary Layer Mean Velocity Profiles. $\beta = 1{\cdot}37$

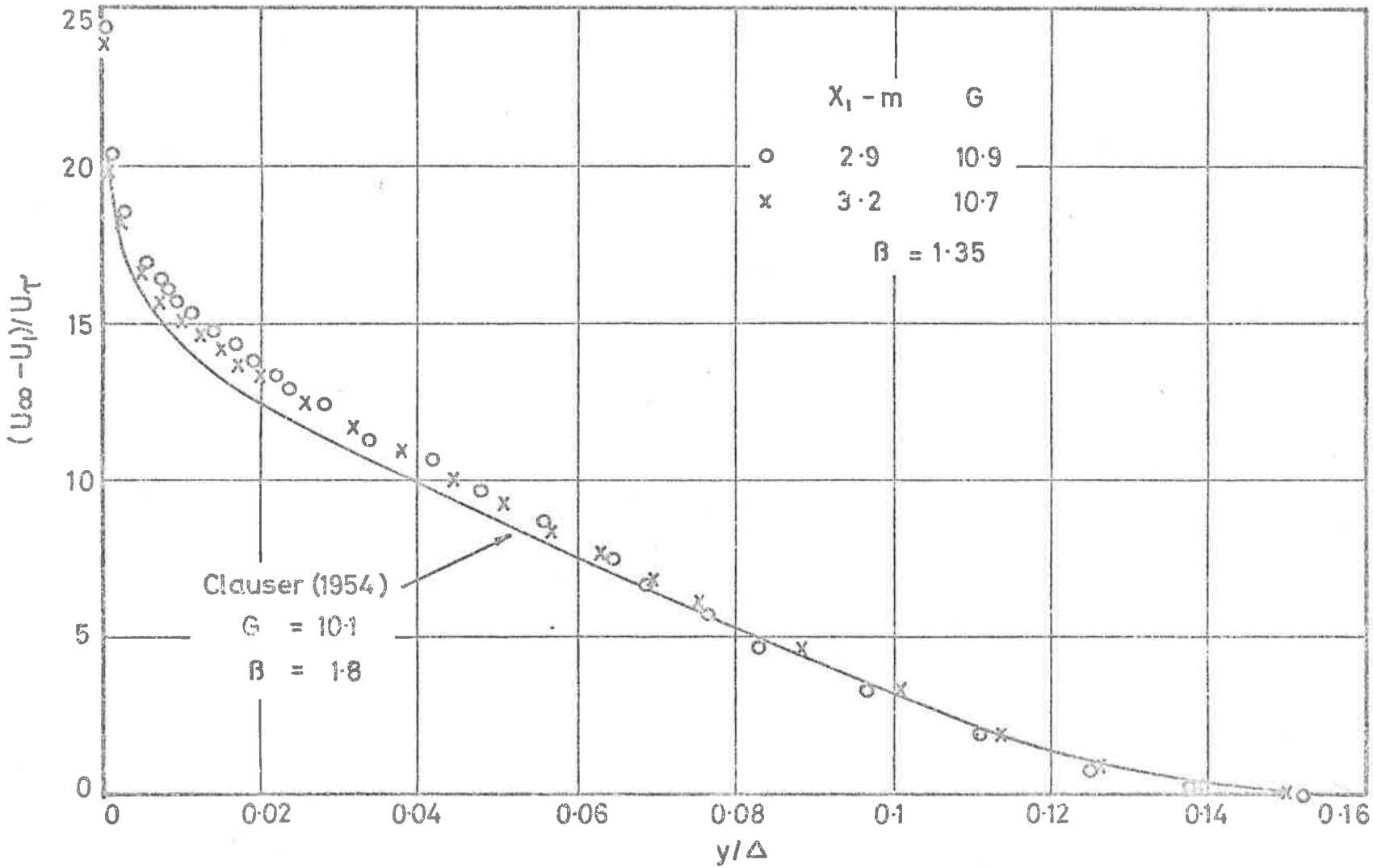

Fig. 69 Boundary Layer Mean Velocity Profiles. Pressure Gradient Layer.

amplifier electronic noise are shown in figures 70 and 71 respectively. A comparison of the two figures shows that, just as in the constant pressure boundary layer measurements, the signal to noise ratio is good everywhere except at the low and high frequency ends of the spectrum where it falls off to about 8 db and less below 200 Hz or above 25 kHz. Consequently, all measurements below 200 Hz or above 25 kHz have been neglected. At the low frequency end of the spectrum where the measurements have been neglected due to the low signal to noise ratio, the distribution of the integrand of Equation (5.1.3) which is still significant at the low frequencies is faired in using the results of the constant pressure layers as a guide. Any error incurred in this procedure is estimated to be less than 3% of the mean square value of the wall pressure fluctuations. The electronic noise present in these measurements is the same as that for the constant pressure case and its effects have been discussed in Section 5.1.2.

The mean square values of the wall pressure fluctuations are obtained from the spectral density distributions using Equation (5.1.3), and result in values of p'/q_∞ of 7.0×10^{-3} and 6.8×10^{-3} for $x_1 = 2.9$ m and 3.2 m respectively. The corresponding values of p'/τ_w are 4.1 and 3.9.

The frequency power spectral density distributions of the wall pressure fluctuations corrected for transducer size effects are shown in figures 72, 73 and 74. The correction procedure used is due to Corcos (1963) and has been outlined in Section 5.1.3. The mean distribution of the spectra for the constant pressure turbulent boundary layer as well as that for the pressure gradient results of Schloemer (1967) (arbitrary pressure

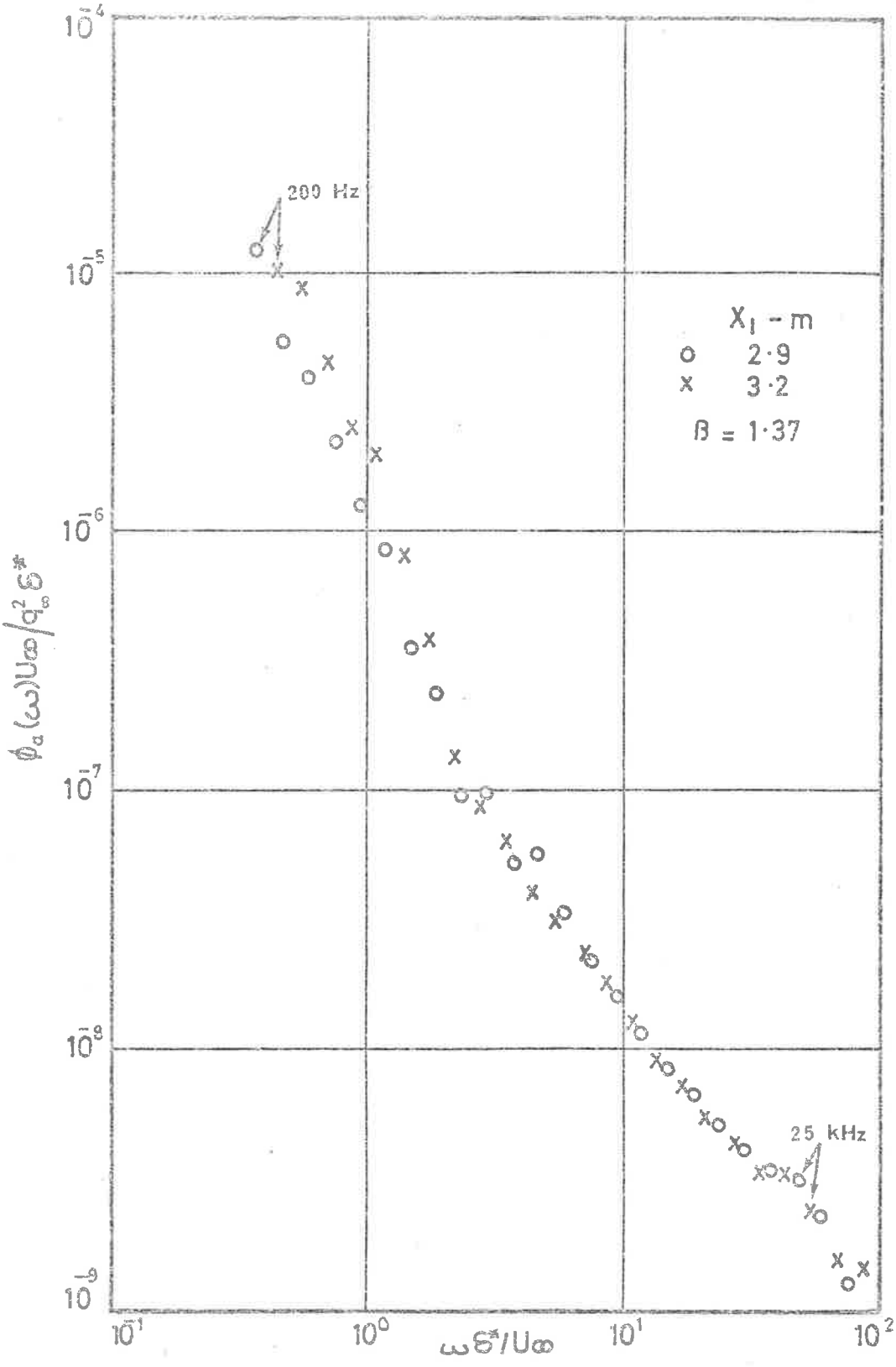

Fig.70 Spectra of Sound Field in Wind Tunnel Working Section.

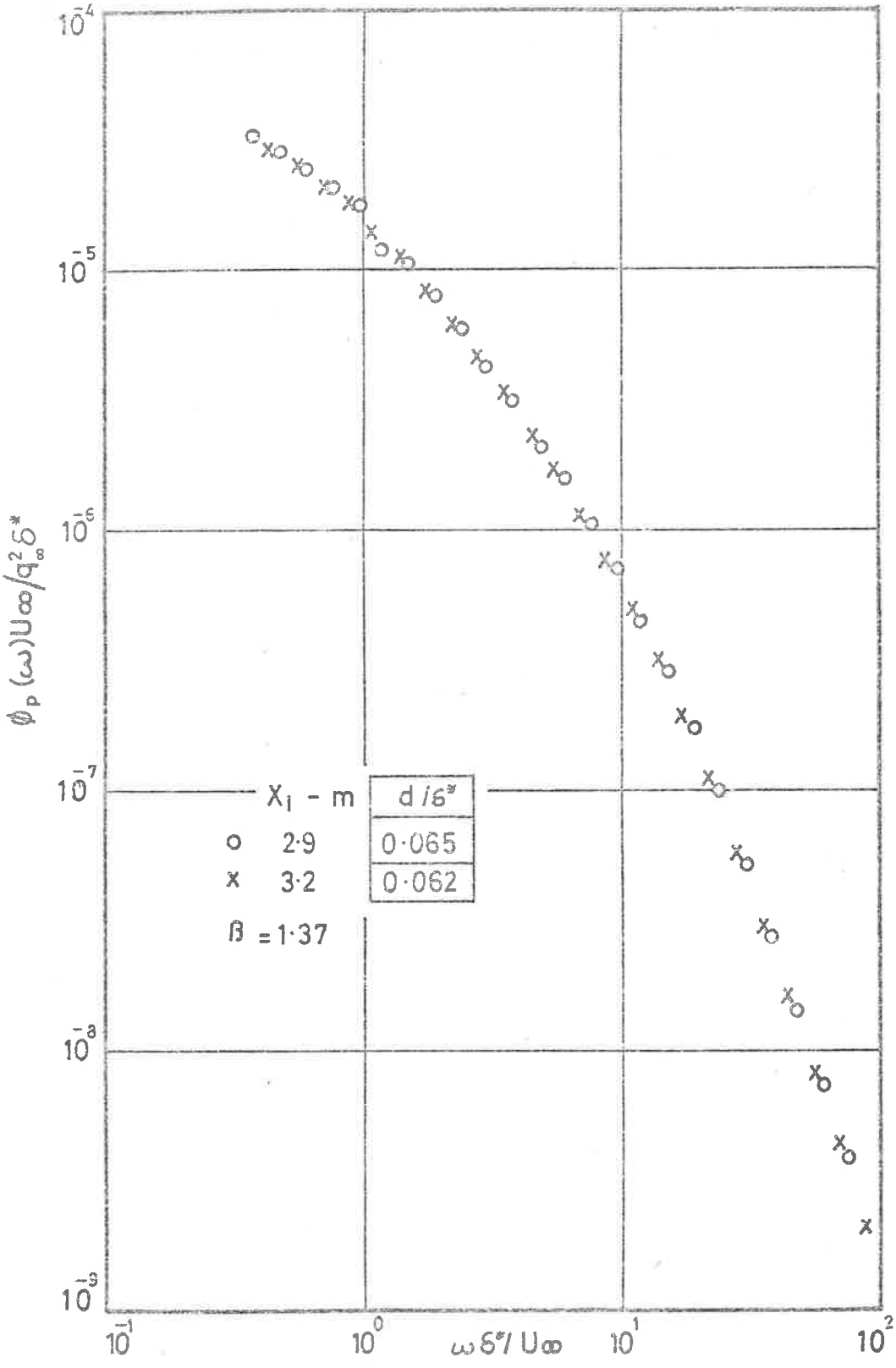

Fig. 71 Spectra of Wall Pressure Fluctuations not corrected for Transducer size.

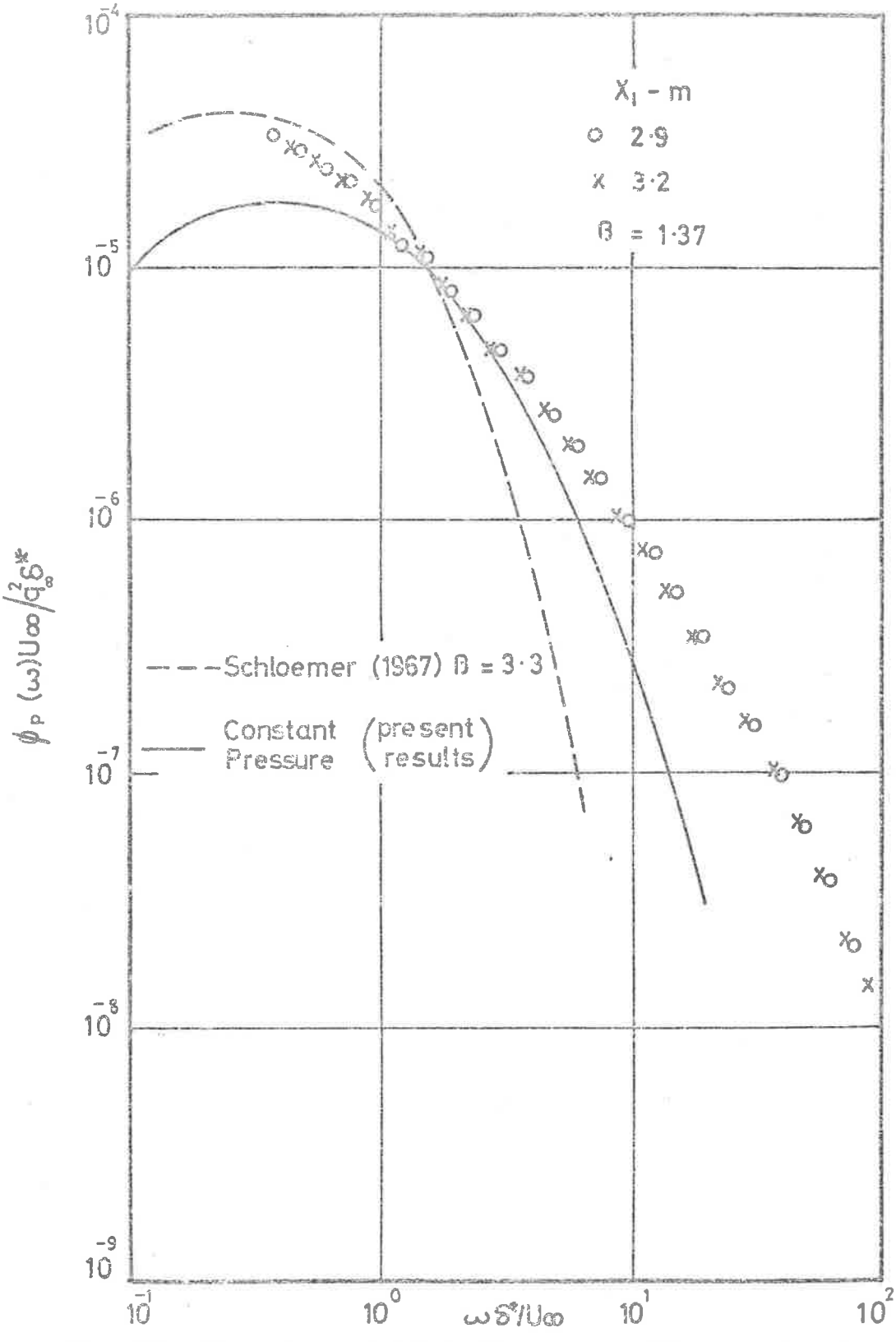

Fig. 72 Spectra of Wall Pressure Fluctuations corrected for Transducer size.

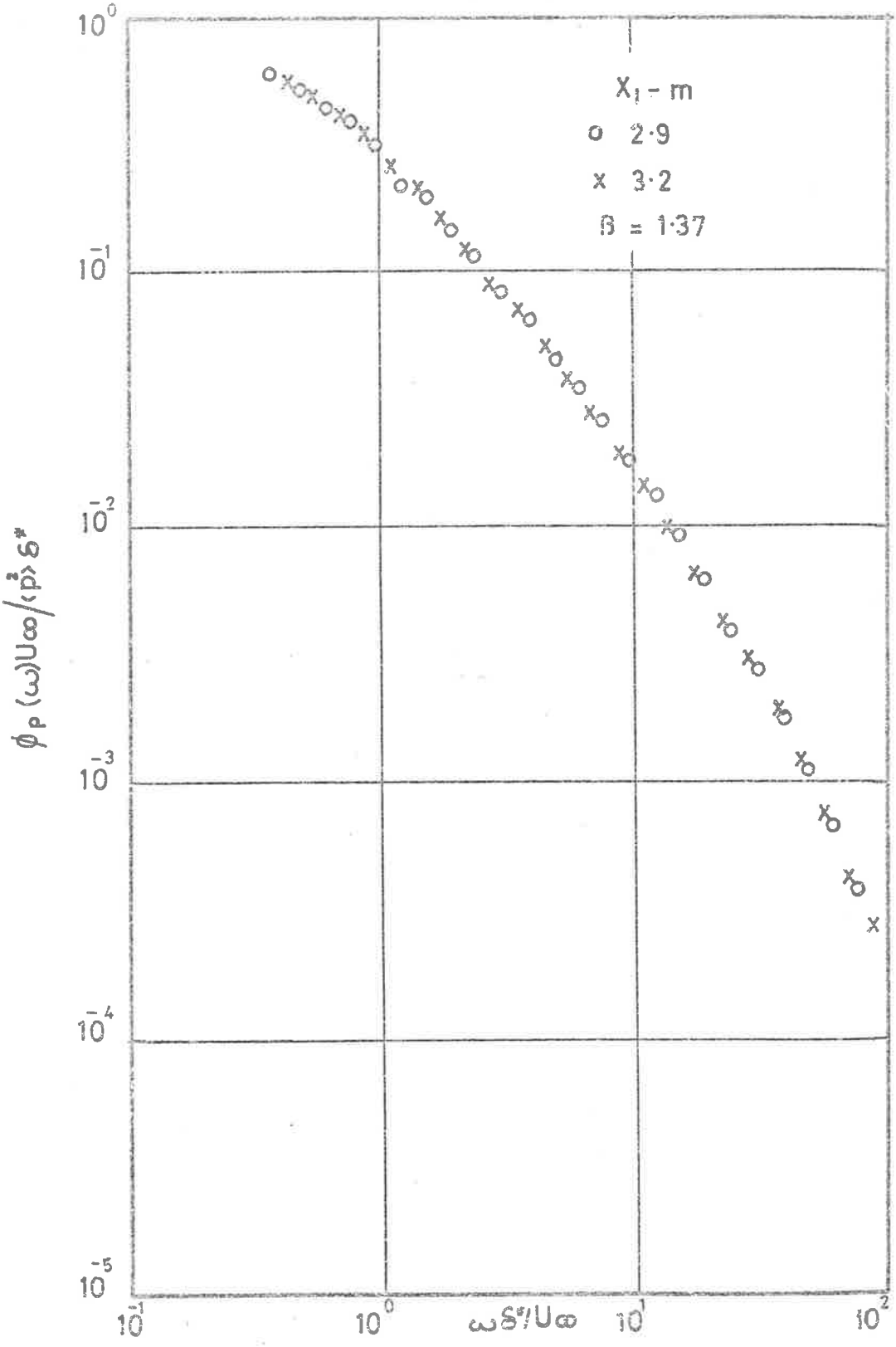

Fig. 73 Spectra of Wall Pressure Fluctuations corrected for Transducer size.

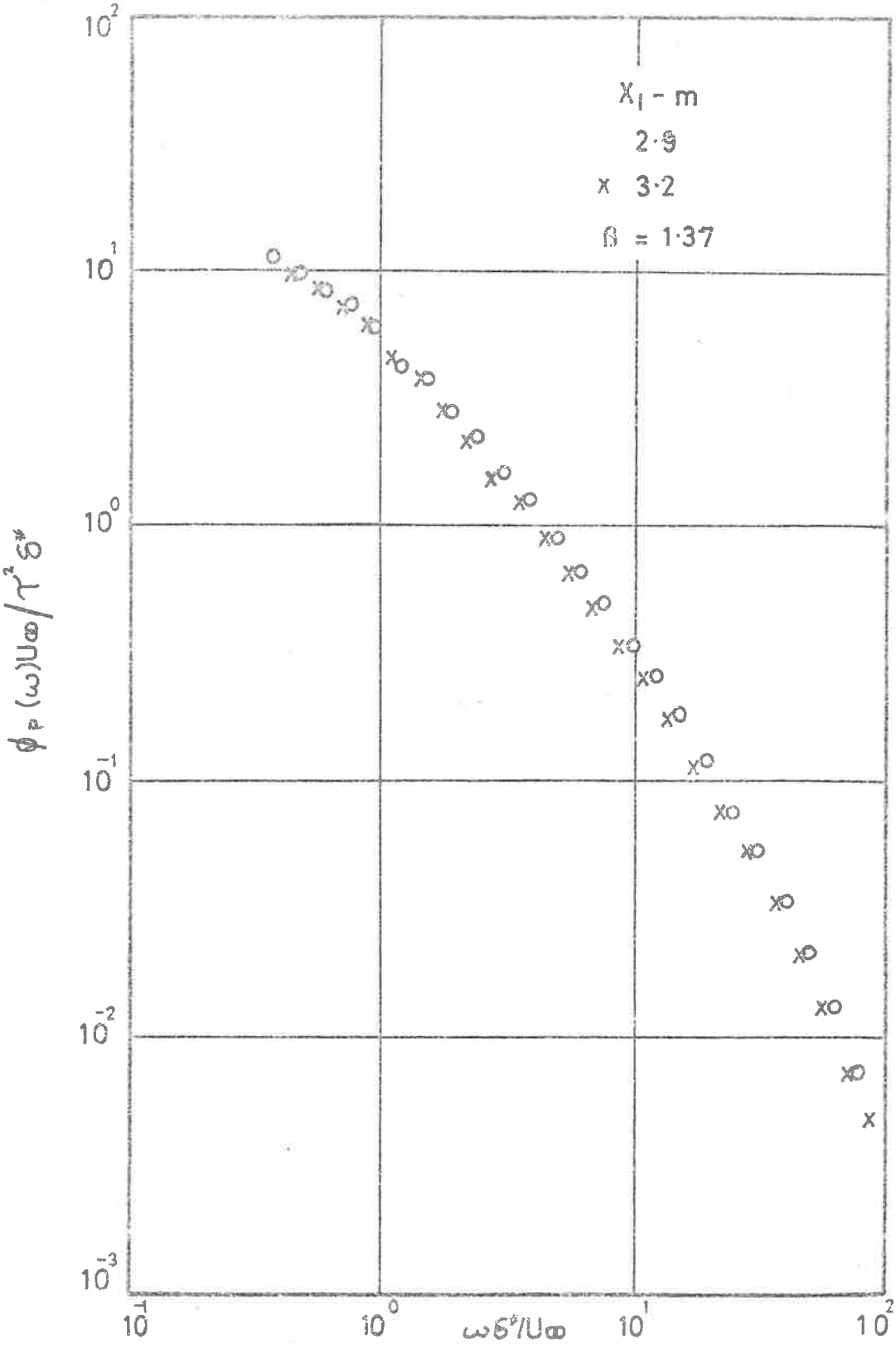

Fig. 74 Spectra of Wall Pressure Fluctuations corrected for Transducer size.

gradient layer) have been included in figure 72 for comparison. It can be seen that the present results for the constant pressure and the pressure gradient turbulent boundary layers are similar in the range $1 < \omega\delta^*/U_\infty < 3$ when non-dimensionalised by the free stream dynamic pressure q. For frequencies for which $\omega\delta^*/U_\infty > 3$ or for which $\omega\delta^*/U_\infty < 1$, the spectra from the pressure gradient layer have higher values than those of the constant pressure layer, and the difference increases with increasing frequency for $\omega\delta^*/U_\infty > 3$ or for decreasing frequency for $\omega\delta^*/U_\infty < 1$. The difference between the spectra of the wall pressure fluctuations in the adverse pressure gradient layer and those of the constant pressure layer at the high frequencies is in accord with Schloemer's results for the distribution of the longitudinal component of the fluctuating velocity which he found to be greater in the inner two-thirds of the boundary layer for the adverse pressure gradient case. Schloemer's results for the spectral density distributions of the wall pressures in an adverse pressure gradient layer exhibited similarity with those of the constant pressure layer for $\omega\delta^*/U_\infty > 2$ whereas for frequencies less than this, the results for the former type of boundary layer were higher than those of the latter. His measurements were made with a transducer which gave a value of d/δ^* of about 0.26 as compared to a value of 0.06 for the present measurements. The difference between the distributions of the spectral density of the wall pressures obtained by Schloemer and those of the present measurements could be due either to the fact that the boundary layers have entirely different histories (unknown for Schloemer's layer) or to the difference in resolution of the transducers used. The latter effect definitely cannot be discounted in the light of Blake's (1970) results which showed

the drastic effects of the relative transducer size on its resolution at high frequencies, although it would be premature to disregard the effects of the possible difference in history.

The mean square values obtained from the frequency spectra corrected for transducer size give $p'/q_\infty = 7.4 \times 10^{-3}$ and 7.1×10^{-3} with $p'/\tau_w = 4.3$ and 4.1 for $x_1 = 2.9$ m and 3.2 m respectively. (A summary of the properties of the adverse pressure gradient boundary layer is given in Table 5.1.) The corresponding Reynolds numbers, Re_δ^*, (which cover only a very small range) are 2.8×10^4 and 3.2×10^4. Thus, although the apparent trend of p'/τ_w with Re_δ^* is contrary to that observed in the constant pressure layer, it may just as well be due either to the loss of signal as a result of the relatively low signal to noise ratio particularly at the low frequency end of the spectrum or to the cumulative effect of probable errors in the measurements which is up to about 6%. The latter effect seems the more likely, and therefore the root mean square pressure will simply be taken as $p'/\tau_w \simeq 4.2$ with $p'/q_\infty \simeq 7 \times 10^{-3}$.

A significant point to note is that, as in the zero pressure gradient layer, the collapse of the spectral density distributions is better in the pressure gradient boundary layer when plotted in the form $\phi_p(\omega) U_\infty / q_\infty^2 \delta^*$ compared with $\phi_p(\omega) U_\infty / \tau_w^2 \delta^*$. This fact, in conjunction with the smaller variation of p'/q_∞ compared with p'/τ_w for the different flow conditions indicates that the free stream dynamic pressure is perhaps a more useful parameter than the wall shear stress, and that at least for engineering purposes the value of p'/q_∞ of 7×10^{-3} may be sufficiently representative

Table 5.1 Summary of Boundary Layer Properties.

Location of point of measurement from start of test section - m	2.9	3.2
Free stream dynamic head q_∞ - N/m^2	8.53×10^2	8.06×10^2
Free stream velocity U_∞ - m/s	37.2	36.2
Displacement thickness δ^* - mm	11.0	12.5
Wall shear stress τ_w - N/m^2	1.45	1.40
Streamwise pressure gradient dp/dx - $(N/m^2)/m$	180	152
Pressure gradient parameter β	1.37	1.36
Clauser family parameter G	10.9	10.7
Momentum thickness θ - mm	7.07	8.25
p'/q_∞	7.4×10^{-3}	7.1×10^{-3}
p'/τ_w	4.34	4.10
Re_{δ^*}	2.84×10^4	3.24×10^4
Re_θ	1.83×10^4	2.13×10^4

of the wall pressure fluctuations for flows which are not subjected to large mean pressure gradients. Schloemer's results which indicate that p'/q_∞ for the favourable pressure gradient layer is also very nearly equal to that for his constant pressure layer adds weight to this observation.

5.2.4 Conclusions.

The measurements of the spectral density of the wall pressure fluctuations which were made in an adverse pressure gradient turbulent boundary layer for which the pressure gradient parameter $\beta = 1.37$ are believed to be the first to be made in an equilibrium turbulent boundary layer under the effects of a finite pressure gradient. The results which give the value of d/δ^* of approximately 0.06, a value which is believed to be the smallest to date, indicate that

(1) The spectral density distribution for the pressure gradient layer is similar to that of the constant pressure layer in the frequency range for which $1 < \omega\delta^*/U_\infty < 3$. For frequencies where $\omega\delta^*/U_\infty > 3$ or $\omega\delta^*/U_\infty < 1$, the spectra from the adverse pressure gradient layer are higher than those of the constant pressure layer.

(2) The root mean square value of the wall pressure fluctuations expressed as p'/τ_w is greater in the adverse pressure gradient layer than that in the constant pressure layer.

(3) In view of the fact that the range of Re_δ^* investigated is so small, no valid comment can be made on the effect of Reynolds number on p'/τ_w or p'/q_∞. All that can be concluded is that $p'/\tau_w = 4.2$ for $Re_\delta^* \simeq 3\times10^4$ with a corresponding value of p'/q_∞ of 7×10^{-3}.

6. CONCLUDING REMARKS.

So far the conclusions have been drawn in direct relations only to specific sections of the work. General conclusions will now be drawn from those presented in Sections 3.4, 5.1.4 and 5.2.4, and these will be examined in relation to the stated objectives of the investigation (Section 1.3).

(1) Calculation Procedures.

It is believed that sound procedures for calculating various properties of the wall pressure fluctuations in constant pressure boundary layers have been developed, and the numerical analysis used has been demonstrated to be reliable. The results obtained for the magnitude of the root mean square pressure and its variation with Reynolds number, and the frequency power spectral density of the fluctuations are in quite good agreement with previously existing experimental data and additional data obtained in the course of the present investigation. From this, it can be concluded that the model of the boundary layer on which the calculations were based give a reasonable representation of reality.

The numerical procedure could be extended directly to calculations for layers with non-zero pressure gradients but, as indicated in Section 3.4, the boundary layer model, in view of the much more limited number of existing experimental data, would be less firmly based. Thus, even though no calculations have been made for layers with non-zero

pressure gradients, the work has gone a long way towards fulfilling the first objective stated in Section 1.3.

(2) Region of the Boundary Layer Making the Most Significant Contributions to the Wall Pressure Fluctuations.

The region of the boundary layer which, according to the calculations, makes the most significant contribution to the wall pressure fluctuations can, as required by the second objective given in Section 1.3, be readily identified. For the boundary layer model used, the calculations show that, at least for constant pressure layers, the inner part of the layer between the wall and x_2/δ = 0.2 to 0.3 makes the dominant contribution (this conclusion applies for both the small and large eddies of the boundary layer model). For layers with adverse pressure gradients, this region can be expected to be concentrated between the wall and even smaller values of x_2/δ (the x_2/δ value decreasing as the pressure gradient increases).

(3) Measurements of Properties of the Fluctuating Wall Pressure Field in Equilibrium Turbulent Boundary Layers with Various Streamwise Pressure Gradients.

Measurements of the root mean square pressure and frequency spectrum of the wall pressure fluctuations at a number of stations in a constant pressure layer have added a useful systematic set of data to those already existing. Measurements of the root mean square value and spectral density of the pressure fluctuations at two stations in a layer with the pressure

gradient parameter $\beta = 1.37$ are believed to be the first such measurements made in an equilibrium layer with a non-zero pressure gradient. For these measurements the ratio d/δ^* was 0.06 which is believed to be the smallest yet achieved.

However, since the design and construction of the wind tunnel and associated instrumentation had to be carried out within the time alloted for the project, the measurements had to be limited to those just mentioned. The third objective outlined in Section 1.3 was, therefore, not completely achieved, although, again, the work did go a long way towards it. The apparatus has been developed to the point from which an extension to much more comprehensive measurements could readily be made.

(4) Effect of Reynolds Number on the Root Mean Square Pressure.

A significant amount of information relevant to the fourth objective (Section 1.3) has been obtained. For constant pressure layers, both the theoretical and experimental aspects of the present study support the indication given by previous experimental work that p'/τ_w increases with increasing Reynolds number. The calculated variation of p'/τ_w (based on turbulence/mean-shear interaction) is from 1.10 to 6.51 as the Reynolds number Re_δ^* increases from 10^3 to 10^7, a trend which is consistent with that found experimentally over a much narrower range of Reynolds number ($5\times10^3 \lesssim Re_\delta^* \lesssim 4\times10^4$). Because of the decrease of τ_w/q_∞ with increasing Reynolds number, changes in Re_δ^* have much less effect on p'/q_∞ than on p'/τ_w: the corresponding p'/q_∞ variation is from 4.7×10^{-3} to 6.6×10^{-3},

that is, by a factor of 1.4 compared with 5.9 as for p'/τ_w.

Consideration of the range of Reynolds number covered by the various experimental investigations clearly shows the need for additional accurate measurements at considerably higher Reynolds numbers. Such data would provide a valuable and much more severe test of the boundary layer model used in this work.

Limitation to the present experimental work does not allow correlation measurements to be made for zero or non-zero pressure gradient layers.

(5) Dominance of Turbulence/Mean-Shear Interaction.

The calculation of the root mean square wall pressure fluctuation and its variation with Reynolds number, and frequency power spectral density of the fluctuations were based on pressure source terms arising from the interaction between the turbulence and mean shear. Since these results are in good agreement with experimental data, they give a strong indication that this interaction is the dominant process which gives rise to the wall pressure fluctuations.

For the constant pressure layer, the work indicates that turbulence/mean-shear interaction is responsible for about 80% of the mean square pressure.

REFERENCES

Bakewell, H.P., Carey, G.F., Libuha, J.J., Schloemer, H.H. and von Winkle, W.A.	1962	Wall Pressure Correlations in Turbulent Pipe Flow. U.S. Navy Underwater Sound Laboratory Report No. 559.
Bannister, F.K. and Mucklow, G.F.	1948	Wave Action Following Sudden Release of Compressed Gas from a Cylinder. Proc. Inst. Mech. Eng., vol 159.
Batchelor, G.K.	1945	On the Concept and Properties of the Idealised Hydrodynamic Resistance. Aust. Council for Aeronautics, Rept. 13
Batchelor, G.K.	1951	Pressure Fluctuations in Isotropic Turbulence. Proc. Camb. Phil. Soc., vol. 47.
Batchelor, G.K.	1953	The Theory of Homogeneous Turbulence. Cambridge University Press.
Blake, W.K.	1970	Turbulent Boundary Layer Wall Pressure Fluctuations on Smooth and Rough Walls. J. Fluid Mech., vol. 44.
Bull, M.K.	1963	Wall Pressure Fluctuations Associated with Subsonic Turbulent Boundary Layer Flow. Ph.D. Thesis, University of Southampton.

Bull, M.K.	1967	Wall Pressure Fluctuations Associated with Subsonic Turbulent Boundary Layer Flow. J. Fluid Mech., vol. 28.
Bull, M.K.	1969a	Velocity Profiles of Turbulent Boundary Layers. Aero. J. Roy. Aero. Soc., vol. 73.
Bull, M.K.	1969b	Mean Shear in a Constant Pressure Turbulent Boundary Layer. A.I.A.A. Journal, vol. 7.
Bull, M.K. and Lim, K.B.	1968	Effects of Reynolds Number on Wall Pressure Fluctuations in Constant Pressure Turbulent Boundary Layers. Paper presented at Third Australasian Conference on Hydraulics and Fluid Mechanics, Sydney.
Bull, M.K. and Lim, K.B.	1969	Calculations of Wall Pressure Fluctuations in Constant Pressure Turbulent Boundary Layers. Paper presented at 4th A.I.N.S.E. Heat Transfer and Fluid Flow Conference, Lucas Heights.
Bull, M.K. and Lim, K.B.	1970	Wall Pressure Fluctuations in a Turbulent Boundary Layer: Interpretation of Contributions of Various Regions to the Space-Time Covariance. I.E. Aust., Mech. and Chem. Eng. Trans.

Bull, M.K. and Willis, J.L.	1961	Some Results of Experimental Investigations of the Surface Pressure Field due to a Turbulent Boundary Layer. University of Southampton, A.A.S.U. Rept. 199
Clauser, F.H.	1954	Turbulent Boundary Layers in Adverse Pressure Gradients. J. Aero. Sciences, vol. 21.
Clauser, F.H.	1956	The Turbulent Boundary Layer. Adv. Appl. Mech., vol. 4.
Coles, D.E.	1954	The Problem of the Turbulent Boundary Layer. Z.A.M.P., vol 5.
Coles, D.E.	1956	The Law of the Wake in the Turbulent Boundary Layer. J. Fluid Mech., vol. 1.
Coles, D.E.	1962	The Turbulent Boundary Layer in a Compressible Fluid. RAND Corp., Rept., R - 403 - PR.
Coles, D.E.	1968	A Young Person's Guide to the Data. AFOSR-IFP-Stanford Conference on Computation of Turbulent Boundary Layers, Standford University.
Collar, A.R.	1939	The Effect of a Gauze on the Veolcity Distributions in a Uniform Duct. A.R.C., R&M 1867.

Corcos, G.M.	1962	Pressure Fluctuations in Shear Flows. U.C.L.A., Inst. of Eng. Res. Rept. Ser. 183, No. 2.
Corcos, G.M.	1963	Resolution of Pressure in Turbulence. J. Acous. Soc. America, vol. 35.
Corcos, G.M.	1964	The Structure of Turbulent Pressure Field in Boundary Layer Flows. J. Fluid Mech., vol. 18.
Doak, P.E.	1960	Acoustic Radiation from a Turbulent Fluid Containing Foreign Bodies. Proc. Roy. Soc., A254.
Dryden, H.L.	1953	Review of Published Data on the Effect of Roughness on Transition from Laminar to Turbulent Flow. J. Aero. Sciences, vol. 20.
Favre, A.J., Gaviglio, J.J. and Dumas, R.	1957	Space-Time Double Correlations and Spectra in a Turbulent Boundary Layer. J. Fluid Mech., vol. 2.
Gardner, S.	1965	On Surface Pressure Fluctuations Produced by Boundary Layer Turbulence. Acoustica, vol. 16.
Grant, H.L.	1958	The Large Eddies of Turbulent Motion. J. Fluid Mech., vol. 4.

Harrison, M. 1958 Pressure Fluctuations on the Wall Adjacent to a Turbulent Boundary Layer. U.S. Navy, David Taylor Model Basin Rept. 1260.

Hinze, J.O. 1959 Turbulence - An Introduction to its Mechanism and Theory. McGraw-Hill.

Hodgson, T.H. 1962 Pressure Fluctuations in Shear Flow Turbulence. Ph.D. Thesis, University of London.

Klebanoff, P.S. 1955 Characteristics of Turbulence in a Boundary Layer with Zero Pressure Gradient. N.A.C.A., Tech. Rept. 1247.

Kraichnan, R.H. 1956a Pressure Field within Homogeneous Anisotropic Turbulence. J. Acous. Soc. America, vol. 28.

Kraichnan, R.H. 1956b Pressure Fluctuations in Turbulent Flow Over a Flat Plate. J. Acous. Soc. America. vol. 28.

Laufer, J. 1954 The Structure of Turbulence in Fully Developed Pipe Flow. N.A.C.A., Tech. Rept., 1174.

Lilley, G.M. 1960 Pressure Fluctuations in an Incompressible Boundary Layer. College of Aeronautics, Cranfield, Rept. 113

Lilley, G.M. 1960 On Surface Pressure Fluctuations in

Turbulent Boundary Layers.
AGARD Rept. 276.

MacMillan, F.A. 1956 Experiments on Pitot Tubes in Shear Flow.
A.R.C. R&M 3028.

MacPhail, D.C. 1939 Experiments on Turning Vanes in an Expansion.
A.R.C. R&M 1876.

Mellor, G.L. and Gibson, D.M. 1966 Equilibrium Turbulent Boundary Layers.
J. Fluid Mech., vol. 24.

Morrison, W.R.B. 1969 Two-Dimensional Frequency-Wave Number Spectra and Narrow Band Shear Stress Correlations in Turbulent Pipe Flow.
Ph.D. Thesis, University of Queensland.

Pankhurst, R.C. and Holder, D.W. 1952 Wind Tunnel Technique.
Pitman and Sons.

Patel, V.C. 1965 Calibration of the Preston Tube and Limitations on Its Use in Pressure Gradients.
J. Fluid Mech., vol 23.

Pope, A. and Harper, J.J. 1966 Low Speed Wind Tunnel Testing.
John Wiley.

Proudman, I. 1951 A Comparison of Heisenberg's Spectrum of Turbulence with Experiment.
Proc. Camb. Phil. Soc., vol. 47.

Reichardt, H. 1951 Vollstandige Darstellung der Turbulenten Geschwindigkeitsverteilung in Glatten

Leitungen.
Zeitschrift fur Angewandte Mathematik
und Mechanik, vol. 31.

Reynolds, O. 1883 An Experimental Investigation of the Circumstances which Determine whether the Motion of Water shall be Direct or Sinuous, and of the Law of Resistance of Parallel Channels.
Phil. Trans. Roy. Soc.,

Richards, E.J., Bull, M.K. and Willis, J.L. 1960 Boundary Layer Noise Research in the U.S.A. and Canada; a Critical Review.
A.R.C., 21, 766.

Sag, T.W. 1963 A New Method for the Numerical Evaluation of Multiple Integrals.
M.Sc. Thesis, University of Adelaide.

Serafini, J.S. 1963 Wall Pressure Fluctuations and Pressure Velocity Correlations in a Turbulent Boundary Layer.
AGARD Rept. 453.

Schlichting, H. 1960 Boundary Layer Theory.
McGraw-Hill.

Schloemer, H.H. 1967 Effects of Pressure Gradients on Turbulent Boundary Layer Wall-Pressure Fluctuations.
J. Acous. Soc. America, vol. 42.

Simmons, L.F.C. 1945 Measurements of the Aerodynamic Forces Acting on Porous Screens.
A.R.C., R&M 2276.

Skudrzyk, E.J. and 1960 Noise Production in a Turbulent Boundary

Haddle, G.P.		Layer by Smooth and Rough Surfaces. J. Acous. Soc. America, vol. 32.
Tani, I. and Hama, F.R.	1945	Experiments on the Permissible Roughness in the Laminar Boundary Layer over a Flat Plate. (in Japanese.) Wartime Research Report I-4.
Tani, I. and Hama, F.R.	1953	Some Experiments on the Effects of a Single Roughness Element on Boundary layer Transition. J. Aero. Sciences, vol. 20.
Tani, I., Hama, F.R. and Mituisi, S.	1954	On the Effect of a Single Roughness Element on Boundary Layer Transition. Rept. Inst. Sci. Tech., Tokyo Univ., vol. 8.
Taylor, G.I.	1921	Diffusion by Continuous Movements. Proc. London Math. Soc., Ser. 2, vol. 20.
Taylor, G.I.	1935	Statistical Theory of Turbulence. Pts. I-IV. Proc. Roy. Soc., A151.
Taylor, G.I.	1938	The Spectrum of Turbulence. Proc. Roy. Soc., A164.
Townsend, A.A.	1956	The Structure of Turbulent Shear Flow. Cambridge University Press.
Tritton, D.J.	1967	Some New Correlation Measurements in a Turbulent Boundary Layer. J. Fluid Mech., vol. 28.
Uberoi, M.S.	1953	Quadruple Velocity Correlations and Pressure Fluctuations in Isotropic Turbulence. J. Aero. Sciences, vol. 20.

White, F.M. 1964 A Unified Theory of Wall Pressure Fluctuations. U.S. Navy Underwater Sound Lab. Rept. 629.

Willmarth, W.W. 1959 Space-Time Correlations and Spectra of Wall Pressure in a Turbulent Boundary Layer. N.A.S.A. Memo. 3-17-59W.

Willmarth, W.W. and Roos, F.W. 1965 Resolution and Structure of the Wall Pressure Field Beneath a Turbulent Boundary Layer. J. Fluid Mech., vol. 22.

Willmarth, W.W. and Wooldridge, C.E. 1962 Measurements of the Fluctuating Pressure at the Wall Beneath a Thick Turbulent Boundary Layer. J. Fluid Mech., vol. 14.

Willmarth, W.W. and Wooldridge, C.E. 1963 Measurements of the Correlation between the Fluctuating Velocities and the Fluctuating Wall Pressure in a Thick Turbulent Boundary Layer. AGARD Rept. 456.

APPENDIX A.

This Appendix contains the major computer programmes used in the calculations of the joint contribution density function, the auto-covariance and the mean square value of the wall pressure fluctuations in a turbulent boundary layer. They are presented as follows:

A-I Evaluation of Equation (3.2.1) for the mean square value of the wall pressure fluctuations.

A-II Evaluation of Equation (B.3) with the scale of the small eddies given by Equation (3.1.14).

A-III Evaluation of Equation (B.3) with the scale of the small eddies given by Equation (3.1.19).

A-IV Evaluation of the small eddy contribution to the mean square wall pressure fluctuation.

A-V Evaluation of the large eddy contribution to the mean square wall pressure fluctuation.

A-VI Programme for the selection of region size required for use in the evaluation of the mean square wall pressure fluctuation.

A-VII Evaluation of Equation (2.6.16) for G^{s}_{13}.

A-VIII Programme for the selection of region size required for use in the evaluation of the auto-covariance of the fluctuating wall pressure.

A-IX Evaluation of Equation (3.2.1) for the auto-covariance of the wall pressure fluctuation.

A-I Numerical Evaluation of Equation (3.2.1) for the case of $\vec{\xi} = \tau = 0$

PROGRAM KBL052

The multiple integral giving the value of $\partial P^*(y_2, \infty)/\partial y_2$ must first be reduced to a form appropriate for numerical analysis. This involves the normalising of the limits and some re-arrangement of the variables concerned. The procedure is detailed below.

Let the value of the integral represented by Equation (3.2.1) be given by

$$I = \frac{\partial P^*(y_2,\infty)}{\partial y_2} = \rho^2 \int_0^\infty dz_2 \; F_{13}(y_2, z_2) \qquad \ldots(A.I.1)$$

where, from Section 2.6,

$$F_{13}(y_2, z_2) = F_{13}(y_2, z_2, \vec{\xi}=0, \tau=0)$$

$$= \frac{2}{\pi} M(y_2)M(z_2)u_2'(y_2)u_2'(z_2)I_{13}(y_2, z_2),$$

$$I_{13}(y_2, z_2) = I_{13}(y_2, z_2, \vec{\xi}=0, \tau=0)$$

$$= \int_{-\infty}^{\infty} dr_1 \int_{-\infty}^{\infty} dr_3 \; R_{22}(y_2, \vec{r}) g_{13}(y_2, \vec{r}),$$

$$R_{22}(y_2, \vec{r}) = R_{22}(y_2, z_2, r_1, r_3, \tau=0)$$

$$= \frac{\langle u_2(y_2) u_2(y_2 + \vec{r}) \rangle}{u_2'(y_2) u_2'(z_2)} \quad ,$$

$$g_{13}(y_2, \vec{r}) = g_{13}(y_2, z_2, r_1, r_3, \tau = 0)$$

$$= \frac{\left[1 - \frac{r_1^2 (y_2 + z_2 + 2m)}{m^2 (y_2 + z_2 + m)} \right]}{m(y_2 + z_2 + m)} \quad ,$$

$$m^2 = (y_2 + z_2)^2 + r_1^2 + r_3^2 \quad ,$$

$$M(y_2) = \partial U_1(y_2) / \partial y_2 \quad ,$$

$$u_2'(y_2) = \langle u_2^2(y_2) \rangle^{\frac{1}{2}} \quad ,$$

$\vec{r} = \vec{z} - \vec{y}$, and

$\langle \ldots . \rangle$ denotes the statistical mean value.

It can be seen that I_{13} is an even function of r_1 and r_3. If we now introduce the friction velocity U_T and the boundary layer thickness δ as normalising parameters, Equation (A.I.1) is written in full as

$$I = \frac{\partial P^*(\frac{y_2}{\delta}, \infty)}{\partial(\frac{y_2}{\delta})}$$

$$= \frac{8\rho^2\delta^2U_\tau^4}{\pi} \int_0^\infty d(\frac{r_1}{\delta}) \int_{-y_2/\delta}^\infty d(\frac{r_2}{\delta}) \int_0^\infty d(\frac{r_3}{\delta})\ M(\frac{y_2}{\delta})M(\frac{r_2}{\delta})\ \frac{u_2(\frac{y_2}{\delta})}{U_\tau}\ \frac{u_2(\frac{r_2}{\delta})}{U_\tau} \cdots$$

$$\cdots\ R_{22}(\frac{y_2}{\delta}, \frac{\vec{r}}{\delta}) g_{13}(\frac{y_2}{\delta}, \frac{\vec{r}}{\delta})$$

$$\approx \frac{8\rho^2\delta^2U_\tau^4}{\pi} \int_0^{c_1} d(\frac{r_1}{\delta}) \int_{-y_2/\delta}^{c_2} d(\frac{r_2}{\delta}) \int_0^{c_3} d(\frac{r_3}{\delta})\ M(\frac{y_2}{\delta})M(\frac{r_2}{\delta})\ \frac{u_2(\frac{y_2}{\delta})}{U_\tau}\ \frac{u_2(\frac{r_2}{\delta})}{U_\tau} \cdots$$

$$\cdots R_{22}(\frac{y_2}{\delta}, \frac{\vec{r}}{\delta}) g_{13}(\frac{y_2}{\delta}, \frac{\vec{r}}{\delta})\ ,$$

for some values of c_1, c_2 and c_3 which are sufficiently large and for

$$M(\frac{y_2}{\delta}) = \frac{\delta}{U_\tau} \frac{\partial U_1(\frac{y_2}{\delta})}{\partial y_2}\ .$$

If we now let

$$r_1' = \frac{r_1}{c_1}\ ,$$

$$r_2' = \frac{r_2+y_2}{c_2+y_2} \quad \text{and}$$

$$r_3' = \frac{r_3}{c_3} ,$$

we have

$$I = \frac{8\rho^2\delta^2U^4}{\pi} c_1(c_2+y_2)\, c_3 \int_0^1 dr_1' \int_0^1 dr_2' \int_0^1 dr_3'\, M(y_2)M\,(c_2+y_2)r_2' \ldots$$

$$\ldots u_2'(y_2)u_2'\left[(c_2+y_2)r_2'\right] R_{22}(y_2, c_1r_1', (c_2+y_2)r_2', c_3r_3') \ldots$$

$$\ldots g_{13}(y_2, c_1r_1', (c_2+y_2)r_2', c_3r_3'), \qquad \ldots.(A.I.2)$$

where r_2' now represents a normalised distance from the boundary surface.

The computer programme written for the evaluation of Equation (A.I.2) is listed below, where the functions representing the mean shear $M(y_2)$, the turbulence intensity $u_2'(y_2)$, the correlation coefficient R_{22} and the geometric term g_{13} have been included as subroutine functions.

Experience has shown that values for H, S, V and U required in the use of Sag's numerical method should be 0.025, 34, 0.86 and 1.50 respectively, where H represents the half mesh size, S is the number of mesh points per dimension, V is the proportion of the transformed space over which the values of the integrand at the mesh points are to be evaluated and U is a weighting factor. For this choice of values of H, S, V and U, the total number of mesh

points considered is 21283 requiring a central processor time of about 93 seconds. As this time is only for one value required for the final manual determination of $\langle p^2 \rangle$ and since the distribution of I with y_2 is a peaky function itself, it can be realised that the determination of $\langle p^2 \rangle$ becomes a laborious and costly affair.

```
      PROGRAM KBL052 (INPUT,OUTPUT)
C  ADAPTATION OF T. SAGS NUMERICAL METHOD FOR THE MEAN SQUARE WALL
C      PRESSURE IN EQUILIBRIUM TURBULENT BOUNDARY LAYER FLOW.
       DIMENSION T(6),X(6),M(6),Y(100),ANS(100),D(100)
       COMMON N,U,C,C1,C2,C3,X2,RE,RK,CPI,PI,YSTRLMT,Z2,Z3
    10 FORMAT (F6.3,F3.0,6F6.2,E9.2,2F5.2,2I4)
    20 FORMAT (F9.6)
    30 FORMAT (/////34X,5H C = ,F5.3,2X,8H FTRA = ,F5.1,2X,8H FTRB = ,
      1F5.1,2X,8H FTRC = ,F5.1)
    40 FORMAT (37X,12H REDELTA* = ,E8.2,2X,5H K = ,F4.2,2X,
      112H COLES PI = ,F4.2)
    50 FORMAT (37X,4H H =,F5.3,5X,4H S =,F3.0,5X,4H V =,F5.2,5X,4H U =,
      1F5.2,/)
    70 FORMAT (37X,2H I,6X,2H Y,4X,18H MEAN OF INTEGRAND,4X,
      113H NO OF POINTS)
    80 FORMAT (36X,I3,3X,F7.5,5X,E12.5,11X,I6)
       PI=3.1415926536
   100 READ 10,H,S,V,U,C,FTRA,FTRB,FTRC,RE,RK,CPI,NII,N
       IF (H.GT.0)110,200
   110 E=PI*3.60/(0.837*RE)
       STEP=0.5
       RLIMIT=50.0
       CI=3.0
       T=1.0
  1200 CIA=CI
       TA=T
       CI=CI+STEP
       IF (CI.GT.RLIMIT)1121,1122
  1121 PRINT 1123
  1123 FORMAT (10X,22H CI* GREATER THAN 50.0)
       GO TO 200
  1122 CY=CI/4.0
       CZ=RK*CI
       T=(1.0+CY+0.5*CY*CY+CY**6/1300.0)*EXP(-CY)-(1.0/(RK*CI)+E*CPI*
      1SIN(E*CI)/RK)
  1300 IF (T*TA)1400,2000,1200
```

```
1400 CIB=CIA
     CIA=CI
     TA=T
     CI=(CIA+CIB)/2.0
1500 CY=CI/4.0
     CZ=RK*CI
     T=(1.0+CY+0.5*CY*CY+CY**6/1300.0)*EXP(-CY)-(1.0/(RK*CI)+E*CPI*
    1SIN(E*CI)/RK)
     IF (T*TA)1600,2000,1700
1600 CIB=CIA
1700 CIA=CI
     TA=T
     CI=(CIA+CIB)/2.0
     IF (ABS(CI-CIA).LT.0.001)2000,1500
2000 YSTRLMT=CI
     A1=S**N
     V0=H**N
     HH=2.0*H
     VV=V*V
     HMA=0.5*H-V
     DO 106 II=1,NII
     READ 20,Y(II)
     Z2=U2Y(C*Y(II))
     Z3=RMS(C*Y(II))
     C1=FTRA*C*Y(II)
     X2=FTRB*C*Y(II)
     C2=X2-C*Y(II)
     C3=FTRC*C*Y(II)
     PRINT 30,C,FTRA,FTRB,FTRC
     PRINT 40,RE,RK,CPI
     PRINT 50,H,S,V,U
     SUM=0.0
     A=0.0
     NPOINTS=0
 140 M(1)=0
     R0=0
```

```
      DO 150 I=1,N
      M(I+1)=A/S**(N-I)
      T(I)=HH*(M(I+1)-S*M(I))+HHA
  150 R0=R0+T(I)*T(I)
      IF (R0-VV)160,170,170
  160 R=SQRT(R0)
      NPOINTS=NPOINTS+1
      CALL TRNS (T,R,DET,X)
      SUM=SUM+DET*G(X,Y(II))
  170 A=A+1
      IF (A-A1)140,180,180
  180 ANS(II)=SUM*V0*8.0*C*C1*C3*X2/3.14159265
      PRINT 70
  190 PRINT 80,II,Y(II),ANS(II),NPOINTS
      GO TO 100
  200 STOP
      END



      SUBROUTINE TRNS (T,R,DET,X)
C     SAGS MULTI-DIMENSIONAL TRANSFORMATION.
      DIMENSION T(6),X(6),W(6)
      COMMON N,U,C,C1,C2,C3,X2,RE,RK,CPI,PI,YSTRLMT,Z2,Z3
      R1=1.0/(1.0-R)
      R2=U*R1
      DET=R1*R2**N
      DO 3 I=1,N
      RX=T(I)*R2
      EX=EXP(2.0*RX)
      EX1=2.0/(EX+1.0)
      W(I)=1.0-EX1
    3 DET=DET*EX1*(2.0-EX1)
      DO 10 I=1,N
   10 X(I)=(W(I)+1.0)/2.0
      RETURN
```

```
      END


      FUNCTION G (X,YG)
C     HOUSEKEEPING ROUTINE.
      DIMENSION X(6)
      COMMON N,U,C,C1,C2,C3,X2,RE,RK,CPI,PI,YSTRLMT,Z2,Z3
      Z1=R22(C*YG,C1*X(1),X2*X(2)-C*YG,C3*X(3))
      Z4=U2Y(X2*X(2))
      Z5=RMS(X2*X(2))
      Z6=GM(X,YG)
      G=Z1*Z2*Z3*Z4*Z5*Z6
      RETURN
      END


C     THE SUBROUTINE FUNCTIONS LISTED BELOW ARE FOR SET 4 CALCULATIONS.


      FUNCTION RMS (YMS)
C     MEAN SHEAR FUNCTION.
      COMMON N,U,C,C1,C2,C3,X2,RE,RK,CPI,PI,YSTRLMT,Z2,Z3
      IF (YMS.GE.1.0)1,2
    1 RMS=0.0
      GO TO 50
    2 YSTARMS=YMS*RE/3.60
      IF (YSTARMS.LE.YSTRLMT)10,20
   10 YSTMS=YSTARMS/4.0
      RMS=(1.0+YSTMS+0.5*YSTMS*YSTMS+YSTMS**6/1300.0)*EXP(-YSTMS)*RE/3.6
      GO TO 50
   20 IF (YMS.GT.0.837)30,40
   30 RMS=((1.0-YMS)/0.163)**0.67/(0.837*RK)
      GO TO 50
```

```
   40 RMS=1.0/(RK*YMS)+PI*CPI*SIN(PI*YMS/0.837)/(0.837*RK)
   50 RETURN
      END


      FUNCTION U2Y(YU2Y)
C     TURBULENCE INTENSITY FUNCTION.
C     RE IS REYNOLDS NUMBER BASED ON DISPLACEMENT THICKNESS.
      COMMON N,U,C,C1,C2,C3,X2,RE,RK,CPI,PI,YSTRLMT,Z2,Z3
      IF (YU2Y.GE.0.2)10,20
   10 U2Y=1.06*EXP(-2.23*(YU2Y-0.20)**2)
      GO TO 70
   20 YRE=RE*YU2Y/3.60
      IF (YRE.GT.600.0)30,40
   30 U2Y=1.06
      GO TO 70
   40 IF (YRE.GT.10.0)50,60
   50 U2Y=0.0838*YRE*YRE/(1.0+0.922*YRE+0.077*YRE*YRE)
      GO TO 70
   60 U2Y=0.00921*YRE*YRE/(1.0-0.0361*YRE+0.01328*YRE*YRE)
   70 RETURN
      END


      FUNCTION R22 (YR22,R1R22,R2R22,R3R22)
C     FUNCTION SATISFIES R22(Y,R1,R2,R3) = R22(Y+R2,R1,-R2,R3).
C     VARIABLE ASSIGNMENTS.....................
C     YR22,R1R22,R2R22,R3R22 ARE DISTANCES IN THE Y,R1,R2,R3 DIRECTIONS
C     RESPECTIVELY.
C     RSCALE IS THE SCALE FACTOR FOR THE VARIATION OF THE CORRELATION
C     COEFFICIENT DUE TO THE SMALL EDDIES.
      IF (YR22.EQ.0.0)10,20
   10 R22=0.0
      GO TO 80
```

```
   20 IF (YR22+R2R22/2.0.LT.0.2)30,40
   30 RSCALE=0.570*(YR22+R2R22/2.0)
      GO TO 50
   40 RSCALE=0.114
   50 IF (R1R22.EQ.0.0.AND.R3R22.EQ.0.0)60,70
   60 R22=0.915*EXP(-ABS(R2R22)/RSCALE)+0.085*EXP(-7.4562*R2R22*R2R22)
      GO TO 80
   70 R1R22S=R1R22*R1R22
      R2R22S=R2R22*R2R22
      R3R22S=R3R22*R3R22
      SQR123=SQRT(R1R22S+R2R22S+R3R22S)
      R22=0.915*(1.0-(R1R22S+R3R22S)/(2.0*SQR123*RSCALE))*EXP(-SQR123/
     1RSCALE)+0.085*(1.0-14.91*R1R22S)*(1.0-264.1*R3R22S+5814.7*R3R22S*
     2R3R22S)*EXP(-(29.824*(R1R22S+R2R22S)+264.12*R3R22S)/4.0)
   80 RETURN
      END
```



```
      FUNCTION GM (X,YGM)
C     GEOMETRIC FUNCTION.
      DIMENSION X(6)
      COMMON N,U,C,C1,C2,C3,X2,RE,RK,CPI,PI,YSTRLMT,Z2,Z3
      A1GM=C1*X(1)
      A2GM=(C2+C*YGM)*X(2)-C*YGM
      A3GM=C3*X(3)
      A4GM=A2GM+C*YGM
      A5GM=A4GM+C*YGM
      D1GM=SQRT(A5GM*A5GM+A1GM*A1GM+A3GM*A3GM)
      D2GM=A5GM+D1GM
      D3GM=D1GM*D2GM
      RUGM=A1GM*A1GM*(2.0+A5GM/D1GM)
      T2GM=1.0-RUGM/D3GM
      GM=T2GM/D3GM
      RETURN
      END
```

A-II Numerical Evaluation of Equation (B.3)

PROGRAM KBL070

This programme is for the determination of I^{s}_{13} using Equation (B.3) derived in Appendix B. The variation of the scale s of the small eddies is given by Equation (3.1.14) as

$$s/y_2 = 0.570 \quad \text{for} \quad 0 \leqslant y_2/\delta \leqslant 0.2$$

$$s/\delta = 0.114 \quad \text{for} \quad 0.2 \leqslant y_2/\delta \leqslant 1.0 \ ,$$

where δ is the boundary layer thickness and y_2 is the distance from the boundary in the direction normal to the boundary. The listing of the programme is given below.

```
      PROGRAM KBL070 (INPUT,OUTPUT)
C  DETERMINATION OF I13 DUE TO THE SMALL EDDIES WITHOUT RECIPROCITY.
C  VARIABLE ASSIGNMENTS.....
C  Y=Y2/SCALE=(Y2/DELTA)*(DELTA/SCALE).
C  R=R2/SCALE.
C  A=2*Y+R.
C  AR=ABSOLUTE VALUE OF R.
C  N DESIGNATES THE TOTAL NUMBER OF R VALUES TO BE READ IN.
C  X(J) = ABSCISSAE VALUES OVER WHICH THE VALUES OF F, F1 ,F AND EXPR
C     ARE TO BE EVALUATED.
C  AREA = VALUE OF THE INTEGRAL OVER THE X-SPACE.
C  PRO = PRODUCT OF AREA WITH THE NECESSARY COEFFICIENTS.
      DIMENSION X(51),F(51),F1(51),F2(51),EXPR(51)
    1 FORMAT (F7.4,I3)
    2 FORMAT (1H1,//42X,5H Y = ,F8.5,5X,6H R2 = ,F8.5,5X,5H A = ,
     1F8.5,///38X,2H X,11X,2H F,10X,3H F1,11X,3H F2,7X,10H INTEGRAND,/)
    3 FORMAT (36X,F6.3,6X,F7.3,6X,F7.4,6X,F8.5,6X,F9.6)
    4 FORMAT (/19X,23H VALUE OF X-INTEGRAL = ,E11.4,10X,42H PRODUCT OF X
     1-INTEGRAL WITH COEFFICIENT = ,E11.4)
  100 READ 1,Y,N
      IF (Y.GT.0.0)110,170
  110 DO 160 I=1,N
      READ 1,R
      AR=ABS(R)
      A=2.0*Y+R
      PRINT 2,Y,R,A
      DO 140 J=1,51
      AJ=J-1
      X(J)=AJ/50.0
      F(J)=X(J)*X(J)*(1.0-2.0*AR+A*A)-2.0*X(J)*(1.0-AR)+1.0
      F(J)=F(J)**1.5
      F1(J)=X(J)*X(J)*(4.0*AR-3.0)+2.0*X(J)*(2.0-AR)-1.0
      IF (J.EQ.1)120,130
  120 F2(J)=0.0
      EXPR(J)=0.0
      GO TO 140
```

```
130 F2(J)=EXP(-(1.0/X(J)-1.0))/X(J)
    EXPR(J)=F1(J)*F2(J)/F(J)
140 PRINT 3,X(J),F(J),F1(J),F2(J),EXPR(J)
    SUM=0.0
    DO 150 K=1,49,2
150 SUM=SUM+EXPR(K)+4.0*EXPR(K+1)+EXPR(K+2)
    AREA=SUM/150.0
    PRO=AREA*A*EXP(-AR)*3.1415927/2.0
160 PRINT 4,AREA,PRO
    GO TO 100
170 STOP
    END
```

A-III Numerical Evaluation of Equation (B.3)

PROGRAM KBL079

This programme is for the determination of I^{s}_{13} using Equation (B.3) derived in Appendix B. It is different from PROGRAM KBL070 in that the variation of the scale s of the small eddies across the boundary layer is given by Equation (3.1.19) as

$$s/\left[\tfrac{1}{2}(y_2+z_2)\right] = 0.570 \quad \text{for} \quad 0 \leqslant \tfrac{1}{2}(y_2+z_2)/\delta \leqslant 0.2$$

$$s/\delta = 0.114 \quad \text{for} \quad 0.2 \leqslant \tfrac{1}{2}(y_2+z_2)/\delta \leqslant 1.0$$

where y_2 and z_2 represent the distances of the two correlation points from the boundary and δ is the boundary layer thickness. The listing of the programme is given below.

```
      PROGRAM KBL079 (INPUT,OUTPUT)
C  DETERMINATION OF I13 DUE TO SMALL EDDIES SATISFYING RECIPROCITY CONDITION.
C  VARIABLE ASSIGNMENTS..........
C  Y=Y2/SCALE=(Y2/DELTA)*(DELTA/SCALE).
C  R=R2/SCALE.
C  SCALE=0.570*(Y2+R2/2.0) FOR Y2+R2/2.0 LESS THAN 0.20, OTHERWISE USE
C     SCALE=0.114.
C  A=2*Y+R.
C  AR=ABSOLUTE VALUE OF R.
C  N DESIGNATES THE TOTAL NUMBER OF R VALUES TO BE READ IN.
C  X(J) = ABSCISSAE VALUES OVER WHICH THE VALUES OF F, F1 ,F AND EXPR
C     ARE TO BE EVALUATED.
C  AREA = VALUE OF THE INTEGRAL OVER THE X-SPACE.
C  PRO = PRODUCT OF AREA WITH THE NECESSARY COEFFICIENTS.
      DIMENSION X(51),F(51),F1(51),F2(51),EXPR(51)
    1 FORMAT (E11.4,I3)
    2 FORMAT (1H1,//20X,6H Y2 = ,E11.4,5X,6H R2 = ,E11.4,5X,5H Y = ,
     1F8.4,5X,5H R = ,F8.4,5X,5H A = ,F8.4,
     2///36X,2H X,11X,2H F,10X,3H F1,11X,3H F2,7X,10H INTEGRAND,/)
    3 FORMAT (36X,F6.3,6X,F7.3,6X,F7.3,6X,F7.4,6X,F8.5,6X,F9.6)
    4 FORMAT (/19X,23H VALUE OF X-INTEGRAL = ,E11.4,10X,42H PRODUCT OF X
     1-INTEGRAL WITH COEFFICIENT = ,E11.4)
  100 READ 1,Y2,N
      IF (Y2.GT.0.0)110,170
  110 DO 160 I=1,N
      READ 1,R2
      IF (Y2+R2/2.0.LT.0.2)111,112
  111 SCALE=0.570*(Y2+R2/2.0)
      GO TO 113
  112 SCALE=0.114
  113 Y=Y2/SCALE
      R=R2/SCALE
      AR=ABS(R)
      A=2.0*Y+R
      PRINT 2,Y2,R2,Y,R,A
      DO 140 J=1,51
```

```
      AJ=J-1
      X(J)=AJ/50.0
      F(J)=X(J)*X(J)*(1.0-2.0*AR+A*A)-2.0*X(J)*(1.0-AR)+1.0
      F(J)=F(J)**1.5
      F1(J)=X(J)*X(J)*(4.0*AR-3.0)+2.0*X(J)*(2.0-AR)-1.0
      IF (J.EQ.1)120,130
  120 F2(J)=0.0
      EXPR(J)=0.0
      GO TO 140
  130 F2(J)=EXP(-(1.0/X(J)-1.0))/X(J)
      EXPR(J)=F1(J)*F2(J)/F(J)
  140 PRINT 3,X(J),F(J),F1(J),F2(J),EXPR(J)
      SUM=0.0
      DO 150 K=1,49,2
  150 SUM=SUM+EXPR(K)+4.0*EXPR(K+1)+EXPR(K+2)
      AREA=SUM/150.0
      PRO=AREA*A*EXP(-AR)*3.141927/2.0
  160 PRINT 4,AREA,PRO
      GO TO 100
  170 STOP
      END
```

A-IV Evaluation of the Small Eddy Contribution to the Mean Square Wall Pressure Fluctuation

PROGRAM EBL083

The computer programme is designed to give the value of the three-fold integral

$$\frac{\partial P(y_2,\infty)}{\partial y_2} = \rho^2 \int_0^\infty dz_2 \; G_{13}(y_2,z_2) \quad , \qquad \ldots(A.IV.1)$$

where G_{13} itself is a double integral in the (r_1,r_3) space defined by Equations (2.6.15) and (2.6.16) and the definition of $P(y_2,z_2)$ is given by Equation (2.5.3) as

$$P(y_2,z_2) = \rho^2 \int_0^{y_2} dy \int_0^{z_2} dz \; G_{13}(y,z)$$

The final integration over y_2 to give

$$\langle p^2 \rangle = \tfrac{1}{2} \int_0^\infty \left[\frac{\partial P(y_2,\infty)}{\partial y_2} \right] dy_2 \qquad \ldots(A.IV.2)$$

is carried out manually.

The listing of the computer programme for the evaluation of Equation (A.IV.1) for any value of y_2 is given below. The function subroutines for the mean shear and the turbulence intensity required to complete the computer programme are the same as those

listed in PROGRAM KBL052 and will not be listed here.

```
      PROGRAM KBL083 (INPUT,OUTPUT)
C
C  DETERMINATION OF THE CONTRIBUTION TO THE MEAN SQUARE WALL PRESSURE
C    IN EQUILIBRIUM TURBULENT BOUNDARY LAYER FLOW TAKING INTO ACCOUNT
C    ONLY THE EFFECTS OF THE SMALL SCALE CORRELATIONS WHICH SATISFY THE
C    RECIPROCAL RELATIONSHIP.
C  NOTE THAT THE CORRELATION FUNCTION IS NORMALISED BY THE PRODUCT OF
C    THE RMS VALUES OF THE TURBULENCE INTENSITIES AT THE TWO POINTS TAKEN.
C
C  ............VARIABLE ASSIGNMENTS............
C
C  YR = (Y2+R2)/DELTA.
C  Y=Y2/SCALE=(Y2/DELTA)*(DELTA/SCALE).
C  R=R2/SCALE.
C  SCALE=0.570*(Y2+R2/2.0) FOR Y2+R2/2.0 LESS THAN 0.20, OTHERWISE USE
C    SCALE=0.114.
C  A=2*Y+R.
C  AR=ABSOLUTE VALUE OF R.
C  X(J) = ABSCISSAE VALUES OVER WHICH THE VALUES OF F, F1 ,F AND EXPR
C     ARE TO BE EVALUATED.
C  AREA = VALUE OF THE INTEGRAL OVER THE X-SPACE.
C  PRO = PRODUCT OF AREA WITH THE NECESSARY COEFFICIENTS.
C  RE = REYNOLDS NUMBER BASED ON THE DISPLACEMENT THICKNESS.
C  CPI = COLES PRESSURE GRADIENT PARAMETER.
C  RK = VON KARMANS CONSTANT.
C  N = NUMBER OF POINTS TAKEN PER DECADE IN THE YR-SPACE.
C  NR = NUMBER OF POINTS TAKEN IN THE R1, R3-SPACE.
C  ND = NUMBER OF DECADES TO BE CONSIDERED IN THE R-SPACE.
C  II = NUMBER OF Y2 VALUES TO BE READ IN FOR A SET REYNOLDS NUMBER.
C
    1 FORMAT (E9.2,2F5.2,4I4)
    2 FORMAT (1H1,/////25X,82H DETERMINATION OF THE CONTRIBUTION TO THE
     1MEAN SQUARE WALL PRESSURE IN EQUILIBRIUM,/26X,80H TURBULENT BOUNDA
     2RY LAYER FLOW TAKING INTO ACCOUNT ONLY THE EFFECTS OF THE SMALL,/3
     35X,62H SCALE CORRELATIONS WHICH SATISFY THE RECIPROCAL RELATIONSHI
     4P.,//41X,12H REDELTA* = ,E8.2,2X,5H K = ,F4.2,2X,12H COLES PI = ,
```

```
     5F4.2,//4X,2H Y,7X,13H ZERO TO E-05,4X,13H E-05 TO E-04,4X,13H E-04
     6 TO E-03,4X,13H E-03 TO E-02,4X,13H E-02 TO E-01,4X,13H E-01 TO E-
     700,4X,18H MEAN OF INTEGRAND,/)
   3 FORMAT (F9.6)
   4 FORMAT (2X,F7.5,6(5X,E12.5),8X,E12.5)
     DIMENSION X(1001),F(1001),F1(1001),F2(1001),EXPR(1001),PRMS(1001),
     1DECADE(6)
     COMMON PI,RE,RK,CPI,YSTRLMT
C
 100 READ 1,RE,RK,CPI,N,NR,ND,II
     IF (RE.GT.0.0)110,240
 110 PRINT 2,RE,RK,CPI
     N1=N-2
     N2=(N-1)/10+1
     NR1=NR-2
     ANR=NR-1
     PI=3.1415926536
     E=PI*3.60/(0.837*RE)
     STEP=0.5
     RLIMIT=50.0
     CI=3.0
     T=1.0
1200 CIA=CI
     TA=T
     CI=CI+STEP
     IF (CI.GT.RLIMIT)1121,1122
1121 PRINT 1123
1123 FORMAT (10X,22H CI* GREATER THAN 50.0)
     GO TO 240
1122 CY=CI/4.0
     T=(1.0+CY+0.5*CY*CY+CY**6/1300.0)*EXP(-CY)-(1.0/(RK*CI)+E*CPI*
    1SIN(E*CI)/RK)
1300 IF (T*TA)1400,2000,1200
1400 CIB=CIA
     CIA=CI
     TA=T
```

```
      CI=(CIA+CIB)/2.0
 1500 CY=CI/4.0
      T=(1.0+CY+0.5*CY*CY+CY**6/1300.0)*EXP(-CY)-(1.0/(RK*CI)+E*CPI*
     1SIN(E*CI)/RK)
      IF (T*TA)1600,2000,1700
 1600 CIB=CIA
 1700 CIA=CI
      TA=T
      CI=(CIA+CIB)/2.0
      IF (ABS(CI-CIA).LT.0.001)2000,1500
 2000 YSTRLMT=CI
      DO 230 L=1,II
      READ 3,Y2
      DO 119 I=1,6
  119 DECADE(I)=0.0
      DO 210 I=1,ND
      D=10.0**(I-ND)
      DO 190 J=1,N
      AAN=N-1
      YRJ=J-1
      YR=YRJ*D/AAN
      R2=YR-Y2
      IF (Y2+R2/2.0.LT.0.2)120,130
  120 SCALE=0.570*(Y2+R2/2.0)
      GO TO 140
  130 SCALE=0.114
  140 Y=Y2/SCALE
      R=R2/SCALE
      AR=ABS(R)
      A=2.0*Y+R
      DO 170 K=1,NR
      AK=K-1
      X(K)=AK/ANR
      F(K)=X(K)*X(K)*(1.0-2.0*AR+A*A)-2.0*X(K)*(1.0-AR)+1.0
      F(K)=F(K)**1.5
      F1(K)=X(K)*X(K)*(4.0*AR-3.0)+2.0*X(K)*(2.0-AR)-1.0
```

```
      IF (K.EQ.1)150,160
  150 F2(K)=0.0
      EXPR(K)=0.0
      GO TO 170
  160 F2(K)=EXP(-(1.0/X(K)-1.0))/X(K)
      EXPR(K)=F1(K)*F2(K)/F(K)
  170 CONTINUE
      SUM=0.0
      DO 180 K=1,NR1,2
  180 SUM=SUM+EXPR(K)+4.0*EXPR(K+1)+EXPR(K+2)
      AREA=SUM/(3.0*ANR)
      PRO=AREA*A*EXP(-AR)
  190 PRMS(J)=PRO*RMS(YR)*U2Y(YR)
      SUM=0.0
      IF (I.EQ.1)200,202
  200 DO 201 J=1,N1,2
  201 SUM=SUM+PRMS(J)+4.0*PRMS(J+1)+PRMS(J+2)
      GO TO 210
  202 DO 203 J=N2,N1,2
  203 SUM=SUM+PRMS(J)+4.0*PRMS(J+1)+PRMS(J+2)
  210 DECADE(I)=SUM*D/(3.0*AAN)
      SUM=0.0
      DO 220 I=1,ND
  220 SUM=SUM+DECADE(I)
      ANS=SUM*RMS(Y2)*U2Y(Y2)
  230 PRINT 4,Y2,DECADE,ANS
      GO TO 100
  240 STOP
      END
```

```
C     THE SUBROUTINE FUNCTIONS  REQUIRED FOR COMPLETENESS OF THE COMPUTER
C     PROGRAMME FOR SET 4 CALCULATIONS ARE THE SAME AS THOSE GIVEN IN APPENDIX
C     A-I AND ARE NOT LISTED HERE.
```

A-V Evaluation of the Large Eddy Contribution to the Mean Square Wall Pressure Fluctuation

PROGRAM KBL085

The programme for the evaluation of the large eddy contribution to the mean square wall pressure fluctuation uses the same main programme as that listed in Appendix A-I. The difference between the two programmes lies in the form of the correlation coefficient. The listing below gives the required correlation coefficient for PROGRAM 085.

```
      FUNCTION R22E (YR22,R1R22,R2R22,R3R22)
C     CORRELATION FUNCTION FOR THE INFLUENCE OF THE LARGE SCALE EFFECTS ONLY.
C     VARIABLE ASSIGNMENTS.....
C     YR22,R1R22,R2R22,R3R22 ARE DISTANCES IN THE Y,R1,R2,R3 DIRECTIONS
C       RESPECTIVELY.
C     RSCALE IS THE SCALE FACTOR FOR THE VARIATION OF THE CORRELATION
C       COEFFICIENT DUE TO THE LARGE EDDIES.
      IF (YR22.EQ.0.0)10,20
   10 R22E=0.0
      GO TO 80
   20 IF (YR22.LT.0.2)30,40
   30 RSCALE=0.570*YR22
      GO TO 50
   40 RSCALE=0.114
   50 IF (R1R22.EQ.0.0.AND.R3R22.EQ.0.0)60,70
   60 R22E=0.085*EXP(-7.4562*R2R22*R2R22)
      GO TO 80
   70 R1R22S=R1R22*R1R22
      R2R22S=R2R22*R2R22
      R3R22S=R3R22*R3R22
      SQR123=SQRT(R1R22S+R2R22S+R3R22S)
      R22E=0.085*(1.0-14.91*R1R22S)*(1.0-264.1*R3R22S+5814.7*R3R22S*
     1R3R22S)*EXP(-(29.824*(R1R22S+R2R22S)+264.12*R3R22S)/4.0)
   80 RETURN
      END
```

A-VI Computer Programme for the Selection of Region Size Required for Use in the Evaluation of Equation (3.2.1)

PROGRAM KBL084

The programme provides for a detailed print-out of the value of the integrand of Equation (A.I.2). This integrand has an oscillatory nature and its absolute value diminishes as the value of r_1, r_2 and r_3 increases. The print-out allows the inspection of the integrand values and the size of the region over which the integration is to be made, that is the values of c_1, c_2, and c_3 are chosen on the basis of the error encountered due to the neglect of the outer regions. It has been found that region sizes chosen such that the value of the integrand at the edge of the region is 10^{-5} of that of the maximum value will give an accuracy of about 0.1% for the subdivisions used in PROGRAM KBL052 without incurring excessive computational times.

The listing of the computer programme for the detailed print-out of the integrand values is given below, where the listing of the subroutinefunctions have been omitted as these functions have already been given in the listing of PROGRAM KBL052

```
      PROGRAM KBL084 (INPUT,OUTPUT)
C    FOR THE GENERATION OF THE INTEGRAND VALUES TO ALLOW THE SELECTION
C      OF THE REGION SIZE REQUIRED TO OBTAIN A SUFFICIENTLY ACCURATE VALUE
C      OF THE MEAN USING 085 WHERE THE CORRELATION FUNCTION IS GIVEN FOR
C      THE EFFECTS OF THE LARGE SCALE TURBULENCE ONLY.
C    NOTE THAT THE CORRELATION FUNCTION IS NORMALISED BY THE PRODUCT OF
C      THE RMS VALUES OF THE TURBULENCE INTENSITIES AT THE TWO POINTS.
      DIMENSION W(51)
      COMMON YSTRLMT,RE,RK,CPI,PI
    5 FORMAT (4F7.2,E9.2,2F5.2,4I4)
   10 FORMAT (F9.6)
   15 FORMAT (////////////32X,5H C = ,F6.4,2X,8H FTRA = ,F6.2,2X,
     18H FTRB = ,F6.2,2X,8H FTRC = ,F6.2,/37X,12H REDELTA* = ,E8.2,
     22X,5H K = ,F4.2,2X,12H COLES PI = ,F4.2,/)
   20 FORMAT (//37X,6H R2 = ,E8.2,4X,6H R3 = ,E8.2,4X,5H Y = ,E8.2,/)
   25 FORMAT (1X,11E12.3)
   30 FORMAT (//37X,6H R1 = ,E8.2,4X,6H R3 = ,E8.2,4X,5H Y = ,E8.2,/)
   35 FORMAT (//37X,6H R1 = ,E8.2,4X,6H R2 = ,E8.2,4X,5H Y = ,E8.2,/)
      PI=3.1415926536
  100 READ 5,C,FTRA,FTRB,FTRC,RE,RK,CPI,NAN,NBN,NCN,NII
      IF (C.GT.0)110,160
  110 E=PI*3.60/(0.837*RE)
      STEP=0.5
      RLIMIT=50.0
      CI=0.0
      T=1.0
 1200 CIA=CI
      TA=T
      CI=CI+STEP
      IF (CI.GT.RLIMIT)1121,1122
 1121 PRINT 1123
 1123 FORMAT (10X,22H CI* GREATER THAN 50.0)
      GO TO 160
 1122 CY=CI/4.0
      CZ=RK*CI
      T=(1.0+CY+0.5*CY*CY+CY**6/1300.0)*EXP(-CY)-(1.0/(RK*CI)+E*CPI*
```

```
     1SIN(E*CI)/RK)
1300 IF (T*TA)1400,2000,1200
1400 CIB=CIA
     CIA=CI
     TA=T
     CI=(CIA+CIB)/2.0
1500 CY=CI/4.0
     CZ=RK*CI
     T=(1.0+CY+0.5*CY*CY+CY**6/1300.0)*EXP(-CY)-(1.0/(RK*CI)+E*CPI*
    1SIN(E*CI)/RK)
     IF (T*TA)1600,2000,1700
1600 CIB=CIA
1700 CIA=CI
     TA=T
     CI=(CIA+CIB)/2.0
     IF (ABS(CI-CIA).LT.0.001)2000,1500
2000 YSTRLMT=CI
     ANA=NAN-1
     ANB=NBN-1
     ANC=NCN-1
     DO 150 II=1,NII
     READ 10,Y
     Z2=U2Y(C*Y,RE)
     Z3=RMS(C*Y)
     C1=FTRA*C*Y
     X2=FTRB*C*Y
     C2=X2-C*Y
     C3=FTRC*C*Y
     PRINT 15,C,FTRA,FTRB,FTRC,RE,RK,CPI
     R2=0.02
     R3=0.0
     DO 120 I=1,NAN
     AR1=I-1
     R1=AR1/ANA
     Z1=R22E(C*Y,C1*R1,(C2+C*Y)*R2-C*Y,C3*R3)
     Z4=U2Y((C2+C*Y)*R2,RE)
```

```
      Z5=RMS((C2+C*Y)*R2)
      Z6=GM(C,C1,C2,C3,Y,R1,R2,R3)
  120 W(I)=Z1*Z2*Z3*Z4*Z5*Z6
      PRINT 20,R2,R3,Y
      PRINT 25,W
      R1=0.0
      DO 130 I=1,NBN
      AR2=I-1
      R2=AR2/ANB
      Z1=R22E(C*Y,C1*R1,(C2+C*Y)*R2-C*Y,C3*R3)
      Z4=U2Y((C2+C*Y)*R2,RE)
      Z5=RMS((C2+C*Y)*R2)
      Z6=GM(C,C1,C2,C3,Y,R1,R2,R3)
  130 W(I)=Z1*Z2*Z3*Z4*Z5*Z6
      PRINT 30,R1,R3,Y
      PRINT 25,W
      R2=0.02
      DO 140 I=1,NCN
      AR3=I-1
      R3=AR3/ANC
      Z1=R22E(C*Y,C1*R1,(C2+C*Y)*R2-C*Y,C3*R3)
      Z4=U2Y((C2+C*Y)*R2,RE)
      Z5=RMS((C2+C*Y)*R2)
      Z6=GM(C,C1,C2,C3,Y,R1,R2,R3)
  140 W(I)=Z1*Z2*Z3*Z4*Z5*Z6
      PRINT 35,R1,R2,Y
      PRINT 25,W
  150 CONTINUE
      GO TO 100
  160 STOP
      END


C     THE SUBROUTINE FUNCTIONS  REQUIRED FOR COMPLETENESS OF THE COMPUTER
C     PROGRAMME FOR SET 4 CALCULATIONS ARE THE SAME AS THOSE GIVEN IN APPENDIX
C     A-I AND ARE NOT LISTED HERE.
```

A-VII Evaluation of Equation (2.6.16) for G^s_{13}

PROGRAM KBL090

The computer programme for the determination of I^s_{13} using Equation (B3) was extended to give the values of G^s_{13} as defined in Equation (2.6.16). The resultant programme is listed below without the function subroutines for the mean shear and the turbulence intensity which are required for completeness of the programme as these are the same as those listed in Appendix A-I.

```
      PROGRAM KBL090 (INPUT,OUTPUT)
C  FOR THE DETERMINATION OF G13 DUE TO THE SMALL EDDIES.
C  VARIABLE ASSIGNMENTS.....
C  Y=Y2/SCALE=(Y2/DELTA)*(DELTA/SCALE).
C  Z=Z2/SCALE
C  R=R2/SCALE.
C  SCALE=0.570*(Y2+R2/2.0) FOR Y2+R2/2.0 LESS THAN 0.20, OTHERWISE USE
C     SCALE=0.114.
C  A=2*Y+R.
C  AR=ABSOLUTE VALUE OF R.
C  N DESIGNATES THE TOTAL NUMBER OF Z VALUES TO BE READ IN.
C  X(J) = ABSCISSAE VALUES OVER WHICH THE VALUES OF F, F1 ,F AND EXPR
C     ARE TO BE EVALUATED.
C  AREA = VALUE OF THE INTEGRAL OVER THE X-SPACE.
C  PRO = PRODUCT OF AREA WITH THE NECESSARY COEFFICIENTS.
      DIMENSION X(51),F(51),F1(51),F2(51),EXPR(51)
    1 FORMAT (2E11.4,I3)
    2 FORMAT (1H1,//////////////////////////,57X,11H YSTRLMT = ,E11.4)
    3 FORMAT (1H1,//29X,6H Y2 = ,E11.4,5X,6H RE = ,E11.4,5X,6H RK = ,
     1F8.4,5X,7H CPI = ,F8.4,
     2///48X,3H Z2,15X,22H VALUE OF G13 FUNCTION,/)
    4 FORMAT (44X,F9.5,19X,E11.4)
  100 READ 1,Y2,RE,N
      IF (Y2.GT.0.0)110,170
  110 PI=3.1415926536
      RK=0.41
      CPI=0.55
      E=PI*3.60/(0.837*RE)
      STEP=0.5
      RLIMIT=50.0
      CI=3.0
      T=1.0
 1200 CIA=CI
      TA=T
      CI=CI+STEP
      IF (CI.GT.RLIMIT)1121,1122
```

```
1121 PRINT 1123
1123 FORMAT (10X,22H CI* GREATER THAN 50.0)
     GO TO 170
1122 CY=CI/4.0
     CZ=RK*CI
     T=(1.0+CY+0.5*CY**2.0+CY**6.0/1300.0)*EXP(-CY)
    1-(1.0/(RK*CI)+E*CPI*SIN(E*CI)/RK)
1300 IF (T*TA)1400,2000,1200
1400 CIB=CIA
     CIA=CI
     TA=T
     CI=(CIA+CIB)/2.0
1500 CY=CI/4.0
     CZ=RK*CI
     T=(1.0+CY+0.5*CY**2.0+CY**6.0/1300.0)*EXP(-CY)
    1-(1.0/(RK*CI)+E*CPI*SIN(E*CI)/RK)
     IF (T*TA)1600,2000,1700
1600 CIB=CIA
1700 CIA=CI
     TA=T
     CI=(CIA+CIB)/2.0
     IF (ABS(CI-CIA).LT.0.001)2000,1500
2000 YSTRLMT=CI
     PRINT 2,YSTRLMT
     PRINT 3,Y2,RE,RK,CPI
     DO 160 I=1,N
     READ 1,Z2
     R2=Z2-Y2
     IF (Y2+R2/2.0.LT.0.2)111,112
 111 SCALE=0.570*(Y2+R2/2.0)
     GO TO 113
 112 SCALE=0.114
 113 Y=Y2/SCALE
     Z=Z2/SCALE
     R=R2/SCALE
     AR=ABS(R)
```

```
      A=2.0*Y+R
      DO 140 J=1,51
      AJ=J-1
      X(J)=AJ/50.0
      F(J)=X(J)*X(J)*(1.0-2.0*AR+A*A)-2.0*X(J)*(1.0-AR)+1.0
      F(J)=F(J)**1.5
      F1(J)=X(J)*X(J)*(4.0*AR-3.0)+2.0*X(J)*(2.0-AR)-1.0
      IF (J.EQ.1)120,130
  120 F2(J)=0.0
      EXPR(J)=0.0
      GO TO 140
  130 F2(J)=EXP(-(1.0/X(J)-1.0))/X(J)
  140 EXPR(J)=F1(J)*F2(J)/F(J)
      SUM=0.0
      DO 150 K=1,49,2
  150 SUM=SUM+EXPR(K)+4.0*EXPR(K+1)+EXPR(K+2)
      AREA=SUM/150.0
      PRO=AREA*A*EXP(-AR)
      G13=RMS(Y2,RE,RK,CPI,YSTRLMT,PI)*RMS(Z2,RE,RK,CPI,YSTRLMT,PI)
     1*U2Y(Y2,RE)*U2Y(Z2,RE)*PRO*2.0
  160 PRINT 4,Z2,G13
      GO TO 100
  170 STOP
      END


C     THE SUBROUTINE FUNCTIONS  REQUIRED FOR COMPLETENESS OF THE COMPUTER
C     PROGRAMME FOR SET 4 CALCULATIONS ARE THE SAME AS THOSE GIVEN IN APPENDIX
C     A-I AND ARE NOT LISTED HERE.
```

A-VIII Computer Programme for the Selection of Region Size required for use in the Evaluation of Equation (3.2.1). PROGRAM KBL095

In the calculation of the auto-covariance of the wall pressure fluctuation, the computer programme written for the determination of I which is defined by Equation (A.I.1) differs from that for the mean square value of the fluctuating wall pressures, the listing of which has been given in Appendix A-I. The difference arises due to the fact that, in general, I_{13} and F_{13} are no longer even functions of r_1 although both are still even functions of r_3. This condition comes about because the correlation term R_{22} is no longer an auto-correlation function but a covariance having space-time dependencies. In Section (3.1) it has been shown that if the pattern of the eddies can be regarded to be frozen it is possible to make use of the available data on the correlation coefficient obtained for zero time delay to provide the necessary covariance for the calculation of the auto-covariance of the wall pressure fluctuation. On this basis we then write Equation (A.I.1) as

$$I = \frac{4\rho^2\delta^2 U_\tau^4}{\pi}\int_{-\infty}^{0} dr_1 \int_{-y_2}^{\infty} dr_2 \int_{0}^{\infty} dr_3 \; T(y_2, r_1 - U_c\tau, r_2, r_3)$$

$$+ \frac{4\rho^2\delta^2 U_\tau^4}{\pi}\int_{0}^{\infty} dr_1 \int_{-y_2}^{\infty} dr_2 \int_{0}^{\infty} dr_3 \; T(y_2, r_1 - U_c\tau, r_2, r_3) \quad \ldots (A.VIII.1)$$

where

$$T(y_2, r_1 - U_c\tau, r_2, r_3) = M(y_2)M(r_2)u_2'(y_2)u_2'(r_2)R_{22}(y_2, r_1 - U_c\tau, r_2, r_3)\ldots$$
$$\ldots\ g_{13}(y_2, r_1, r_2, r_3)$$

and $M(y_2)$, $u_2'(y_2)$, R_{22} and g_{13} are as defined in Section 3.1.

The computer programme written to calculate and give detailed print-out of the values of T is listed below.

```
      PROGRAM KBL095 (IMPUT,OUTPUT)
C   AUTOCORRELATION OF PRESSURE FLUCTUATIONS.
C   FOR THE GENERATION OF THE INTEGRAND VALUES TO ALLOW THE SELECTION OF
C       THE REGION SIZE REQUIRED TO OBTAIN A SUFFICIENTLY ACCURATE VALUE
C       OF THE MEAN USING 096 WHERE THE CORRELATION FUNCTION IS GIVEN FOR
C       THE COMBINED EFFECTS OF THE SMALL AND LARGE SCALE EDDIES WITH TIME
C       AS WELL AS SPACE DEPENDENCIES.
C   THE CORRELATION FUNCTION IS BASED ON THE FROZEN PATTERN OF THE EDDIES
C       AND USES THE FORM SUGGESTED BY LILLEY AND HODGSON.
C   THE SCALE FUNCTION WILL PERMIT IT TO SATISFY THE CONDITION THAT
C       R22(Y,R1,R2,R3,TAU) = R22(Y+R2,R1,-R2,R3,TAU)
C   TAU IS THE TIME DELAY NON-DIMENSIONALISED BY THE FREE STREAM VELOCITY
C       AND THE BOUNDARY LAYER THICKNESS.
C   NOTE THAT THE CORRELATION FUNCTION IS NORMALISED BY THE PRODUCT OF
C       THE RMS VALUES OF THE TURBULENCE INTENSITIES AT THE TWO POINTS.
C   MEAN SHEAR IN THE EQUILIBRIUM TYPE TURBULENT BOUNDARY LAYER PER M.K.B.
C   THE RMS VALUE OF THE TURBULENCE INTENSITY COMPONENT IN THE DIRECTION
C       PERPENDICULAR TO THE WALL IS PER M.K.B. FITTED CURVE TO LAUFER AND
C       KLEBANOFF DATA.
      DIMENSION W(51)
      COMMON YSTRLMT,RE,RK,CPI,PI,ALPHA,ANN,DELRA,URATIO,UO
    5 FORMAT (4F7.2,E9.2,2F5.2,F6.3,2F5.2,F6.3,E9.2,/4I4)
   10 FORMAT (F7.4)
   15 FORMAT (1H1,////////////////38X,51H REYNOLDS NUMBER BASED ON DISPL
     1ACEMENT THICKNESS = ,E10.3,////34X,25H VON KARMAN CONSTANT K = ,F3
     2.2,15X,22H COLES PARAMETER PI = ,F3.2,////40X,52H RATIO OF COLES D
     3ELTA TO BOUNDARY LAYER THICKNESS = ,F4.3,////32X,68H POWER LAW IND
     4EX FOR WAKE FUNCTION IN THE OUTER PART OF THE LAYER = ,F4.2,////3X
     5,126H RATIO OF DISPLACEMENT THICKNESS AND FREE STREAM VELOCITY PRO
     6DUCT TO BOUNDARY LAYER THICKNESS AND FRICTION VELOCITY PRODUCT = ,
     7F4.2,////24X,85H RATIO OF (FREE STREAM VELOCITY - COLES FREE STREA
     8M VELOCITY) TO FRICTION VELOCITY = ,F4.3,////39X,54H RATIO OF FREE
     9 STREAM VELOCITY TO FRICTION VELOCITY = ,F4.1,////16X,95H TIME DEL
     1AY NON-DIMENSIONALISED BY THE FREE STREAM VELOCITY AND THE BOUNDAR
     2Y LAYER THICKNESS = ,E9.2,/1H1)
   20 FORMAT (//32X,5H C = ,F6.4,2X,8H FTRA = ,F6.2,2X,8H FTRB = ,F6.2,2
```

```
     1X,8H FTRC = ,F6.2)
  25 FORMAT (//37X,6H R2 = ,E8.2,4X,6H R3 = ,E8.2,4X,5H Y = ,E8.2,/)
  30 FORMAT (1X,11E12.3)
  31 FORMAT (1H1)
  35 FORMAT (//37X,6H R1 = ,E8.2,4X,6H R3 = ,E8.2,4X,5H Y = ,E8.2,/)
  40 FORMAT (//37X,6H R1 = ,E8.2,4X,6H R2 = ,E8.2,4X,5H Y = ,E8.2,/)
     PI=3.1415926536
 100 READ 5,C,FTRA,FTRB,FTRC,RE,RK,CPI,ALPHA,ANN,DELRA,URATIO,TAU,NAN,
    1NBN,NCN,NII
     IF (C.GT.0)110,160
 110 E=PI*DELRA/(ALPHA*RE)
     STEP=0.5
     RLIMIT=50.0
     CI=3.0
     T=1.0
1200 CIA=CI
     TA=T
     CI=CI+STEP
     IF (CI.GT.RLIMIT)1121,1122
1121 PRINT 1123
1123 FORMAT (10X,22H CI* GREATER THAN 50.0)
     GO TO 160
1122 CY=CI/4.0
     T=(1.0+CY+0.5*CY*CY+CY**6/1300.0)*EXP(-CY)-(1.0/(RK*CI)+E*CPI*
    1SIN(E*CI)/RK)
1300 IF (T*TA)1400,2000,1200
1400 CIB=CIA
     CIA=CI
     TA=T
     CI=(CIA+CIB)/2.0
1500 CY=CI/4.0
     T=(1.0+CY+0.5*CY*CY+CY**6/1300.0)*EXP(-CY)-(1.0/(RK*CI)+E*CPI*
    1SIN(E*CI)/RK)
     IF (T*TA)1600,2000,1700
1600 CIB=CIA
1700 CIA=CI
```

```
      TA=T
      CI=(CIA+CIB)/2.0
      IF (ABS(CI-CIA).LT.0.001)2000,1500
 2000 YSTRLMT=CI
      UO=USTAR(1.0)
      PRINT 15,RE,RK,CPI,ALPHA,ANN,DELRA,URATIO,UO,TAU
      ANA=NAN-1
      ANB=NBN-1
      ANC=NCN-1
      DO 150 II=1,NII
      READ 10,Y
      Z2=U2Y(C*Y)
      Z3=RMS(C*Y)
      C1=FTRA*C*Y
      X2=FTRB*C*Y
      C2=X2-C*Y
      C3=FTRC*C*Y
      YSTAR=C*Y*RE/DELRA
      PRINT 20,C,FTRA,FTRB,FTRC
      R2=0.02
      R3=0.0
      SDIST=(C2+C*Y)*R2/2.0
      XTAU=TAU*USTAR(SDIST)/UO
      DO 120 I=1,NAN
      AR1=I-1
      R1=AR1/ANA
      Z1=R22F(C*Y,C1*R1+XTAU,(C2+C*Y)*R2-C*Y,C3*R3,TAU)
      Z4=U2Y((C2+C*Y)*R2)
      Z5=RMS((C2+C*Y)*R2)
      Z6=GM(C,C1,C2,C3,Y,R1,R2,R3)
  120 W(I)=Z1*Z2*Z3*Z4*Z5*Z6
      PRINT 25,R2,R3,Y
      PRINT 30,W
      R1=0.0
      DO 130 I=1,NBN
      AR2=I-1
```

```
      R2=AR2/ANB
      SDIST=(C2+C*Y)*R2/2.0
      XTAU=TAU*USTAR(SDIST)/UO
      Z1=R22F(C*Y,C1*R1+XTAU,(C2+C*Y)*R2-C*Y,C3*R3,TAU)
      Z4=U2Y((C2+C*Y)*R2)
      Z5=RMS((C2+C*Y)*R2)
      Z6=GM(C,C1,C2,C3,Y,R1,R2,R3)
  130 W(I)=Z1*Z2*Z3*Z4*Z5*Z6
      PRINT 35,R1,R3,Y
      PRINT 30,W
      R2=0.02
      SDIST=(C2+C*Y)*R2/2.0
      XTAU=TAU*USTAR(SDIST)/UO
      DO 140 I=1,NCN
      AR3=I-1
      R3=AR3/ANC
      Z1=R22F(C*Y,C1*R1+XTAU,(C2+C*Y)*R2-C*Y,C3*R3,TAU)
      Z4=U2Y((C2+C*Y)*R2)
      Z5=RMS((C2+C*Y)*R2)
      Z6=GM(C,C1,C2,C3,Y,R1,R2,R3)
  140 W(I)=Z1*Z2*Z3*Z4*Z5*Z6
      PRINT 40,R1,R2,Y
      PRINT 30,W
      IIHALF=II/2
      IF (II-IIHALF*2.EQ.0)145,150
  145 PRINT 31
  150 CONTINUE
      GO TO 100
  160 STOP
      END


      FUNCTION RMS (YMS)
      FUNCTION USTAR(YU)
C  FOR THE DETERMINATION OF THE MEAN VELOCITY IN THE BOUNDARY LAYER.
```

```
C  IT SHOULD BE NOTED THAT SOME OF THE CONSTANTS USED ARE ONLY VALID
C       FOR CONSTANT PRESSURE GRADIENT LAYERS.
      COMMON YSTRLMT,RE,RK,CPI,PI,ALPHA,ANN,DELRA,URATIO,UO
      IF (YU.GT.1.0)100,110
  100 USTAR=UO
      GO TO 180
  110 YUSTAR=YU*RE/DELRA
      YUC=1.194*YU
      IF (YU.GT.ALPHA)120,130
  120 USTAR=5.0*URATIO*(1.0-((1.0-YU)/(1.0-ALPHA))**ANN)+(ALOG(YUSTAR)*2
     1.0*CPI-ALOG(YUC))/RK
      GO TO 180
  130 IF (YU.LE.ALPHA.AND.YUC.GT.0.08)140,150
  140 USTAR=5.0+(ALOG(YUSTAR)+CPI*(1.0-COS(PI*(YUC-0.08)/0.92)))/RK
      GO TO 180
  150 IF (YUSTAR.GT.YSTRLMT.AND.YUC.LE.0.08)160,170
  160 USTAR=5.0+ALOG(YUSTAR)/RK
      GO TO 180
  170 USTAR=14.22-(14.22+2.55*YUSTAR+0.194*YUSTAR*YUSTAR+0.00577*YUSTAR*
     1*3+0.00036*YUSTAR**4+0.00018*YUSTAR**5+0.00000075*YUSTAR**6)*EXP(
     2-YUSTAR/4.0)
  180 RETURN
      END


C     FURTHER SUBROUTINE FUNCTIONS REQUIRED FOR COMPLETENESS OF THE
C     COMPUTER PROGRAMME BUT WHICH HAVE NOT BEEN LISTED HERE CAN BE FOUND IN
C     THE PROGRAMME LISTING IN APPENDIX A-I FOR THE CASE OF SET 4 CALCULATIONS.
```

A-IX Evaluation of Equation (3.2.1) for the Auto-Covariance of the Wall Pressure Fluctuations.

PROGRAM KBL097.

The method of calculation of the auto-covariance of the wall pressure fluctuations is the same as that of Method I for the calculation of the mean square value. Equation (3.2.1) can be written in the form given in Equation (A.VIII.1) to take into account the asymmetry of the I_{13} function about the (r_2,r_3)-plane brought about by the time delay. Sag's (1963) numerical routine generates mesh points in the positive quadrant only and the required negative values of r_1 are obtained by reflection about the (r_2,r_3)-plane. The listing of the computer programme for the evaluation of I defined by Equation (A.VIII.1) is given below. The values for H, S, V and U are the same as those given in Appendix A-I.

```
      PROGRAM KRL097 (INPUT,OUTPUT)
C   ADAPTATION OF T. SAGS NUMERICAL METHOD FOR THE AUTO CORRELATION OF THE WALL
C     PRESSURE IN EQUILIBRIUM TURBULENT BOUNDARY LAYER FLOW.
C  THE CORRELATION FUNCTION IS BASED ON THE FROZEN PATTERN OF THE EDDIES
C     AND USES THE FORM SUGGESTED BY LILLEY AND HODGSON.
C  THE CORRELATION FUNCTION IS GIVEN FOR THE COMBINED EFFECTS OF THE SMALL AND
C     LARGE SCALE EDDIES WITH TIME AS WELL AS SPACE DEPENDENCIES.
C  THE SCALE FUNCTION WILL PERMIT IT TO SATISFY THE CONDITION THAT
C     R22(Y,R1,R2,R3,TAU) = R22(Y+R2,R1,-R2,R3,TAU)
C  TAU IS THE TIME DELAY NON-DIMENSIONALISED BY THE FREE STREAM VELOCITY
C     AND THE BOUNDARY LAYER THICKNESS.
C  NOTE THAT THE CORRELATION FUNCTION IS NORMALISED BY THE PRODUCT OF
C     THE RMS VALUES OF THE TURBULENCE INTENSITIES AT THE TWO POINTS.
C  MEAN SHEAR IN THE EQUILIBRIUM TYPE TURBULENT BOUNDARY LAYER PER M.K.B.
C  THE RMS VALUE OF THE TURBULENCE INTENSITY COMPONENT IN THE DIRECTION
C     PERPENDICULAR TO THE WALL IS PER M.K.B. FITTED CURVE TO LAUFER AND
C     KLEBANOFF DATA.
      DIMENSION T(6),X(6),M(6),Y(100),ANS(100),D(100)
      COMMON N,U,C,C1,C2,C3,X2,Z2,Z3,YSTRLMT,RE,RK,CPI,PI,ALPHA,ANN,DELR
     1A,URATIO,UO,TAU
   10 FORMAT (E9.2,2F5.2,F6.3,2F5.2,F6.3,E9.2,2I4)
   15 FORMAT (1H1,/////////////////38X,51H REYNOLDS NUMBER BASED ON DISPL
     1ACEMENT THICKNESS = ,E10.3,////34X,25H VON KARMAN CONSTANT K = ,F3
     2.2,15X,22H COLES PARAMETER PI = ,F3.2,////40X,52H RATIO OF COLES D
     3ELTA TO BOUNDARY LAYER THICKNESS = ,F4.3,////32X,68H POWER LAW IND
     4EX FOR WAKE FUNCTION IN THE OUTER PART OF THE LAYER = ,F4.2,////3X
     5,126H RATIO OF DISPLACEMENT THICKNESS AND FREE STREAM VELOCITY PRO
     6DUCT TO BOUNDARY LAYER THICKNESS AND FRICTION VELOCITY PRODUCT = ,
     7F4.2,////24X,85H RATIO OF (FREE STREAM VELOCITY - COLES FREE STREA
     8M VELOCITY) TO FRICTION VELOCITY = ,F4.3,////39X,54H RATIO OF FREE
     9 STREAM VELOCITY TO FRICTION VELOCITY = ,F4.1,////16X,95H TIME DEL
     1AY NON-DIMENSIONALISED BY THE FREE STREAM VELOCITY AND THE BOUNDAR
     2Y LAYER THICKNESS = ,E9.2,/1H1,/////9X,2H C,7X,5H FTRA,5X,5H FTRB,
     35X,5H FTRC,6X,2H H,7X,2H S,6X,2H V,7X,2H U,7X,2H Y,4X,18H MEAN OF
     4INTEGRAND,4X,13H NO OF POINTS,/)
   20 FORMAT (F6.3,F3.0,6F6.2,E9.2)
```

```
  25 FORMAT (8X,F5.3,5X,F5.1,5X,F5.1,5X,F5.1,5X,F4.3,6X,F2.0,6X,F3.2,5X
    2,F4.2,4X,F6.5,5X,E12.5,11X,I6)
      PI=3.1415926536
 100  READ 10,RE,RK,CPI,ALPHA,ANN,DELRA,URATIO,TAU,NII,N
      IF (RE.GT.0)110,200
 110  E=PI*DELRA/(ALPHA*RE)
      STEP=0.5
      RLIMIT=50.0
      CI=3.0
      T=1.0
1200  CIA=CI
      TA=T
      CI=CI+STEP
      IF (CI.GT.RLIMIT)1121,1122
1121  PRINT 1123
1123  FORMAT (10X,22H CI* GREATER THAN 50.0)
      GO TO 200
1122  CY=CI/4.0
      CZ=RK*CI
      T=(1.0+CY+0.5*CY*CY+CY**6/1300.0)*EXP(-CY)-(1.0/(RK*CI)+E*CPI*
     1SIN(E*CI)/RK)
1300  IF (T*TA)1400,2000,1200
1400  CIB=CIA
      CIA=CI
      TA=T
      CI=(CIA+CIB)/2.0
1500  CY=CI/4.0
      CZ=RK*CI
      T=(1.0+CY+0.5*CY*CY+CY**6/1300.0)*EXP(-CY)-(1.0/(RK*CI)+E*CPI*
     1SIN(E*CI)/RK)
      IF (T*TA)1600,2000,1700
1600  CIB=CIA
1700  CIA=CI
      TA=T
      CI=(CIA+CIB)/2.0
      IF (ABS(CI-CIA).LT.0.001)2000,1500
```

```
2000 YSTRLMT=CI
     UO=USTAR(1.0)
     PRINT 15,RE,RK,CPI,ALPHA,ANN,DELRA,URATIO,UO,TAU
     DO 190 II=1,NII
     READ 20,H,S,V,U,C,FTRA,FTRB,FTRC,Y(II)
     A1=S**N
     V0=H**N
     HH=2.0*H
     VV=V*V
     HHA=0.5*H-V
     YSTAR=C*Y(II)*RE/DELRA
     Z2=U2Y(C*Y(II))
     Z3=RMS(C*Y(II))
     C1=FTRA*C*Y(II)
     X2=FTRB*C*Y(II)
     C2=X2-C*Y(II)
     C3=FTRC*C*Y(II)
     SUM=0.0
     A=0.0
     NPOINTS=0
 140 M(1)=0
     R0=0
     DO 150 I=1,N
     M(I+1)=A/S**(N-I)
     T(I)=HH*(M(I+1)-S*M(I))+HHA
 150 R0=R0+T(I)*T(I)
     IF (R0-VV)160,170,170
 160 R=SQRT(R0)
     NPOINTS=NPOINTS+1
     CALL TRNS (T,R,DET,X)
     SUM=SUM+DET*G(X,Y(II))
 170 A=A+1
     IF (A-A1)140,180,180
 180 ANS(II)=SUM*V0*4.0*C*C1*C3*X2/3.14159265
 190 PRINT 25,C,FTRA,FTRB,FTRC,H,S,V,U,Y(II),ANS(II),NPOINTS
     GO TO 100
```

```
  200 STOP
      END


      FUNCTION USTAR(YU)
C  FOR THE DETERMINATION OF THE MEAN VELOCITY IN THE BOUNDARY LAYER.
C  IT SHOULD BE NOTED THAT SOME OF THE CONSTANTS USED ARE ONLY VALID
C       FOR CONSTANT PRESSURE GRADIENT LAYERS.
      COMMON N,U,C,C1,C2,C3,X2,Z2,Z3,YSTRLMT,RE,RK,CPI,PI,ALPHA,ANN,DELR
     1A,URATIO,UO,TAU
      IF (YU.GT.1.0)100,110
  100 USTAR=UO
      GO TO 180
  110 YUSTAR=YU*RE/DELRA
      YUC=1.194*YU
      IF (YU.GT.ALPHA)120,130
  120 USTAR=5.0+URATIO*(1.0-((1.0-YU)/(1.0-ALPHA))**ANN)+(ALOG(YUSTAR)+2
     1.0*CPI-ALOG(YUC))/RK
      GO TO 180
  130 IF (YU.LE.ALPHA.AND.YUC.GT.0.08)140,150
  140 USTAR=5.0+(ALOG(YUSTAR)+CPI*(1.0-COS(PI*(YUC-0.08)/0.92)))/RK
      GO TO 180
  150 IF (YUSTAR.GT.YSTRLMT.AND.YUC.LE.0.08)160,170
  160 USTAR=5.0+ALOG(YUSTAR)/RK
      GO TO 180
  170 USTAR=14.22-(14.22+2.55*YUSTAR+0.194*YUSTAR*YUSTAR+0.00577*YUSTAR*
     1*3+0.00036*YUSTAR**4+0.000018*YUSTAR**5+0.00000075*YUSTAR**6)*EXP(
     2-YUSTAR/4.0)
  180 RETURN
      END


C     FURTHER SUBROUTINE FUNCTIONS REQUIRED FOR COMPLETENESS OF THE
C     COMPUTER PROGRAMME BUT WHICH HAVE NOT BEEN LISTED HERE CAN BE FOUND IN
C     THE PROGRAMME LISTING IN APPENDIX A-I FOR THE CASE OF SET 4 CALCULATIONS.
```

APPENDIX B REDUCTION OF I^s_{13} TO A SINGLE INTEGRAL

For the case $\vec{\xi} = \tau = 0$, I^s_{13} can be represented by $I^s_{13}(y_2, r_2)$, and then eq. (2.6.15) , with the insertion of the appropriate expression for g_{13} and transformation to polar coordinates, gives

$$I^s_{13}(y_2,r_2) = (1-a_2) \int_0^\infty dk\ k \int_0^{2\pi} d\theta\ \exp\left(-\frac{\sqrt{r_2^2+k^2}}{s}\right) \quad \ldots$$

$$\ldots \left[1 - \frac{\sqrt{r_2^2+k^2}}{2s} + \frac{r_2^2}{2s\sqrt{r^2+k^2}}\right]$$

$$\ldots \frac{1}{m(y_2+r_2+m)} \left[1 - \frac{k^2(y_2+r_2+2m)}{m^2(y_2+r_2+m)} \cos^2\right]$$

$$= 2\pi \int_0^\infty dk\ k\ \exp\left(-\frac{\sqrt{r_2^2+k^2}}{s}\right) \left[1 - \frac{\sqrt{r_2^2+k^2}}{2s} + \frac{r_2^2}{2s\sqrt{r_2^2+k^2}}\right]$$

$$\ldots \frac{1}{m(y_2+r_2+m)} \left[1 - \frac{k^2(y_2+r_2+2m)}{2m^2(y_2+r_2+m)}\right]$$

$$= 2\pi \int_0^\infty dk\ k\ \exp\left(-\frac{\sqrt{r_2^2+k^2}}{s}\right) \left[1 - \frac{\sqrt{r_2^2+k^2}}{2s} + \frac{r_2^2}{2s\sqrt{r_2^2+k^2}}\right] \ldots$$

$$\ldots \frac{1}{(a^2+k^2)^{3/2}} \qquad \ldots(B.1)$$

where $k^2 = r_1^2 + r_3^2$,

and $a = y_2 + r_2$

If we now put

$$X = \frac{\sqrt{r_2^2+k^2}}{s} \quad ,$$

$$R_2 = \frac{r_2}{s} \quad ,$$

and $A = \frac{a}{s}$, equation (B.1) becomes

$$I^s_{13}(y_2,r_2) = \pi A \int_{|R_2|}^{\infty} \frac{e^{-X}}{(X^2+A^2-R_2^2)^{3/2}} \left(X - \frac{X^2}{2} + \frac{R_2^2}{2}\right) dX \qquad \ldots(B.2)$$

which, for numerical evaluation, can be further simplified to

$$I^s_{13}(y_2,r_2) = \frac{\pi A}{2} e^{-|R_2|} \int_0^1 \frac{F_1(Z,R_2).F_2(Z)}{\left[F_3(Z,R_2,A)\right]^{3/2}} dZ, \qquad \ldots(B.3)$$

where $F_1(Z,R_2) = Z^2(4|R_2|-3) + 2Z(2-|R_2|) - 1,$

$F_2(Z) = \frac{1}{Z} \exp(1 - \frac{1}{Z})$, and

$F_3(Z,R_2,A) = Z^2(1-2|R_2| + A^2) - 2Z(1-|R_2|) + 1.$

Simpson's rule was used to obtain the value of $I^s_{13}(y_2,r_2)$ with the Z-region subdivided into 100 equal parts. This gives a

numerical accuracy of better than 0.01%. The computer programmes employed in the numerical evaluation of Equation (B.3) are given in Appendix A-II and Appendix A-III for s given by Equations (3.1.14) and (3.1.19) respectively.

APPENDIX C.

THE 3-PHASE TO DC THYRISTOR CONTROLLED POWER SUPPLY

The power necessary for the running of the wind tunnel DC motor comes from the rectification of the available 3-phase AC supply for the armature windings and the rectification of one of the phases for the field coils. Solid state devices have been selected in the construction of the power supply for reasons of

(i) compactness,

(ii) reliability and ruggedness,

(iii) availability in the required voltage/current ratings, and

(iv) relative low costs.

The basic circuit for the rectification of the 3-phase supply is given in fig. C-1 and the details of the principles involved can be found in the GE SCR Manual.

The initiation and hence the control of conduction is through the application of the required voltage at the gates of the SCR's by the use of firing circuits and a range of supply voltages from 0 to 540 volts can be made available by varying the point of conduction. Fig. C-2 shows the resultant DC due to partial as well as full conduction. In the actual layout of the power supply, the three phases from the bus-bars have been connected to a three phase Heinnemann "Control" circuit breaker and a three phase "Power" contractor - see fig. C-3. The circuit breaker has been labelled "Control" as it supplies power to the safety, as well as the firing circuits, and the contactor has the job of providing up to 100 kw

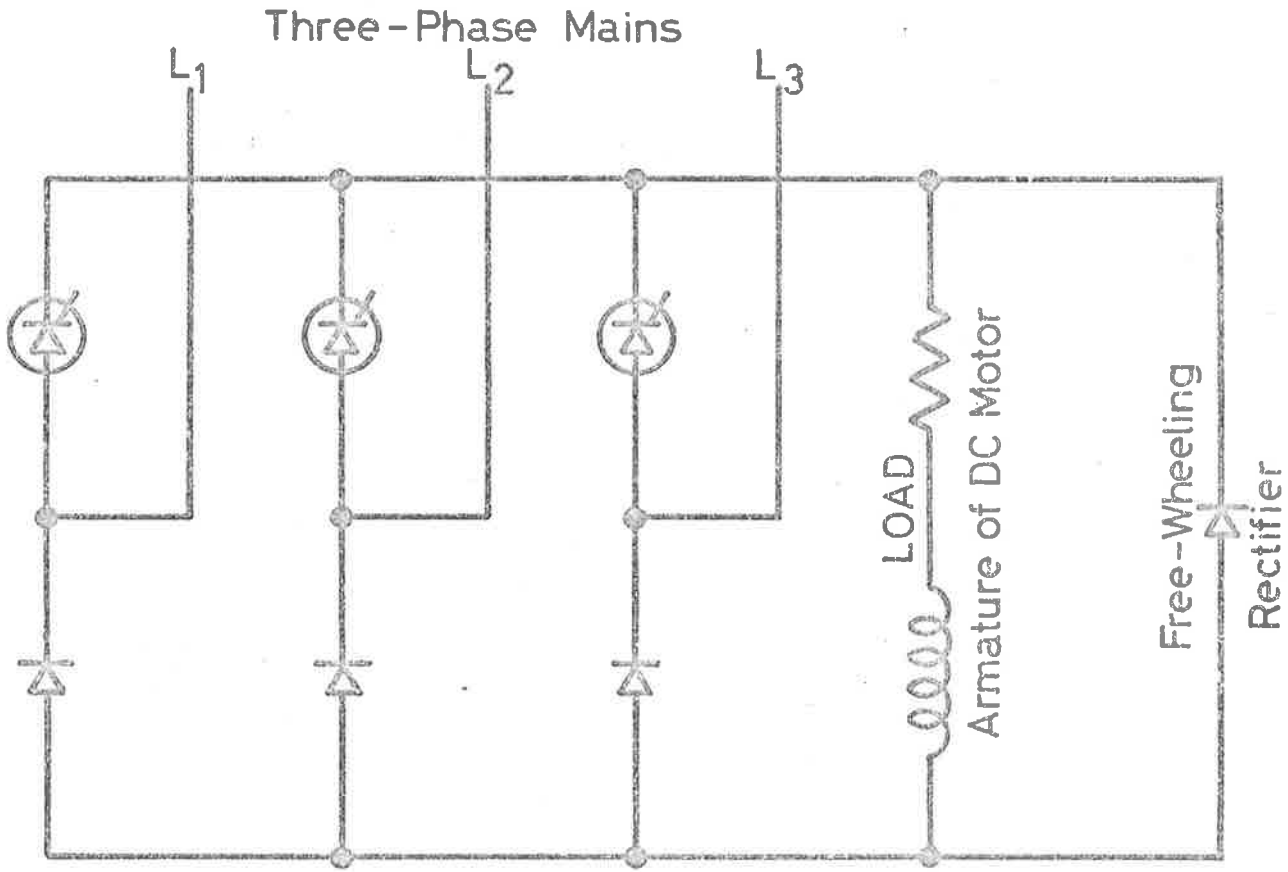

Fig. C-1. Three-Phase Full-Wave SCR Bridge.

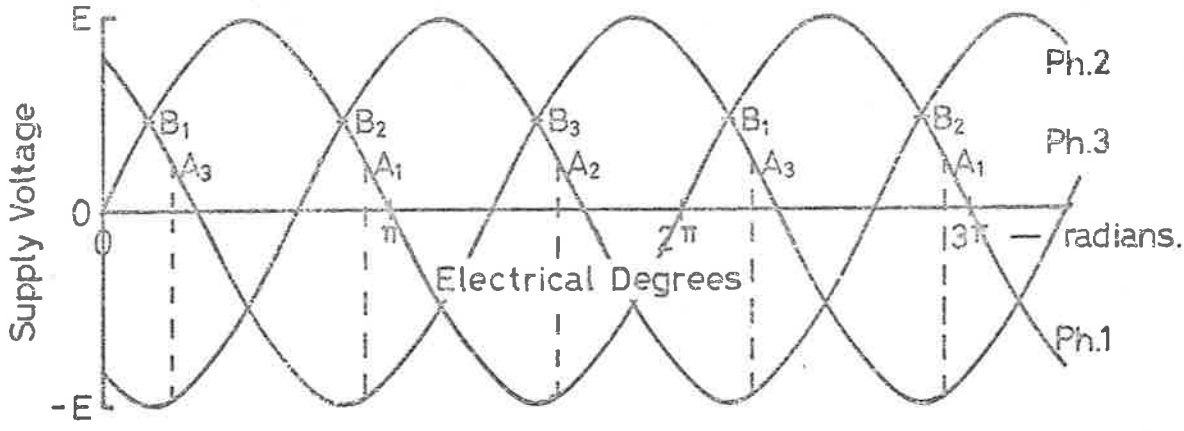

(a) Three Phase Mains to SCR Bridge.

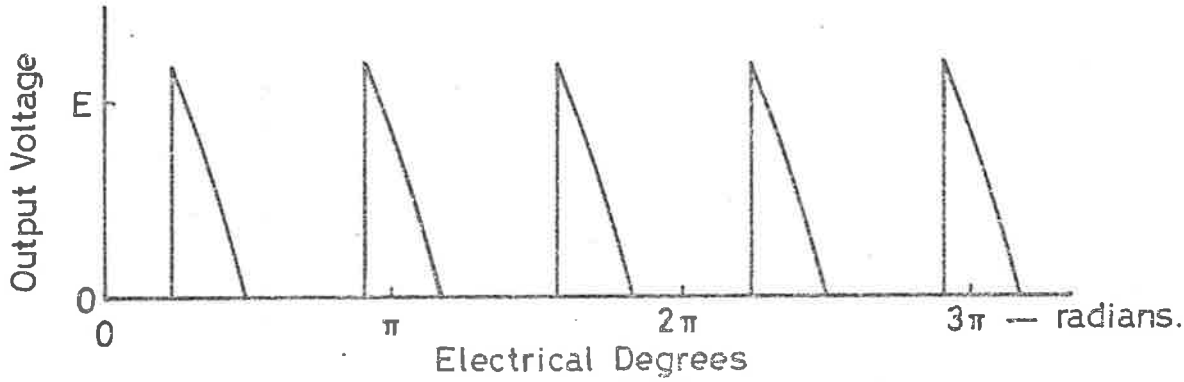

(b) Partial Conduction - SCR's Triggered at A_1, A_2 and A_3 for Phases 1, 2 and 3 respectively.

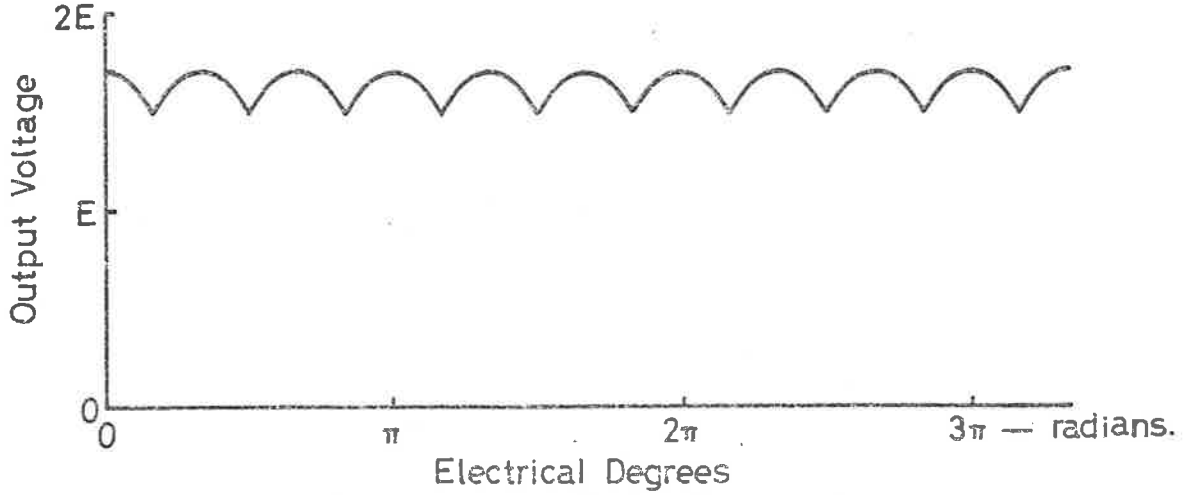

(c) Full Conduction - SCR's Triggered at B_1, B_2 and B_3 for Phases 1, 2 and 3 respectively.

Fig. C-2 Resultant DC from Thyristor Controlled Full-Wave Bridge at Partial and at Full Conduction.

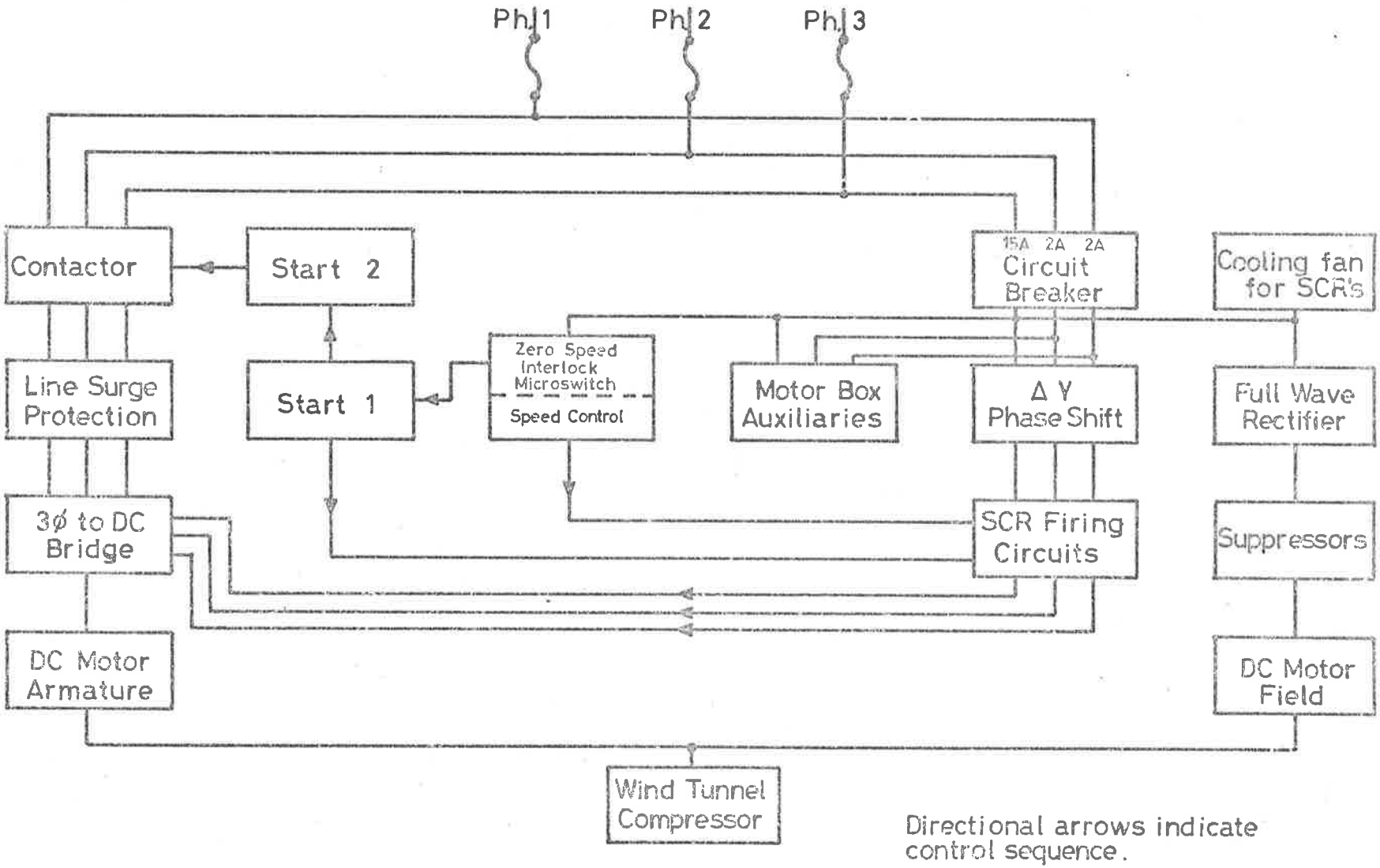

Fig. C-3. Block diagram of Wind Tunnel DC Power Supply.

to the armature windings.

A number of safety devices have been built into the power supply system. They have been incorporated to prevent

(i) the starting up of the wind-tunnel without the removal of the front cover protecting the honeycombs,

(ii) the conduction of armature current unless the field coils of the DC motor have been energised,

(iii) the three-phase SCR bridge from being energised before the influence of the firing circuit could be established, and

(iv) the three-phase bridge from initial conduction in other than the zero-volts output condition, i.e. with the speed control potentiometer on the zero position.

Fig. C-4 shows the circuit diagram used to achieve the required protection. It can be seen that only one of the three phases has been used throughout the control circuit, and this is denoted as phase Φ_1. The 15A line from the circuit breaker has been used to supply power to the pull-in coil of the three-phase contactor.

In the starting-up procedure, the control circuit breaker must first be closed. Two of the three phases, Φ_2 and Φ_3, will immediately be energised and be indicated by the lights on the front panel. To energise the controlling phase, phase Φ_1, the front cover of the wind tunnel must be removed and must also be positioned in its wall bracket where two micro-switches in series detect its presence by being closed. The "live" state of phase Φ_1 should then be indicated

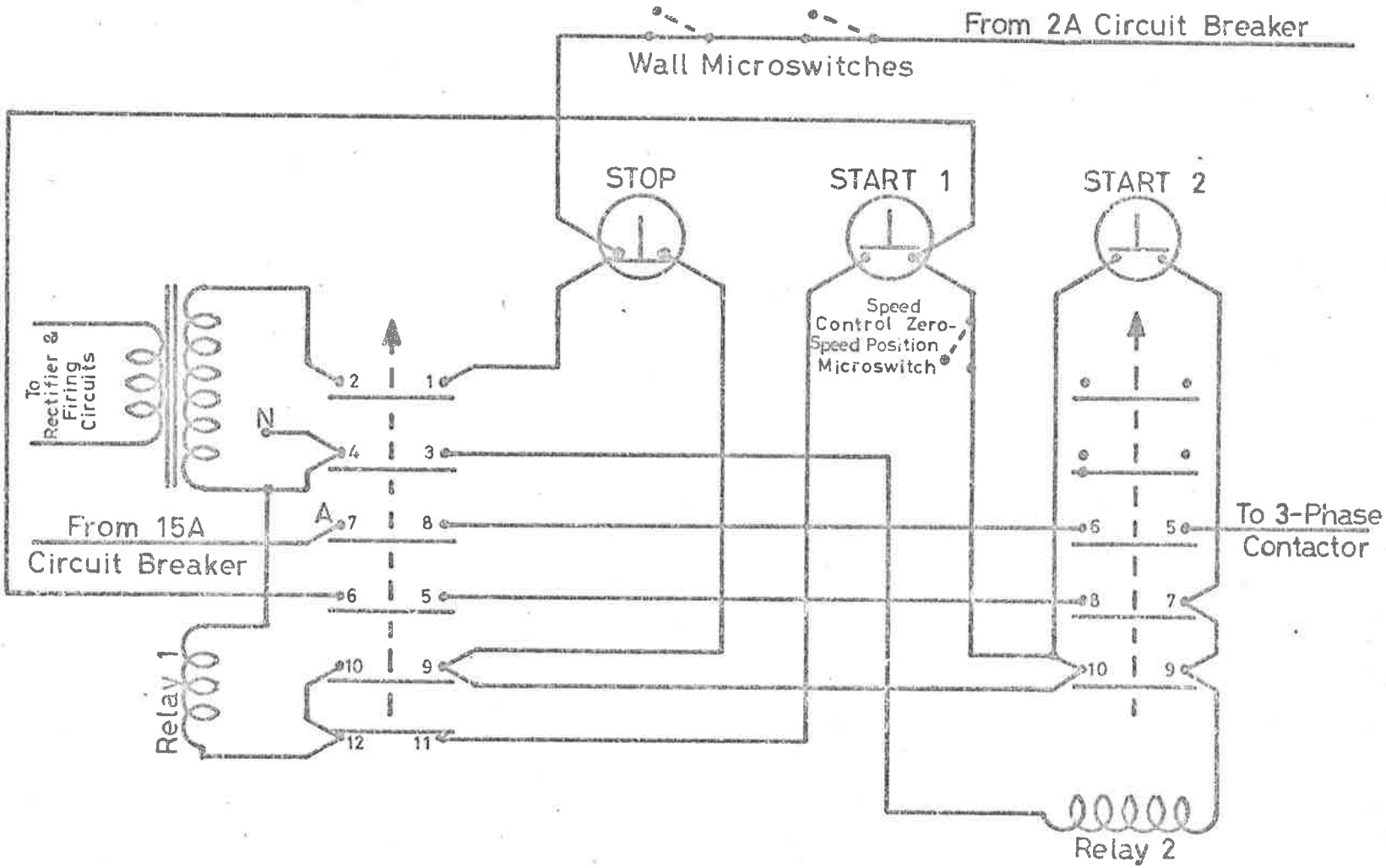

Fig. C-4. Control Protection Circuit.

by the panel light. The three phases would then be available to the auxiliaries such as the oil scavange pump, the motor box exhaust fan, the SCR cooling fan and the hour meter - the latter two being run only on phase *1. The field coils would also be energised through the DC available from the full-wave rectification of phase *1. The only other requirement for the running of the DC motor is the supply of variable DC to the armature, and this is achieved in two stages. Firstly, the firing circuit must be energised. Secondly, and only then, the three phase SCR bridge can be energised. This safeguard has been adopted to prevent full conduction from occurring at the moment of switching on, for the firing circuits have been found to issue pulses at switch-on and these pulses have been noted to be of sufficient magnitude to cause the SCR's to conduct. To this end two start buttons in conjunction with a microswitch and two relays have been employed. The speed control is a potentiometer which varies the instant at which gating or the initiation of conduction occurs in each of the SCR's with respect to each of the three supply phases. From fig. C-2, it can be seen that if gating occurs at A, B and C for each of the threes phases, no DC output will be available even though the gating should be repeated with each cycle. This must then be the zero-speed position for the speed control potentiometer, and to ensure that there should be no conduction at the initial switch on, a microswitch has been installed in the line carry power to START *1 such that it (the microswitch) can only be made with the speed control potentiometer in the zero position. Only when this condition has been achieved can the hold-

in coil of relay $^{*}1$ be energised when START $^{*}1$ is pushed in. Power should now be supplied to the firing circuit and should also be available to START $^{*}2$ and the hold-in coil of relay $^{*}2$. Pushing in START $^{*}2$ will now allow relay $^{*}2$ to provide power to the three phase contactor which will then close thus bringing in the three-phase supply to the SCR bridge. Note that it is still necessary to have the speed control potentiometer at the zero position to that the microswitch remained closed before START $^{*}2$ can be energised and relay $^{*}2$ closed. The speed control can now be rotated from the zero position to give the required conduction and hence the necessary compressor speed. In the event of the failure of the power supply to the field coils due to the failure of phase $^{*}1$, the control mechanism and circuitry which have been made to rely on this phase have been set up so that relays $^{*}1$ and $^{*}2$ fall out and all power to the three phase bridge will be automatically terminated. This precaution is taken to prevent the motor from "running-away".

A further series of protection have been incorporated at the supply end of the three phase between the bus-bars and the SCR's. These consist of series inductances, resistors, capasitors and fuses to cope with line surges.

Fig. C-5 shows the details of the protection circuit.

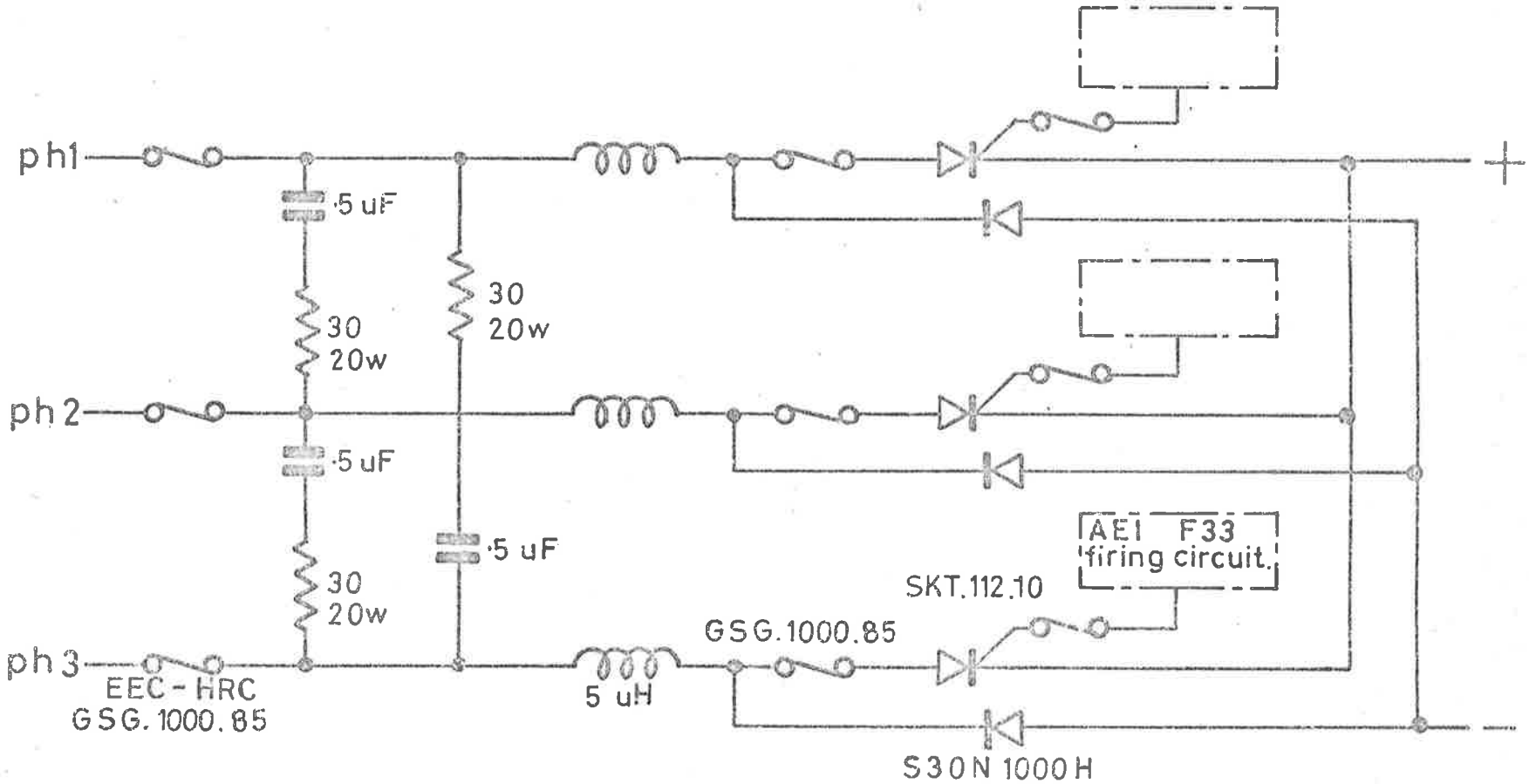

Fig C-5 SCR bridge with associated protection.

APPENDIX D SONIC CHOKE DIMENSIONS

The detailed dimensions giving the form of the nose of the centre-body and nozzle of the choke are presented in Table D.1. The profile of the nose of the centre-body has been calculated from the relationship

$$y_1 = (r_1^2 - x_1^2)^{\frac{1}{2}} - z_1 \quad ,$$

where

r_1 = 254.00mm (10.000 inch),

z_1 = 212.09mm (8.350 inch),

y_1 is the radius of the centre-body cross-section at a distance x_1 upstream from the first shoulder - see figure D.1(a). The shape of the nozzle used in the sonic choke has been generated using the relationship

$$y_2 = (r_2^2 - x_2^2)^{\frac{1}{2}} - z_2 \quad ,$$

for $0 \leqslant x_2 \leqslant 97.72\text{mm}$,

where r_2 = 489.61mm (19.276 inch),

z_2 = 423.37mm (16.668 inch)

and

$$y_2 = z_3 - \left[r_3^2 - (L - x_2)^2 \right]^{\frac{1}{2}} \quad ,$$

for $97.72\text{mm} \leqslant x_2 \leqslant 148.17\text{mm}$,

where r_3 = 252.73mm (9.9501 inch),

z_3 = 304.04mm (11.970 inch),

L = 148.17mm (5.8333 inch)

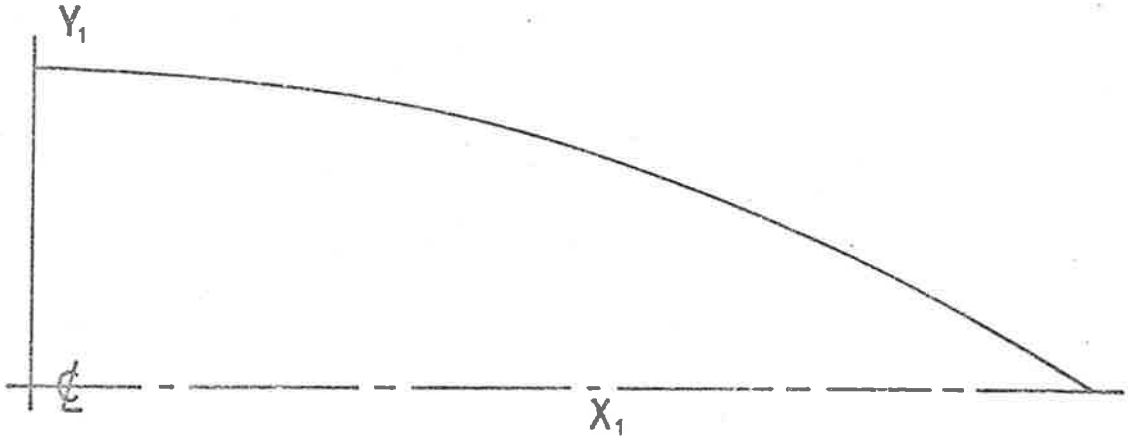

a) Form of Choke Centrebody Nose.

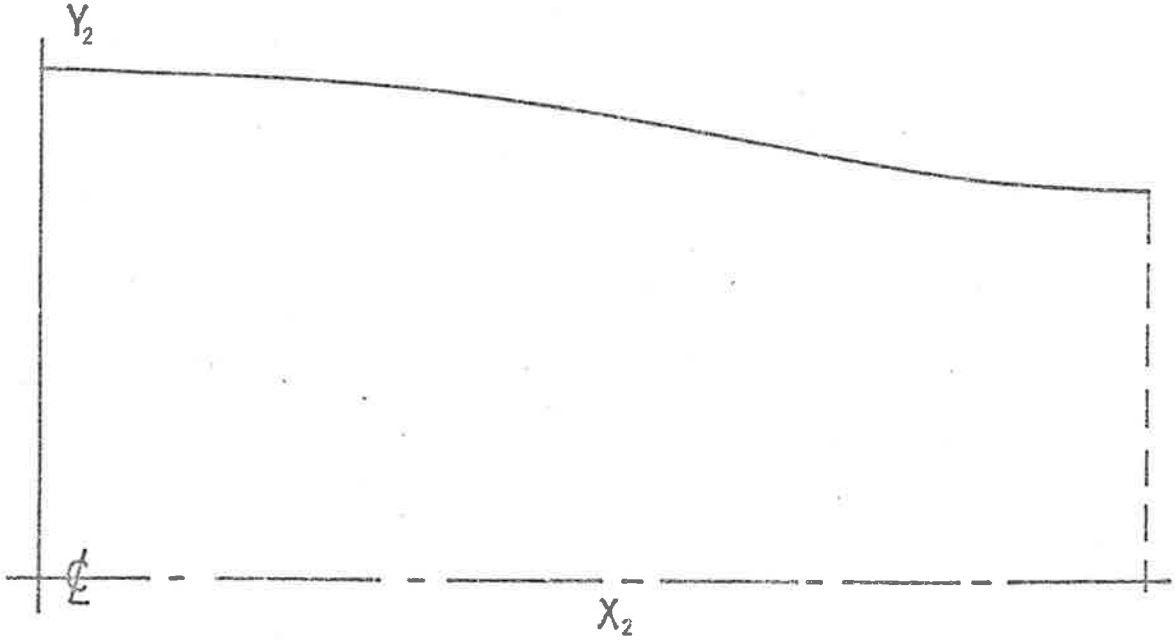

b) Form of Choke Nozzle.

Fig. D1 Co-ordinate System for Sonic Choke Section.

and y_2 is the internal radius of the nozzle cross-section at a distance x_2 from the downstream end - see figure D.1(b).

Table D.1 Ordinates of Sonic Choke Centre-Body Nose and Nozzle

(a) Centre-body Nose

x_1 mm	y_1 mm
0	41.91
10.00	41.71
20.00	41.12
30.00	40.13
40.00	38.74
50.00	36.94
60.00	34.72
70.00	32.07
80.00	28.98
90.00	25.43
100.00	21.40
110.00	16.86
120.00	11.78
130.00	6.12
139.76	0.0

(b) Nozzle

x_2 mm	y_2 mm
0.00	66.29
10.00	66.16
20.00	65.83
30.00	65.32
40.00	64.60
50.00	63.68
60.00	62.55
70.00	61.21
80.00	59.66
90.00	57.90
97.72	56.39
100.00	55.94
110.00	54.21
120.00	52.92
130.00	51.96
140.00	51.44
148.17	51.31

The calculated values for y_2, for $x_2 = 0$ and 10.00mm are 66.24mm and 66.14mm respectively. The first two values have been changed to fair the nozzle into the existing diffuser.